**Development of Electro-Anaerobic Membrane Bioreactor (EAnMBR) for treatment
of high-strength industrial wastewater**

Valeriy Troshin

A Thesis

In the Department of

Building, Civil and Environmental Engineering

Presented in Partial Fulfillment of the Requirements

for the Degree of

Doctor of Philosophy (Civil Engineering) at

Concordia University

Montreal, Quebec, Canada

October 2016

CONCORDIA UNIVERSITY
SCHOOL OF GRADUATE STUDIES

This is to certify that the thesis prepared

By: Valeriy Troshin

Entitled: Development of Electro-Anaerobic Membrane Bioreactor (EAnMBR) for treatment of high-strength industrial wastewater

and submitted in partial fulfillment of the requirements for the degree of

Doctor of philosophy (Civil Engineering)

complies with the regulations of the University and meets the accepted standards with respect to originality and quality.

Signed by the final Examining Committee:

Dr. R. Jayakumar, CSE	Chair
Dr. H. Zhou	External Examiner
Dr. V. Titorenko, Biology	Examiner to Program
Dr. J. Hadjinicolaou, BCEE	Examiner
Dr. T. Stathopoulos, BCEE	Examiner
Dr. M. Elektorowicz, BCEE	Thesis Supervisor

Approved by _____ Dr. F.Haghighat _____
                                Chair of Department or Graduate Program Director

October 2016   Dr. A. Asif _____
                              Dean of Faculty

ABSTRACT

Development of Electro-Anaerobic Membrane Bioreactor (EAnMBR) for treatment of high-strength industrial wastewater

Valeriy Troshin, Ph. D.
Concordia University, 2016

The main objective of this research was to develop an advanced system for industrial wastewater treatment which could produce an excellent quality effluent. The subsequent objectives were: i) to reduce the initial concentration of carbon, nutrients, and color-forming substances compared to conventional treatment systems, ii) to investigate removal mechanisms in the new system under electric field, iii) to optimize the system by studying the relationship between various operating parameters. To achieve these objectives an innovative compact electro-anaerobic membrane bioreactor (EAnMBR) was designed and its high performance was researched in two operational configurations. In the EAnMBR, physicochemical, biological and electrokinetic processes interacted simultaneously permitting to control the effluent quality and sludge properties. The dark-color molasses-based wastewater containing the high concentrations of chemical oxygen demand (53,000 mgL^{-1}), total nitrogen (2,300 mgL^{-1}), total phosphorus (150 mgL^{-1}), was selected for this research and submitted to multi-phase studies. The research allowed to define optimal operational conditions leading to removal of carbon, nutrients by 99% and to complete discoloration in the EAnMBR system. The novel system was compared with anaerobic membrane bioreactor showing performance superiority of EAnMBR in respect to COD, sludge volume reduction and filterability by 10%, 54% and 7%, respectively. A separate experimental phase was dedicated to optimize the energy balance in the novel system by the surface response method. The EAnMBR demonstrated outstanding results which make it a promising advanced wastewater treatment technology for various applications, e.g. in food, agriculture and defence industries.

Acknowledgment

I would like to express my sincere gratitude to my advisor, Dr. Maria Elektorowicz, for her continuous support throughout this long and exciting journey that made this work possible. I am especially thankful for her invaluable advice and compassion. I also appreciate the freedom I was given to develop and manage my PhD research.

Dedication

To my wonderful parents. Dear Mom, thank you very much for your support. Dad, I wish you were able to see this work completed. Your influence is evident on every page.

Table of Contents

List of Figures

List of Tables

1. Introduction

This chapter outlines the problem and focuses on the thesis scope, structure and emphasis.

1.1. Background

Water is an essential life-sustaining element and our planet's most precious natural resource [1, 2]. While 70% of the world's surface is covered by water, 97.5% of that is salt water. Of the remaining 2.5% that is fresh water almost 68.7% is frozen in ice caps and glaciers. Only one percent of the total water resources on earth is available for human use [2].

Water is vital for life, but also crucial for economic development [1]. Today 2.6 billion of people, which is one third of the world population, cannot use improved sanitation facilities and 884 million still do not have a basic human right to access to safe drinking water from improved sources [3, 4].

As the world population tripled in the 20th century reaching 6.1 billion in 2000, the use of renewable water resources has grown sixfold, more than twice the rate of population growth [1, 3]. Projections recently issued by the United Nations suggest that world population could pick 8.9 billion in 2050, but in alternative scenarios could be as high as 10.6 billion and no less than 7.4 billion [5].

The increase in Gross National Product (GNP) in most countries and progressing industrialisation combine to create a demand for clean water in the urban and rural areas in many countries and will continue to expand substantially in the coming years [1].

Climate change is also contributing to degradation of water quality and its availability [6]. Clean water, an essential component for many industries, is becoming a scarce resource and a new road map to sustainable water management needs to be focused on. An effective approach to the growing demand must include not only raising public awareness but also implementation of new and innovative technologies for industrial wastewater treatment, in order to reduce constantly growing pressure on fresh water supplies [7].

These technologies should be environmentally beneficial and based on principles of waste reduction, treatment localization and recovery of valuable resources from wastewater which can be used further.

Despite the abundance of available technologies for industrial wastewater treatment, there has been growing interest from scientific community [8-18] and industry [19] to other possible alternatives.

This has been dictated by social and economic challenges resulting from urgent demand for energy savings, constrains of traditional treatment, increasingly stringent quality standards set for treated effluents and searching ways to treat wastewater, especially from industrial sources more environmentally friendly. Due to the nature of such wastewaters, they are significantly more difficult to treat. Because of these factors, currently available technologies face challenges to meet the demand for wastewater treatment without unacceptably increasing cost. Hence, there is a place for medium or small- scale treatment systems that could be used for treatment of wastewaters coming from industrial sources.

Minimization of waste generation is a growing necessity as current wastewater treatment practices lead to the point when wastewater treatment plants are recognized as point-sources of contamination. Oxygen depletion, metals of environmental concern, solids formed during technological process, carbon dioxide and nitrous oxide emissions are the problems associated with wastewater treatment.

Localized treatment solves the problem of wastewater transport to treatment plants and treated water back to the point of origin. Local treatment of discharges from small and medium-scale point sources is more flexible, can be tuned for a particular type of wastewater which eliminates problems associated with treatment of highly-mixed and complex wastes.

Wastewater contains valuable chemical compounds such as metals, phosphorous, nitrogen and many other which otherwise lost in a landfill as a waste without any beneficial use.

Traditional treatment of wastewater broadly divided on physical, chemical and biological methods in different combinations depending on the nature of wastewater and enforced by local authorities standards for the discharged water quality.

Physical separation involves the processes that do not necessarily change chemical structure of wastewater and includes sedimentation, flotation, filtration, membrane separation, adsorption, ion exchange, and gas-liquid exchange.

Treatment systems that are suitable for large-scale wastewater producers take advantage of physical processes like sedimentation with gravity as energy source. However, reliance on gravity settling is not often appropriate, especially in urban areas where free space may be in deficit.

Chemical methods include precipitation [20], ion exchange, coagulation-flocculation [21], and oxidation-reduction of targeted substances [22].

The direct introduction of a chemical coagulant into the solution in order to destabilize established equilibrium in the system and promote phase separation is a traditional and well-established chemical method. Typically, in the chemical coagulation process, sulphates and chlorides of aluminium or iron are added as inorganic coagulant reagents [23, 24]. Hydrolysis results in release of a series of metal hydrolyzed species carrying a charge. Synthetic coagulants [25, 26] and pre-hydrolyzed aluminium and iron coagulants and silica-modified coagulants are also applied [27-31].

Principal disadvantages are the problems associated with large amount of sludge produced, corrosion, the high operating costs of chemical addition and solids handling and disposal.

Oxidation of pollutant may be accomplished by introduction of air or strong oxidizing agents such as ozone [32], potassium permanganate [33, 34], Fenton reagent, hypochlorite ion, by ultraviolet (UV) radiation or photocatalysis [35].

Biological wastewater treatment may involve aerobic [36], anoxic [37] or anaerobic microorganisms [38-48] . The biological activity of the microorganisms is of extreme importance to the successful treatment of wastewater [49], and activated sludge process is the most widely used technology for municipal and industrial wastewater treatment today [50]. However, wastewater may contain compounds that are inhibitory or toxic to the biological community [49]. Population shifts within the microbial community may result in changes in the plant operating conditions and cause sludge quality problems such as poor sludge settling, compaction, and dewatering [50].

There is also a concern that effluent toxicity may actually be created in the biological treatment process itself as soluble microbial products (SMP) could be more toxic than the original organic compounds present in the wastewater [41].

Electrochemically based processes of separation can be one of possible alternatives. This technology is based on creation of potential difference between electrodes submerged into the wastewater. Resulting electrical field liberates ions from anode and cathode and causes their directed movement in the solution initiating the process of electrocoagulation. At the anode-electrolyte and cathode-electrolyte interface electrons are released and captured accordingly which leads to electrolytic oxidation or reduction of undesirable constituent and its removal

from solution by sedimentation and electroflotation. The combination of these processes can be precisely adjusted to suit the treatment requirements.

The electrochemical methods of separation also include photoelectrocatalysis and chemically-assisted electrooxidation and photoelectrocatalysis [35].

Physical, chemical and biological changes occur simultaneously when electric field applied to the water.

Available alternatives need to be assessed on a multitude of cost aspects, energy requirements, operational experience, process reliability and environmental impact. However, the selection of the best alternative is generally based on cost-effectiveness [37].

Electrochemical technologies are not only comparable with other technologies in terms of cost effectiveness [51-55], but proved to be efficient in terms of contaminant removal efficiency in many cases [56, 57]. In some situations, electrochemical technologies may be indispensable in treating wastewaters containing refractory pollutants which cannot be removed by other methods [58].

1.2. Thesis Scope

This research focused on development of a novel compact system that combined physico-chemical, biological and electrokinetic treatment methods, and assessment of wastewater effluent quality parameters as metrics of treatment effectiveness and biological activity. Experimental studies were conducted on synthetic and raw molasses-based industrial wastewater in the environmental laboratory at Concordia University.

1.3. Thesis Emphasis

Because the project had an outlook towards application of a novel system for treatment of highly recalcitrant industrial wastewaters, the research conducted on real wastewater was extremely important. In-depth analysis was pursued to design a novel system suitable for real-life application.

1.4. Thesis Structure

This thesis consists of six chapters. The remainder of this thesis is organized as follows: Chapter 2 provides information on properties of molasses-containing industrial wastewaters and examines the research previously conducted on treatment methods and systems for such

wastewaters. It also defines hypothesis and objectives of this thesis based on conclusions drawn from the comprehensive literature review.

Chapter 3 describes the experimental methodology including the major considerations in designing the EAnMBR system and introduces a detailed description for the experimental work such as research strategy, experimental setup, equipment, materials and chemicals, sampling and analytical methods. Chapter 4 provides results and discussion for Phase I of the research including preliminary trials on batch systems in order to evaluate optimal electrokinetic parameters in terms of current density, voltage gradient and exposure mode for optimal biological treatment.

The results of the experimental study in Phase II provide insight into operation of the novel system in AnMBR (Stage I) and EAnMBR (Stage II) configuration for the two-month period and impact on carbon, nutrients removal and decolourization of synthetic wastewater. Mechanisms of carbon and nutrients removal by anaerobic membrane and anaerobic electro-bioreactor have also been studied on synthetic wastewater and discussed in details.

Phase III covers application of the EAnMBR for treatment of a raw industrial wastewater in AnMBR (Stage I) and EAnMBR (Stage II) configuration for the six-month period. Chapter 5 describes surface response method optimization of the EAnMBR for carbon, nutrients and color removal from wastewater. Controlled experiments were carried out in the laboratory to examine optimal operating conditions in terms of pH, current density and concentration of mixed liquor for these specific pollutants removal.

Chapter 6 covers novel findings of the research and suggestions for further work.

2. Literature Review

This chapter presents a comprehensive literature review of the previous research related to the topics of this work.

2.1. Molasses Wastewater Characterisation

Wastewater resulting from molasses production technological processes is a complex mixture of various organic and inorganic substances. As most of the industry utilizes beet molasses as a main feed component for the large-scale production, contaminants encountered in the wastewater come mainly as a result of usage of this source of carbon and biological activity during the process of fermentation, and is especially difficult to treat due to extremely high concentration of pollutants [59].

Secondary treatment of this fermentation wastewater such as a combination of aerobic, anoxic and anaerobic processes removes the bulk of the loading; however, the wastewater still cannot meet regulations for discharge into the municipal sewage system [60-63].

Further treatment by various methods is generally effective for the color removal, however high concentrations of nitrogenous compounds, sulfur and COD remain a problem [64-72].

A well-known problem of membrane filtration processes is fouling. Chemical coagulation removes color and COD relatively effectively, however has a number of drawbacks. Adsorption on activated carbon could generate large amounts of sludge, while advanced oxidation processes are associated with a high energy demand [61, 62, 73-76].

Therefore, it is necessary to describe and assess the major components of concern in yeast wastewater in order to find an optimal solution in terms of bringing the discharge quality below the regulatory limits.

Regardless of the differences in technological trains, the underlying concepts and processes may have some similarities. At the same time, molasses wastewater produced by food industry has far more differences, making it a unique substance itself in each particular case. Despite this fact, several major components are similar to any molasses wastewater.

This chapter begins by examining some of the key components that are shared by all wastewaters such as color-forming substances, carbon, nitrogenous compounds, sulphur-containing agents and solids.

2.1.1. Color-forming Substances

Sugar beets do not contain color-forming agents, but they contain chromogenic compounds [59]. The number of color-conferring materials that can be found in the wastewater is enormous. They include not only ketones, dicarbonyls, acrylamides, and heterocyclic amines, all of which contribute to flavour, but also melanoidins and advanced glycation end-products [77]. Some are referred in the literature under various names such as acrylamid, caramelan, caramelene, carameline, saccharan and fuscazinic acid [59, 78]. Besides, furfural derivatives are formed simultaneously with volatile compounds (aldehydes, such as acrolein).

In addition, carbohydrates, substances such as phenol-iron complexes, melanins and caramels also participate in the formation of color, and are responsible for the change of the optical properties of the liquid phase.

The extent of color formation is related primarily to pH, pressure, temperature and reaction time [77-79]. Variations in pH influence the structure of the chromophoric compounds [77]. The effect of high pressure on each reaction separately will depend on the type of reaction. For example, reactions involving the formation of hydrogen bonds are known to be favoured by high pressure because bonding results in a decrease in volume of the molecules [78]. However, according to the literature, formation of color-forming substances increases threefold for each ten centigrade degree rise in the temperature and time of processing which affects molecular weight of the chromophores, with increasing molecular weight upon heating [77].

Another major contributor is the reactions between bases and acids, but browning products are formed also, to a certain extent, from the decomposition of saccharose [59].

The major color-forming agents that appear in the course of sugar manufacturing and passed along the technological train, and further to the wastewater can be divided into the following groups [59]: melanoidins, polyphenolic-metal complexes, melanins and caramels, and further described in more detail in the following sections.

2.1.1.1. Melanoidins

Three theories on melanoidins formation have been proposed, all based on the Maillard reaction (MR). According to the first one, high-molecular weight colored structures are formed by cyclizations, retroaldolizations, dehydration, rearrangement, isomerization, and condensation of low-molecular weight products of sugars and amino acids produced by MR,

and intermediates such as furans, pyrroles, pyrrolopyrroles, and their derivatives in the later stages of MR reaction [77, 80, 81].

The second theory states that high-molecular weight melanoidins are derived from cross-linking chromophoric low-molecular weight polymers and reactive amino acid side chains such as lysine, arginine, or cysteine [77].
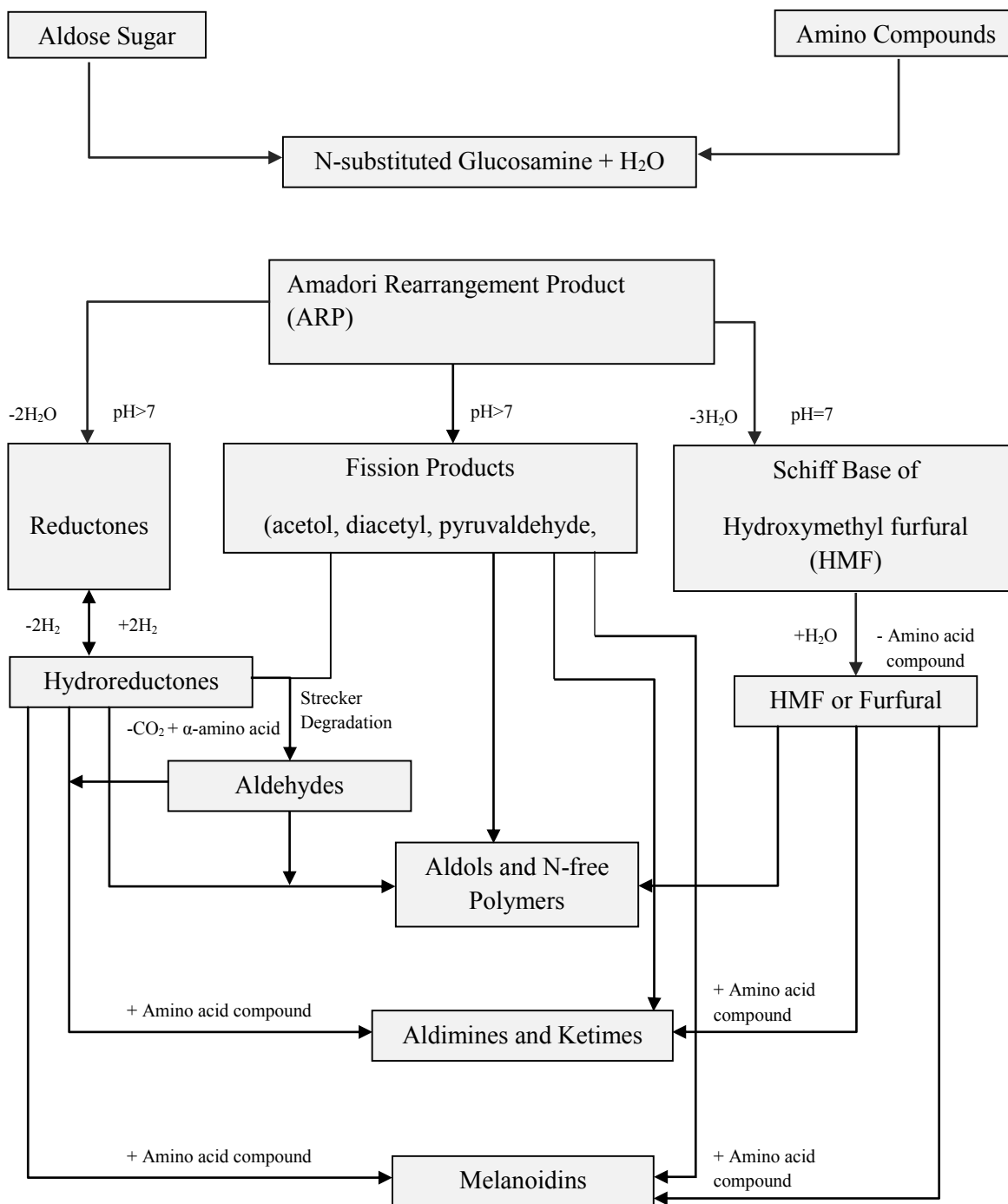
Figure 2.1. Formation of melanoidin [82, 83]

The third theory proposes that the melanoidin skeleton is built primarily from sugar degradation products branched with amino compounds, such as amino acids. It has been demonstrated in model systems that melanoidins are formed by aldol condensations of highly reactive a-dicarbonyl compounds, which are the main intermediates during the early stages of the MR, and partially branched by amino compounds [77, 84]. Three consecutive steps that lead to the formation of melanoidins in MR are illustrated in Fig. 2.1.

In the first stage of the reaction, reducing sugars react with amino compounds to form a Schiff base which is then stabilized by the Amadori product [77, 85, 86]. In the second stage, the Amadori product degradation gives rise to a variety of highly reactive carbonyl compounds [82].

During this stage, a-dicarbonyls, aldehydes, furaldehydes and furanone, are generated, which rapidly react with each other in an aldol-type condensation. In addition, degradation of aldose sugars leads to the formation of furaldehydes and furanones as well, for instance furan-2-carboxaldehyde and furan-2-aldehyde in the late stage of the reaction [77].

A range of reactions takes place in the advanced stages of the MR, including cyclizations, dehydrations, retro-adolizations, rearrangements, isomerizations and additional condensations. Ultimately, these intermediate products react with amino acids to form low molecular weight products, leading to the production of high molecular weight products by polymerisation [80].

It has been reported that in the absence of chlorogenic acids the melanoidins behave as anionic hydrophilic polymers, which can form stable complexes with metal cations [77, 80].

The type of sugar was shown to be a significant parameter for obtaining melanoidins with high iron affinity, and glucose led to stronger binding than lactose [87].

Despite ubiquity of research, the structures of the resulting melanoidin polymers mainly remain a mystery. This can partially be attributed to the amorphous and insoluble nature of these polymers [88].

Recently, the formation of microspherules without amines has been observed under conditions associated with the formation of humins which were called "pseudomelanoidins" [80, 88]. This observation under laboratory conditions suggests that humins and melanoidins are structurally similar.

It has been demonstrated that the polymer can form similar gelatinous globules and can also contain furans and pyrroles, when formed from erythrose in the presence of ammonium acetate

[88]. This suggests that in some industrial processes melanoidins can be removed from the final products, e.g., sugar crystals, by adsorption [80].

Research has been performed on the partial structure of melanoidins [81, 86, 88-90].

Melanoidins produced in model MR systems heated for more than 24 h are predominantly of molecular weights greater than 10 kDa, demonstrating predominance of high-molecular weight chromophores [77, 80, 87]. However, other studies also demonstrate formation of pigments associated with low-molecular weight polymers if other conditions are applied (glucose and fructose heated with amino acids to 100 ^{0}C for 2 h) [91].

Blue and red pigments which subsequently undergo transformation and acquire brown pigmentation have been isolated from alkali aqueous xylose-glycine, glucose-glycine and xylose-b-alanine reactions conducted under pH 8.1 in presence of 60% ethanol at 26.5 ^{0}C for 48 h. The blue pigments were determined to have a novel chemical structure consisting of two pyrrolopyrrole rings combined with a methine bridge [86].

The attempt to control the formation of melanoidins and its intermediates from nonenzymatic browning reaction by pH control using model melanoidins prepared with a strong buffer shows dependence of melanoidins stability on pH of the environment. The greater stability of the melanoidins prepared with pH control might, therefore, have been attributed to a higher content of pyrrole and reductone compounds as well [77, 79].

Assessments of model systems in laboratory conditions demonstrated the antimicrobial properties of melanoidins, and antimicrobial activity towards gram-positive and gram-negative microorganisms have recently been compared [77, 92]. Results of the studies demonstrate that melanoidins exhibit higher antimicrobial activity towards gram-positive microorganisms and high-molecular fractions of melanoidins exhibit higher antimicrobial activity against *E. coli* than low-molecular fractions. A higher microcidal activity was found in samples prepared at higher temperatures. Strong antimicrobial activity was observed in both pure melanoidins, as well as the bounded melanoidin compounds linked to these melanoidins [93]; however, the bound melanoidin compounds fraction contributed to the antimicrobial activity of melanoidins the most [77, 94, 95].

At low concentrations of melanoidins, antimicrobial activity exhibit a bacteriostatic activity, mainly mediated by the formation of iron chelates from the culture medium [77]. However, bactericidal activity at higher concentrations was found to be predominant [92, 96].

If bacterial strains are able to produce siderophores for iron acquisition, the formation of the siderophores-Fe^{3+} complex by melanoidins is observed, which could decrease the virulence of pathogenic bacteria [77].

Finally, melanoidins at high concentrations can both destroy the outer and inner cell membranes by chelating Mg^{2+} ions from the outer membrane, leading to a destabilization of the inner cell membrane and eventual cell lyses [92, 96]. The higher antimicrobial activity shown towards gram-positive microorganisms is attributed to the absence of a protective outer membrane, which makes this type of microorganisms more susceptible to antibiotic activity of melanoidins[96]. These findings suggest that the antimicrobial activity of melanoidins may affect the effectiveness of biological treatment methods of molasses-based wastewater.

2.1.1.2. Polyphenolic-metal Complexes

Variety of non-biodegradable and toxic pollutants such as phenolic compounds (pyrogallol, catechol, hydroquinone, and their derivatives bearing heterocyclic fragments) presents in the wastewater and may form chromogenic chelate complexes. In a series of the studied synthetic phenolic compounds, pyrocatechol derivatives possess the maximum antioxidant capacity (AOC) and leads to a yellow-green discoloration of sugar molasses. It is understood that the color results from the formation of a pyrocatechol-iron complex [59, 97].

2.1.1.3. Enzymatic Browning

Enzymatic browning is a chemical process which occurs in fruits and vegetables by the enzyme polyphenol oxidase, which results in brown pigments.

Beet tyrosinase, for instance, which belongs to the polyphenol-oxidases. In the presence of oxygen, the enzyme catalyzes the first steps in the biochemical conversion of phenols to produce quinones, which undergo further polymerization to yield dark, insoluble polymers referred to as melanins. This reaction, known as melanin-formation, requires only enzymatically catalyzed oxidation for its initiation and then proceeds as a chain reaction passing through red and red-brown intermediate stages to orthoquinone-like compounds. The reaction is not only dependent on the presence of air, but also on the pH. The reaction does not occur at pH <5 or pH >8 [59].

An example of the formation of melanins from a simple polyphenol, tyrosine, is illustrated in Fig. 2.2.

```
        ┌─────────────┐
        │   Tyrosine  │
        └─────────────┘
              │   Phenoloxidase + O₂
              │    ⤵
              └──────────────→ ┌──────────┐
                  Slow         │   Dopa   │
                               └──────────┘
                                    │  Phenoloxidase + O₂
                                    │   ⤵
                                    └──────────→ ┌──────────────┐
                                        Fast     │ Dopaquinone  │
                                                 └──────────────┘
                                                        │ Fast
                                                        ↓
                                                 ┌──────────────────┐
                                                 │  Leuco Compound  │
                                                 └──────────────────┘
                                                        │ + O₂
        ┌──────────────┐                                │
        │  Dopachrome  │←───────────────────────────────┘
        └──────────────┘        Fast
              │ + CO₂
              ↓
┌────────────────────┐
│ 5,6-Dihydroxyndole │←──────── Slow
└────────────────────┘
        │ + O₂
        └──────────→ ┌─────────────────────┐
            Fast     │  Indole 5,6-Quinone │
                     └─────────────────────┘
                              │ + O₂
                              └──────────→ ┌──────────┐
                              Relatively Slow │ Melanin │
                                           └──────────┘
```
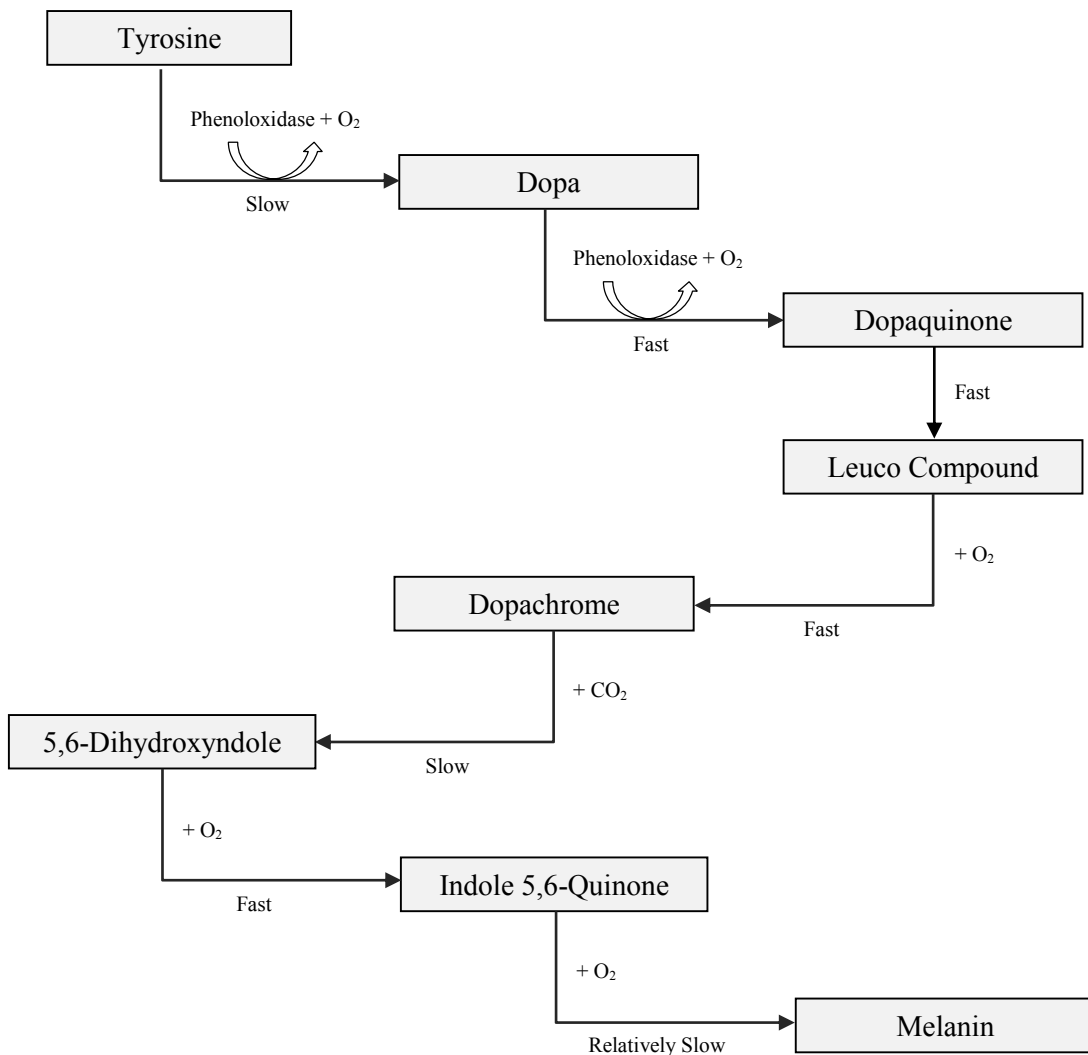
Fig. 2.2. Formation of melanin [98]

2.1.1.4. Caramels

Caramelization is one of the most important types of browning processes in food-production industry along with MR and enzymatic browning. Caramels are the result of the process of removal of water from carbohydrates such as glucose and sucrose followed by isomerization and polymerisation steps. Despite the fact that caramelization process is still poorly understood, a reaction can proceed in series of the following steps.

During the first stage of reaction saccharose is decomposed into simpler sugars- glucose and fructose. This step is followed by a condensation, in which the individual sugars lose water and react with each other to form, for instance, difructose-anhydride.

The next step is the isomerization of aldoses to ketoses and further dehydration process. The last series of reactions include both fragmentation reactions (flavor compounds formation such as diacetyl) and polymerization reactions (color-forming polymers such as caramelans ($C_{24}H_{36}O_{18}$, caramelens ($C_{36}H_{50}O_{25}$, caramelins $C_{125}H_{188}O_{80}$ formation). At constant pH the formation of caramels is directly proportional to the effective temperature- caramelization starts at relatively high temperatures as compared to the other browning reactions, and depends on the type of carbohydrate [59].

2.1.2. Nitrogen

Nitrogen and its derivatives removal from wastewater are a major concern for many industries as many municipal wastewater treatment plants limit accepted concentrations for these compounds [99].

A number of new processes based on partial nitrification, anaerobic ammonia oxidation, aerobic deammonification, nitrifier denitrification, and others have been recently developed in the domain of wastewater treatment [100].

Two processes deserve particular attention. Anaerobic microbial ammonium oxidation, or the anammox process occurs at high ammonium concentrations and depends on the availability of nitrite as an electron acceptor. In limited oxygen conditions, anammox consortia of microorganisms are usually accompanied by aerobic ammonium-oxidizing bacteria that oxidize ammonium to nitrite and, at the same time, protect anammox organisms from oxygen poisoning [101].

Recent advancements also include a new Denitrifying Ammonium Oxidation process (deamox). The concept of this process combines the recently discovered anammox reaction which takes place in autotrophic denitrifying conditions and employs sulphide as an electron donor for the production of nitrite from nitrate within an anaerobic biofilm [100]. To generate sulphide and ammonia, authors proposed an Upflow Anaerobic Sludge Bed (UASB) reactor as a first step of the process and evaluated it under various conditions [70]. The UASB effluent was split and partially fed to a nitrifying reactor in order to generate nitrate and the remaining part was directly supplied to the deamox reactor where this stream was mixed with the nitrified effluent. After a 410 day experiment at volumetric nitrogen loading rates above 1000 mg NL^{-1}d^{-1}, the total nitrogen removal efficiency was established around 90% [100]. However, there were some limitations observed regarding mass-transfer for denitrification attributed mostly

to the structure of sludge aggregates which are presumably formed with the outer layers of sulfide-oxidizing denitrifies and the inner layers of anaerobic ammonia oxidisers [70].

Initially, the deamox was developed as a mainly sulphide-driven process [70, 99, 100, 102]. However, it was extended to the organic-driven one, as another major drawback of this technology would be a possible deficiency of sulphide as an electron donor. This can be overcome by replacement of sulphides by volatile fatty acids. However, in this case removal efficiency of nitrate removal is reduced [103].

The phylogenetic analysis of the deamox microbial community reveals similarities with microorganisms involved in the anammox process [101]. The presence of nucleotide sequences of the microorganisms involved in the main reactions of the carbon, nitrogen, and sulfur cycles, including nitrifying, denitrifying, and anammox bacteria. In the bacterial clone library, 16S rRNA gene sequences of the phyla *Proteobacteria*, *Bacteroidetes*, *Chloroflexi*, *Firmicutes*, *Verrucomicrobia*, *Lentisphaerae*, *Spirochaetales*, and *Planctomycetes*, and other groups, were detected. In the archaeal clone library, nucleotide sequences of methanogens belonging to the orders *Methanomicrobiales*, *Methanobacteriales*, and *Methanosarcinales* were found [101]. Although cost effective, the biological process of nitrogen removal, especially in anaerobic conditions however, can be very long due to a slow growth of microbial community [99, 100].

Very limited research was conducted on assessment of removal efficiency of nitrogen associated with melanoidin [72]. Authors fractionated dissolved organic nitrogen (DON) by molecular weight and used chemical coagulation to study effect of dosage on various fractions. An alum dose of 30 mgL^{-1} was required to obtain maximum DON removal from the analysed samples. However, no significant removal of DON occurred in the <10 kDa molecular weight fractions using of aluminium for coagulation from wastewater effluents, highlighting that alum was more effective at removing compounds which had MW >10 kDa only.

2.1.3. Phosphorus

Phosphate can be separated by multiple physical, chemical, and biological methods. Biological methods are advantageous in terms of economy and produce less amount of solids compared to physical and chemical methods, however they have also disadvantages such as lower phosphorous removal efficiency and longer treatment time. Polyphosphate-accumulating organisms (PAOs) release phosphorous during the anaerobic phase and remove it during the

aerobic phase by accumulating phosphorus as polyphosphate [104]. Aluminum sulphate and ferric chloride are commonly used coagulants, however their usage is associated with higher costs for the purchase, generation of higher volume of sludge and its disposal [105].

Enhanced biological phosphorous removal processes can lower the total phosphorous (TP) concentrations in the effluent up to 0.1–0.2 mgL^{-1}, however, supplemental additions of conventional coagulants, poly-aluminum chloride (PACl) or lime are often necessary to maintain acceptable effluent TP concentrations [104, 106].

As an alternative, MBR have been gained popularity in the advanced wastewater treatment, including phosphorous removal [83]. This method of advanced treatment allows to achieve extremely high removal efficiency of phosphorous, however, it comes with a high maintenance cost as the membrane must be cleaned periodically or even replaced to combat membrane fouling [104]. Recently, various types of inorganic coagulants such as $FeCl_3 \cdot 6H_2O$, $Fe_2(SO_4)_3 \cdot 5H_2O$, $FeClSO_4$, $PFS_{0.3}$, PAC A9-M, PAC-A16, $Al_2(SO_4)_3 \cdot 18H_2O$, FO4350SSH, $NaAlO_2$ have been studied for the fouling reduction performance in MBRs [107]. Based upon the obtained results, $FeCl_3 \cdot 6H_2O$, $FeClSO_4$ and $Fe_2(SO_4)_3 \cdot 5H_2O$ exhibited relatively better performance. Specifically, $FeCl_3 \cdot 6H_2O$ and $FeClSO_4$ contributed both to sludge filterability enhancement as well as to SMP removal, while the effect of $Fe_2(SO_4)_3 \cdot 5H_2O$ on fouling control was mainly shown as a decrease of the respective TMP values. However, besides membrane fouling control, the effects of chemical coagulants addition on real MBR systems is associated with larger amount of sludge. Electrokinetic processes for phosphorous removal have also been attempted [104, 106]. An MBR reactor with a flat-sheet membrane and the electrokinetic process were studied to improve phosphorous removal efficiency and membrane permeability. The combination allowed to achieve PO_4^{3-}-P and TP removal efficiencies of 89.2% and 79.9%, respectively. The TP removal efficiency (79.9%) of the MBR system equipped with the electrokinetic unit was two times higher than that (41.0%) of other MBR systems with chemical coagulation process. The PO_4^{3-}-P removal efficiency (77.2%) of the MBR with the EC was also significantly higher than that (59.0%) of the MBR with conventional coagulation.

2.1.4. Sulphur-containing Substances

Sulfate is a source of considerable operational difficulties in anaerobic processes associated with generation of sulfides, loss of electrons, contamination of gas streams and equipment corrosion. Wastewater from the yeast industry contains extremely high concentrations of

sulfate (up to 5,900 mg L^{-1}) [70, 99, 100, 108]. A high sulfate content can be a source of the destabilization of the anaerobic treatment processes due to the hydrogen sulphide formation, especially if the $COD/(SO_4)^{2-}$ ratio is below 10 [108].

The main source of sulfate in the wastewater originated in the fermentation industry is the use of sulphuric acid for pH control. In addition, sulfur dioxide is used for bleaching to prevent colorization in sugar manufacturing. H_2SO_4 is relatively inexpensive and can be transported in a highly concentrated form (> 96%) [109].

Metal sulfide precipitates are more stable than metal hydroxides that are sensitive to pH change. Wastewater from the yeast industry is usually deficient in electron donors and requires external supplies in order to achieve sulfate reduction. Commonly used electron donors include hydrogen, methanol, ethanol, acetate, lactate, propionate, butyrate, sugar, and molasses [110]. Theoretically, conversion of 1 mol of sulfate requires 0.67 mol of chemical oxygen demand or electron donors [110]. However, for every mole of sulfate reduced, one mole of potential methane gas is lost; therefore the methane yield may be considerably reduced [111]. Methods to manage sulfide include biological oxidation, precipitation by metals, and removal in the gas stream with either sulfide removal in a caustic scrubber, reaction with packed beds of iron or zinc. An alternative to biological reduction is to remove sulfate from the wastewater by ion exchange, ion selective membranes and crystallization of sulfate minerals [111].

The calcium-aluminum-sulfate or ettringite is precipitated in the presence or with the addition of aluminum and calcium at high pH. It has been shown that during the formation of this mineral the sulfate levels can drop to less than 200 mgL^{-1} with a reasonable concentration of aluminum and calcium [111, 112]. The mineral jarosite, which is formed by the combination of iron, sulfate and another cation such as ammonium, potassium or sodium is commonly precipitated at acidic pH (<2.8) in the metallurgical recovery of zinc, where iron (III) must first be removed from solution [111].

2.1.5. Solids

A considerable fraction of refractory compounds remains after biodegradation even if the advanced methods of biological treatment implemented. The significant part of these compounds is represented by solids and often present in the original water or may also be produced as a result the biological processes [76].

Solids content in influent may range from 835 mgL^{-1} to 3,795 mgL^{-1} in terms of suspended solids (SS) and 810 mgL^{-1} to 1750 mgL^{-1} in terms of volatile suspended solids (VSS) [61, 75, 113].

VSS/TSS ratios are above 0.75 for all streams in the process which are an indicator of high organic content of the wastewater [114].

Concentration of total dissolved solids (TDS) may be as high as 6,300 mgL^{-1}. Increased conductivity of about 10.4 µScm^{-1} and Cl^{-} is 2,460 mgL^{-1} is a result of sodium chloride usage in the filtration process in order to increase the osmotic pressure of the yeast cream[114, 115]. Rotary drum filter, tank and equipment cleaning, evaporation process and cleaning streams are the major contributors to the high content of dissolved and suspended solids in the wastewater coming from yeast manufacturing plant [114].

Alkalinity is also present in significant quantities and may reach 1,980-2,349 mgL^{-1} CaCO$_3$ [75, 115].

2.2. Current Methods of Molasses Processing Wastewater Treatment

Molasses-based technological processes are among the most severely-polluting industries generating large volumes of recalcitrant wastewater. Different processes employing biological as well as physical-chemical methods have been employed to treat this type of wastewater. Anaerobic treatment is the most widely used method as over 80% BOD removal can be achieved [64, 71, 100]. In addition, energy recovery in the form of biogas is another major factor which makes it attractive [116, 117].

Further treatment to reduce residual organic and color includes secondary biological treatment employing fungi and bacteria, and physical-chemical methods such as adsorption, coagulation-flocculation, oxidation, and membrane filtration [65, 71, 74, 101, 106, 118-122].

This chapter examines the concepts and presents a review of the current state-of-art in biological and physical-chemical methods applied to the treatment of molasses-based wastewater. Bench-scale, pilot and industrial studies are considered in the following sections. Furthermore, limitations in the existing processes are summarized and potential areas for further research are discussed.

2.2.1. Physico-chemical Treatment

This chapter separates physical-chemical treatment details into eight major sections: adsorption, coagulation and flocculation, ozonation, advanced oxidation, Fenton's reagent, photocatalysis, membrane filtration, evaporation and combustion.

2.2.1.1. Adsorption

The decolorization study of a yeast wastewater factory by adsorption on activated carbon charcoal showed that these adsorbents have great capacity for adsorption and the total organic carbon, and color removal [65]. The COD and the DOC can be significantly reduced as well. The size of particles is an important parameter. Activated carbon of 150-250 μm at 30 gL^{-1} of solution leads to a total color removal and to up to 50% removal of the COD and DOC. To obtain the same removal efficiency, 130 gL^{-1} of 425-850 μm of activated carbon is required. The study of the kinetics of the discoloration shows that the adsorbent instantly reaches a saturated state with a saturation rate almost equivalent to the rate of its diffusion in the liquid phase. It shows also that the adsorption of the COD and the DOC follows the Langmuir adsorption isotherm, and that they are respectively equal to 231 and 213 mggL^{-1} for the nonactivated carbon (150-250 μm) and 103 mgg^{-1} for the activated carbon (425-850 μm) regarding the COD. The Freundlich adsorption model fit well the COD and DOC adsorption for the nonactivated carbon as well [65]. Another study revealed that the adsorption mechanism of melanoidin onto activated carbon involves mainly physical adsorption by electrostatic interactions and is favored in acidic pH. Breakthrough curves of melanoidin adsorption followed the characteristic "S" shape with good fit of the Thomas model [123].

It was also clearly demonstrated that an activated carbon with a significant distribution of both micropores and mesopores and a significant amount of macropores that are assumed to act as conduits providing access to micro- and mesopores, have a good adsorption efficiency for compounds such as tannic acid and melanoidins [74].

Although wastewater contains a majority of low-size particles (<1 nm) that may be preferentially adsorbed in micropores; activated carbon with micropores alone may not be suitable [74]. The selection of activated carbon containing both micropores and mesopores can be beneficial for adsorption of tannic acid, melanoidins and similar compounds. The role of activated carbon surface groups and macropores for adsorption needs of compounds specific to yeast wastewater needs to be further investigated, however. The major drawback of

adsorption is a large amount of waste produced, equipment clogging and the need for adsorbent regeneration.

2.2.1.2. Coagulation and Flocculation

Coagulation-flocculation is regarded as a simple and cost-effective means for color removal from molasses wastewater [124]. Besides, it is the most widely practiced process for removing colloidal particles in wastewater treatment [125].

Coagulation performance by hydrolyzing metal salts is strongly influenced by aqueous chemistry and raw water characteristics. Variables, such as pH, coagulant type and dose, are well recognized being significant factors affecting the process [71, 125, 126]. For instance, it has been shown that the optimum dosage of the coagulant increases with the increase in initial pH. In the pH range tested, the appropriate initial pH should be higher than 7 to ensure effective removal of coloring agents [127]. Ferric chloride and aluminum sulfate were compared in terms of removal efficiency [125]. It has been found that ferric chloride is the most effective in removing melanoidins from bio-treated molasses wastewater, achieving color and COD removal efficiencies of 98% and 89%, respectively at the optimal dosage, whereas aluminum sulfate was found the least effective among the conventional coagulants. The optimal dosage of ferric chloride expressed in terms of the ratio of metal to organic carbon removed was found in the range of 0.73-0.81g Fe^{3+} g^{-1} COD [124].

The ability of alum to remove the color and dissolved organic nitrogen (DON) associated with melanoidin has also been evaluated [72]. Study shows that alum dose of 30 mgL^{-1} as aluminium was sufficient to reach maximum removal of color (75%), DON (42%) and dissolved organic carbon (DOC) (30%) present in melanoidin containing effluent. Alum was shown to preferentially remove DON with a molecular weight >10 kDa over small molecular weight DON. Not all humic substances can be removed by aluminum sulfate, however.

There is a linear relationship between color removal and COD reduction [126]. However, there is still a 30% COD residual after almost all the color has been removed which is a result of the formation of complex organic compounds known as soluble microbial products (SMP) arising from anaerobic/aerobic treatment.

Besides conventional coagulants, polyelectrolytes are commonly used either as coagulant aids in wastewater treatment process to increase the settling rate, reduce operation costs, and provide better dewatering characteristics of sludge and reduce sludge volume [125]. It has

been demonstrated that cationic polyacrylamide (PAM) may significantly reduce the effluent turbidity, hence enhancing removal efficiency. Under optimal conditions, the removal efficiency of COD and color can be reached as high as 72% and 90% respectively [127]. Anaerobic biological treatment of the wastewater enhances the coagulation efficiency markedly, with $FeCl_3$ achieving 94% color and 96% COD removal, while chlorohydrate (ACH) and a low MW polydiallyldimethylammonium chloride (polyDADMAC) show 70% and 56% removal efficiency, respectively [71]. The improved decolorization can be attributed to the decrease in low MW organics (<500 Da) and biopolymers by the biological treatment, leading to reduced competition with melanoidins for interaction with coagulant/flocculant [71].

Molecular weight fractionation before and after coagulation experiments indicated that cationic polymer addition can increase the removal of all molecular weight fractions of DON with the highest molecular weight fraction (410,000 Da) being preferentially removed [119]. Rapid mixing conditions are suggested as most important parameters in the entire coagulation step as well. The appropriate rate was determined to be between 300 and 500 rpm [127].

Generated during coagulation step sludge could be a problem in full-scale operation. The iron sludge had much better SVI compared to alum which is an important parameter for further sludge handling and disposal [59].

2.2.1.3. Ozonation

Ozone is a powerful oxidant applied for wastewater treatment. Once dissolved in aqueous phase, ozone reacts with organic compounds in two different ways: by direct oxidation as molecular ozone or by indirect reaction through formation of secondary oxidants like free radicals, in particular the hydroxyl radicals. Both ozone and hydroxyl radicals are strong oxidation agents capable of oxidizing a number of compounds [128].

The main operating parameters affecting efficiency of ozonation process in wastewater treatment include pH, bicarbonate ion concentration, temperature and mixing rate.

The elimination of bicarbonate ion, strong inhibitor of hydroxyl radical reactions, showed an improvement in both color and COD reduction efficiencies [62]. According to the study, acidification for the purpose of removing bicarbonate ion resulted in a shift of color-forming agents to smaller molecular weights. The highest efficiencies were achieved at an elevated temperature of 40 ^{0}C. Color and COD reductions in this case can be achieved about 90% and

37%, respectively. Stirring rate may have a positive effect during the first stage of the reaction showing that mass transfer plays a role only during the initial reaction phase when direct attack of ozone molecules to aromatic compounds of colored substances was the predominant pathway [62].

Hydraulic residence time and applied ozone mass flow rate on color and organic matter removal were also studied [67]. Increasing the hydraulic residence time or ozone mass flow leads to a considerable increase in the ozone consumption, with similar color and organic matter reduction percentages. Operating with a hydraulic residence time of 45 minutes and applied ozone mass flow rate of 1.7 gh^{-1}, color and COD removal rates were about 80% and 14%, respectively.

Color reduction can be mainly attributed to direct oxidation reactions between ozone and chromophores, whereas the indirect oxidation pathway contributes to the reduction of the COD content [67].

The moderate COD removal results by pure ozone led to evaluation of treatment efficiency of ozone coupled with low-cost and non-toxic iron oxide employed as a heterogeneous catalyst for the treatment of wastewater [120]. In the presence of the Fe_2O_3 catalyst, ozone becomes more effective in reducing both COD and color-forming substances since the catalyst is responsible for enhancing the formation of hydroxyl free radicals, which are very reactive towards organic compounds.

When used for pretreatment, ozonation can increase anaerobic biodegradability. However the low concentration in the ozonised feed represents a limitation for possible recycling aimed at biogas production. Anoxic biodegradability can also be improved, reducing both the need for an external carbon source and concentration of nitrogen in the effluent. On average, the ozone pretreatment resulted in an increased biodegradable fraction from zero to 33% without noticeable toxicity on biomass. This ozone dose also resulted in 45% of nitrogen removal by biological denitrification [76].

Application of ozone oxidation for tertiary treatment of yeast wastewater has also been assessed [61]. Research shows that using ozone for posttreatment may result in the reduction of organic fraction by up to 49% if an ozone dose in the range of 1.2-2.5 mgmg^{-1} is applied.

Unfortunately, ozone itself is unstable and can decompose rapidly to molecular oxygen in a gaseous phase. As a result, ozone cannot be held or transported a long distance, and must be produced for immediate use on place [120]. As was found, ozonation pretreatment adversely

affects methane production [129]. Attempt to couple ozonation and adsorption processes did not show a synergistic effect on color and COD removal [130].

2.2.1.4. Advanced Oxidation

The advanced oxidation technology for wastewater treatment usually involves application of Fenton's reagent, ultraviolet irradiation (UV), hydrogen peroxide or their combination, often supported by conventional ozonation, and is based on the production of chemical radicals with an extremely high oxidation potential.

2.2.1.4.1. Fenton's Reagent

Fenton's reagent, which involves homogeneous reaction and is environmentally acceptable, is a mixture of hydrogen peroxide and iron salts (Fe^{2+} or Fe^{3+}) which produces hydroxyl radicals ultimately leading to decolorization of the effluent and non-biodegradable organics destruction [128].

An additional argument supporting the application of these systems is the ability to generate inert gaseous products of degradation and to oxidize hydrogen sulphide and sulphides to sulphates. It may be particularly interesting in the case of anaerobic treatment of wastewater [131].

Recent research evaluated the removal of both COD and color by applying three different chemical oxidation methods namely ozonation, ozonation with hydrogen peroxide, and Fenton's Oxidation [75]. It was noticed that H_2O_2 significantly reduced the reaction time for the ozone dosages; however, COD and color removal efficiency was not remarkable. In the Fenton's oxidation studies, however, the removal efficiencies of COD and color for 30 min reaction time for three different types of effluents were found about 86 and 92%, respectively which is significantly higher than combination of ozone and H_2O_2.

Both the dosages of H_2O_2 and Fe^{2+} are strongly dependent on the COD concentration in the wastewater. COD and color removal is also dependent on the initial COD level- higher initial COD concentrations resulted in lower removal rates [75].

Fenton oxidation of biologically pre-treated effluent of full-scale wastewater treatment plant was also investigated [113]. The 600 mgL^{-1} H_2O_2 and 600 mgL^{-1} Fe^{2+} dose was adequate to achieve a removal efficiency of 97%. However, the best results have been reached if Fe^{2+} /H_2O_2 dosage was 1,200 mgL^{-1} Fe^{2+}/800 mgL^{-1} H_2O_2 at pH 4 and the reaction time of 20 min

for mineralization of DOC and COD. For these conditions, the maximum color removal efficiency was obtained as high as 99%, and maximum DOC and COD removal efficiencies were obtained as 90 and 88% accordingly [113]. Higher results may be achieved (reduction of the total COD above 90%) if additional neutralization by application of lime as an aid is implemented [131]. Optimized combination of coagulation-Fenton's process for winery wastewater treatment was researched [132]. At the initial pH of 3, H_2O_2 concentration of 1.18 Lm^{-3} and reaction time 8 h, COD removal of 56.6% was achieved. Besides, a biodegradability enhancement of 60% was attained reaching a BOD5/COD ratio of 0.4. However, the final COD removal efficiency was 74%.

2.2.1.4.2. Photocatalysis

Photocatalysis or UV irradiation of H_2O_2 can also be used as the mechanism for the hydroxyl radical generation for organic compounds degradation. UV/H_2O_2 was shown to effectively remove the color associated with melanoidin [133]. However, the process was less effective in removing the DON and DOC present in the synthetic melanoidin solution. At the optimum H_2O_2 dose (3,300 mgL^{-1}), with an initial melanoidin concentration of 2,000 mg L^{-1}, the removal of color, DOC and DON were 99%, 50% and 25%, respectively. The nitrogen cleaved from the large organic melanoidin compounds appeared to form low molecular weight compounds (<1 kDa), ammonia and nitrogen gas. No oxidation of the nitrogen to NO_2 or NO_3 was observed in this study.

Discoloration and mineralization of yeast wastewater were investigated by using $Ce\text{-}Fe/Al_2O_3$ as a heterogeneous photo-Fenton catalyst in fluidized bed reactor [121]. The results show that TOC can be reduced from 347.6 mgL^{-1} to 10.8 mgL^{-1} and color reduced from 500 units to 0 at initial pH 6.0, H_2O_2 and concentration of 1,000 gL^{-1}, catalyst loading of 5 gL^{-1}, reaction duration of 120 min and reaction temperature of 30 ^0C.

2.2.1.5. Membrane Filtration

Pressure-driven membrane processes such as ultrafiltration (UF) and nanofiltration (NF) have been evaluated in many recent studies and found several practical applications in the field of wastewater treatment [134-138].

However, literature on membrane process application for COD removal and reduction of color-forming substances in industrial wastewater, especially molasses-based is extremely rare.

A recent study has been conducted with the purpose of evaluating the feasibility of membrane treatment of yeast production wastewater [122]. The effluent from the anaerobic stage was treated in order to reduce coloring agents and COD concentration and reducing the load on the downstream aerobic stage. For this purpose microfiltration (MF), ultrafiltration and nanofiltration membranes with differing molecular weight cut-offs (MWCOs) were tested. To evaluate the effectiveness of membrane processes in treating the waste stream, researchers measured optical density (OD) and COD along with permeation fluxes. Effects of pretreatment methods (coagulation and coarse filtration) and feed composition on OD, color, COD were also studied. Gel filtration analysis was employed to characterize feed and permeate streams in terms of MW distribution of organics. Maximum rejections obtained were 94%, 89% and 72% for OD, color and COD, respectively, when 0.8 μm microfiltration membrane and 400 Da NF membranes were used in series. Research suggests that chemical precipitation and conventional filtration were not adequate for pretreatment operations; however, MF was demonstrated to be effective for this purpose [122].

2.2.1.6. Evaporation and Combustion

Although no indication of direct application of thermal decomposition in yeast wastewater treatment has been found, this method has been applied for distillery spent wash which has similar raw components including molasses. A novel catalytic thermal pretreatment or catalytic thermolysis (CT) has been proposed to recover the majority of energy content with subsequent COD and BOD removal [128]. The initial pH had profound effect on the COD removal efficiency by applying thermolysis. At 140 ^{0}C and 3 kg m^{-3} catalyst loading, and optimum pH of 2, a maximum removal rate of 60% COD has been reached.

The CT process resulted in the formation of settleable solid residue and the slurry obtained after the thermolysis demonstrated good filtration parameters. At 140 ^{0}C and pH 2, the solid residue had a C:H atomic ratio of 1:1.08 with a heating value of 21.77 MJ kg^{-1}.

The residue can be used as a source of energy for the combustion furnaces and the product ash can be mixed with organic fertilizers and used in agricultural or horticultural industries [128].

2.2.2. Biological Treatment

Biological treatment plays a major role in food manufacturing wastewater treatment. In fact this is the primary and the most common method of plant effluent purification in yeast production [60, 63, 64, 68, 114, 139].

Biological processes are divided into aerobic, anaerobic, or combinations of both, and are often combined with physical-chemical treatment for pre or post treatment in order to enhance the efficiency and kinetics of the process [64, 66, 71, 76, 105, 122, 140-142].

This section covers the details of various biological methods of molasses-based wastewater treatment along with focus on equipment associated with primarily anaerobic treatment.

2.2.2.1. Mixed Cultures Processes

Since in many large-scale applications it is difficult to implement treatment by only pure microbial cultures, mixed culture studies have been carried out by several researchers for degradation of effluents containing color-forming substances and high concentration of COD in laboratory conditions [143-145]. As the metabolic processes of microorganisms in mixed consortia generally complement one another, the syntrophic interactions present in mixed communities lead to better performance in the mineralization of the organic components in the wastewater [128].

The degradation of four synthetic melanoidins, namely GGA, GAA, SGA, and SAA by three Bacillus isolates, *Bacillus thuringiensis* (MTCC 4714), *Bacillus brevis* (MTCC 4716) and *Bacillus sp.* (MTCC 6506) was conducted recently [144]. Results show that activity of consortium of these strains lead to significant reduction in the COD along with the decolorization of all four types of melanoidins. The medium that contained single source of carbon (glucose) demonstrated higher degree of removal (by up to 15%) than that containing both carbon and nitrogen electron donor. The addition of 1% glucose as a supplementary carbon source was essential for co-metabolism of melanoidin complex [144].

The toxicity test on tubificid worm (*Tubifex tubifex*, Müller), demonstrated significant reduction of toxicity with melanoidins removal by the three *Bacillus sp.* [143]. Authors isolated and characterized fifteen rhizosphere bacteria of *Phragmites australis* found in distillery effluent contaminated sites. These microorganisms included *Microbacterium hydrocarbonoxydans*, *Achromobacter xylosoxidans*, *Bacillus subtilis*, *B. megaterium*, *B.*

anthracis, *B. licheniformis*, *A. xylosoxidans*, *Achromobacter sp.*, *B. thuringiensis*, *B. licheniformis*, *B. subtilis*, *Staphylococcus epidermidis*, *Pseudomonas migulae*, *Alcaligens faecalis*, *B. cereus* which collectively brought about 76% melanoidin reduction and 85–86% BOD and COD removal in the effluent within 30 days [128].

Another microbial consortium of *Pseudomonas aeruginosa* PAO1, *Stenotrophomonas maltophila* and *Proteus mirabilis* has been isolated from distillery effluent contaminated sites following bioaugmentation [145]. These strains exhibited rapid degradation of the effluent resulting in 67% decolorization and 51% COD reduction within 72 h in the presence of very low sources of nutrients.

The major disadvantage of mixed-culture treatment, therefore, is that it is necessary to add nutrients as well as to dilute the concentrated effluent to obtain optimal microbial activity. Enzymatic pretreatment of wastewaters has been shown to increase the degradation efficiency of sub- sequent biological treatment processes [146]. The levels required by regulatory organisms still may not be achieved in many cases.

2.2.2.1.1. Aerobic Processes

After primary anaerobic treatment, the partially purified wastewater still contains high concentrations of organics, BOD, COD, suspended solids and remains highly colored, and, thus, cannot be directly discharged into the municipal sewer network.

Therefore, most processes include aerobic degradation as a secondary step (after anaerobic treatment) as most aerobic systems are highly effective at COD reduction provided there is adequate oxygen supply [146].

2.2.2.1.2. Anaerobic Processes

The anaerobic process is a complex multistage process, involving hydrolysis, acidogenesis, acetogenesis and methanogenesis and incorporates interaction of various symbiotic, synergetic and antagonistic microorganisms [116]. The anaerobic microbial communities can broadly be divided into three major groups of organisms, namely hydrolytic fermentative, syntrophic acetogenic and methanogenic bacteria.

The conventional anaerobic process presents several advantages as compared to aerobic treatment. It has a higher capacity for degrading highly-concentrated organic substances, produces less sludge, requires less energy, and generates biogas [128].

Carbon dioxide, hydrogen and methane can be generated during the process and possibility to increase the hydrogen production yield, which has the higher calorific value, has recently attracted significant attention from the scientific community [147-150].

The anaerobic ecosystem is the result of complex interactions among microorganisms of several different species [151]. The major groupings of bacteria and reaction they mediate are: (i) fermentative bacteria, (ii) hydrogen-producing acetogenic bacteria, (iii) hydrogen-consuming acetogenic bacteria, (iv) carbon dioxide-reducing methanogens, and (v) aceticlastic methanogens. The reactions they mediate are presented in Figure 2.3.
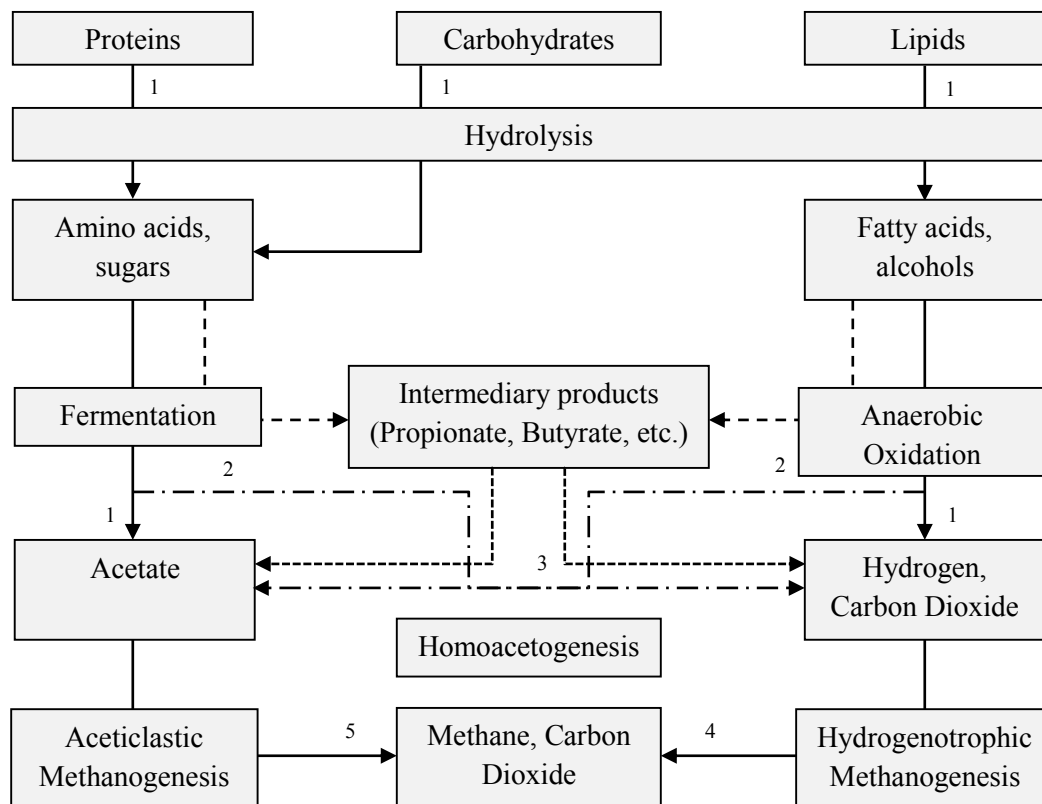
Figure 2.3. Reactive scheme for the anaerobic digestion of polymeric materials (Adapted from [151])

1) Hydrolysis, where enzymes excreted by fermentative bacteria convert complex material into less complex, dissolved compounds which can pass through the cell walls and membranes of the fermentative bacteria.

2) Acidogenesis, where the dissolved compounds present in cells of fermentative bacteria are converted into a number of simple compounds which are then excreted. The compounds

produced during this phase include volatile fatty acids (VFAs), alcohols, lactic acid, CO_2, H_2, NH_3 and H_2S, as well as new cell material.

3) Acetogenesis (intermediary acid production) where digestion products are converted into acetate, hydrogen (H_2) and CO_2, as well as new cell material.

4) Methanogenesis, where acetate, hydrogen plus carbonate, formate or methanol are converted into methane, CO_2 and new cell material. In this global scheme, the following sub-processes can be distinguished (Figure 2.3):

1) Hydrolysis of biopolymers:

- hydrolysis of proteins

- hydrolysis of polysaccharides

- hydrolysis of fats

2) Acidogenesis/fermentation:

- anaerobic oxidation of amino acids and sugars

- anaerobic oxidation of higher fatty acids and alcohols

3) Acetogenesis:

- formation of acetic acid and H_2 from intermediary products (particularly VFAs)

- homoacetogenesis: the formation of acetic acid from H_2 and CO_2

4) Methanogenesis:

- methane formation from acetic acid

- methane formation from hydrogen and carbon dioxide

Figure 2.3 provides degradation path of organic materials to the end products CH_4 and CO_2. The homoacetogenic process involves the conversion of acetate, the major CH_4 precursor and H_2/CO_2. In practice, other back reactions may occur also, e.g. the formation of higher VFA or alcohols out of acetate and propionate. These backward reactions are very important in case of malfunctioning or perturbation of the anaerobic reactor or when a specific reaction is deliberately pursued. Under normal AnWT applications, i.e. stable reactor performance under mesophilic conditions, acetate is the major precursor of CH_4 (about 70% of the COD flux). COD removal takes place owing to the fact that the end product of the reaction chain, CH_4, is gaseous and highly insoluble in water. In the case of the presence of alternative electron acceptors, like NO^{3-} and SO_4^{2-}, other bacterial groups will be present in the anaerobic reactor as well, such as denitrifies and sulphate reducers [102].

In a recently described approach, an electrical input to a modified microbial fuel cell (MFC) provided the energy necessary to convert organic acids, such as acetate, to hydrogen [148, 149].

Methanogens represent a major group of microorganisms in anaerobic process and are commonly considered to be strictly aerophobic organisms for which oxygen being toxic and inhibitory. Studies and practical experience have, however, revealed increased solubilisation of organics and the possibility of maintaining high methane generation activity in the presence of significant aerobic loads in anaerobic large-scale digestion [152, 153]. The positive impact of oxygenation on methane yield is more pronounced at conditions characterized by low hydrolysis rate coefficients (slowly degradable feed) and low biomass concentrations. The optimum oxygenation point moves towards zero when the hydrolysis rate coefficient and the biomass concentration increase [153].

Despite economic advantages and reliability, anaerobic treatment, however, is sensitive to organic shock loadings, variations in pH and demonstrates slow growth rate of anaerobic microorganisms resulting in longer hydraulic retention times (HRT). Therefore, precise tuning of the system is often necessary.

2.2.2.2. Pure Cultures Processes

In order to increase the efficiency of wastewater treatment, research has focused on treatment by pure microbial cultures [154]. However, problem of external nutrient addition, feed dilution and pilot-scale application still exist and should be addressed more thoroughly. The following sections summarize available data on application of bacterial, algal, and fungal cultures in wastewater treatment targeting both decolorization and COD reduction in effluent.

2.2.2.2.1. Bacterial

Various bacterial cultures capable of both bioremediation and decolorization of anaerobically treated distillery spent wash have been isolated [128].

Decolorization of molasses wastewater by immobilized cells of *Pseudomonas fluorescence* on porous cellulose carrier achieved 76% decolorization in 24 h at 30 ^{0}C. The decolorization efficiency can be further increased to 94% by coating cellulose carrier with collagen [128, 154].

An acetogenic strain from vegetable and juice samples which decolorized the molasses pigment medium and anaerobically treated distillery effluent to 73–76% within 5 days when supplemented with glucose and nitrogen sources. In replacement culture system involving six replacements, the strain showed constant decolorization and decrease in BOD and COD values of 58.5–82.2% and 35.5–71.2%, respectively. The maximum adsorption yield of this strain observed from the dead (autoclaved) cells. It was two times higher than that of living cells [155, 156] .

Oxidation of melanoidins thus is possible by removing almost all the high molecular weight compounds associated with melanoidins in untreated wastewater.

Recently, the decolorization of four synthetic melanoidins i.e., glucose-glutamic-acid (GGA), glucose-aspartic acid (GAA), sucrose-glutamic acid (SGA), and sucrose-aspartic-acid (SAA), were investigated using three strains: *Bacillus thuringiensis*, *Bacillus brevis* and *Bacillus sp*. The extent of color degradation of the melanoidins separately by each isolate was in the 1-31% range [144, 154].

2.2.2.2.2. Algal

The ability of a marine filamentous, non-heterocystous strain *Oscillatoria boryana* BDU 92181 to use the 5% melanoidin as nitrogen and carbon source leading to decolorization has recently been reported [157]. The organism generates hydrogen peroxide, hydroxyl ions and molecular oxygen all strong oxidizing agents during the process of photosynthesis resulting in 60% decolorization of melanoidin. As follows, cyanobacteria could use melanoidin as a better nitrogen source than carbon. Moreover, it has been shown that *Oscillatoria boryana* BDU 92181 forms natural coagulant by releasing proteins, lipopolysaccharides, polyhydroxybutyrate (PHB), polyhydroxy-alkanoates (PHA), etc. COO^- and ester sulphate (OSO^{3-}) functional groups form complexes with cationic sites resulting in flocculation of the organic matter in the effluent.

2.2.2.2.3. Fungal

Increasing attention has been directed towards utilizing fungal activity for decolorization of melanoidin-containing wastewater [128]. White rot fungus secreting ligninolytic enzymes can be effective in degrading xenobiotics and organic pollutants [154].

Molasses wastewater was decolorized and its COD was reduced in static cultivation using the fungi *Coriolus versicolor*, *Funalia trogii*, *Phanerochaete chrysosporium* and *Pleurotus pulmonarius* [118]. The effect of cotton stalk on decolorizing and COD removing capability of four fungi was also determined. In the concentration range from 10 to 30% wastewater was effectively decolorized by *C. versicolor* and *F. trogii*. The color was reduced up to 71% depending on waste concentration. Cotton stalk addition stimulated the decolorization activity of all fungi providing electron donor. Vinasse concentration had also a positive effect on biomass production, at its higher concentration the biomass production remarkably increased which can be explained by higher concentration of both organic and inorganic compounds added.

2.2.2.3. Combined Methods of Biological Treatment

The effluent coming from fermentation yeast industry, as stated previously, is highly colored and carries a large amount of organics. Existing anaerobic/aerobic biological treatment technologies reduce the BOD, but are unable to completely remove the color-forming substances and associated chemical oxygen COD from the wastewaters, therefore regulatory limits cannot be met.

Many efforts have been focused on combination of biological processes with physical and chemical methods of treatment in order to enhance biodegradability of the effluent [60, 62, 63, 76, 106, 120, 139, 158].

Combined with coagulation/flocculation process, biological treatment demonstrates better performance. An alum dose of 30 mg L^{-1} as aluminium was sufficient to reach maximum removal of color (75%), DON (42%) and dissolved organic carbon (DOC) (30%) present in melanoidin containing effluent [72]. Another study demonstrated anaerobic biotreatment of the wastewater was enhanced by the coagulation remarkably, with $FeCl_3$ achieving 94% color and 96% COD removal [71]. It was also demonstrated that removal efficiency of $Al_s(SO_4)_2$ and $FeCl_3$ at optimum dosage concentrations dependant on effluent quality. Both removed almost 90% of the color and up to 80% of the COD [126].

The use of ozone combined with biological treatment was investigated for molasses fermentation wastewater containing highly concentrated, biorefractory compounds [76]. Ozonation applied at the ozone dose of 0.5 g O_3 g^{-1} COD led to an increase in biodegradability.

On average, the pretreatment resulted in an increased biodegradable fraction from zero to 33% without noticeable toxicity to the biomass.

2.2.3. Electrochemical Treatment Processes

This chapter covers the theoretical aspects of electrochemical treatment of wastewater. After reviewing the history of development, this chapter examines in more detail the electrokinetic phenomena and introduces electrochemically-assisted membrane separation in wastewater treatment.

2.2.3.1. Historical Overview

The application of electric potential in wastewater treatment can be traced back into the nineteenth century.

In 1877 an American engineer Eugene Hermite received patents in Britain and France to treat wastewater by mixing it with a portion of sea water and electrolysing it for disinfection purpose. Based on these patents, a treatment plant was built in 1889 in London and was in operation until 1899. Another plant with iron electrodes for treating canal water was built the same year in Salford, England. Seawater was added as a chlorine source for disinfection [159].

In the United States series of patents were issued in the beginning of twentieth century [160-169]. In 1901 the United States Patent and Trademark Office issued a patent to Jean Marie Auguste Lacomme on a device for purification of water [165]. The device consisted of minimum a pair of electrodes shaped to form a pipe when properly combined. The edges of each anode and cathode were provided with flanges for assembling and insulating material between them. The system also consisted of series of metal rods integrated to the casing and extended inward into the pipe. The device could be integrated into the municipal water main and worked in a continuous mode.

An insoluble anode with high surface area made of perforated lead sheets was patented in 1919 [160].

In the United States, electrolytic sludge treatment plants were commissioned as early as 1911 in Santa Monica, California and Oklahoma City, Oklahoma and were operated until 1930. Both plants employed steel electrodes connected in series [159]. Solids removal efficiency at Santa Monica plant was 50% [170]. However, operation costs were high due to sludge handling and disposal problems [159].

In the Soviet Union a unit with iron electrodes for electrochemical coagulant generation was first used at the Shaturskaya GRES power station in 1925 [171]. Another early report from 1938 on implementation of electrical field in wastewater treatment showed the ability to treat tannery effluent [172].

Applicability of electrocoagulation as a method of treatment was trialed on industrial wastewater from food-production industry in 1965 and on municipal wastewater in 1969 in the Soviet Union [173, 174].

The use of gas as of a buoyant media to treat wastewater was first mentioned in a German patent in 1877 [175]. Based on this principle gases were generated by reaction of acids with suspended sulfides and carbonates. It was not until 1904 that production of gases by electrolysis for wastewater treatment was first referred to in a British patent [176].

In the United States, the concept of wastewater treatment by electroflotation first appeared in a patent issued in 1913 [167]. The apparatus consisted of an electrode chamber with a set of electrodes and a flotation tank. Wastewater entered the electrode chamber from the bottom and was forced to move upward along baffled electrode plates. From this gas-producing chamber liquid was carried to the flotation tank where it entered at the bottom and was separated from contaminants by buoyant microbubbles formed during the process of electrolysis.

In 1917 J. D. Kynaston proposed a wastewater treatment reactor with baffled aluminium anodes and carbon cathodes placed horizontally and connected in series [164].

In Canada A. T. Stuart patented horizontally arranged electrodes with developed surface area for improved electroflotation in 1918 [168].

Numerous patents were issued in the United States on electroflotation wastewater treatment in1920s and by 1930s this process became widespread in industrial applications [175].

Application of electrolytically generated gases in wastewater treatment has been given considerable attention in 1960s: research on emulsified sewage purification from oil refineries was reported in1962 [177].

2.2.3.2. Electrochemical Coagulation

In the process of electrocoagulation, electrical current passes through sacrificial metal electrodes (Fe or Al often the most economically-feasible choice) submerged into the aqueous phase, dissolving them and generating corresponding metal ions that yield Fe (II) and/or Fe

(III) or Al (III), (or other metals) aqua complexes along with hydroxide ion depending on the pH of the environment. The metal ions generation takes place at the anode and hydrogen gas is released from the cathode [178-181].

These species act as coagulants neutralizing charge of colloids and sweeping other particles out of wastewater by means of gravity forces.

The major processes that take place during the EC process may be summarized as follows [35]:

(i) Electrical current initiates reactions on electrodes surface, metal ions migrate from anode towards cathode, and H_2 gas is released at the cathode;

(ii) Coagulants start forming in the aqueous phase during the migration of ions;

(iii) Removal of impurities with coagulants by gravity and/or buoyancy forces;

(iv) Other electrochemical and chemical reactions involving reduction of organic impurities and metal ions at the cathode and coagulation of colloidal particles.

Other ions such as chloride are also oxidized at the anode, and are actively involved in the electrochemical reactions. Either the chlorine ion or its derivatives can initiate additional metal consumption in by-reactions. The more detailed description of factors affecting electrocoagulation follows later in the chapter.

2.2.3.3. Aluminum Anode

Anodic and cathodic reactions for systems with aluminium anodes and cathodes have been a subject of extensive research [19, 182-187].

Aluminium is frequently used as the sacrificial anode for electrocoagulation [188]. In the process of electrocoagulation, when the DC field is applied, Al^{3+} metal ions are generated due to the electrooxidation of the sacrificial aluminum anode and released into aqueous phase. The oxidation of water prodcues hydrogen (H+) and oxygen gas at the anode whereas hydrogen gas and hydrogen oxide (OH⁻), due to the water reduction, are generated at the cathode.

The release of Al^{+3} results in the aggregation (flocculation) of colloidal particles through reducing the value of zeta potential to a level where the Van der Waal's forces are greater than the repulsive forces between the charged colloids. The generated Al^{+3} cations also react with the free OH⁻ in water to initially form monomeric species such as $Al(OH)^{+2}$, $Al(OH)_2^{+1}$ and $Al(OH)_4^-$. These species are converted into polymeric colloids such as [189], $Al_{13}(OH)_{34}^{+5}$, which eventually transform into a long chain of Al(OH)(s). These cationic hydroxide

complexes can effectively remove the negatively charged organic materials through the electrostatic forces to neutralize the charge [189]. These complexes have large surface area up to 1 μm capable of adsorbing and trapping the soluble and organic colloidal particles, which are easily separated from the liquid medium by sedimentation or H_2 flotation [190]. In addition to the formation of aluminum hydroxide complexes, electrokinetic system enhances the interactions between the solid surfaces to facilitate the flocculation process [191-194]. Aluminium floc formation requires a certain amount of available alkalinity to permit rapid hydrolysis [182, 186, 187, 195, 196]. Recycling of spent coagulant is also possible [197]. Researchers have also reported that the amount of electrolytically produced aluminium flocculent required for good results with rendering plant effluent is less than direct chemical addition [51, 198].

2.2.3.4. Iron or Steel Anode

When an iron or steel anode is utilized in EC, Fe^{2+} is dissolved in the wastewater from Fe oxidation at the anode (standard potential $E^0 = 0.44$ V) as follows:

$$Fe \rightarrow Fe^{2+} + 2e^-$$
(2.1)

hydroxide ion and H_2 gas are generated at the cathode from the reaction ($E^0 = 0.83$ V):

$$2H_2O + 2e^- \rightarrow 2OH^- + H_2(g)$$
(2.2)

OH production from reaction (2.3) causes an increase in pH during electrolysis. Insoluble $Fe(OH)_2$ precipitates at $pH > 5.5$ and remains in equilibrium with Fe^{2+} up to pH 9.5 or with monomeric species such as $Fe(OH)^+$, $Fe(OH)_2$ and $Fe(OH)_3$ at higher pH values. The formation of insoluble $Fe(OH)_2$ can be written as

$$Fe^{2+} + 2OH^- \rightarrow Fe(OH)_2(s)$$
(2.3)

and the overall reaction for the electrolytic process from the sequence of reactions (2.1 – 2.3) is:

$$Fe + 2H_2O \rightarrow Fe(OH)_2(s) + H_2(g)$$
(2.4)

In the presence of O_2, dissolved Fe^{2+} is oxidized to insoluble $Fe(OH)_3$:

$$4Fe^{2+} + 10H_2O + O_2(g) \rightarrow 4Fe(OH)_3(s) + 8H^+ \tag{2.5}$$

and protons can be directly reduced to H_2 gas at the cathode:

$$8H^+ + 8e^- \rightarrow 4H_2(g) \tag{2.6}$$

The corresponding overall reaction obtained by combining reactions (2.1), (2.3) and (2.4) is:

$$Fe + H_2O + O_2(g) \rightarrow Fe(OH)_3 + H_2(g) \tag{2.7}$$

In acidic media of pH < 5.0, however, a greater quantity of Fe anode than that expected from Faraday law following reaction (2.7) is dissolved owing to the chemical attack of protons. $Fe(OH)_3$ coagulates from pH > 1.0, i.e., it is present in much stronger acidic media than $Fe(OH)_2$. Then, this precipitate can be in equilibrium with soluble monomeric species as Fe^{3+}, $Fe(OH)^{2+}$, $Fe(OH)^{3+}$, $Fe(OH)_3$ and $Fe(OH)_4^-$ as a function of the pH range. Among them, hydroxo-iron cations have a pronounced tendency to polymerize at pH 3.5–7.0 to give polymeric cations such as $Fe_2(OH)_2^{4+}$ and $Fe_2(OH)_4^{2+}$.

2.2.3.5. Factors Affecting Electrocoagulation

Electrocoagulation is efficient in removing suspended solids as well as emulsions [199-208]. However, several variables may affect the efficiency of the process. Important factors influencing the process are presented in this section.

2.2.3.5.1. Current Density

The supply of current to the electrocoagulation system determines the amount of Al^{3+} or Fe^{2+}, or any other ions released from the respective electrodes. For aluminum, the electrochemical equivalent mass is 335.6 mg(Ah)$^{-1}$. For iron, the value is 1,041 mg(Ah)$^{-1}$ [209, 210]. However, when too large current is used, there is a high chance of wasting electrical energy in heating up the water. More importantly, large current density would result in a significant decrease in current efficiency. In order for the electrocoagulation system to operate for a long period of time without maintenance, its current density is suggested to be 20–25 Am^{-2} unless there are measures taken for a periodical cleaning of the surface of electrodes [206]. The current density selection should be made with other operating parameters such as pH, temperature as well as flow rate to ensure a high current efficiency.

The current efficiency for aluminum electrode can be 120–140% while that for iron is around 100% [19].

The over 100% current efficiency for aluminum is attributed to the pitting corrosion effect especially when there are chlorine ions present [73]. The current efficiency depends on the current density as well as the types of the anions. Significantly enhanced current efficiency, up to 160%, was obtained when low frequency sound was applied to iron electrodes [178].

The quality of the treated water depends on the amount of ions produced (mg) or charge loading, the product of current and time (Ah) [19].

The operating current density or charge loading can be determined experimentally if there are not any reported values available. There is a critical charge loading required. Once the charge loading reaches the critical value, the effluent quality does not show significant improvement for further current increase [211].

2.2.3.5.2. Presence of Chloride Ion

Sodium chloride is usually employed to increase the conductivity of the water or wastewater to be treated.

Besides its ionic contribution in carrying the electric charge, it was found that chloride ions could significantly reduce the adverse effect of other anions such as HCO_3^-, SO_4^{2-} [73, 212]. The existence of the carbonate or sulfate ions would lead to the precipitation of Ca^{2+} or Mg^{2+} ions that forms an insulating layer on the surface of the electrodes. This insulating layer would sharply increase the potential between electrodes and result in a significant decrease in the current efficiency.

It is, therefore, recommended that among the 100% anions present, there should be 20% Cl^- to ensure a normal operation of electrocoagulation in water treatment [73].

The addition of NaCl would also lead to the decrease in power consumption because of the increase in conductivity.

2.2.3.5.3. Effect of pH

The effects of pH of water or wastewater on electrocoagulation are reflected by the current efficiency as well as the solubility of metal hydroxides [19]. When there are chloride ions present, the release of chlorine also would be affected. It is generally found that the aluminum current efficiencies are higher at either acidic or alkaline condition than at neutral. The

treatment performance depends on the nature of the pollutants with the best pollutant removal found near pH of 7. The power consumption is, however, higher at neutral pH due to the variation of conductivity. When conductivity is high, pH effect is not significant.

The effluent pH after electrocoagulation treatment would increase for acidic influent but decrease for alkaline influent. This is one of the advantages of this process. The increase of pH at acidic conditions was attributed to hydrogen evolution at the cathodes [159]. In fact, besides hydrogen evolution, the formation of $Al(OH)_3$ near the anode would release H^+ leading to decrease of pH. In addition, there is also oxygen evolution reaction leading to pH decrease. When there are chlorine ions, there are following chemical reactions taking place:

$$2Cl^- - 2e^- \rightarrow Cl_2 \tag{2.8}$$
$$Cl_2 + H_2O \rightarrow HOCl + Cl^- + H^+ \tag{2.9}$$
$$HOCl \rightarrow OCl^- + H^+ \tag{2.10}$$

Hence, the increase of pH due to hydrogen evolution is more or less compensated by the H^+ release reactions above. For the increase in pH at acidic influent, the increase of pH is believed to be due to CO_2 release from hydrogen bubbling, due to the formation of precipitates of other anions with Al^{3+}, and due to the shift of equilibrium towards left for the H^+ release reactions. As for the pH decrease at alkaline conditions, it can be the result of formation of hydroxide precipitates with other cations, the formation of $Al(OH)_4^-$.

$$Al(OH)_3 + OH^- \rightarrow Al(OH)_4^- \tag{2.12}$$

The pollutant removal efficiencies were found to be the maximum near neutral pH using aluminum electrode [19, 213-215].

When iron electrode was used in textile printing and dying wastewater treatment, alkaline influent was found to give better color as well as COD removal efficiency [216-218].

2.2.3.5.4. Temperature

Although electrocoagulation has been around for over 100 years, the effect of temperature on this technology was not very much investigated. The research from the former USSR demonstrates that the current efficiency (CE) of aluminum increases initially with temperature

until about 60 ^{0}C where a maximum CE was found; further increase in temperature results in a decrease of CE [219-229]. The increase of CE with temperature was attributed to the increased activity of destruction of the aluminum oxide film on the electrode surface. When the temperature is too high, there is a shrink of the large pores of the $Al(OH)_3$ gel resulting in more compact flocs that are more likely to deposit on the surface of the electrode. Similar to the current efficiency, the power consumption also gives a maximum at slightly lower value of temperature, 35 ^{0}C for treating oil-containing wastewater. This was explained by the opposite effects of temperature on current efficiency and the conductivity of the wastewater. Higher temperature provides a higher conductivity, hence a lower energy consumption.

2.2.3.6. Electrochemical Oxidation

Electrochemical oxidation or electro-oxidation (EO) is a conventional electrochemical procedure for removing recalcitrant organic pollutants from variety of wastewaters [230, 231]. This process consists of the following steps [35]:

(i) Direct electron transfer to the anode, which yields very poor performance in terms of degradation.

(ii) Generation electrolysis products from water discharge at the anode (such as physisorbed hydroxyl radical (OH)) or chemisorbed oxygen (in the lattice of a metal oxide (MO) anode). The action of these oxidizing species leads to a total or partial decomposition of recalcitrant organic species, accordingly. The existence of indirect or mediated oxidation with different heterogeneous species formed from water discharge allowed to propose two main approaches for the pollution abatement in wastewaters by EO [35]:

(i) The electrochemical conversion method, in which refractory organics are selectively transformed into biodegradable compounds, usually carboxylic acids, with chemisorbed oxygen.

(ii) The electrochemical combustion (or electrochemical incineration) method, where organics are completely mineralized, i.e., oxidized to CO_2 and inorganic ions, with physisorbed OH. This radical is the second strongest oxidant known after fluorine, with a high standard potential ($E0 = 2.80$ V) that ensures its fast reaction with most organics giving dehydrogenated or hydroxylated derivatives up to conversion into CO_2.

In both cases high cell potentials are applied for the simultaneous oxidation of pollutants and water, thus maintaining the anode activity. The use of low cell voltages avoiding O_2 evolution

frequently causes the loss of anode activity because some by-products formed from direct anodic oxidation can be adsorbed on its surface and hence, this procedure is not feasible in practical applications. It has also been suggested that the nature of the anode material affects both the selectivity and efficiency of the EO process.

At the anode, the color removal and COD reduction proceeds only in the presence of chloride [232]. Therefore, the color reduction in the yeast effluent being treated is, most probably, due to the reaction between the generated chlorine/hypochlorite and the organic species. The chlorine/hypochlorite oxidizes the COD and is then reduced to chloride ion.

The mechanisms of the oxidation of organic matter and the formation of hydroxyl radicals on an oxide anode are represented below [233]:

$$2Cl^- \rightarrow Cl_2 + 2e^- \tag{2.13}$$

$$4OH^- \rightarrow O_2 + 2H_2O + 4e^- \tag{2.14}$$

$$Cl_2 + H_2 \rightarrow OH^+ + Cl^- + HOCl \tag{2.15}$$

$$HOCl \rightarrow H^+ + OCl^- \tag{2.16}$$

$$\text{Organics} + 3OCl^- \rightarrow CO_2 + H_2O + 3Cl^- + \text{Product} \tag{2.17}$$
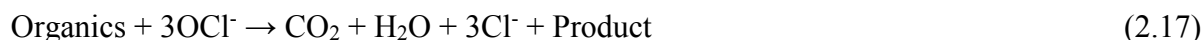
At the cathode surface a hydrogen peroxide is formed by reduction of atmospheric oxygen. The color removal and COD reduction depends upon the generation of H_2O_2, pH, presence of a catalyst. Also the degradation of organics depends upon the formation of $OH^\bullet$ radical and the nature of organic molecule. Therefore, the following reactions take place [233]:

$$2H_2O + 2e^- \rightarrow H_2 + 2OH^- \tag{2.18}$$

$$O_2 + 2H^+ + 2e^- \rightarrow H_2O_2 \tag{2.19}$$
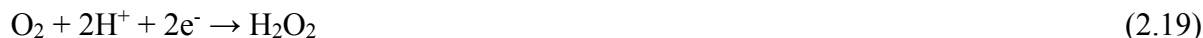
This demonstrates that the hydrogen peroxide is the product of the electron transfer to oxygen. However, if oxygen is reduced by a four-electron process, water is formed as the end product [232]:

$$O_2 + 4H^+ + 4e^- \rightarrow 2H_2O \tag{2.20}$$
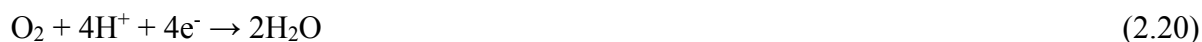
Hydrogen peroxide can reduce further to water:

$$H_2O_2 + 2H^+ + 2e^- \rightarrow 2H_2O \tag{2.21}$$

In alkaline media, the reaction stoichiometry is given by:

$$O_2 + H_2O + 2e^- \rightarrow OH{-} + HO_2^- \tag{2.22}$$

$$HO_2^- + H_2O + 2e^- \rightarrow 3OH^- \tag{2.23}$$
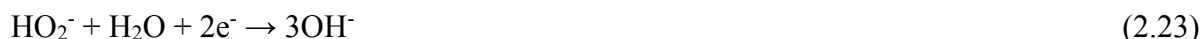
The per-hydroxyl ion (HO_2^-) is formed by hydrogen peroxide dissociation in base:

$$H_2O_2 \rightarrow H^+ + HO_2^- \tag{2.24}$$

The exact mechanisms of electrochemical oxidation are complex and not yet entirely understood.

2.2.3.7. Electroflotation

Electroflotation is the process of electrolytic gases generation resulting from electrolysis processes.

The use of gas as of a buoyant media to treat wastewater was first mentioned in a German patent in 1877 [175]. Based on this principle gases were generated by reaction of acids with suspended sulfides and carbonates. It was not until 1904 that production of gases by electrolysis for wastewater treatment was first referred to in a British patent [176].

Application of electrolytically generated gases in wastewater treatment has been given significant attention in 1960s [177, 234]. Currently, many researchers have focused on implementation of this process in wastewater treatment [235-239].

Bubble size distribution is of great importance in flotation as smaller bubbles cause an increase in interfacial area and, therefore, an increase in the efficiency of the separation process [240, 241].

Furthermore, the zeta potential of both particles and bubbles can be of great importance in separation using flotation. So, if the particles are negatively charged, bubbles with a slightly positive charge would achieve the optimum removal efficiency [241].

The particles to be removed in effluent treatment are normally less than about 20 μm and close to neutral buoyancy, and the concentration is also very dilute as low as 20 ppm [242].

Despite the long history of EF, the lack of ideal anodes with long service lives, low O_2 evolution overpotentials, and acceptable costs is still a serious problem that needs to be solved imminently [243].

2.2.3.8. Photoassisted Electrochemical Methods

Heterogeneous photocatalysis involves the conversion of organic pollutants to LMW species and even to their complete mineralization through the generation of highly reactive free radical oxidants. This treatment can be performed various types of lamps such as mercury lamps and a metal oxide as catalyst [244]. Titanium dioxide is one of the most useful catalysts showing several advantages compared to others, due to its high photochemical stability, low toxicity and reduced costs [245]. The heterogeneous photocatalysis systems are based on the absorption of photons with energy greater than 3.2 eV, which corresponds to wavelengths lower than ~ 390 nm, to initiate the electron excitation, related to a charge separation event (gap band), i.e. one electron promotion at the conductive band (e_{CB}^-) and a positive hole at valence band (h_{VB}^+), as represented in Equation 2.52 (bands formed by the evolvement of molecular orbitals of TiO_2 as it is packed into a lattice). The h_{VB}^+ can oxidize H_2O molecules and OH^- ions adsorbed at the particle surface (TiO_2) producing •OH radicals (Equations 2.25 and 2.26). The hydroxyl radical is a short-lived and extremely powerful agent in the organic substances oxidation, degrading and mineralizing them to CO_2, H_2O and inorganic ions.

$$TiO_2 + vh \rightarrow e_{CB}^- + h_{VB}^+ \tag{2.25}$$

$$H_2O(ads) + h_{VB}^+ \rightarrow \bullet OH + H^+ \tag{2.26}$$

$$OH(ads)^- + h_{VB}^+ \rightarrow \bullet OH \tag{2.27}$$

The presence of such dissolved oxygen is very important for heterogeneous photocatalysis because it can make the recombination process on TiO_2 (h_{VB}^+/e_{CB}^-) more difficult and maintain the electroneutrality of the TiO_2 particles. This condition makes the treatment practicable for industrial scale application in the environment conditions. However, according to the literature, for the TiO_2 photocatalysis process to succeed, the COD must be lower than 800 mgL^{-1}.

2.2.3.9. Electrochemically-assisted Membrane Separation

Commercial anaerobic membrane separation bioreactors have been used for treating municipal wastewater and process streams within many industries and provide a simple, reliable and small footprint alternative to conventional biological treatment methods, producing a high-quality effluent at high organic loading rates. Although biological treatment is the most preferred option, single step biological treatment is often insufficient to deal with high strength wastewater such as yeast manufacturing effluent. Co-treatment processes, however, may increase either kinetic degradation rate or degradability; enhance gas production, reactor performance, and significantly improve quality of effluent [73, 115, 126, 246-251]. Improving the rate can also allow process intensification, with the faster kinetics allowing for the same performance in a smaller digester, and thus decreasing hydraulic retention time (HRT). There is therefore an increased need to review and analyze the different options for co-treatment in terms of mechanism, costs, and performance.

Co-treatment may be implemented either before or after the anaerobic reactor. Both pre-treatment and post-treatment can be performed simultaneously as well.

A combined system consisted of EC pre-treatment followed by anaerobic digestion in anaerobic fixed-film bed reactor (AFFBR) has shown promising results for the treatment of high strength pharmaceutical wastewater [250]. EC as pre-treatment was successful in removing COD, BOD and color in the range of 22.8–24.2%, 34.50–36.70% and 69.2–70.3% respectively at pH 7.2 and current density between 40–120 Am^{-2}. The ratio of total volatile acids to alkalinity (TVA/ALK) remained always less than 0.8 throughout the study indicating the reactor stability and that there was no significant accumulation of volatile acids. This suggests that the reactor could be conveniently operated up to a loading of 4 $kgCODm^{-3}$ d and HRT of 2 days and achieve removal of 80% COD and 85.4% BOD. Operational problems such as clogging of the filter media were never observed during the entire period of reactor operation. The anaerobic co-digestion of glycerol together with the wastewater generated during biodiesel manufacturing, combined with EC pretreatment processes has also been investigated [251]. Following the EC pre-treatment, the mixture showed a high level of anaerobic biodegradability (around 100%), permitting a substantial quantity of methane to be obtained (310 mL CH_4g^{-1} $COD_{removed}$). TVA/ALK ratio values were always found to be lower than 0.30–0.40, thus indicating that the process operated without the risk of acidification.

Removal rates of COD and BOD after EC step (COD decreased by 6.25%, while soluble COD decreased by 13.60%) are in line with the other research [250].

Investigation on the remediation efficacy of chemical coagulation-flocculation and EC post-treatment of anaerobic biorefinery process water containing high concentrations of biorecalcitrant, colored organic melanoidins and polyphenols has shown similar removal efficiency [126]. Despite both methods removed up to 99% of the visible color (UV_{475}) and 80% of the COD, research suggests that EC has the potential to offer a simpler, more environmentally friendly post-treatment disposal of the coagulated sludge [73]. Energy consumption was also investigated for this type of wastewater by conducting batch experiments in the EC cells over the range of current efficiency from 2 to 100 Am^{-2} using aluminum electrodes. EC was shown to be capable of removing 90–98% of the color and 70–80% of the COD, irrespective of current density or EC reactor design [115].

Another study on simulated wastewater from an unbleached Kraft pulp mill suggests that the chemical coagulation process using ferric chloride and aluminum sulfate was a better alternative for treating the effluent from the upflow anaerobic sludge blanket (UASB) reactor than the EC process [247]. This study however lacks of economic analysis of the costs involved with the sludge disposal. Findings from experimental study on poultry manure wastewater clearly shows advantage of EC technology used as a post-treatment unit at initial pH of 5.0, a current density of 15 $mAcm^{-2}$, and an electrolysis time of 20 min [249]. Toxicity tests also proved that the EC effluent complied with regulations and did not cause any acute toxicity symptoms and showed 100% survival of tested fish even at the end of the additional 120 h of exposure.

Most of wastewater discharge guidelines are more stringent with regards to Fe than Al. However, despite Al current efficiency is high, thus reducing energy consumption, it is known to be prone to passivation [115].

The electrochemical treatment using dimensionally-stable Ti/Pt–IrO_2 electrode without pretreatment was investigated for the anaerobic digestion effluent from an energy plant using pig excreta and kitchen garbage as the substrate [248]. It was shown that ammonia could be completely removed in 5 h using an electric current of 1 A; however, 620 mgL^{-1} of ammonia still remained when an electric current of 0.5 A was used. In addition, total organic carbon, inorganic carbon, and turbidity removals reached 51.4, 73.8, and 95.5%, respectively. Hence,

it was affirmed that the direct treatment of the anaerobic digestion effluent with the Ti/Pt–IrO$_2$ electrode not only was possible but also could achieve good treatment efficiencies.

An integrated process involving a combination of pretreatment with electro-Fenton method, digestion in anaerobic filter and post-treatment stage was also investigated [246]. After electro-Fenton, the COD of the crude wastewater dropped to approximately 68% of the initial value, and the COD/BOD$_5$ ratio decreased from 5.84 before to 2.26 after. Pre-treatment resulted in decreasing the toxic effect of this wastewater on anaerobic digestion and in gradual increase in methanogenic activity. Inhibition on *V. fischeri* was reduced to 66.9% after pretreatment by electro-Fenton and to 45.2% in the anaerobic effluent. Yet, microtoxicity of Electro-Fenton anaerobic-treated stream remained high due to the residual VFA. For this purpose, EC post-treatment was carried out using the same electro-Fenton reactor, in order to remove the residual polyphenols, COD and color. Study shows that the electrolysis process was able to remove 70.55% of TSS, 91% of the color and 70% of the residual COD. Moreover, the analysis of ortho-diphenols showed a removal efficiency of 97% while polyphenolic compounds were not detected. The anaerobic process applied as post-treatment reached a loading rate of 10g COD l^{-1}d^{-1} without any apparent toxicity [246].

Based on the literature review, it can be concluded that little has been done to investigate electrokinetic pre- and posttreatment for membrane purification of molasses wastewater. Co-treatment based on combination of electrokinetics and anaerobic membrane separation bioreactor is interesting and promising alternative as it may ensure the compliance with regulatory requirements otherwise unattainable in many cases, and generate energy.

Analysis of 698 peer-reviewed articles published from 1970 to 2016 has been performed using Compendex and Engineering Village databases. Although, the best possible efforts have been made to provide consistent and reliable analysis, it should be pointed that a certain number of publications might not have been included in this research. Interestingly enough, this analysis demonstrates a constant increase of attention from scientific community towards application of electrokinetics in the wastewater treatment.

2.3. Anaerobic Treatment Systems

Anaerobic systems can be operated as single-phase or two-phase systems [128]. Single-phase systems involve only one reactor for the microorganisms to decompose organics, whereas two-phase systems separate the acidogenic and methanogenic processes. The majority of full-

scale applications and research effort has been concentrated on a single-stage anaerobic digestion (AD) within the mesophilic (25–45 ^{0}C) or thermophilic (45–65 ^{0}C) temperature ranges. However, some laboratory-scale experiments have also been carried out at psychrophilic temperature ranges, which has illustrated that low-temperature AD of effluents (< 20 ^{0}C) is also feasible, and can now be considered as an alternative to thermophilic or mesophilic AD [252-254].

Approximately 67% of the membrane reactors currently in operation have been completely-stirred reactors (CSTRs), 15% fixed-bed, or anaerobic filter (AF), 10% UASB or UASB hybrid, 7% fluidized bed (FB), and 2% septic tank (ST) [255].

This section begins by examining the normal operational and design considerations of contemporary anaerobic reactors currently employed in food wastewater treatment industry, followed by a thorough explanation of the reactor-specific features.

2.3.1. Completely-stirred Reactor

The most common reactor type used for anaerobic treatment of wastewaters is the completely-stirred reactor CSTR. The main drawback of this type, the fact that the active biomass is continuously washed out from the system leading to long retention times, has been overcome in a number of systems based on immobilization of the active biomass [256]. For dimensioning the size of CSTRs both the OLR and the HRT are the parameters applied most frequently in practice [257]. Stable CSTR operation requires HRTs of 15 to 3–0 days. However, reduction of the HRT in CSTRs risks washout of the active biomass, with consequent process failure [256].

Slow growth rate of syntrophic and methanogenic bacteria is another major problem of this type of reactor. 80–90% COD reduction within a period of 10–15 days have been reported [128].

2.3.2. Suspended Bed Reactor

UASB reactor and its hybrids is one of the most widely used reactors utilized for anaerobic treatment of various types of high-strength wastewaters [154, 258].

Membrane use in UASB hybrid reactor can reduce the capital cost of high-rate reactor designs, for example, by eliminating the need for a solids/liquid/gas separator in a UASB [255, 259].

In UASB reactors, the granulated bed acts as a filter for the SS, increasing residence time. Therefore, the UASB reactor may achieve high COD and SS removals at very short HRT making it perfect choice for highly-concentrated wastewaters treatment.

The UASBs are rarely applied for low-strength wastewater treatment with COD concentration lower than 1,500 to 2,000 mgL^{-1} as the development of granules in the UASB reactors is very difficult in this case scenario [256].

2.3.3. Fixed Bed Reactor

This type of reactor involves immobilization of microorganisms on an inert support in order to limit the loss of biomass from washout and enhance the microbial activity per unit of reactor volume.

Different types of substrate materials have been utilized for this purpose and different flush out methods have been developed to reduce the possibility of plugging. Generally, with upward directed flow, and HRT of few hours to days, and OLR of 0.4–27 kgm^{-3}d^{-1}, this reactor may run in recycle mode to permit dilution or control pH [256].

The AF reactor demonstrated higher efficiency compared to UASB reactor for molasses containing wastewater as it could be operated at higher OLR (19 kg COD m^{-3}d^{-1}) than UASB (12.5 kg COD m^{-3}d^{-1}) and higher COD removal efficiencies at OLR of 10 kg COD m^{-3}d^{-1} can be achieved [128].

The better performance of the fixed film reactor can be attributed to its ability to retain higher biomass at higher OLR.

2.3.4. Fluidized Bed Reactor

Fluidized bed reactors (FBR) contain an appropriate media such as sand, gravel or synthetic materials for bacterial attachment and growth. The reactors can be operated either in the upflow or down flow regimes. Bed expansion is managed by applying high inflow rates, usually by effluent or biogas recycling, and elevated height/diameter ratios. Studies on distillery effluent treatment in a down-flow fluidized bed system using ground perlite resulted in 75–95% reduction in COD content [154]. The utilization of a carrier material is advantageous in the down-flow configuration as it requires a lower fluidization velocity which prevents the possibility of clogging.

FB reactors can be operated as ultra-high-loaded anaerobic reactors (up to 30 kg COD $m^{-3}d^{-1}$) to treat effluents from the chemical, biochemical, and biotechnological industries [256].

2.3.5. Anaerobic Hybrid Reactor

The anaerobic hybrid reactor (AHR) was developed to combine the advantages of AF and UASB reactors. The performance of AHRs depends on contact of the wastewater with both the suspended growth in the sludge layer and the attached biofilm in the material matrix. Hence, AHR configurations generally have better operating characteristics than fully packed reactors. If an AHR has to maintain a high solid retention, a key factor to be attended to is having support materials to form a filter inside the reactor. The significance of the media is arguably comparable to granular sludge in an upflow-sludge bed-type reactor.

2.3.6. Anaerobic Membrane Bioreactor

Membranes provide exceptional suspended solids removal and complete biomass retention and can significantly improve biological treatment process, but their commercial application for anaerobic treatment has been limited [255].

Single-stage reactors demonstrate lower COD removal efficiency if compared to multistage CSTR reactor configurations regardless of substrate complexity. The CSTR configuration exposes the membrane to the reactor bulk MLSS, whereas UASB reactors expose the membrane only to the residual effluent TSS [260]. For instance, the effluent from a UASB AnMBR was 300-550 mg TSS L^{-1}, while the MLSS of a CSTR AnMBR reactor is commonly >10,000 mgL^{-1} [255]. Higher solids concentrations in the reactor usually lead to lower fluxes, however.

Membranes can also simplify the design of high-rate reactor designs, and thus, reduce the capital cost as solids/liquid/gas separator in a UASB is no longer a necessity.

Two-phase AnMBRs have also been studied. The membrane may be positioned after the first-phase acid reactor, second-phase methane reactor, or after both reactors [261-265]. The location of the membrane unit within a two-phase system can have a significant impact on performance. For a two-phase system, a COD removal efficiency of 52% observed when no membranes were used, compared to 78% when a membrane was used after the methane-phase reactor and 92% when a membrane was used after the acid-phase reactor. The effluent suspended solids concentration decreased from 361 mgL^{-1} in a conventional

configuration to 4 mgL^{-1} with a membrane placed after the acid-phase and to 0% after the second stage [255].

A two-phase AnMBR with a submerged membrane in the acidogenic reactor was tested to increase the sludge retention time SRT and to enhance the solid separation [266]. The pilot plant experiment was performed for wastewater treatment for one year. The membrane material consisted of mixed esters of cellulose of 0.5 μm pore size. COD removal efficiency was 80% and the methane production showed 0.32 m^{3}kg^{-1} COD removed for the submerged membrane system in the anaerobic digester. Authors noticed significant cake resistance of the membrane, and implemented preliminary filtration with a stainless-steel filter and air backwash in order to minimize the cake resistance. Among the tested preliminary filters, the 63 μm pore filter demonstrated the best performance. By cleaning with alkali first and acidic solutions later, the performance increased up to 89%.

The conventional acid reactor is a CSTR with a short HRT operated at low pH. However, this design is not suitable for degradation of every substrate. For example, the degradation of long-chain fatty acids, aromatics, and some proteins is not thermodynamically favourable in normal acid-phase reactors as the syntrophic relationships needed to consume reducing equivalents have been eliminated [255]. A membrane acid reactor, on the other hand, can separate the SRT from the HRT to allow the growth of hydrogenotrophic methanogens at a shorter HRT and low pH. As hydrogen reacts with reducing equivalents, conditions become favourable.

2.3.7. Two-stage Reactor

Conventional biogas processes described previously have long been focusing on methane production. However, a two-stage anaerobic process producing both hydrogen and methane from organic wastes have also been given attention recently as hydrogen is considered to be a clean and environmentally friendly gas, oxidized to pure water as a combustion product, thus, eliminating greenhouse gases emission [267].

A two-stage AD system is capable of optimizing the fermentation steps of each stage in separate reactors or compartments under different environmental conditions. It is clear that the microorganisms that work in the anaerobic digestion processes (hydrolytics, acetogenics and methanogenics have different physiological and nutrient requirements, levels of sensitivity to the environmental conditions and growing kinetics [268]. As a result, the overall efficiency and kinetics of the process are higher than those of conventional single-stage operations in

which all primary and secondary organisms and all associated biochemical reactions are conducted under the same identical environmental conditions in a single unit [150].

In the primary acid fermentation stage, the end-products of the reactions are formate, acetate, lactate, ethanol, carbon dioxide, hydrogen and C_3 and higher volatile fatty acids [128].

The secondary stage constitutes acetotrophic methane fermentation where the end products are methane and carbon dioxide.

Microbial community analysis in a two-stage process with molasses as a single source of carbon revealed that *Clostridium butyricum* was the major hydrogen-producing bacteria and methanogens consisted of hydrotrophic *Methanobacterium beijingense* and acetotrophic bacteria *Methanothrix soehngenii* [269]. Research demonstrated that in the first-stage process, hydrogen could be efficiently produced from diluted molasses with the highest production rate of 2.8 L-H_2 /L-reactor×d at the optimum HRT of 6 h. In the second-stage process, methane could be also produced from residual sugars and VFAs with a production rate of 1.48 L-CH_4 /L-reactor×d at the optimum HRT of 6 d, at which overall COD removal efficiency of the two-stage process was determined to be 79.8%.

Microbial community structures were also assessed in a two-stage anaerobic digestion system treating food waste-recycling wastewater [270]. The reactors were operated for 390 d at 10 different HRTs ranging from 25 to 4 d. Stable operation was achieved with the overall COD removal efficiency of 73.0-85.9% at organic loading rate of up to 35.6 g COD $L^{-1}d^{-1}$. The research also reports a shift in performance due to changes in microbial structure from *Aeriscardovia*- and *Lactobacillus amylovorus*-related species to one dominated by *Lactobacillus acetotolerans*- and *Lactobacillus kefiri*-like organisms at the first stage and from *Methanoculleus*- to Methanosarcina-like organisms in methanogenic stage.

2.4. Summary of Critical Review

As it was outlined throughout the literature review presented in this chapter, food industrial wastewater plants effluents pose environmental hazard to receiving treatment facilities mainly due to the contents of carbon, nitrogen and phosphorus, particularly if the receiving plant is not designed to perform tertiary nutrients removal. Industrial effluents also contain higher concentration of pollutants compared to domestic wastewater streams and often colored.

These nutrients are the major stimulants of eutrophication and they should be eliminated from the effluent before discharge into the aquatic environment. The ever stringent regulations

require the retrofitting of the existing wastewater facilities to meet the disposal requirements and reduce the concentration of the pollutants as much as possible. In conventional treatment plants, the removal of C, N, P and color requires several physico-chemical and biological reactors or zones within one reactor working simultaneously at different operating conditions to create the optimum environment for the removal of each individual pollutant. The anaerobic and sequential anaerobic/aerobic reactors are by far the most widely applied methods to remove carbon, through the oxidation of the organic materials by the microbial biomass.

Despite the fact that anaerobic treatment provides better results than aerobic process and remains primary method of treatment, research on application of MBRs for anaerobic industrial wastewater remains elusive.

Nitrogen removal involves sequential aerobic and anoxic biological reactions to achieve complete transformation of the influent ammonium into nitrogen gas. Carbon source is added into the anoxic reactor to sustain the heterotrophic denitrifies responsible for conversion of nitrate into gas, which is associated with high cost.

Phosphorus removal involves the recycling of biomass into anaerobic and aerobic zones in order to promote the accumulation of phosphate by micro-organisms in a process known as enhanced biological phosphorus removal (EBPR). Coagulants such as aluminum sulfate and ferric chloride are common phosphorus precipitants that are used as alternatives to the EBPR process or in cases where lower phosphorus concentrations are required.

Color removal from industrial effluents is also a significant challenge. No common solution is available, however oftentimes chemical treatment methods are used.

The elimination of all these pollutants in one single reactor is a challenging task.

In addition, membrane fouling prevents long-term high performance of membrane units in biological reactors and sludge dewatering/volume reduction significantly affect the cost of solids management. Therefore, reduction of specific resistance to filtration (SRF) may greatly enhance performance of membrane units and sludge volume index (SVI) can significantly lower cost of solid waste management. To decrease the amount of sludge generated in AnMBR applications several approaches have been taken, however majority of the conducted studies, describe chemical coagulation as a primary method. In this case, aluminum and iron salts for coagulation have been introduced into aqueous phase as described in the literature. However, the addition of chemicals to the MBR system usually leads to side effects the most common

of which are increasing the amount of sludge, producing by-products, poor quality of bio solids.

Therefore, a novel advanced wastewater treatment system for industrial wastewater treatment capable to provide an innovative hybrid wastewater treatment method by integrating anaerobic biological process, membrane treatment and electrochemical phenomena into a single compact unit is required.

Therefore, research and development of the novel system providing the favorable interactions between three main processes: physico-chemical, biological and electrokinetic phenomena are required to address these issues.

2.5. Hypothesis and Research Objectives

In the previous sections, it was discussed that many food industries fail to produce effluents with the quality that would meet standards imposed by local and federal governments. Therefore, there is a need for a novel and more efficient method of the industrial wastewater treatment.

In order to overcome many common problems found in present industrial wastewater treatment technologies, a new technology was proposed in this research. The novel system combines membrane reactor, anaerobic biological treatment and electrokinetic processes in a single compact unit suitable for treatment of recalcitrant industrial wastewaters.

2.5.1. Hypothesis

The application of electrokinetics in combination with aerobic membrane bioreactors has already demonstrated promising results for domestic wastewater treatment and could be considered as a feasible method of advanced treatment [134, 135]. Therefore, the central research hypothesis was that the electrokinetic phenomena could enhance removal of carbon, nutrients and color from high-strength wastewaters sourced from food industry in anaerobic reactor equipped with a hollow fiber membrane and metal electrodes. The detailed objectives of this research are presented in the following sections.

2.5.2. Research Objectives

As a prerequisite, a sufficient understanding of how electrochemical methods can enhance anaerobic membrane wastewater treatment process suitable for industrial applications was

required. Thus, the central research objective was to develop a novel electro-anaerobic membrane bioreactor (EAnMBR) and investigate removal paths and mechanisms in the new system under electric potential applied.

2.5.3. Objectives with Respect to Major Pollutants

Based on the comprehensive study of literature, the molasses-containing wastewater was selected for the research as it contains extremely high concentrations of carbonaceous, nitrogenous components and phosphorous, and is dark-brown colored. Therefore, the new system must be capable to significantly reduce the concentration of pollutants and produce an effluent of excellent quality.

2.5.3.1. Carbon

Effluents arising from food industrial processes, i.e. molasses fermentation are not only highly colored, but also carry a large organic load. Existing anaerobic/aerobic biological treatment methods are relatively effective for the BOD reduction, however unable to remove the COD from this type of wastewater.

The objective of this research was to study how various operating parameters such as voltage gradient, current density and electrical exposure mode (time-On: time-Off) can increase COD removal efficiency.

2.5.3.2. Nitrogen

Nitrogen and its derivatives removal from wastewater are a major concern for food producing industries as many municipal wastewater treatment plants limit accepted concentrations for these compounds (e.g. TKN). Protein-containing compounds have also been implicated with polysaccharides as an important component of organic foulant on membranes in wastewater treatment.

Therefore, the objective of the thesis was to determine how various operating parameters such as voltage gradient, current density and electrical exposure mode (time-On: time-Off) affect nitrogenous compounds removal efficiency.

2.5.3.3. Phosphorous

Phosphorous removal is important for wastewater discharge quality and maintenance of membrane permeability.

The objective of the study was to analyze how various operating parameters: voltage gradient, current density and electrical exposure mode (time-On: time-Off) can increase phosphorous removal efficiency.

2.5.3.4. Color-forming Substances

Highly-dispersed and colored colloidal systems containing melanoidins, lignins, waxes, and caramels remain challenge for conventional methods of treatment.

The investigation was focused on electrokinetically enhanced improvement of the color removal to an acceptable level and to maximize discoloration in anaerobic conditions.

2.5.4. Objectives with Respect to Operating Parameters

Operating parameters play a major role in successful treatment. Therefore, the major objectives related to operation parameters were to define operation complexity with respect to interaction and coexistence of a number of electrochemical, biological and separation processes and to define the most affecting parameters where interactions take place that can enhance effluent characteristics.

3. Materials and Research Methods

This section presents procedures applied to the experimental phase of the thesis.

3.1. Materials

Anaerobic inoculate from anaerobic digester in wastewater treatment plant in Saint Hyacinth as well as two wastewaters (synthetic and industrial) were used. The samples were stored in polyethylene containers and refrigerated prior being used in the study.

3.1.1. Anaerobic biomass

Anaerobic sludge acquired from a local plant was stored at 4 ^{0}C for no longer than a month to avoid deterioration of properties due to the prolonged storage prior seeding. The biomass was incubated prior inoculation at the temperature of 35 ^{0}C before seeding.

3.1.2. Synthetic Wastewater Characterization

The synthetic wastewater studied in this research was designed to simulate industrial wastewater with high content of nutrients, organic carbon and dissolved solids based on C:N:P ratio 110:5:1. Table 3.1 presents the values of the key characteristics of the synthetic wastewater.

Table 3.1. Composition of the synthetic wastewater

Component	Chemical Formula	Molecular Weight, gmol^{-1}	Concentration, mgL^{-1}
Glucose	$C_6H_{12}O_6$	180.00	3,230.00
Peptone	-	-	252.00
Yeast Extract	-	-	300.00
Sodium Acetate	CH_3COONa	82.03	287.00
Ammonium Sulphate	$(NH_4)_2SO_4$	132.10	940.00
Potassium Phosphate	KH_2PO_4	136.10	50.00
Monopotassium Phosphate	K_2HPO_4	136.09	100.00

Magnesium Sulphate	$MgSO_4 \cdot 7H_2O$	169.02	40.00
Sodium Bicarbonate	$NaHCO_3$	83.00	25.00
Potassium Chloride	KCl	74.55	25.00
Manganese Sulfate Monohydrate	$MnSO_4 \cdot 2H_2O$	169.02	4.50
Calcium Chloride	$CaCl_2 \cdot 2H_2O$	147.00	4.00
Iron (III) Chloride Hexahydrate	$FeCl_3 \cdot 6H_2O$	270.29	0.40

3.1.3. Industrial Wastewater Characterization

The process wastewater was obtained from a discharge outlet of effluent prior treatment facility attached to a local industrial yeast processing plant. Table 3.2 presents the values of the key characteristics of the raw wastewater samples.

Table 3.2. Composition of the industrial wastewater

Parameter	Value
pH	5.2 ± 0.2
Volatile Acids as HOAc, mgL^{-1}	$8,740 \pm 2.0$
N Total, mgL^{-1}	$2,300 \pm 4.0$
P Total, mgL^{-1}	150 ± 2.0
COD, mgL^{-1}	$53,300 \pm 1,000$
SO$_4$-S, mgL^{-1}	$8,350 \pm 8.0$
Color Pt-Co, mgL^{-1}	$20,000 \pm 10$
TDS, mgL^{-1}	$7,200 \pm 5.0$
Redox Potential, mV	-81 ± 1.0
Conductivity, µSm^{-1}	346 ± 1.0

At the time of sampling, the plant was not able to reach the allowable limits in effluent due to its high carbon and nitrogen contents. The wastewater had an excessive dark-brown color.

3.2. Research Methods

Different physiochemical and biochemical parameters were analyzed in this research to assess the performance of the EAnMBR system.

3.2.1. Data Collection Process

The following measurements were performed during the study: COD, VFA, N, P, changes of current density, monitoring pH, EC, floc zeta potential, TSS, VSS, SVI, and color.

In batch experiments, liquid samples were withdrawn every day. In the continuous flow experiments, samples were taken twice per week from the treated effluent storage tank for analysis with a 10-ml plastic syringe (Fisher Scientific Ltd).

All samples were filtered with 0.45 µm syringe filters before analysis to remove all non-dissolved solids, which could affect the analytical techniques. All samples were diluted to concentrations within the range measured.

3.2.2. Analytical Techniques

Techniques provided coverage of the experimental phase of the research and used to assess qualitatively and quantitatively the composition of the wastewater are presented in the following sections. Summary of measured parameters and analytical methods are summarized in Table 3.3.

Table 3.3. Analytical Methods

Parameter	Method(s)
COD	method 8000, Hach, approved by EPA USA
VFAs (CH$_3$COOH)	Hach Method 10240 approved by EPA USA
Total Nitrogen	Hach Method 10208 approved by EPA
Ammonia Nitrogen (NH$_3$-N)	Hach Method 10208 approved by EPA USA
Nitrate (NO$_3$-N)	Hach Method 8192 approved by EPA USA
Nitrite (NO$_2$-N)	Hach Method 8039 approved by EPA USA
Phosphorous as TP	Hach Method 10210 approved by EPA USA

Sulfur as (SO_4^{2-})	Hach Method 10227 approved by EPA USA
TSS, VSS, SVI	According to Standard Methods
Specific Resistance to Filtration (SRF)	Vacuum filtration apparatus (Buchner funnel test)
Zeta Potential	Zeta meter analyzer (Zeta meter 3.0$^+$, USA)
Dissolved Oxygen (DO)	DO meter (YSI, Model 52, USA)
pH, ORP, Electrical Conductivity	Denver Instrument, pH meter model 215, USA
Particles Size Distribution (PSD)	Partica LA-950V2 laser diffraction particle size analysis system Horiba, USA
Color	Color disc/APHA Platinum method using Cobalt Standard Hach Color Test

3.2.2.1. Chemical Oxygen Demand

The COD samples were centrifuged at 4000 rpm for 20 minutes prior measurements were conducted using TNT plus vials (method 8000, Hach, approved by EPA USA).

According to the method, the concentration of COD (mgL^{-1}) is defined as the concentration of consumed O_2 (mgL^{-1}) to oxidize the organic matter in a sample. In this method, the samples were digested with potassium dichromate, a strong oxidizing agent, in the reactor for two hours. The organic compounds in the sample became oxidized and dichromate ion became reduced to green chromic ion. After samples were cooled down to the room temperature, their absorbance was read by a UV-VIS spectrophotometer.

3.2.2.2. Volatile Fatty Acids

For determination of Volatile Acids by the Esterification method, Hach Method 10240 approved by EPA USA using TNTplus™ vials and results were provided as HOAc (acetate), mgL^{-1}.

Volatile fatty acids in the sample react with diols in acidic environment and form fatty acid esters. The esters then reduced by Fe^{3+} to form a red-colored complex. The concentration of VFA was measured based on photometric method and the color of the formed complex. A

wastewater sample of 0.05 L volume was centrifuged at 4000 rpm for 20 minutes prior measurements.

3.2.2.3. Nitrogen Fractionation

All measurements of Nitrogen species are presented in mgL^{-1}. For determination of Total Nitrogen (TN, N_{tot}) in this research, the Persulfate Digestion method was selected, using TNTplus™ vials (Hach Method 10208 approved by EPA). TN is the sum of Total Kjeldahl Number (TKN), NO_2 and NO_3. It can also be calculated as $NH_4^+ + NO_2^- + NO_3^- +$ organic-Nitrogen.

Inorganic and organic nitrogen compounds are digested with peroxodisulfate and are oxidized to nitrate. The nitrate ions react with 2,6-dimethylphenol in a solution of sulfuric and phosphoric acid to form a nitrophenol. Inorganic nitrogen is the sum of $NH_4^+ + NO_2^- + NO_3^-$.

For determination of ammonia as NH_3–N, the Salicylate Digestion method was selected, using TNTplus™ vials (Hach Method 10031 approved by EPA). Ammonium ions react at pH 12.6 with hypochlorite ions and salicylate ions in the presence of sodium nitroprusside as a catalyst to form indophenol. The amount of color formed is directly proportional to the ammonia nitrogen present in the sample. The measurement wavelength is 690 μm.

Nitrate and Nitrite were measured as NO_3 –N using TNTplus™ vials (Hach Method 8192 and 8039 respectively that was approved by EPA). In this method, Cadmium metal reduces nitrate in the sample to nitrite. The nitrite ion reacts in an acidic medium with sulfanilic acid to form an intermediate diazonium salt. The salt couples with gentisic acid to form an amber colored solution. The measurement wavelength is 500 μm for spectrophotometers.

Total Kjeldahl Number (TKN) is the sum of $NH_4 +$ organic-Nitrogen. TKN was measured in accordance with the Hatch Method 10242 approved by EPA using TNTplus™ vials. TKN is the sum of organic nitrogen and ammonia. In the simplified TKN method, inorganic and organic nitrogen are oxidized to nitrate by digestion with peroxodisulfate. The nitrate ions react with 2,6-dimethylphenol in a solution of sulfuric and phosphoric acid to form a nitrophenol. Oxidized forms of nitrogen in the original sample (nitrite + nitrate due to sample preservation) are determined in the second test vial and then subtracted, which results in TKN. Dissolved Organic Nitrogen (DON) was calculated as the difference between filtered with 0.45 μm Millipore express filters TKN and NH_4–N nitrogen.

3.2.2.4. Phosphorous

Ortho- and Total Phosphorus (phosphate) in the research was measured by the Ascorbic Acid method, Hach Method 10210 (total) using TNTplus™ vials.

Ammonium molybdate and antimony potassium tartrate react in an acid medium with dilute solutions of phosphorus to form an antimony-phospho-molybdate complex. This complex is reduced to an intensely blue-colored complex by ascorbic acid. The color is proportional to the phosphorus concentration and is measured at 650 or 880±5 µm.

3.2.2.5. Sulfur

In this research sulfur was measured as SO_4^{2-} in mgL^{-1} by the Turbidimetric method, Hach Method 10227 using TNTplus™ vials. In this method, sulfate ions in the sample react with barium chloride in aqueous solution and form a precipitate of barium sulfate. The resulting turbidity is measured photometrically at 880 µm.

3.2.2.6. Total Suspended Solids and Volatile Suspended Solids

The total suspended solids (TSS) data is critical in determining the operational behavior of the treatment system and its efficiency. Volatile suspended solids data (VSS) is critical in determining the operational behavior and biological concentration in the system. The tests were conducted according to the Standard Methods as described in Appendix A on a stand depicted on Figure A.1.

3.2.2.7. Sludge Volume Index

SVI was used to monitor settling characteristics of sludge according to standard method 2710D "The determination of sludge volume index" [271].

The SVI is the volume in milliliters occupied by 1 gram of a suspension after 30 minutes of settling. The SVI in this study was monitored by the settled volume method. Equipment required for this test included a one liter graduated cylinder, latex gloves and safety glasses. The sludge sample was homogenized before being placed in the cylinder. The volume of the sludge was recorded at 30 minutes as the settled volume. The SVI was calculated as per equation 3.1:

$$\text{SVI}, (\text{mgg}^{-1}) = \frac{\left(\frac{\text{mL}}{\text{L}}\right) \times 1000\text{mg}}{\text{Suspended Solids} \ (\text{mgL}^{-1}) \times \text{g}}$$ (3.1)

3.2.2.8. Electrical conductivity, pH and Dissolved Oxygen

Electrical conductivity (EC), pH and dissolved oxygen were measured using an HQ30d single-input multi-parameter meter (Hach, USA). Current density was calculated as current (A) passing between the electrodes divided by the anode surface area (m^2).

3.2.2.9. Particle Size Distribution

The particle size distribution (PSD) of the aggregates were determined with Partica LA-950V2 laser diffraction particle size analysis system (Horiba, USA). Measurements were conducted on volume distribution. 0.05 to 0.10 L of the activated sludge was taken by a syringe with 2 mm opening in order to preserve particles aggregates. The sample was then stirred carefully in the syringe before placing into the instrument.

A wastewater sample of 50 ml volume was centrifuged at 4000 rpm for 20 minutes. The supernatant was separated and mixed with a few drops of the activated sludge. The mixture was injected into the electrical cell of zeta meter 3.0+ (Zeta -Meter Inc., USA) for floc zeta potential measurement. The final value was given as the average of 10 readings.

3.2.2.10. Current Density

Charge carrying between the electrodes depends on the ionic conductance and surface conductance. Ionic conductance refers to carrying charge by the soluble free ions in the bulk solution, while surface conductance is carried out by the ions in the electric double layer at the solid liquid interface [136]. Therefore, the current passing between the two electrodes is proportional to the concentration of soluble ions, the concentration of suspended solids and the voltage gradient. These three main factors collectively determine the final value of the current generated. The same value of voltage gradient may generate different currents passing through the reactor based on the concentration of soluble salts and MLSS. However, the magnitude of electrical current between the electrodes is the factor affecting the major electrokinetic processes. Based on that, current density was used in this research as a basis to make comparisons with the changes of effluent quality. The batch bioreactors occasionally

were replenished with wastewater in order to maintain the same current density during the experiments.

3.2.2.11. Zeta Potential

Zeta potential was measured daily in the supernatant after settling 50 ml of the mixed liquor for 30 min. A wastewater sample of 50 ml volume was then centrifuged at 4000 rpm for 20 minutes. The supernatant was separated and mixed with a few drops of the activated sludge. The mixture was injected into the electrical cell of zeta meter 3.0+ (Zeta -Meter Inc., USA) for floc zeta potential measurement. The final value was given as the average of 10 readings.

3.2.2.12. Color

The true color (after filtration, 0.45 µm) of the samples was measured by in Pt-Co units by Color disc/APHA Platinum method using Cobalt Standard Hach Color Test Kit. A visual comparison method (color matching) was employed to determine color concentration. The tubes were rinsed with deionized water before and after the test. A wastewater sample (diluted if necessary) was added to a vial and the kit was placed in front of a halogen lamp. The wheel then was rotated until the sample matched a reference color and concentration was displayed in a window. If the color match was between two segments, the value that is in the middle of the two segments was used.

3.2.3. Statistical Analysis

Several different processes take place simultaneously in waste-water treatment process leading to the difficulty in understanding the whole system. Moreover, the nature of influents is constantly changing over time, resulting in an important variability of the system. Application of statistical methods allowed assessing treated effluent quality parameters with a certain degree of confidence. The multiple monitored parameters were subjected to analysis by the following methods.

As relationships between random error, standard deviation, confidence interval and number of measurements exist, it was necessary to take a sufficient number of samples. Therefore, samples were measured in triplicate from each sampling point.

The acquired wastewater characteristics were calculated as arithmetic mean of the values in the database. The arithmetic mean was preferred over the median, as it allowed to correct

outliers and skewed distributions. While numerical information was presented in tabular form, it was far more effective to visualize the data in graphic form. For this research histogram and scatter charts were used for data representation.

3.2.4. Experimental Methodology

Field testing is indispensable for garnering information regarding the processes, however, understanding of the fundamental mechanisms of successful anaerobic treatment of yeast wastewater containing recalcitrant compounds remains elusive in the field. No studies have ever investigated electro-anaerobic treatment of such a wastewater; therefore laboratory experiments were designed to simulate the essential features of the future functional field systems. The experimental part of the research was performed in 4 Phases.

The variable used for the optimization was the current density. The flowchart of the methodological approach is depicted on Figure 3.1. The Phase I experiments were designed for a batch operation to study the relationship between the electrical operating parameters and physical-chemical effluent properties over the operating period of 120 h. A preliminary experimental phase was conducted on a series of small-scale electrobioreactors (without the operation of the membrane module) to identify the best electrokinetic conditions so as not to inhibit the biological activity in the EAnMBR system in the later Phases of the research. These electrical operating parameters included voltage gradient, current density, and exposure time to electrical field (time-On: time-Off), i.e. mode of operation. The following effluent quality parameters were measured: N_{tot}, COD, P_{tot}, color, pH, Zeta potential (ζ-potential), oxidation-reduction potential, TDS, and conductivity. The main objective of the Phase II was designing a novel system and to determine its efficiency for wastewater treatment in continuous flow mode based on the outcome from Phase I. The Phase II was conducted in 2 Stages. The Stage I extended from day 1 to day 30 without applying DC in order to simulate an AnMBR for a reference efficiency baseline.

Phase I
(Day 1-5)

Preliminary Design and Operation in Batch Mode

Objective:

To determine optimal electrical operating parameters
for Phase II and Phase III

Assessment Metrics:

Electrical	COD	ε-potential
N_{tot}	Color	Conductivity
P_{tot}	ζ-potential	TDS

Phase II
(Day 1-60)

Synthetic Wastewater Continuous Flow

Objective:

To design EAnMBR
To determine efficiency of synthetic wastewater

Stage I (Day 1-30)	**Stage II** (Day 31-60)

Assessment Metrics:

VFAs	COD	TSS
N species	Color	Conductivity
P	VSS	SVI

Figure 3.1. Flow chart of the methodological approach

Stage II lasted from day 31 to day 60 when operating as EAnMBR with DC applied. Both stages were conducted on a synthetic wastewater. For both stages, the following measurements were performed: COD, VFAs, and nitrogen species, namely N_{tot}, TKN, ammonia, nitrate-nitrite, DON, P, S, TSS, VSS, SVI, and pH.

The primary goal of the Phase III of this study was to evaluate the performance of the novel system for industrial wastewater treatment in continuous flow mode. The Phase III was conducted in two Stages. The Stage I of Phase III extended from day 1 to day 60 without applying DC in order to simulate a conventional AnMBR, and Stage II lasted from day 61 to day 120 when operating as EAnMBR with electrical current applied. Both stages were conducted on an industrial wastewater. For both stages the measurements similar to those in Phase II were performed.

The research objective of the Phase IV was an optimization of operating parameters of EAnMBR for specific removal of COD, nitrogen, phosphorus and color from the influent industrial wastewater by surface response method.

3.2.4.1. Preliminary Design and Operation

As it was stated in the hypothesis, the electrical operating parameters are paramount for a successful treatment process of molasses containing industrial wastewater. The primary aim of this stage was to investigate and to optimize the effects of pre-treatment and operating parameters such as current density, pH, and colloids stability on the performance of electro-anaerobic reactor in terms of COD, nitrogen, phosphorous and color reduction and exposure time of microbial community to the electric field. Phase 1 experiments were conducted to study the relationship between the electrical operating parameters and physical-chemical effluent properties over the operating period of 120 h.

3.2.4.1.1. Phase I: Batch Experimental Setup

Experimental setup of Phase I consisted of a series of 1-L batch electrokinetic bioreactors, control reactor for reference and supporting system which included the following components (Fig. 3.2):

• Electric power supply
• Power Controller
• Electro-Anaerobic Reactors (EA Reactors)

• Control Anaerobic Reactor

• Gas Release System

The power supplies were connected to the vessels by the shortest possible insulated cables with appropriate current ratings, terminated with bolt-on crimp-lugs.
Electrodes were affixed to a Plexiglas frame in order to keep them in a vertical position. The space between the electrodes was adjusted accordingly.

The porous (40% opening) flat aluminum anode and stainless steel mesh cathode were chosen based on previous research [272].
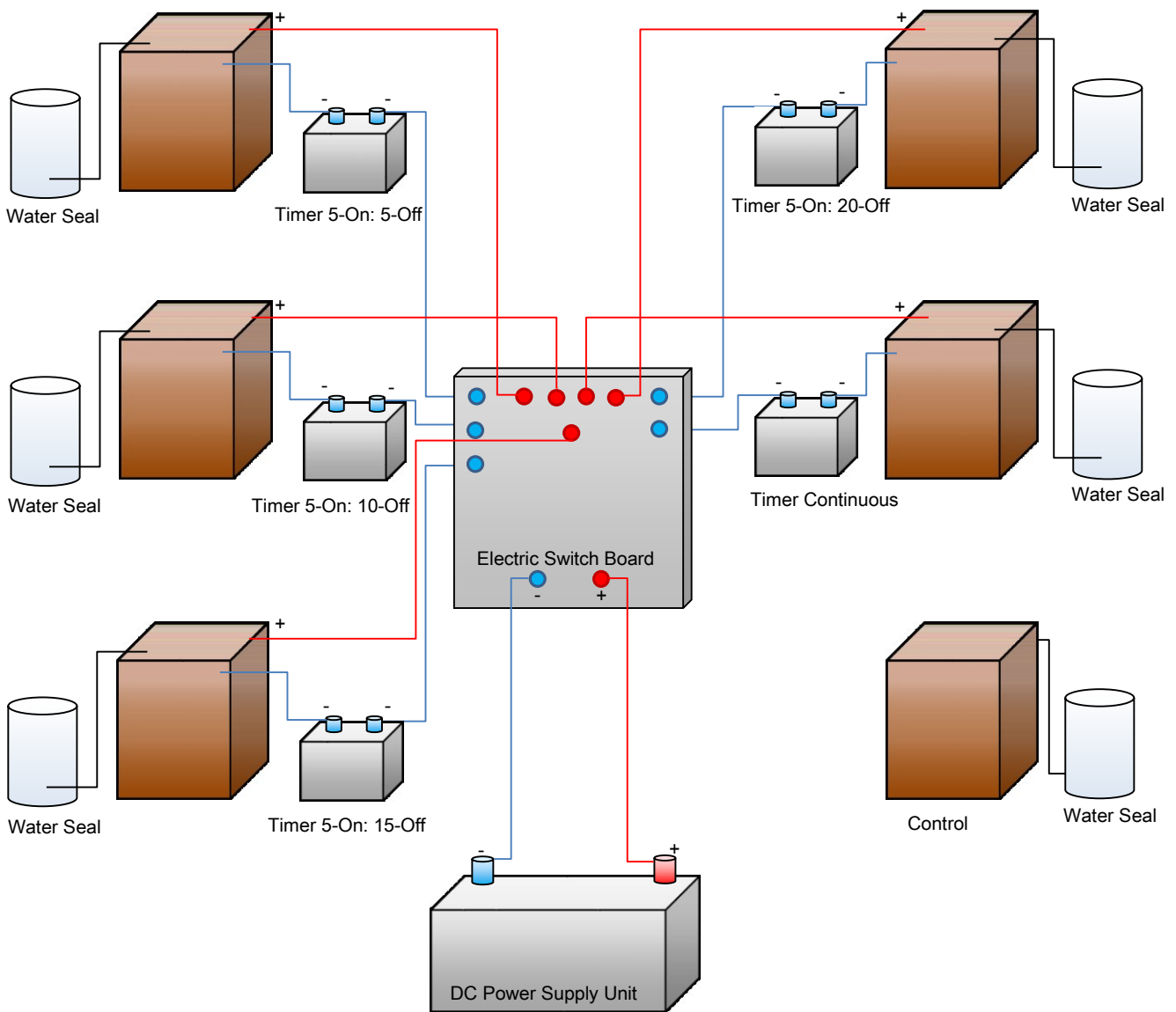
Figure 3.2 Phase I Experimental System Setup

The reactors design simulated the electrokinetic anaerobic membrane bioreactor without membrane module. Anaerobic sludge was stored at 4 ^{0}C for no longer than a month to avoid deterioration of sludge properties due to the prolonged storage. Two voltage gradients were selected based on 1.0, and 1.5 Vcm-1 to provide different current densities between the electrodes. The voltage gradients were selected based on the results of a previous study [136]. Five different electrical exposure modes (5-On: 5-Off, 5-On: 10-Off, 5- ON: 15-Off, 5-On: 20-Off and continuous-On) were selected to run the bioreactors for a minimum of 120 h for testing electro-kinetic processes and to project the long term impact of DC field on the anaerobic microbial community. Each run consisted of five anaerobic electrobioreactors and one control anaerobic bioreactor operated side by side as a control.

All the reactors were monitored during the experiments in order to maintain the anaerobic condition within the vessels.

DC power supply (TES 6230) and all electrodes were connected through a central distribution panel. A switch-timer was connected to the circuit between the distributor and the cathode in order to control the sludge exposure time to DC. Current density was calculated as follows:

Current density (Am^{-2}) = Electrical current (A) / Effective surface area of electrode (m^2)

Three current densities were selected for this experiment, 12, 15 and 20 Am^{-2}. The former value of current density was chosen based on the results of a previous research as it improved effluent properties of interest [136]. The summary of the parameters selected for the experiments in Phase I such as current densities and the exposure modes are represented in (Table 3.4). The range of values was selected to test the system at various working conditions that could be adopted in later phases of the study. A control reactor (E7) without electrical current applied was run side by side for comparison. The design of the system permitted to connect and run six reactors simultaneously. Each run was operated for a period of 120 hours. No synthetic water was added into the reactors, the current density was maintained constant by adjusting the voltage. In this stage, the effluent quality parameters in terms of N, P, COD, Color removal efficiency, pH, Redox Potential and Conductivity were measured and analyzed as indicators.

Table 3.4. Operating conditions of the batch electrocoagulation anaerobic reactors

Experiment №	Duration, h	Current Density, Am^{-2}	Voltage, Vcm^{-1}	Exposure Time, min
E1	120	12	1.0	5'-on/5'-off
				5'-on/10'-off
				5'-on/15'-off
				5'-on/20'-off
				continuous -on
E2	120	12	1.5	5'-on/5'-off
				5'-on/10'-off
				5'-on/15'-off
				5'-on/20'-off
				continuous -on
E3	120	15	1.0	5'-on/5'-off
				5'-on/10'-off
				5'-on/15'-off
				5'-on/20'-off
				continuous -on
E4	120	15	1.5	5'-on/5'-off
				5'-on/10'-off
				5'-on/15'-off
				5'-on/20'-off
				continuous -on
E5	120	20	1.0	5'-on/5'-off
				5'-on/10'-off
				5'-on/15'-off
				5'-on/20'-off
				continuous -on
E6	120	20	1.5	5'-on/5'-off
				5'-on/10'-off
				5'-on/15'-off
				5'-on/20'-off
				continuous -on
E7	120	N/A	N/A	N/A

3.2.4.2. AnMBR Design and Operational Considerations

Understanding of the fundamental mechanisms of successful anaerobic treatment of molasses wastewater containing recalcitrant compounds remains elusive in the field. No studies have ever investigated electro-anaerobic treatment of such a wastewater; therefore laboratory experiments were designed to simulate the essential features of the novel functional system. Based on the research conducted in batch experiments described in the previous chapter, the main focus of the next step was development a system incorporating membrane physical and anaerobic biological treatment methods in a compact AnMBR system in order to provide quality parameters of effluent containing highly-colored and recalcitrant components.

In the following sections, the design considerations and criteria for development of the AnMBR system are discussed in details.

3.2.4.2.1. AnMBR Design Considerations

Design of the AnMBR system is important for the uniform phase distribution inside the system and, thus, increasing the treatment performance. The design considerations for the reactor included the following:

a) Location of the membrane module in the bioreactor must not affect the uniform aqueous phase motion;

b) Homogenous mixing conditions and distribution should promote flocs formation in the aqueous phase;

c) Assembly in the system design should not interfere with the wastewater entering the reactor and directing toward the membrane module;

d) Gases forming by microorganisms' activity and electrokinetic processes must freely leave the system through water seals in order to avoid accumulation in the upper part of the AnMBR and- to prevent air entering the system.

e) The system must be properly sealed in order to maintain anaerobic conditions.

3.2.4.2.2. AnMBR Operational Considerations

Operation condition considerations included the following:

a) The AnMBR design and configuration should incorporate the requirements for simultaneous anaerobic biodegradation and physical separation processes taking place inside the bioreactor;

b) Design took into consideration the following fluid motions in the AnMBR: wastewater supply, movement of gases, formation of colloids and their settling, fluid movement toward the membrane module;

To achieve the overall objectives of the designed configuration, the following major parameters were controlled and optimized during the AnMBR operation: hydraulic retention time (HRT), and sludge retention time (SRT). The strategy of this study was based on operating the AnMBR at constant flux and long SRT.

3.2.4.2.3. AnMBR Design

To meet the requirements, the MBR system was designed according to the following criteria:

a) A cylindrical ultrafiltration Zeeweed-1 (GE, Canada) membrane module with 0.04 µm pore size and 0.047 m^2 surface area was placed vertically in the center of a completely sealed 20 L polyethylene encasing and operated under flux of 12 $Lm^{-2}min$. Lifetime of the membrane is 6-8 years [273, 274];

b) A uniform distance between the membrane module and the reactor shell were maintained in order to minimize the potential detrimental effect of an acidic/oxidation zone on microbial organisms;

c) Two baffles were installed inside to keep the distance and allowed upward movement of biologically-produced gases which facilitated removal of microbial flocs forming on the membrane surface and downward movement of flocs aggregates. These baffles would serve as electrodes at the later stages of the research;

d) Transfer pumps were connected to the shell in order to supply the wastewater and to the membrane outlet to extract the aqueous phase of the sludge liquor at a constant flow rate; the system includes the following components (Figure 3.4):

- Anaerobic Reactor
- Heated Blanket
- Temperature Sensor
- Temperature Control Unit
- Membrane Module
- Influent Transfer Pump
- Effluent Transfer Pump
- Water Seals
- Wastewater Storage Tank
- Treated Effluent Storage Tank
- Sludge Disposal Storage Tank
- Sampling Point (SP)
- Transmembrane Pressure (TMP) Meter

Figure 3.4. Simplified design configuration of the AnMBR system

The proposed design of the AnMBR system broadly divides the hybrid anaerobic reactor into two zones: External Zone is located between the external wall of the reactor to the external baffle, and Internal Zone is from the internal baffle to the membrane module. In the External Zone, processes such as coagulation and sedimentation take place as well as anaerobic biodegradation; whereas in the Internal Zone, further anoxic biodegradation, flotation and membrane filtration take place.

The designed MBR is governed by the following major fluid motions (Figure 3.5):
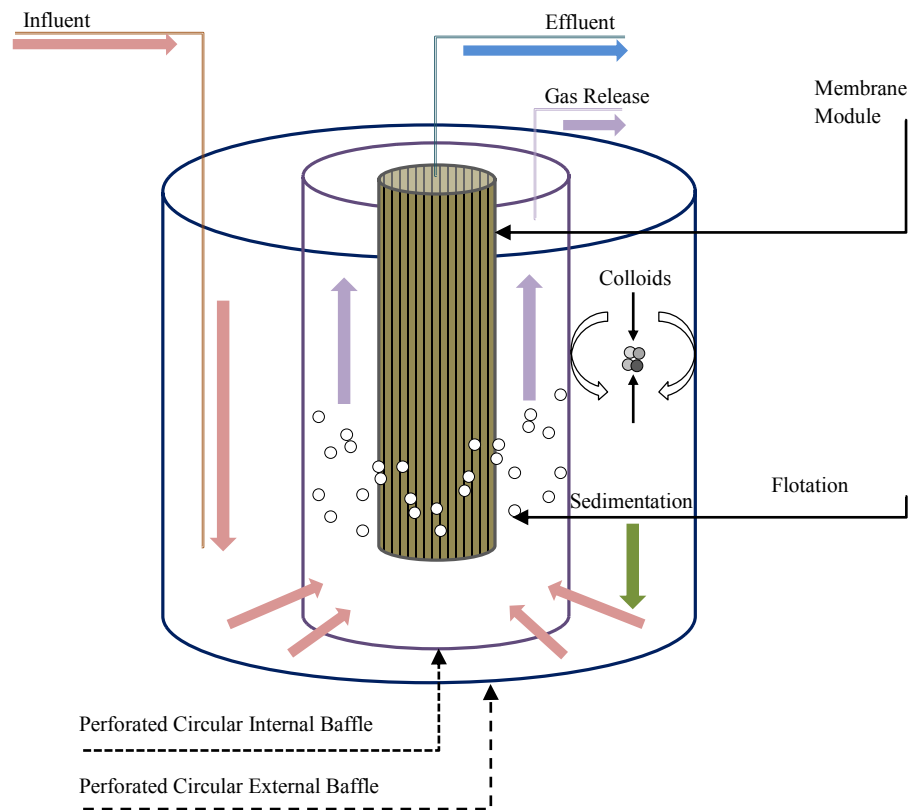
Figure 3.5. Major types of fluid motions in the AnMBR system

a) Industrial wastewater supply. The wastewater is supplied across the perforated baffle and undergoes biological and physical-chemical treatment between the baffles on its way towards the membrane module;

b) Upward movement. These gases help in the MBR system achieving uniform mixing of the aqueous phase in the system and reducing the fouling rate of the membrane;

c) Formation of flocs and sedimentation mainly due to the biological activity and physical-chemical phenomena;

d) Treated water moves through the membrane module due to a vacuum pump connected to the membrane module. Biological activity is to: temperature, pH, electron donor and microelements. The recommend range of pH for microorganism is 5-9 [134]. Based on the preliminary assessment, the pH of the system is kept within this range.

3.2.4.3. EAnMBR Design and Operational Considerations

Based on the research conducted in batch trials described in the previous chapter, the main focus of the next step is to develop a system incorporating electrokinetic, membrane physical and anaerobic biological treatment methods in a compact EAnMBR system in order to provide quality parameters of effluent containing highly-colored and recalcitrant components better than conventional systems.

In the following sections, the design considerations and criteria for development of new EAnMBR system are discussed in details.

3.2.4.3.1. EAnMBR Design Considerations

Positioning of the electrodes in the EAnMBR system is important for the uniform distribution of the DC field inside the system. The design considerations for the reactor included the following:

a) Location of the membrane module in the bioreactor must not affect the uniform electrical direct current distribution;

b) Electrical field should not have an impact on the longevity of membrane material;

c) Electrodes should maintain an adequate current density within the system;

d) Homogenous DC field distribution should promote flocs formation in the aqueous phase;

e) Electrode assembly in the system design should not interfere with the wastewater entering the reactor and directing toward the membrane module;

f) Selection of electrode material is important to reduce membrane fouling of EAnMBR. Aluminum and stainless steel are readily available materials and proven to be effective for

electrocoagulation process [134]. The selection of electrode material is also important for microbial community. For instance, iron is a necessary microelement for the microbial activity. It is an important component of many enzymatic reactions and involved in the metabolic pathways of microorganisms. However, some higher concentrations of iron might create inhibitory conditions for microbial growth [275], [276]. Aluminum in high concentrations can also act as an inhibitor of biological reactions [134].

g) Gases forming by microorganisms' activity and electrokinetic processes must freely leave the system and not accumulate in the upper part of the EAnMBR.

h) The system must be properly sealed in order to maintain anaerobic conditions.

3.2.4.3.2. EAnMBR Operational Considerations

Operation condition considerations include the following:

a) The EAnMBR design and configuration should incorporate the requirements for simultaneous biodegradation, electrokinetic phenomena, and physical separation processes taking place inside the bioreactor;

b) Design should consider the following fluid motions in the EAnMBR: wastewater supply across the anode, movement of gases, formation of colloids and their settling, fluid movement through cathode toward the membrane module;

c) Appropriate DC field should be applied to support electrolysis; the selected DC field cannot be supplied in a continuous mode due to presence of microbial culture. Preliminary tests demonstrated excellent results for 1 Vcm^{-1} and 1.5 Vcm^{-1}, which can be applied to the cultures, whereas COD, N, P and color reduction can be enhanced. This result is in agreement with one obtained in the previous research [134, 136]. According to the study, the impact of an applied DC field below 0.28 Vcm^{-1} may be insignificant, and a DC electric field greater than 1.4 Vcm^{-1} may be harmful for biological activity.

To achieve the overall objectives of the designed configuration, the following five major parameters should be controlled and optimized during the EAnMBR operation: applied direct current (DC), exposure time of microbial community to DC, hydraulic retention time (HRT),

and sludge retention time (SRT). The strategy of this study was based on operating the EAnMBR at variable transmembrane pressure and long SRT.

3.2.4.3.3. EAnMBR Design

To meet the requirements, the EAnMBR system was designed according to the following criteria:

a) A cylindrical ultrafiltration Zeeweed-1 (GE, Canada) membrane module with 0.04 μm pore size and 0.047 m^2 surface area was placed vertically in the center of a completely sealed 20 L polyethylene encasing;

b) Two cylindrical perforated electrodes (aluminum anode and stainless steel cathode) were placed around the membrane module at a distance allowing free hydraulic motion of aqueous phase. Perforated electrodes considered in the design in order to facilitate free feed and flow towards the membrane module;

c) A uniform distance between the electrodes maintained in order to minimize the potential detrimental effect of an acidic/oxidation zone on microbial organisms;

d) Such a distance should also allow free upward movement of electrolytic and bio gases, which will facilitate removal of microbial flocs forming on the membrane surface and downward movement of flocs aggregates;

e) Transfer pumps were connected to the shell in order to supply the wastewater and to the membrane outlet to extract the aqueous phase of the sludge liquor at a constant flow rate;

f) A direct current power supply connected with an electrical timer was used to provide the required current density and exposure mode (time-ON: time-OFF). The power supply was connected to the EAnMBR by the shortest possible insulated cables with appropriate current ratings, terminated with bolt-on crimp-lugs;

g) In the context of this research, the electrolyte is the wastewater to be treated.

The system includes the following components (Figure 3.7):

• Electric power supply
• Timer

- Anaerobic Reactor

- Heated Blanket

- Temperature Sensor

- Temperature Control Unit

- Membrane Module

- System of Circular Electrodes

- Influent Transfer Pump

- Effluent Transfer Pump

- Water Seal for Anode Zone Gas

- Water Seal for Cathode Zone Gas

- Wastewater Storage Tank

- Treated Effluent Storage Tank

- Sampling Point (SP)

- Transmembrane Pressure (TMP) Meter
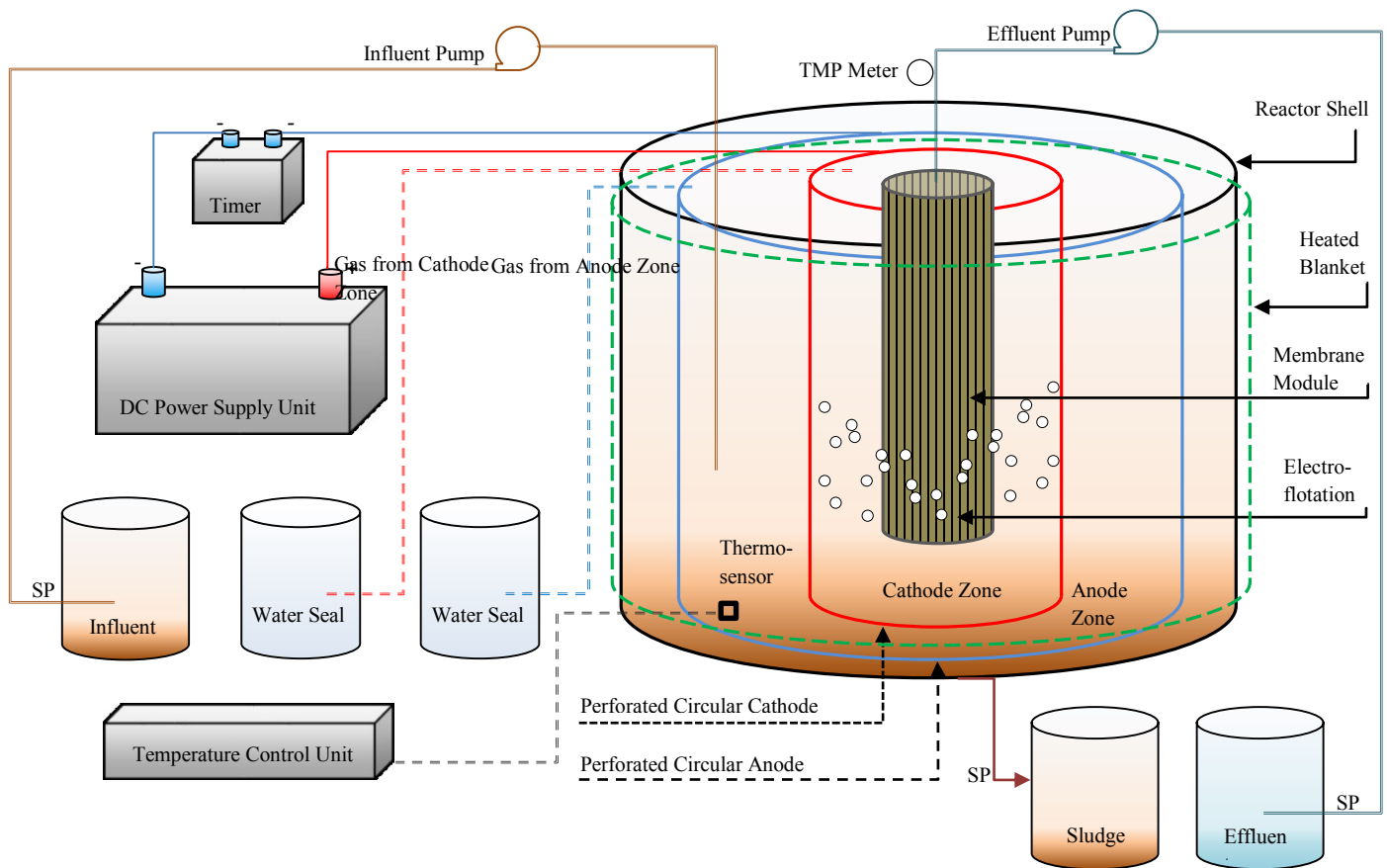
Figure 3.7. Simplified design configuration of the EAnMBR system

The selected design of the EAnMBR system broadly divides the hybrid anaerobic reactor into two zones: Anode Zone is located between the external wall of the reactor to the anode, and Cathode Zone is from the cathode to the membrane module. In Anode Zone, electrokinetic processes such as electrocoagulation and electrosedimentation take place as well as anaerobic biodegradation; whereas in Cathode Zone, further anoxic biodegradation, electroflotation and membrane filtration take place. However, the reactor is design as complex mix reactor. The designed EAnMBR is governed by the following major fluid motions (Figure 3.8):
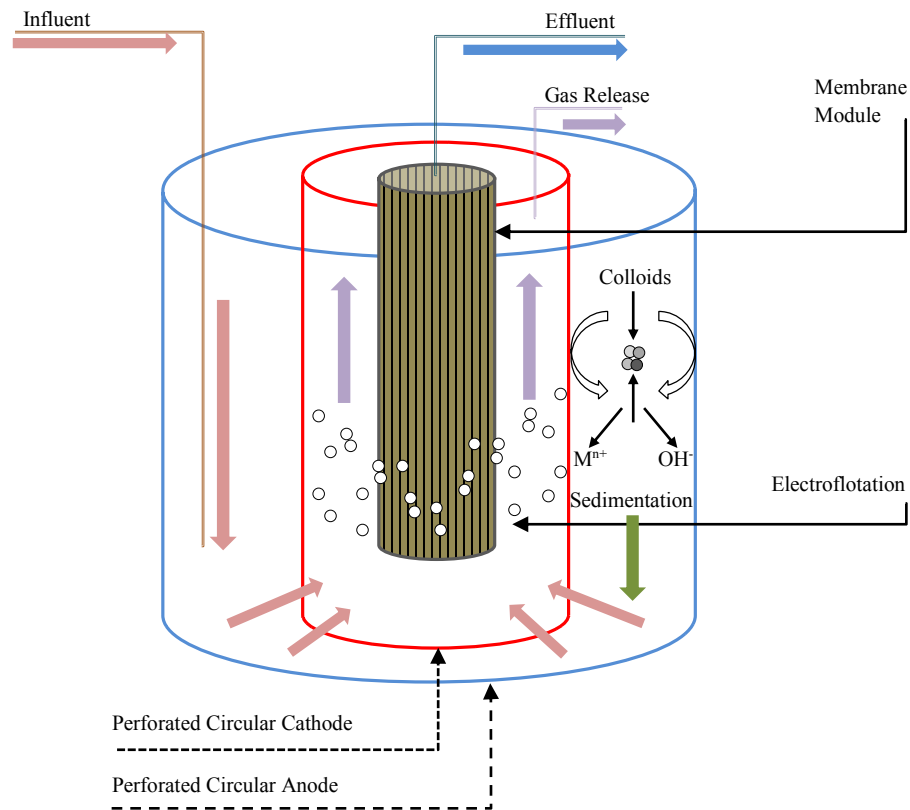
Figure 3.8. Major types of fluid motions in the EAnMBR system

a) Industrial wastewater supply. The wastewater is supplied across the perforated anode and undergoes biological and electrochemical treatment between the anode and cathode on its way towards the membrane module;

b) Electrolytic and bio gases upward movement. Electroflotation is used in EAnMBR system for achieving uniform mixing of the aqueous phase in the system zones and reducing the fouling rate of the membrane;

c) Formation of flocs and sedimentation mainly due to the principles of electrokinetic phenomena;

d) Treated water moves through the perforated cathode toward the membrane module due to a vacuum pump connected to the membrane module. Biological activity is influenced by the environmental conditions in the bioreactor: temperature, pH, electron donor and microelements. Electrical DC field will affect all these parameters, i.e. when a DC field in terms of a voltages gradient (Vcm^{-1}) is applied between anode and cathode, oxidation and reduction reactions will take place at the electrodes. Water oxidation generates hydrogen (H^+) and oxygen gas at the anode ($1/2\ H_2O \rightarrow e^- + H^+ + 1/4\ O_2$), whereas water reduction produces hydroxyls and hydrogen gas at the cathode ($2H_2O + 2e^- \rightarrow 2OH^- + H_2$). This will increase the acidity in the Anode Zone and reduce the pH; simultaneously, pH will increase in the Cathode Zone. The recommend range of pH for microorganism is 5-9 [134]. An interrupted supply of electrical field is needed to preserve the viability of microbial consortia. DC with appropriate voltage gradient is also required for an effective electrokinetic processes in order to create flocs in the bioreactor.

3.2.4.4. Continuous Flow Experimental Setup

Circular perforated aluminum and stainless steel baffles were affixed to a supporting Plexiglas frame in order to keep them in a vertical position. The porous (40% opening) circular baffles promoted the adequate mixing in the reactor.

Experimental setup of Phase II, III, IV consisted of the EAnMBR and supporting system as described previously is depicted on Figure 3.6.

The reactor was monitored during the experiment in order to maintain the anaerobic condition within the system. Synthetic and industrial water was supplied into the reactor by an influent transfer pump and the treated effluent was evacuated from the reactor by an effluent transfer pump. Excess of anaerobic sludge was wasted manually. During the start-up, the reactor was operated anaerobically in a batch mode for 48 h. After start-up, the operation of the AnMBR reactor was subsequently switched to a continuous mode. The effluent quality parameters in terms of N, P, COD, volatile fatty acids, color removal efficiency, pH, redox potential and conductivity were measured and analyzed as the performance indicators.
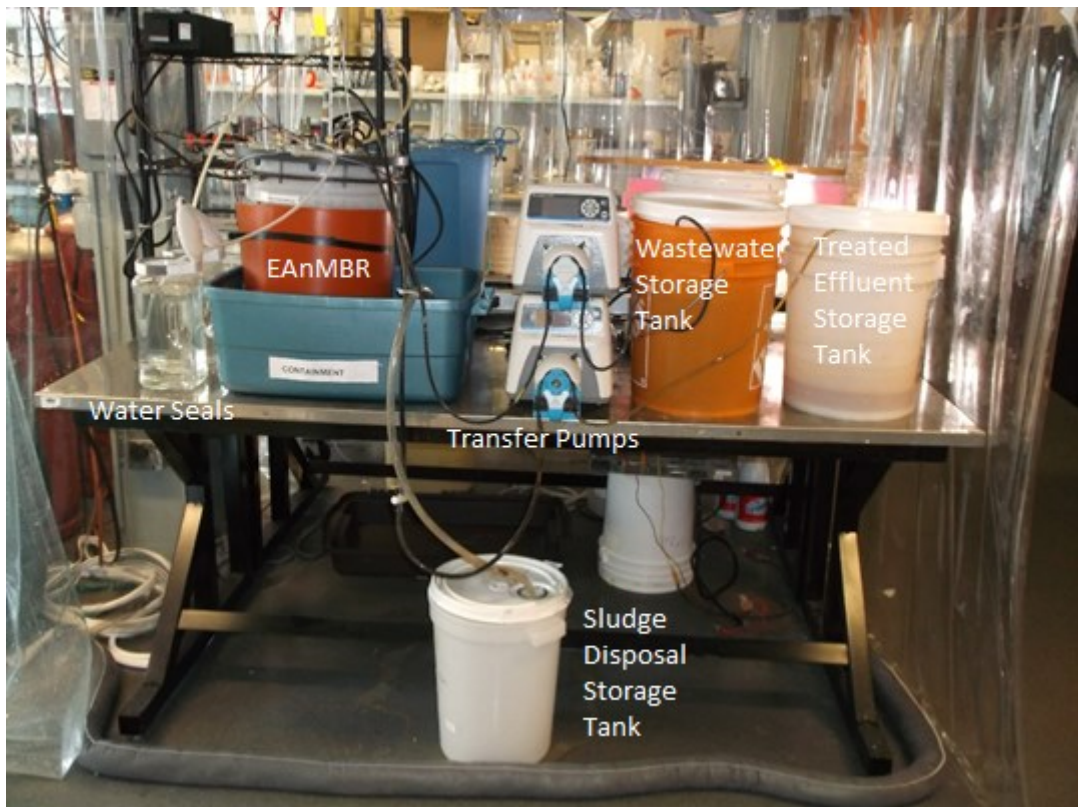
Figure 3.6. General view of experimental system setup

3.2.4.4.1. Phase II: Synthetic Wastewater Continuous Flow

This section presents experimental setup in Phase II. It highlights the operating conditions of the EAnMBR system when a perforated cylindrical aluminum sheet was used as the anode while the cathode was made of a perforated iron mesh of cylindrical shape. The operational period of this phase was divided into two sequential stages and extended for 60 days. The objectives were as follows:

i)   The AnMBR (without DC) lasted for 30 days.

ii)   The objective of the Stage II, which extended for 30 days, was to investigate the performance of the EAnMBR system when the DC was applied to the synthetic solution in conjunction with the operation of the membrane module. The mode 5 minutes ON: 20 minutes OFF was used during the DC supply.

The activated sludge electro-bioreactor, with working volume 10 L, was fed with the synthetic wastewater as described in Table 3.1. The activated sludge had been acclimated at mesophilic

80

conditions (35-37 ^{0}C) to this synthetic wastewater for approximately two months to achieve stable conditions prior the beginning of the experiments. Achieving the steady-state condition in the Stage I was not the goal of the experiment, but rather assessment of the system before the Stage II, where electrokinetic phenomena were applied- the primary interest of the study. During the Phase II the steady-state conditions were well developed (> 2SRT).

The process was closely monitored for multiple parameters including the physical-chemical and biological parameters: pH, temperature, MLSS, MLVSS, specific resistance to filtration (SRF), zeta potential, as well as COD, nitrogen species such as ammonia (NH_3-N), nitrate (NO_3-N), nitrite (NO_2-N) and orthophosphate (PO_4^{3-}-P). Phase II was divided into two stages: Stage I, which was considered the reference stage for comparison purposes, was extended for 30 days without input of DC. The main objective of extending this stage for 30 days was to give the anaerobic bacteria a sufficient time to replicate and research performance of the system in AnMBR configuration.

The impact of applying a DC field to the system operating in EAnMBR configuration was studied in the Stage II. The objective was to investigate the performance of the EAnMBR when a DC is applied to the system. The duration of Stage II was 30 days and the operating mode of the DC power supply was 5 minutes ON: 20 minutes OFF simultaneous with the operating membrane module. Table 3.5 provides detailed conditions under which the process was run and monitored during Phase II. After 3 weeks of operating period, the excess amount of sludge was removed from the reactor daily in the amount of 5% of the reactor volume. The conventional analysis of the samples and SRF analysis was performed on the withdrawn sludge samples. Therefore, on average, about 470 mLday^{-1} of sludge volume was removed from the electro-bioreactor, corresponding to average sludge retention time (SRT) of 21 days. The process was operated under variable transmembrane pressure. The permeate flux decreased with time because of the fouling phenomenon, however insignificantly because of anaerobic and electrolytic gases prevented excessive fouling. Due to this reason, no back washing for the membrane module was performed during the operation.

Table 3.5. Phase II operating conditions

Parameter	Stage I	Stage II
Operation Time, days	30	30
SRT, days	21	21
HRT, days	4	4
Flow Rate, mLh^{-1}	0.85±0.1	0.85±0.1
Voltage Gradient, Vcm^{-1}	0	1±0.1
DC Exposure ON:OFF, min	0	5:20
DC Application	No	Yes, simultaneously with membrane operation
Temperature, ^{0}C	36±1	36±1

Methodologies of sampling techniques and analytical methods performed in the Phase II were described in details in Chapter 3.

3.2.4.4.2. Phase III: Industrial Wastewater Continuous Flow

This the main objective of Phase III was to assess the efficiency of the EAnMBR in terms of carbon, nutrients and color removal in comparison to AnMBR. The Phase consisted of two stages operated of 60 days each. In this Phase, the vessel was operated as an anaerobic membrane reactor (AnMBR) during Stage I and anaerobic electro membrane reactor (EAnMBR) in Stage II.

The impact of applying a DC field in the EAnMBR performance was studies in the Stage II. The objective was to investigate the performance of the EAnMBR when a DC is applied to the system. High-strength molasses-based industrial wastewater was applied in both stages. The mode 5 minutes ON: 20 minutes OFF was used for the DC supply in Stage II.

The AnMBR and EAnMBR with working volume of 10 L, was fed with an industrial wastewater as described in Table 3.2. The sludge from Phase II was used in the Phase III and acclimated to new conditions at 36 ^{0}C for 21 days to achieve stable conditions prior to the experiments.

The process was monitored for various parameters including the physico-chemical and biological, namely: pH, temperature, MLSS, MLVSS, specific resistance to filtration (SRF), zeta potential, COD, nitrogen species such as ammonia (NH_3-N), nitrate (NO_3-N), nitrite (NO_2-N), orthophosphate (PO_4^{3-}-P) and color. The main objective of extending this stages for 60 days was to give the anaerobic reactor to reach steady state conditions.

The impact of applying a DC field in the EAnMBR performance was studied in the Stage II. The objective was to investigate the performance of the EAnMBR when a DC was applied to the system. Table 3.6 provides detailed conditions under which the process was run and monitored during Phase II. The excess amount of sludge was removed to maintain SRT of 21 days. The process was operated with a constant variable pressure. The pressure slightly increased with time because of the fouling phenomenon, however not to extent to reduce membrane performance (< 15 kPa over the course of the study). Subsequently, no back washing for the membrane module was performed during the operation period, thus the system remained completely sealed.

Table 3.6. Phase III operating conditions

Parameter	Stage I	Stage II
Operation Time, days	60	60
SRT, days	21	21
HRT, days	4	4
Flow Rate, mLh^{-1}	0.85	0.85
Voltage Gradient, Vcm^{-1}	0	1
DC Exposure ON:OFF, min	0	5:20
DC Application	No	Yes, simultaneously with membrane operation
Temperature, ^{0}C	36	36

Methods of sampling and analytical techniques performed in the Phase III were provided in details in Chapter 3.

3.2.4.4.3. Phase IV: Modeling and Optimization

The objective of the Phase IV was to assess impact of environmental parameters such as pH, sensitivity of the EAnMBR system with respect to electrical field variation and biological parameters in terms of MLSS on C, N, P and color removal. pH was varying from 6 to 8, the current density from 15 to 20 Am^{-2} and MLSS from 6 to 8 gL^{-1}. The experimental setup for the Phase IV replicated the Phase III. The first 30 days (Stage I), the EAnMBR was run under current density of 20 Am^{-2}. From day 31 to 60 (Stage II), the system was operated under 17.5 Am^{-2}. From day 61 to 90 (Stage III), the reactor was operated under 15 Am^{-2}. pH and liquor concentration were adjusted according to the design matrix. The minimum, midpoint and maximum values for pH of the electrolyte were 5, 7 and 8 respectively. The concentration of mixed liquor was adjusted between 5 and 8 gL^{-1} with 6 gL^{-1} as midpoint. The response surface design was conducted using Minitab® 17.1.0 software package. All the experiments were carried out under constant temperature (35 ± 1 ^{0}C). The electrolyte pH was adjusted with HCl and NaOH. The samples were collected at regular time intervals and analyzed for pollutants degradation using procedures similar to Phase III

4. Results and Discussion

This chapter provides the results of the experimental part of the research.

4.1. Phase I: Results and Discussion

The discussion of the results of the Phase I was built on identifying the current densities, voltage gradient and exposure modes that could maximize the removal efficiency of carbon in terms of COD, phosphorous, nitrogen, and color.

4.1.1. Current Density and Wastewater Conductivity

Changes of electrical conductivity (EC) and current density (CD) over the duration of the experiment are presented in Figures 4.1-4.8 (operation regime 5-On: 5-Off, 5-On: 10-Off, 5-On: 15-Off, 5-On: 20-Off, continuous electrical current supply and no electric current supply for control reactor). Running the batch bioreactors with replenishment of the waste water resulted in changes of concentration of dissolved solids over the time of the experiment. From the biological point of view, the concentration lowering occurred when the carbon source was supplied to the bioreactors. The decrease of dissolved solids was observed when the sludge still was able to provide an electron donor to support building new cells, whereas the increase of dissolved solids appeared when there was a lack of electron donor. Then, the indigenous phase presumably dominated, especially at 5-On: 5-Off operational regime when the microbial community was most affected by the electrical field. During the endogenous phase when the electron donor was limited (picks at 48 hours of operation on the Figures 4.1-4.8), the microbial community released the intra soluble ions into the bulk solution, leading presumably to increase of EC at a larger scale. The initial increase of EC clearly seen for all essays, especially at short time off operational mode can also be attributed to inability of some microorganisms to adapt to electric current applied to the system, thus releasing intra soluble ions into the solution due to the cell lysis.
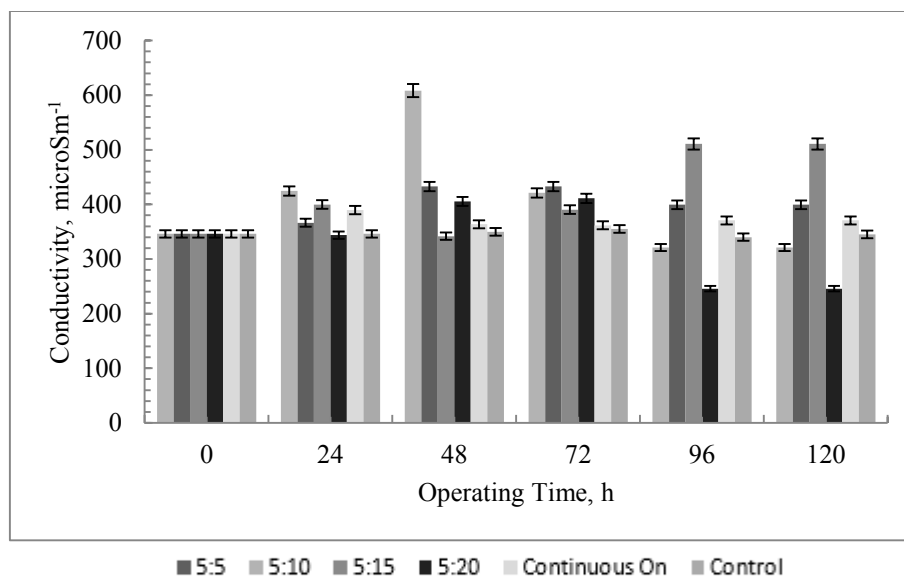
Figure 4.1. E1: Electrical conductivity over 120h at 12 Am^{-2} and voltage 1.0 Vcm^{-1}
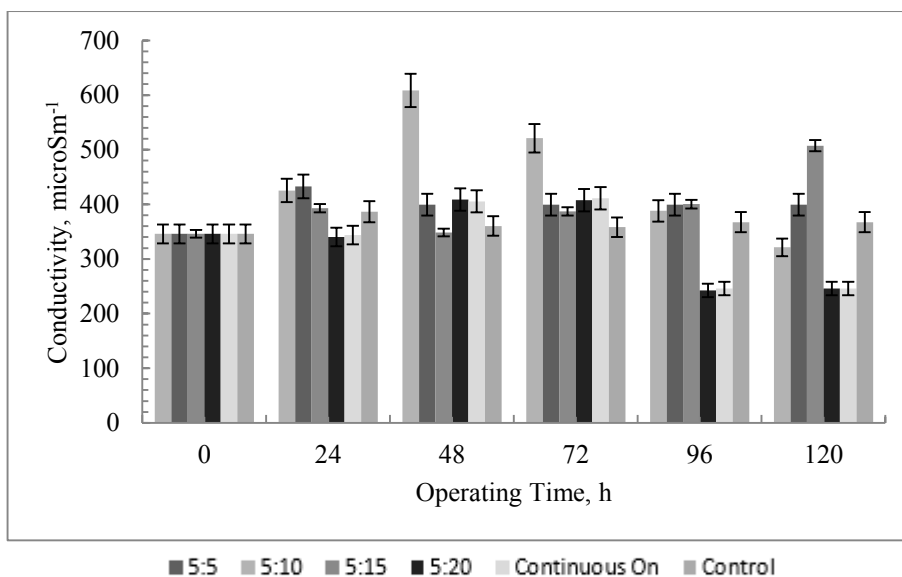
Figure 4.2. E2: Electrical conductivity over 120h at 12 Am^{-2} and voltage 1.5 Vcm^{-1}
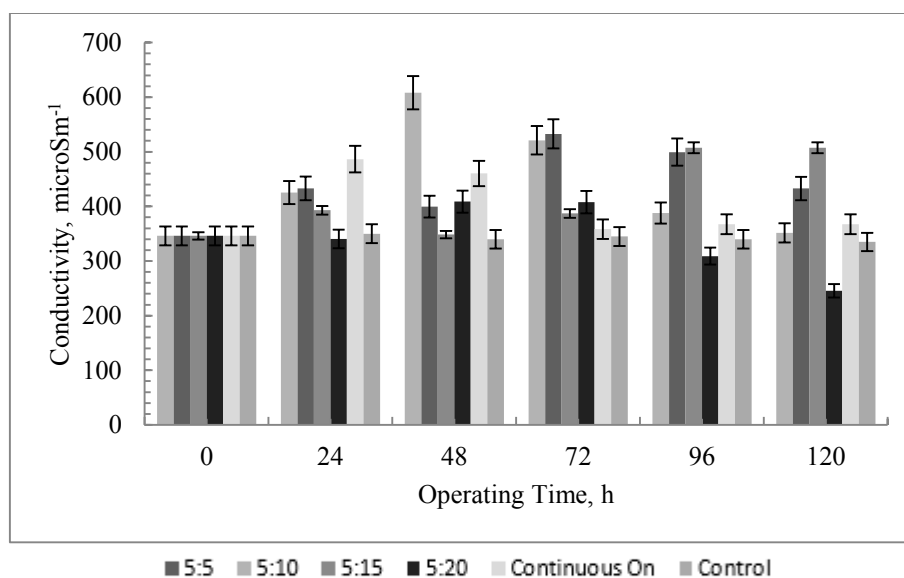
Figure 4.3. E3: Electrical conductivity over 120h at 15 Am^{-2} and voltage 1.0 Vcm^{-1}
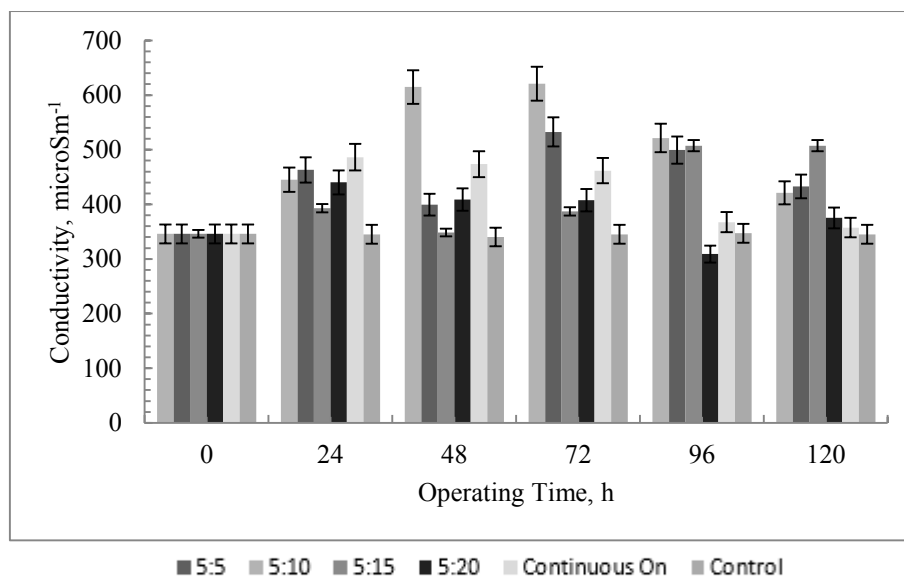
Figure 4.4. E4: Electrical conductivity over 120h at 15 Am^{-2} and voltage 1.5 Vcm^{-1}
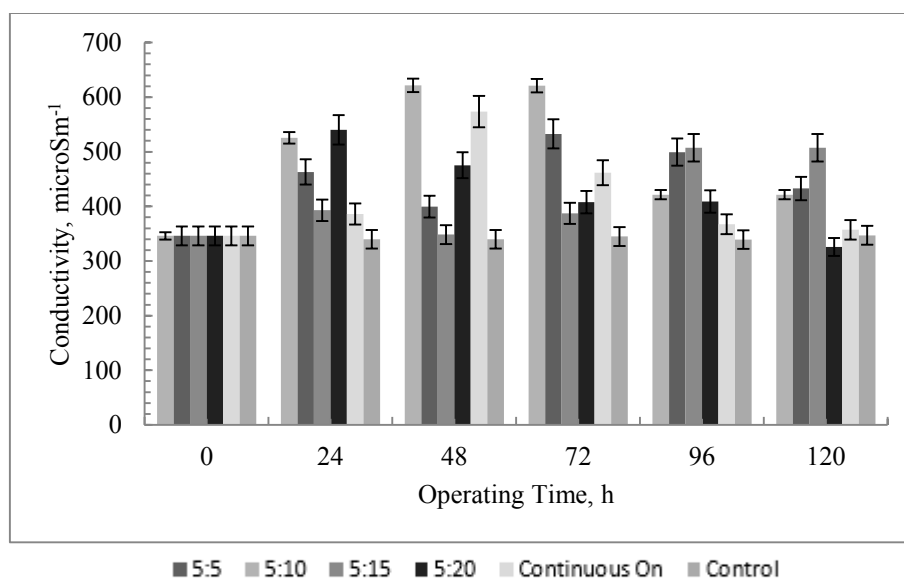
Figure 4.5. E5: Electrical conductivity over 120h at 20 Am^{-2} and voltage 1.0 Vcm^{-1}
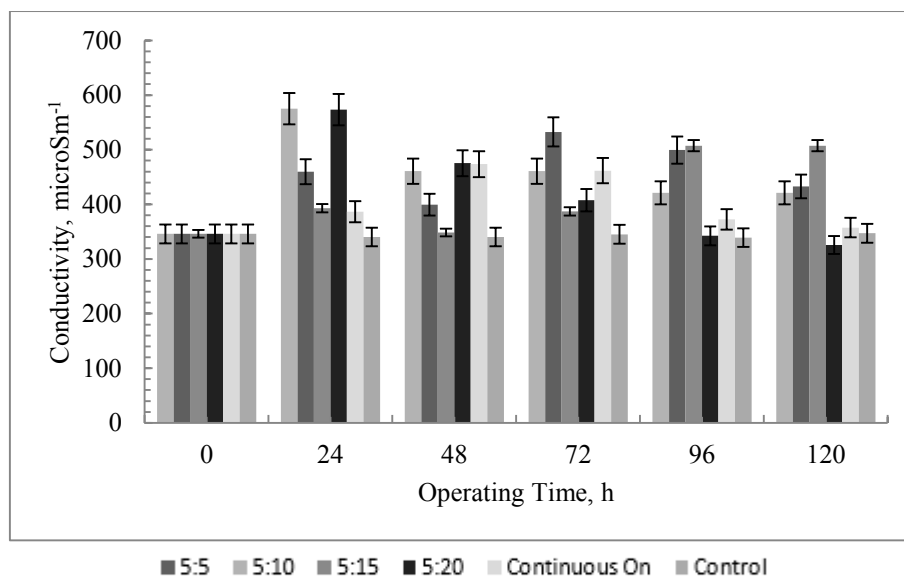
Figure 4.6. E6: Electrical conductivity over 120h at 20 Am^{-2} and voltage 1.5 Vcm^{-1}

From a chemistry of the process, a reduction of dissolved solids in the bioreactors under all operated current densities was also a result of the electrophoretic migration of ions towards the electrodes and deposition on the cathode and anode surfaces.

For all the essays a substantial increase of EC was observed after 24 hours for all electrical modes up to 100%, especially for the essays with short time off regimes, while in the control reactor there were no significant changes observed.

Increase of the dissolved solids concentration and EC can also reflect bonds breaking in high

and low weight organic polymers and phenol-metal complexes that constitute melanoidin compounds.

These mechanisms are responsible for the majority of soluble salts produced in the first hours of operation. After the initial phase, EC started to stabilize as the carbon sources depleted and indigenous phase dominated. After 72 hours of operation, the rate of ions deposition on electrodes exceeded the rate of ions released by cell lysis and polymers destruction. The constantly higher EC for 5-On: 5-Off and 5-Off: 10-On compared to the other operational regimes can be attributed to inability of microbial community to recover from electric current applied with shorter periods of relaxation. EC dropped from its peak at 24 hours (except for 5-On: 5-Off) for up to 30% for 5-On: 10-Off, 50% for 5-On: 15-Off. The most stable EC after 24 hours spike until the end at 120 hours was demonstrated by 5-On: 20-Off operation for essays E5 and E6. The 5-On: 10-Off, 5-On: 15-Off and the continuous ON mode exhibited regular spikes of the current density. These drops in current density can be related to the formation of an organic layer deposition on the anodes, thus reducing the current conductivity between the electrodes. Depositions on anode surface by this process were mostly observed under continuous-ON electrical mode under higher current densities (E2, E4, E6) and for the 5-On: 5-Off, 5-On: 10-Off, 5-On: 15-Off electrical modes. At voltage gradient of 0.5 Vcm^{-1} and 1.0 Vcm^{-1} and current density 12 Am^{-2} a gradual decrease in EC for all electrical modes until the end of the experiment and no extreme drops in current density were detected as the current density was not able to support electrophoretic migration of negatively charged particles towards the anode.

It was concluded that the continuous-ON mode and other modes with shorter periods of relaxation (5-On: 5-Off, 5-On: 10-Off, 5-On: 15-Off) are not recommended for the next phases of the study.

4.1.2. Effect of Current Density and Operational Regime on pH

Electrokinetic process results in decrease of pH at the anode due to release of H$^+$ ions into the aqueous phase, while pH increases at the cathode zone due to the generation of hydroxide ions. Experimental results demonstrated that current densities ranging between 12 up to 20 Am^{-2} indeed caused an increase of wastewater pH. The maximum increase that was observed under current density of 12 to 20 Am^{-2} at the continuous-On mode and 5-On: 5-Off, 5-On:10-Off for all essays (Figure 4.7-4.12). Therefore, direct current at current density up to 20 Am^{-2} may

cause spikes of pH to a level that might negatively affect the biological activity and the pH adjustment might be necessary with the addition of HCl and NaOH. However, this experiment was conducted on batch systems. Under continuous flow in Stage 2, the system is expected to be less susceptible to severe fluctuations of pH because the aqueous phase will be continuously replenished by the influent wastewater, which has pH around 5.23. Thus, the increase of pH noticed might be neutralized by the buffering capacity of the feed wastewater.
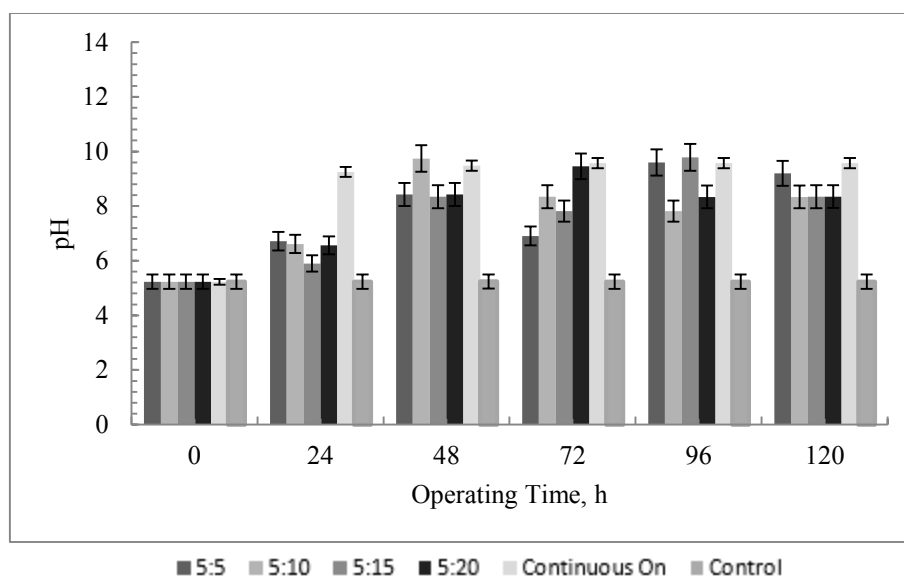
Figure 4.7. E1: pH over 120h at 12 Am^{-2} and 1.0 Vcm^{-1}
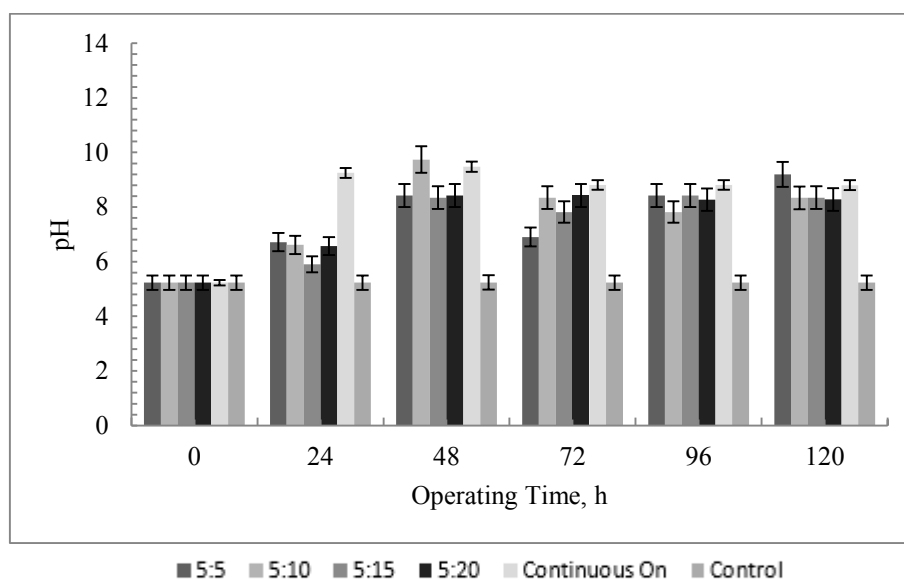
Figure 4.8. E2: pH over 120h at 12 Am^{-2} and 1.5 Vcm^{-1}
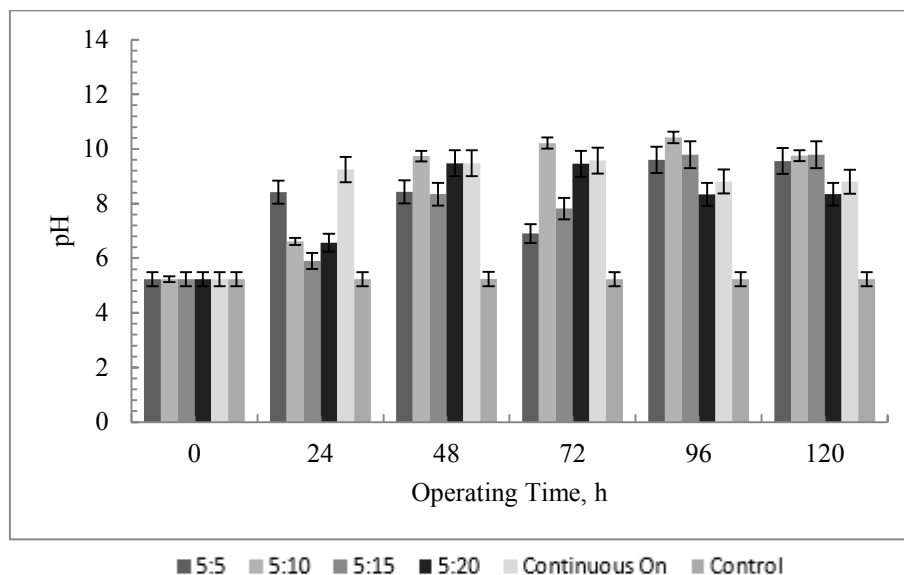
Figure 4.9. E3: pH over 120h at 15 Am^{-2} and 1.0 Vcm^{-1}
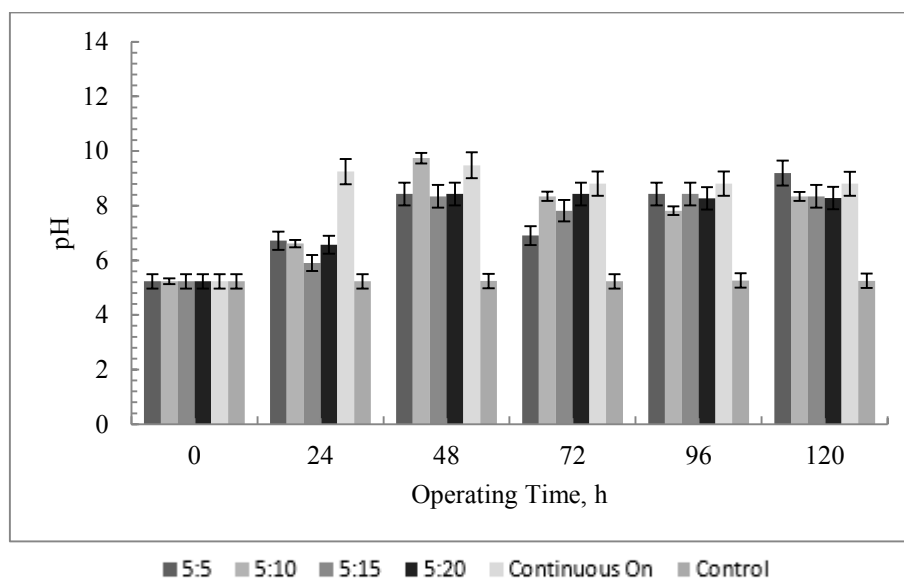
Figure 4.10. E4: pH over 120h at 15 Am^{-2} and 1.5 Vcm^{-1}
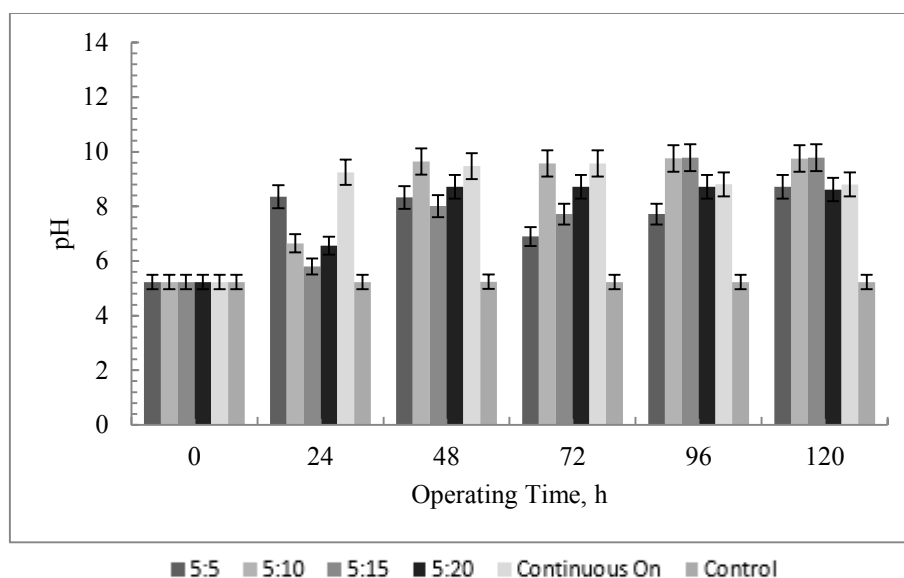
Figure 4.11. E5: pH over 120h at 20 Am^{-2} and 1.0 Vcm^{-1}
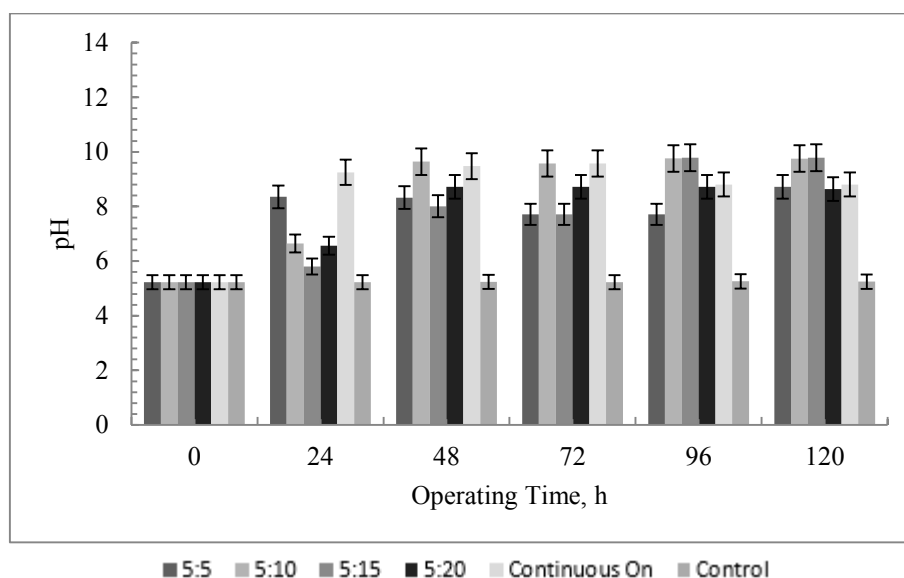
Figure 4.12. E6: pH over 120h at 20 Am^{-2} and 1.5 Vcm^{-1}

These observations highlight the significance of pH control as a variable that can be electrokinetically controlled to improve treatment performance.

4.1.3. Effect of Current Density and Operational Regime on Carbon in Aqueous Phase

EC application prompts COD removal as soon as the current flows resulting in a rapid decrease in COD between 80-92% removed after 120 min operation.

Changes of COD removal efficiencies depending on current densities variations are presented in Figures 3.15 to 3.20. At current density 12 Am^{-2}, the removal efficiency of the COD was in the range of 77 % to 86% for $1Vcm^{-1}$ (Figure 4.13) and 77% to 96% for 1.5 Vcm^{-1} (Figure 4.14). The highest removal efficiency at 12 Am^{-2} by the end of the experiment was obtained at continuous-ON and 5-On: 20-Off modes.

Higher efficiency rate was achieved at current density 15 Am^{-2}, where the COD removal rate was in the range from 85% to 86% for $1Vcm^{-1}$ (Figure 4.15) and slightly lower (85% to 90%) for 1.5 Vcm^{-1} (Figure 4.16). The removal efficiency pattern was similar to all the time-On: time-Off regimes at 15 Am^{-2}, however the highest 90% was obtained at 5-On: 20-Off mode.

Higher value of current density (20 Am^{-2}) was similarly effective for COD removal (up to 96%), (Figures 4.17, 4.18).

Therefore, all current densities were more effective in the removal of COD at timer regimes with the longer time-Off (> 85% and >95% reduction after 96 hours at 5-On: 15-Off and 5-On: 20-Off correspondingly). Short time-Off periods provide enough time for dissolution of Al^{+3} and formation of hydrated species, while high concentration of suspended solids provides larger surface area to interact electrically with the organic colloids (about 80% reduction after 96 hours at 5-On: 5-Off and 5-On: 10-Off correspondingly). As the results demonstrated, longer time-On cycles were required to substantially reduce COD concentration in the wastewater. Therefore, less COD was represented in form of suspended colloids, and rather in dissolved form. The insignificant performance increase of COD removal (Fig. 4.13 - 4.15) was attributed to longer time required for the larger aluminum polymers species formation. Based on the results, operating at current densities higher than 20 Am^{-2} and electrical mode with short time-Off cycles is not recommended.
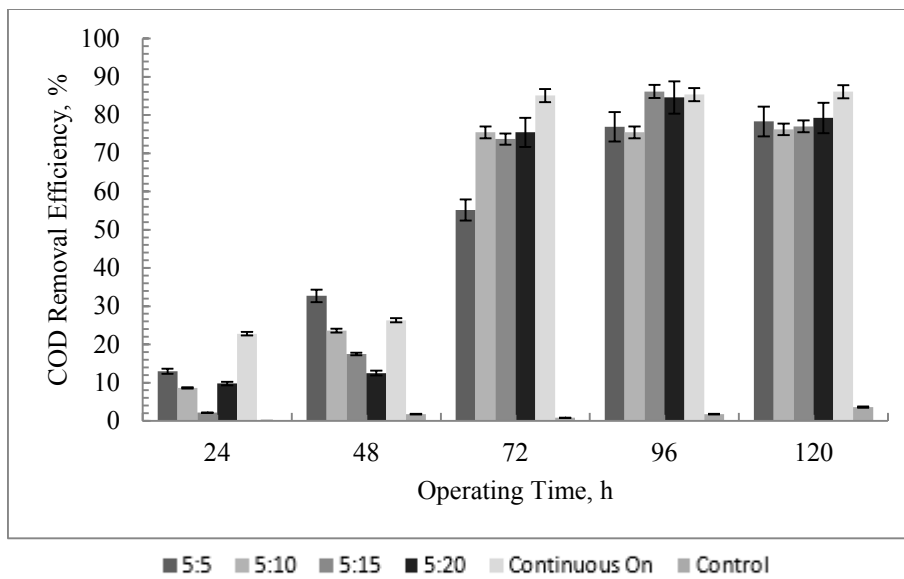
Figure 4.13. E1: COD removal efficiency over 120 h at 12 Am^{-2} and 1.0 Vcm^{-1}
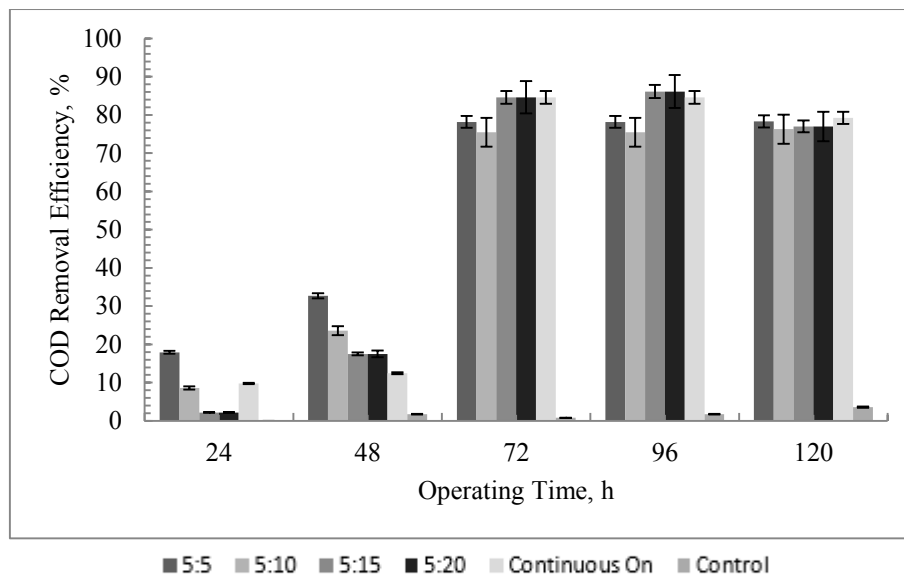
Figure 4.14. E2: COD removal efficiency over 120 h at 12 Am^{-2} and 1.5 Vcm^{-1}
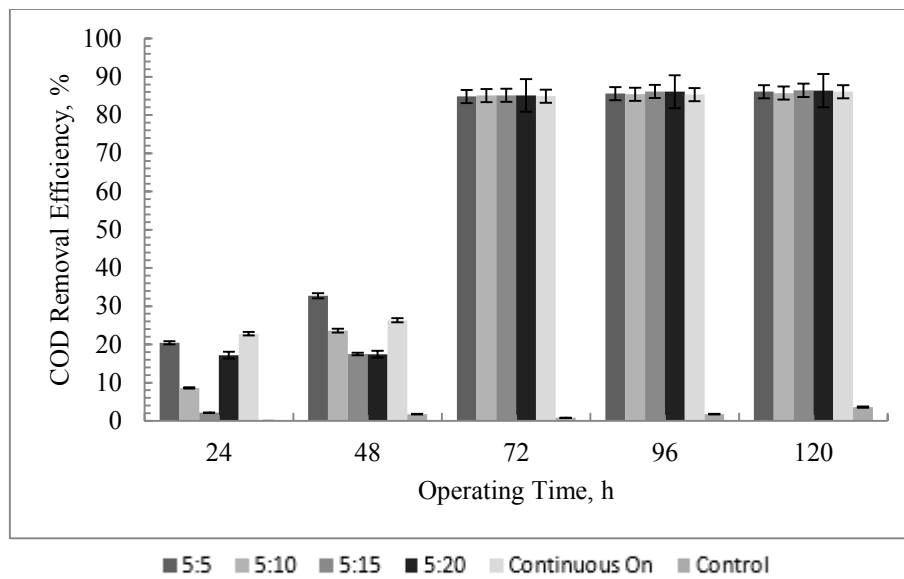
Figure 4.15. E3: COD removal efficiency over 120 h at 15 Am^{-2} and 1.0 Vcm^{-1}
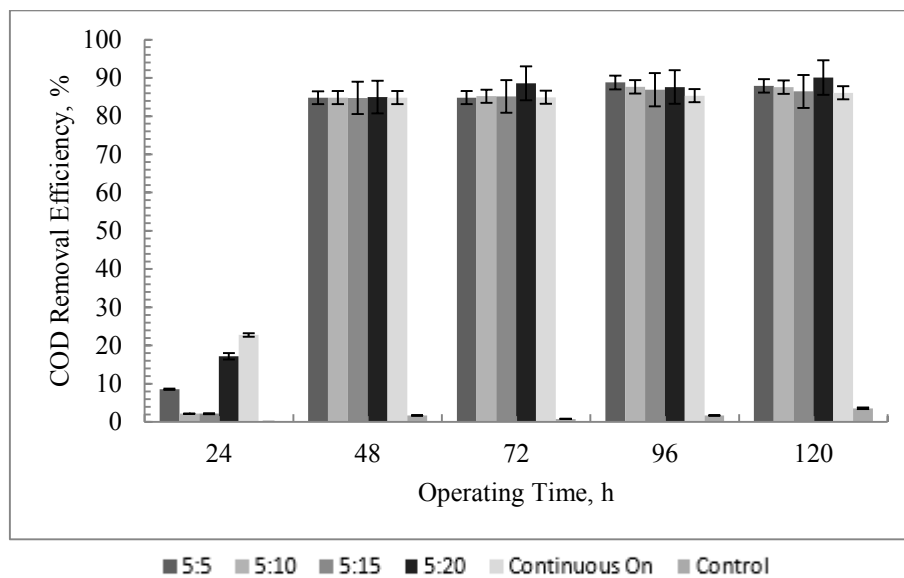
Figure 4.16. E4: COD removal efficiency over 120 h at 15 Am^{-2} and 1.5 Vcm^{-1}
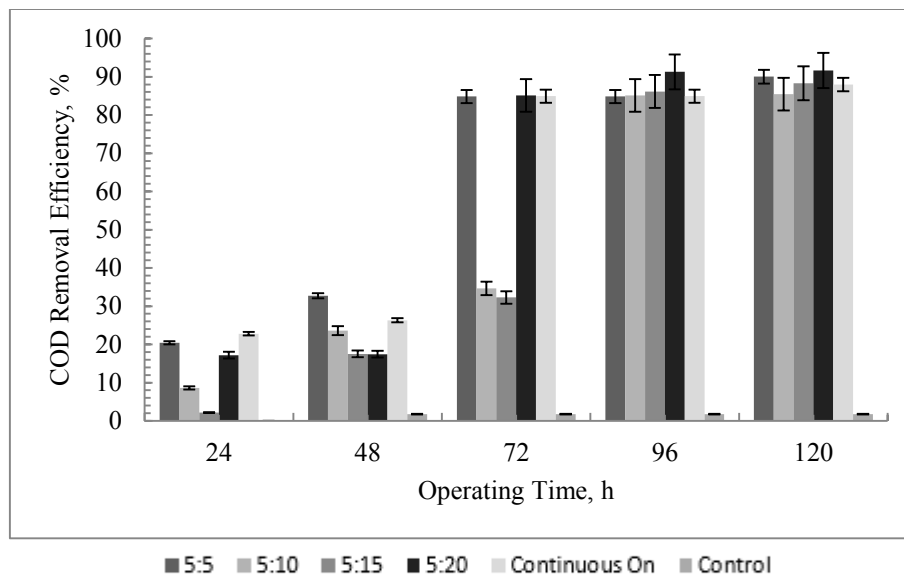
Figure 4.17. E5: COD removal efficiency over 120 h at 20 Am^{-2} and 1.0 Vcm^{-1}
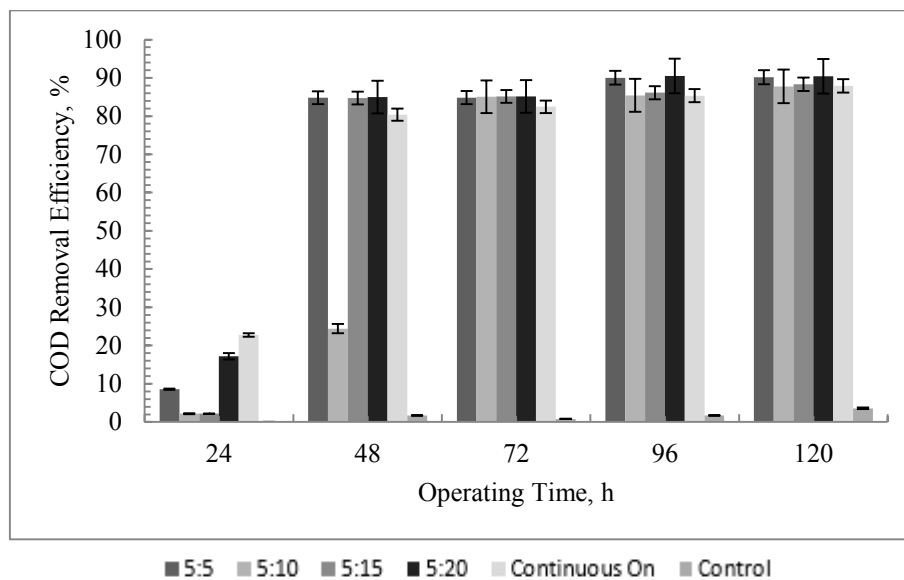
Figure 4.18. E6: COD removal efficiency over 120 h at 20 Am^{-2} and 1.5 Vcm^{-1}

4.1.4. Effect of Current Density and Operational Regime on Nitrogen in Aqueous Phase

In the experiments for evaluating the effect of current density, 12, 15 and 20 Am^{-2} were applied to the system of reactors respectively. The variations in nitrogen removals over the period of experiment are shown in Figures 4.19-4.24.
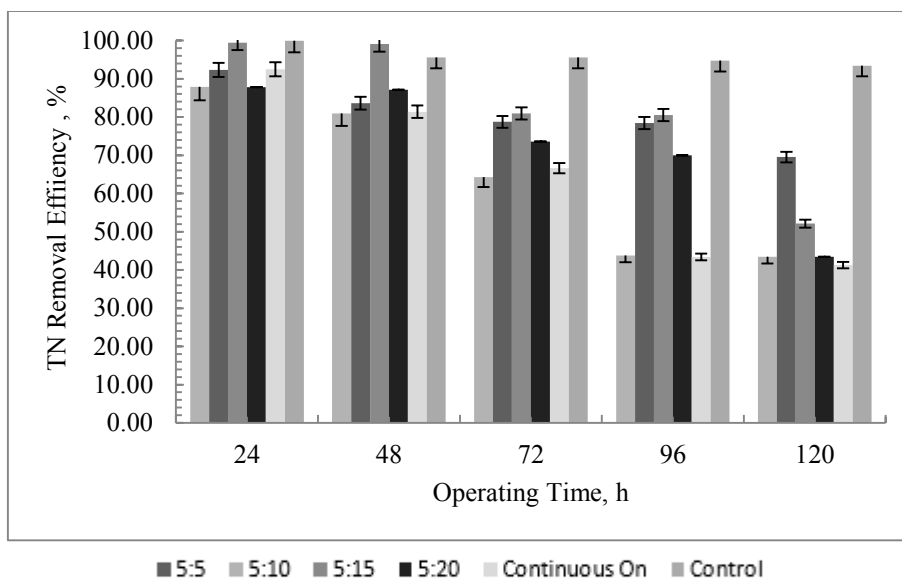
Figure 4.19. E1: TN removal efficiency over 120 h with 12 Am^{-2} and 1.0 Vcm^{-1}
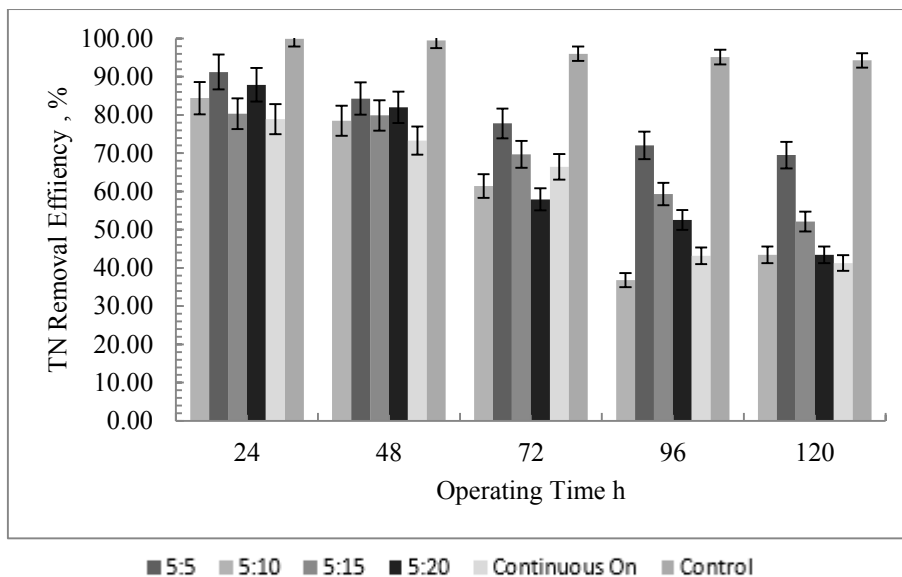
Figure 4.20. E2: TN removal efficiency over 120 h with 12 Am^{-2} and 1.5 Vcm^{-1}
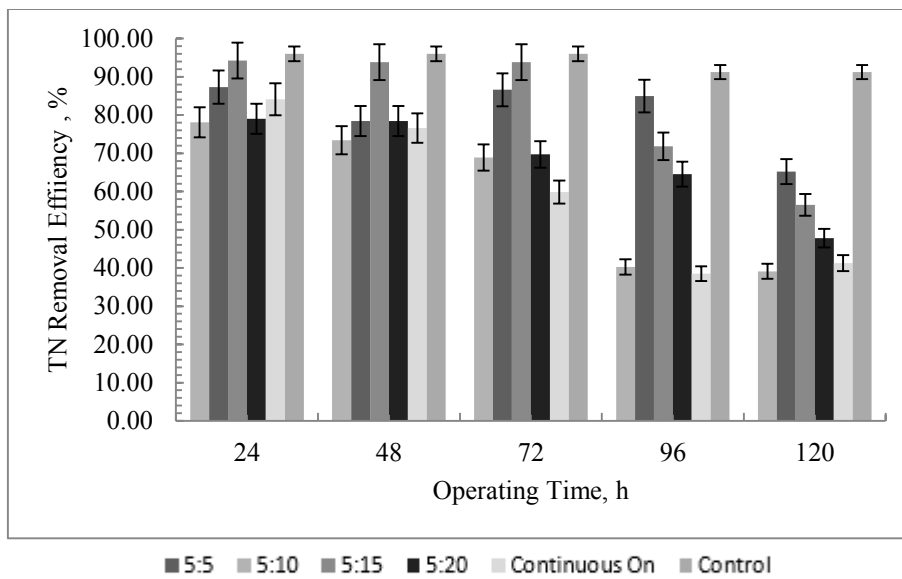
Figure 4.21. E3: TN removal efficiency over 120 h with 15 Am^{-2} and 1.0 Vcm^{-1}
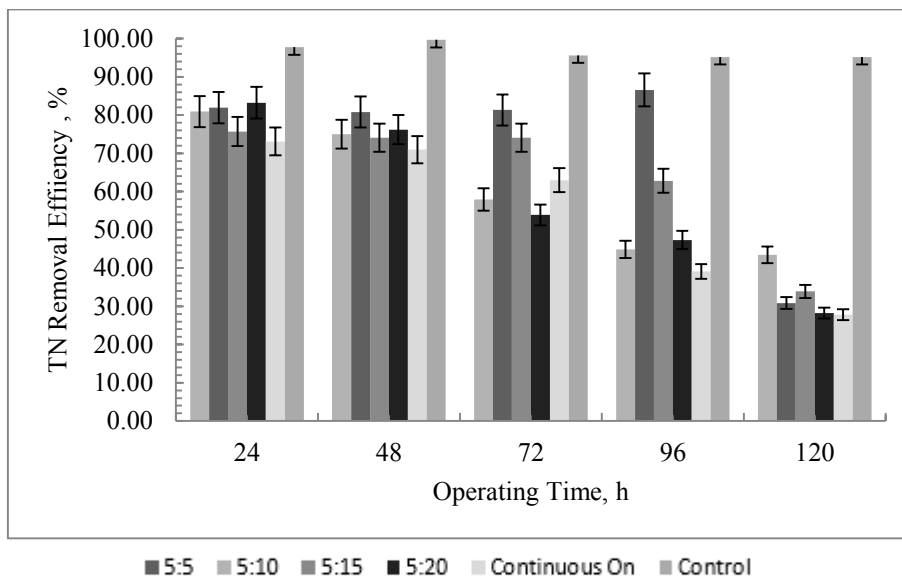
Figure 4.22. E4: TN removal efficiency over 120 h with 15 Am^{-2} and 1.5 Vcm^{-1}
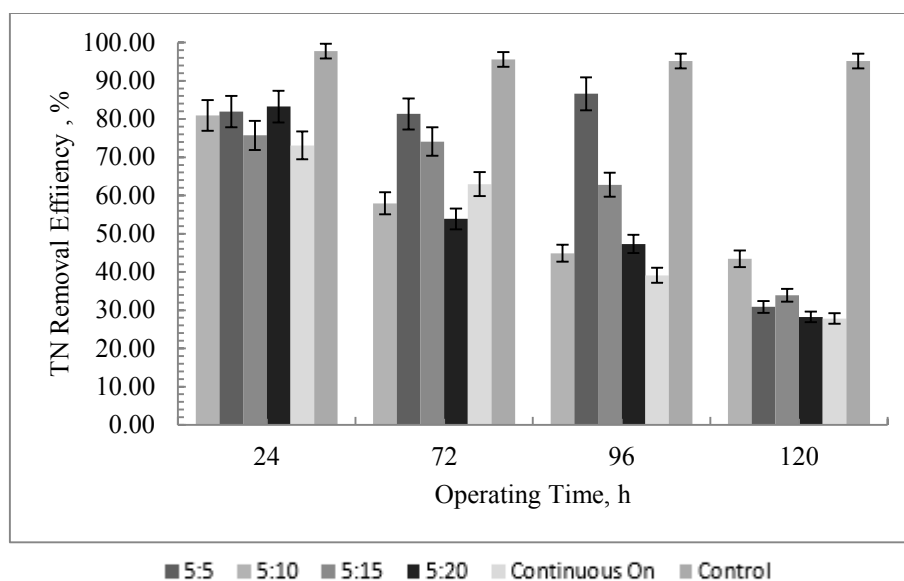
Figure 4.23. E5: TN removal efficiency over 120 h with 20 Am^{-2} and 1.0 Vcm^{-1}
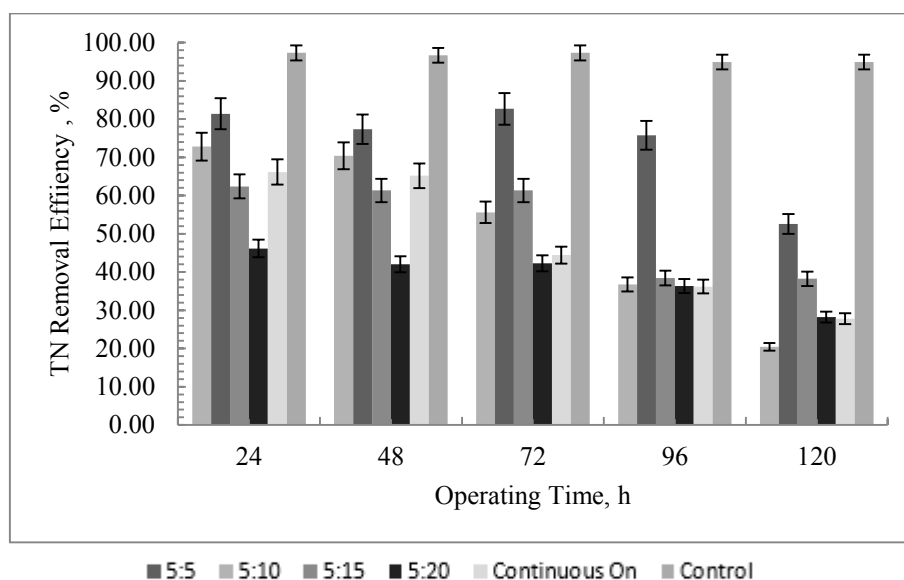
Figure 4.24. E6: TN removal efficiency over 120 h with 20 Am^{-2} and 1.5 Vcm^{-1}

With increasing initial Al^{3+} concentration over the time, degradation rate increased for all the essays. However, nitrogenous compounds were still present at significant levels at this point with 81% and 95% remaining for the essays with lower current density applied (E1 and E2 respectively). Better removal efficiency up to 20% was demonstrated with voltage of 1.5 Vcm^{-1} for all time-on: time-off.

99

For the essays E3 and E4 with current density 15 Am^{-2} applied, similar pattern was observed, however, with slightly better performance for 1.5 Vcm^{-1} and shorter exposure modes (5-On:15-Off, 5-On: 20-Off) and continuous regime.

For the essays with 20 Am^{-2}, the best result was achieved with 5-On: 20-Off mode for the essay E6 with up to 65% nitrogen removed during the initial 24 hours of operation.

After 24 hours, the pattern was similar to all the essays: the concentration of nitrogen gradually decreased. However, some fluctuations were observed for 5-On: 5-10 time cycles as the deposits formed on the electrodes preventing release of Al^{3+}.

The removal N in 120 min reached 59% for 12 Am^{-2}, 15 Am^{-2} and 80% respectively for 20 Am^{-2}.

Based on the experimental results, all current densities were effective in the removal of TN at all time cycles. Short time-off periods provided enough time for dissolution of Al^{+3} and formation of hydrated species which interacted with nitrogenous compounds, while high concentration of suspended solids provides larger surface area to interact electrically with the colloids.

However, longer time-on cycles were performing slightly better and substantially reduced the concentration of TN in the wastewater, especially by the end of runs. Thus, TN was represented both in form of suspended colloids and in dissolved form.

It follows that the nitrogenous bonds in the waste wastewater constituents started to degrade after 24 hours of the experiment and appeared to be degraded, probably to amino acids and sugars which can be an electron donor for biological decomposition in subsequent phases of this study.

Based on the results, operating at current density 20 Am^{-2} and electrical mode with longer time-off cycles are recommended.

4.1.5. Effect of Current Density and Operational Regime on Phosphorous in Aqueous Phase

The results of this study demonstrated the ability of the process to achieve up to 76% of phosphorus (measured as P_{tot}) removal efficiency.

The process of TP removal starts as soon as the current flows through the system resulting in a rapid decrease of TP concentration after 24-48 hours of operation depending on the current density and voltage (Figures 4.25-4.30).

At current density 12 Am^{-2}, the removal efficiency of the TP was in the range from 35% to 62% for $1Vcm^{-1}$ (Figure 4.25) and 41% to 69% for 1.5 Vcm^{-1} (Figure 4.26) by the end of the run. The highest removal efficiency at 12 Am^{-2} by the end of the experiment was obtained at shorter time cycles such as continuous-On, 5-On: 5-Off and 5-On:10-Off modes.

Higher removal efficiency was achieved at 15 Am^{-2} and $1Vcm^{-1}$, where the P removal rate was up to 65% (Figure 4.27) and 76% for 1.5 Vcm^{-1} (Figure 4.28). The removal efficiency pattern was similar to all the regimes at 15 Am^{-2}, however with higher removal rate at the beginning (0-24 hours) where the greater efficiency was demonstrated by 5-On: 5-Off and 5-On: 20-Off modes.

Higher value of current density (20 Am^{-2}) was slightly less effective if compared to 15 Am^{-2} (up to 70%), which can be seen on Figures 4.29, 4.30, nonetheless demonstrating good results especially for 5-On: 5-Off and 5-On: 20-Off regimes after 48 hours.

Therefore, higher current densities were more effective in the removal of P_{tot} for timer regimes with the short and longer time-off.

As calcium chloride is used in the technological process of yeast production, the wastewater is characterized by high concentration of calcium [108]. Short time-off periods provide dissolution of Al^{+3} and formation of hydrated species, while high concentration of suspended solids provides larger surface area to interact electrically with the organic colloids. Under these conditions the high phosphorous removal efficiency could be attributed to precipitation of insoluble $Ca_3(PO4)_2$ and $AlPO_4$.

Based on the results, operating at current density 15-20 Am^{-2} and electrical mode with longer relaxation timing is recommended.

The measurement of calcium concentration in the influent wastewater and effluent was not conducted in the present study and the problem of the formation and removal of potential inorganic precipitate requires future study.
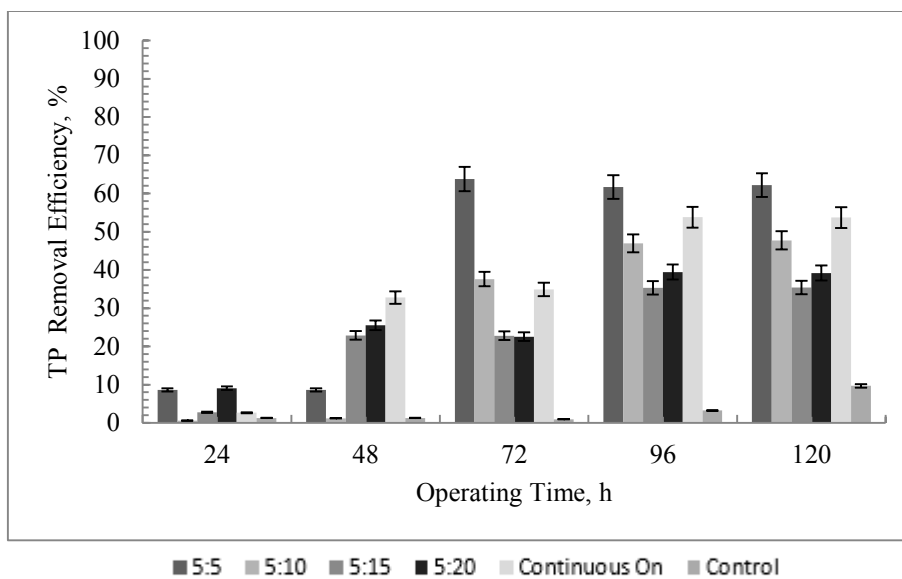
Figure 4.25. E1: TP removal efficiency over 120 h with 12 Am^{-2} and 1.0 Vcm^{-1}
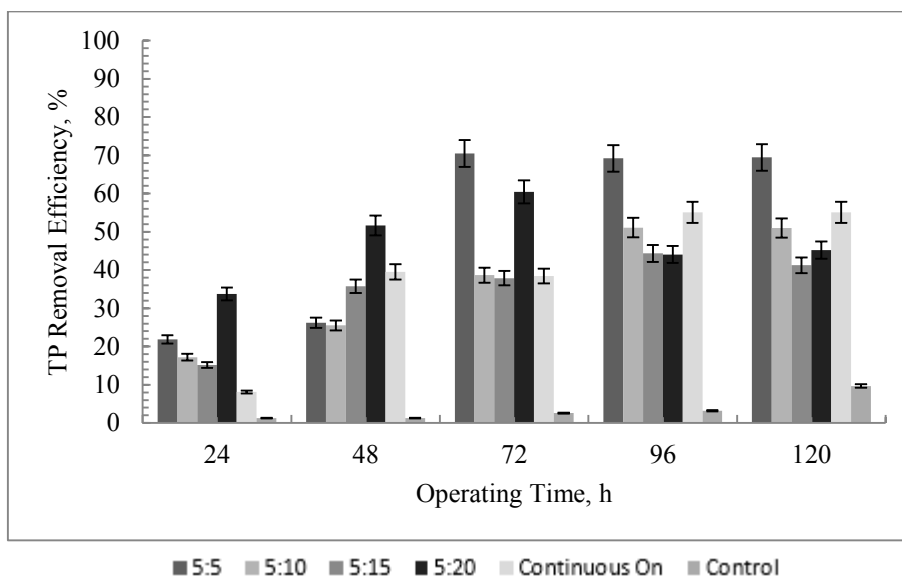
Figure 4.26. E2: TP removal efficiency over 120 h with 12 Am^{-2} and 1.5 Vcm^{-1}
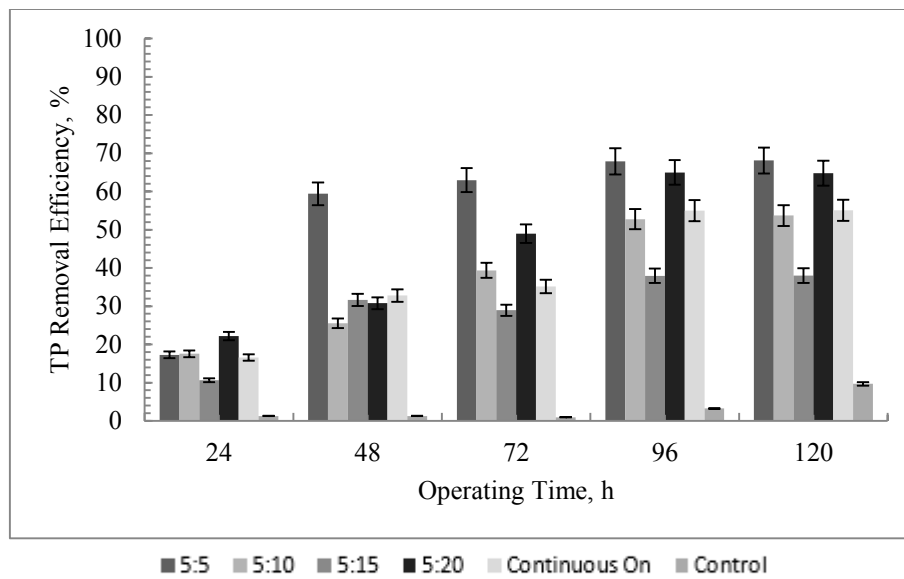
Figure 4.27. E3: TP removal efficiency over 120 h with 15 Am^{-2} and 1.0 Vcm^{-1}
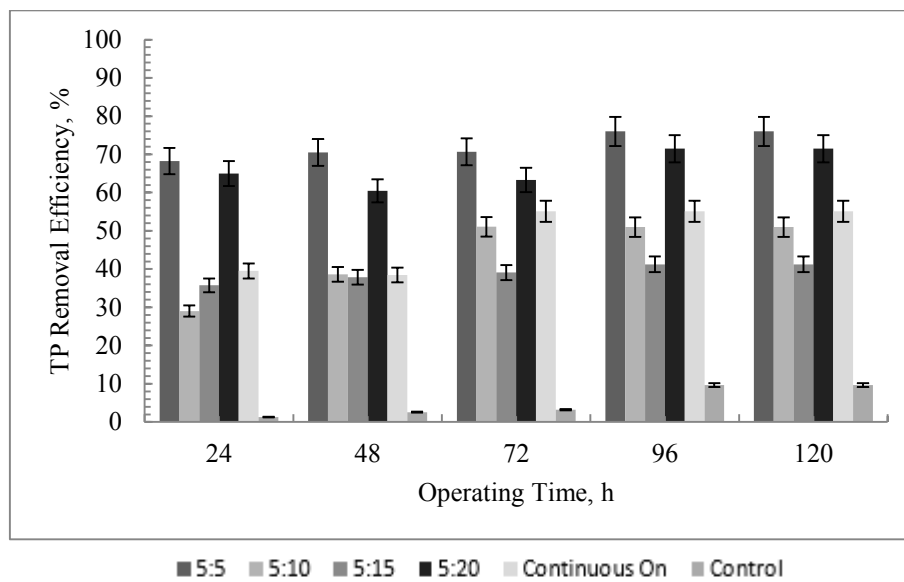
Figure 4.28. E4: TP removal efficiency over 120 h with 15 Am^{-2} and 1.5 Vcm^{-1}
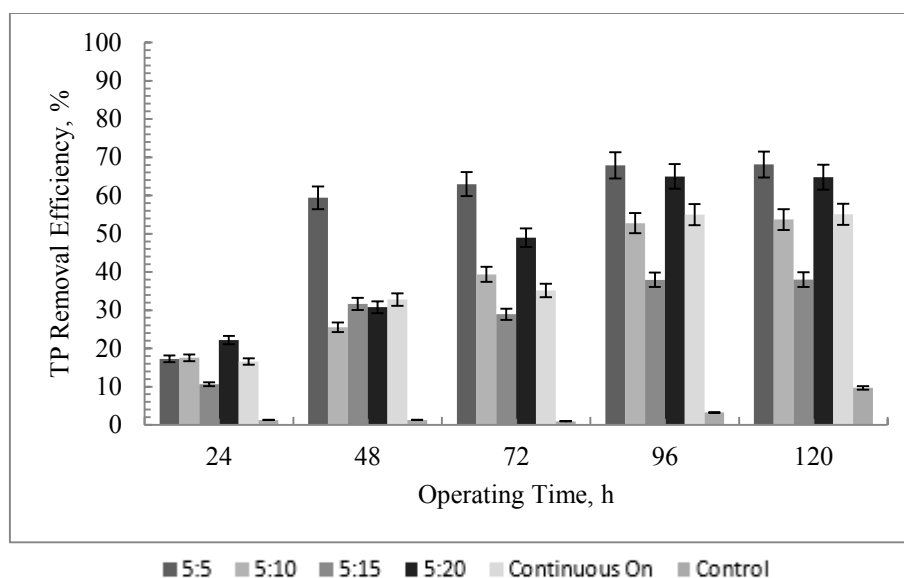
Figure 4.29. E5: TP removal efficiency over 120 h with 20 Am^{-2} and 1.0 Vcm^{-1}
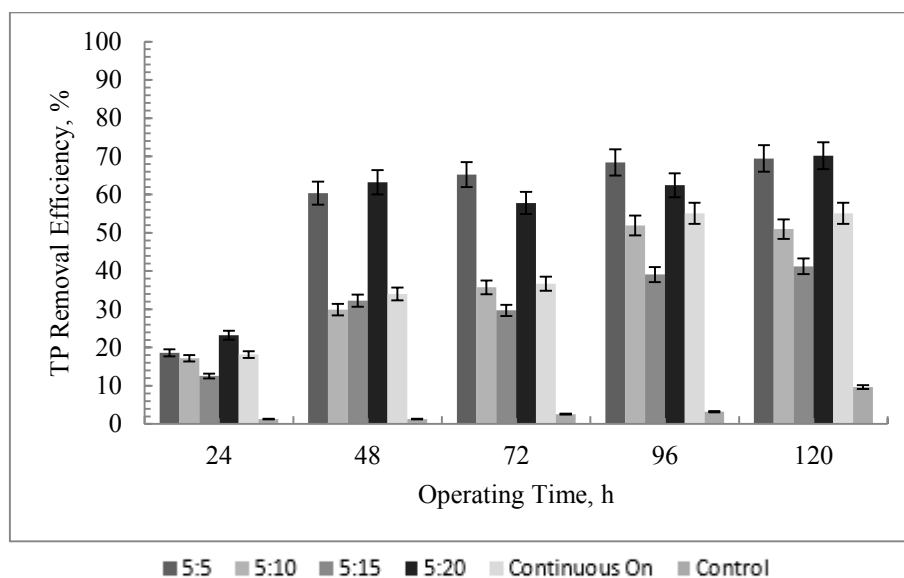
Figure 4.30. E6: TP removal efficiency over 120 h with 20 Am^{-2} and 1.5 Vcm^{-1}

4.1.6. Effect of Current Density and Operational Regime on Decolorization of Melanoidins-containing Wastewater

The melanoidin compounds are negatively charged and carried toward the anode by electrophoretic motion where they interact with the Al^{3+} cations and other hydrolysis products when the process of coagulation takes place [126].

During the experiment, there was a short lag phase observed for E1-E6 at all operational regimes for about 24 hours, followed by a rapid decolourisation stage that removed up to 81% of the colour after 24 hours, corresponding to a release of Al metal into solution from anode (Figures 4.31-4.36).

Similar behaviour was observed for all runs E1-E6 for the period from 24 to 48 hours with the removal rate rapidly accelerated thereafter and a maximum 96% decolourisation was achieved after a run time of 120 min for essay E4 and E6 at 5-On:5-Off and 5-On:20-Off. The lowest removal efficiency (91%) was achieved for essay E1 and E2. These observations correlate with other study which reported a very similar profile for the removal of melanoidin [105]. The pH value of 8-12 reached by the end of the runs with the highest pH for essay E6. The temperature of the treated effluent also increased to approximately 21 ^{0}C. The maximum color removal effect was achieved at the pH range 8 and higher. In comparison, the control reactor E7 demonstrated only 5% of color removal efficiency. The higher removal rates were observed with higher current densities and pH (essays E4 and E6). The removal mechanisms of color substances were attributed to the electro-coagulation of the organic materials, microbial flocs and aluminum hydroxides species in the solution. Based on the results of the experiment, higher current densities and pH are two factors that can attribute to the color removal as well.
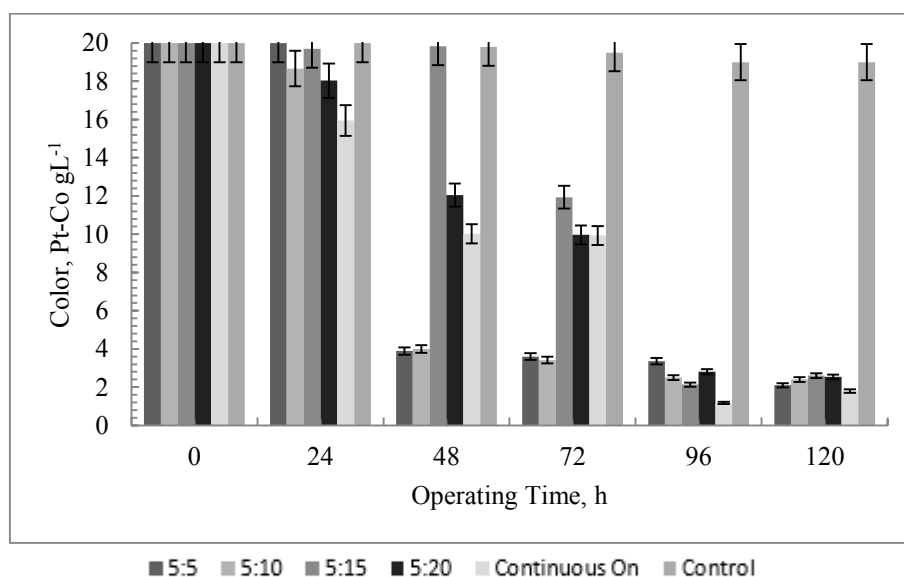
Figure 4.31. E1: Color removal over 120 h with 12 Am^{-2} and voltage 1.0 Vcm^{-1}
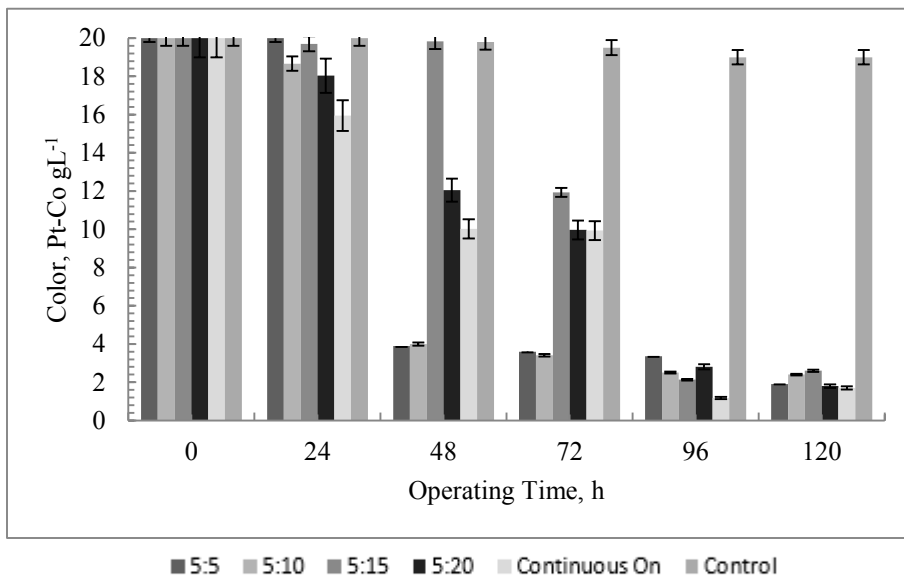
Figure 4.32. E2: Concentration of color after exposure to EK treatment over 120 h with 12 Am^{-2} and 1.5 Vcm^{-1}
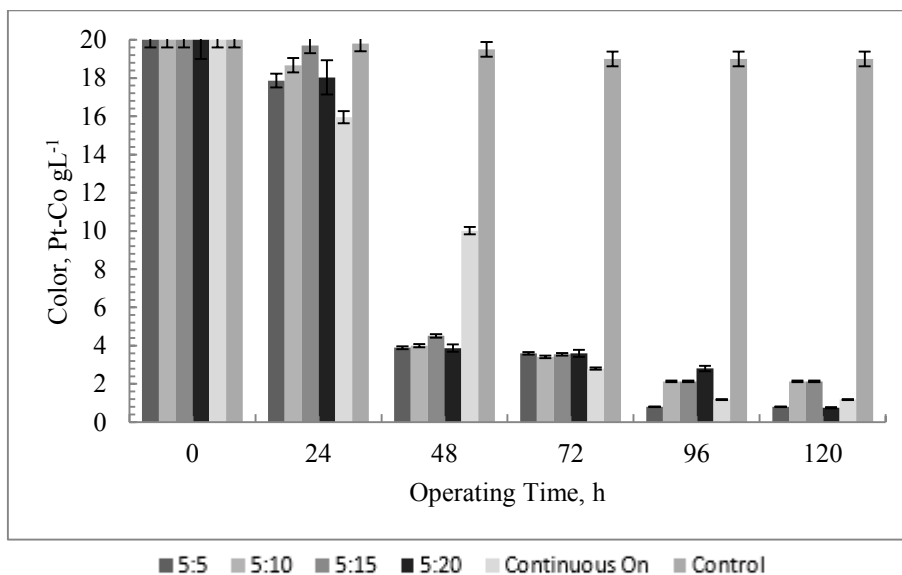
Figure 4.33. E3: Concentration of color after exposure to EK treatment over 120h with 15 Am^{-2} and 1.0 Vcm^{-1}
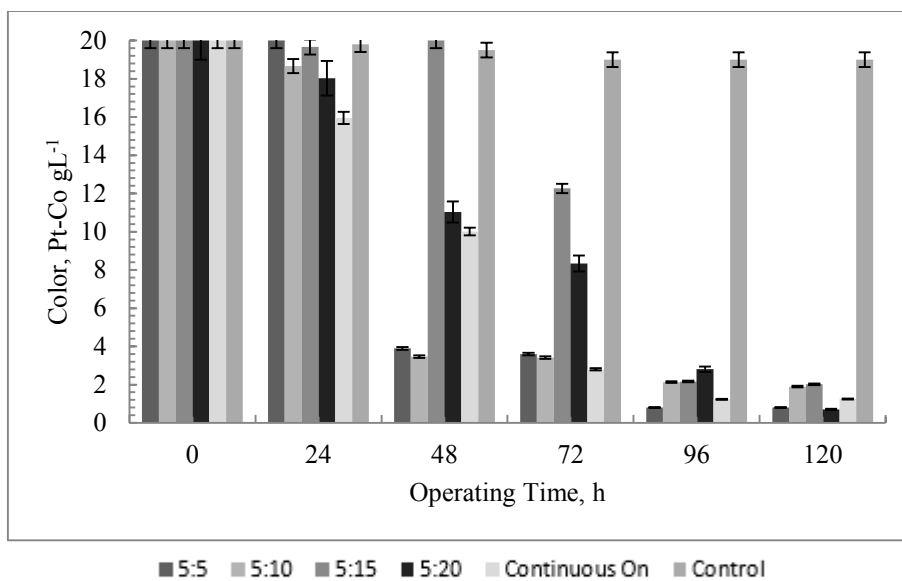
Figure 4.34. E4: Concentration of color after exposure to EK treatment over 120h with 15 Am^{-2} and 1.5 Vcm^{-1}
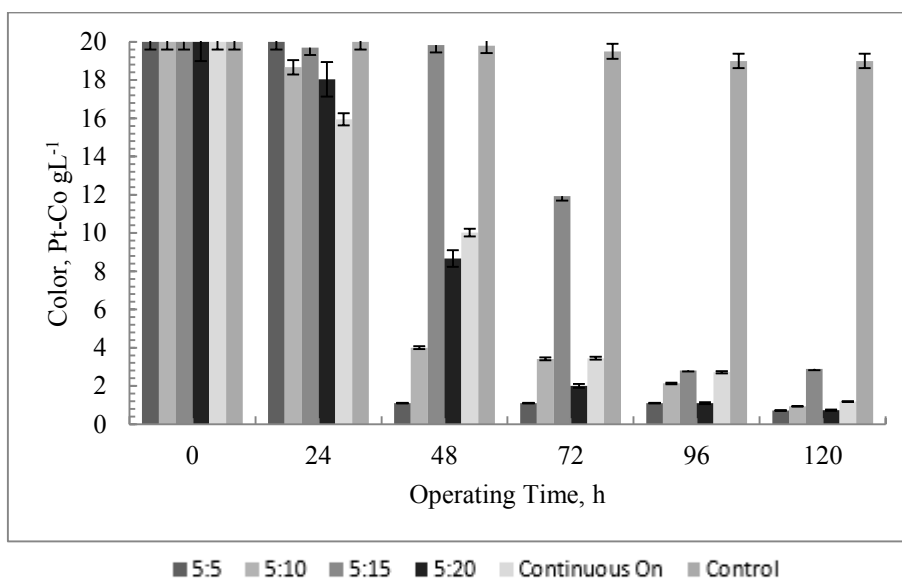
Figure 4.35. E5: Concentration of color after exposure to EK treatment over 120h with 20 Am^{-2} and 1.0 Vcm^{-1}
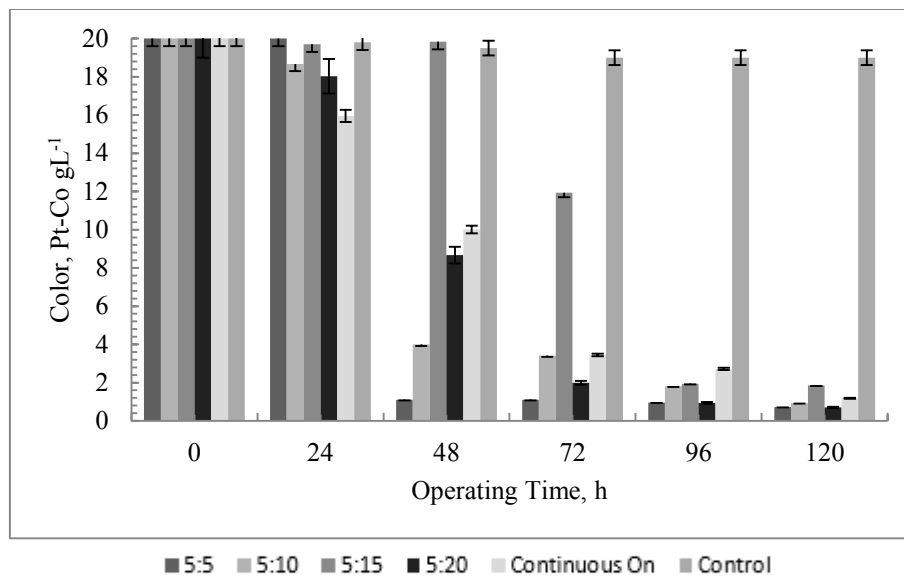
Figure 4.36. E6: Concentration of color after exposure to EK treatment over 120h with 20 Am^{-2} and 1.5 Vcm^{-1}

4.1.7. Relationship between Current Density and Colloids Zeta Potential

Zeta potential is useful in determining the magnitude of attraction-repulsion forces between particles and stability of a colloid system. The closer the magnitude of zeta potential to zero, the less repulsion forces between particles are observed, leading to decrease the stability level of a system.

Tri-valent Ions introduced from aluminum anode into solution were expected to neutralize the negative charge on the colloid surfaces and reduce the repulsive forces between the particles, thus improving settling characteristics. The zeta potential of the control waste water sample without applying any electrical field was in between -15 to -40 mV.

The suspended particles in the wastewater, as can be seen from the previous section, vary in the range of sizes. Therefore, to encompass as wide range of zeta potential values as possible, all particle sizes should be included during the sampling. In this study, the determination of particles zeta potential was done based on tracking all pools based on methodology developed in a previous research [136]. The results are represented in Tables 4.1 to 4.3.

Table 4.1. Zeta potential change after EK treatment at 12 Am^{-2}

Time, h	5:5	5:10	5:15	5:20	Continuous	Control
0	-20-40	-20-40	-20-40	-20-40	-20-40	-15-40
24	-5+5	-5+5	-10+15	-5+5	-5+5	-15-40
48	-6+10	-2+6	-10+15	-3+5	-6+8	-15-40
72	0+5	0+5	-10+15	-2+4	-5+5	-15-40
96	-6+8	-5+5	-10+15	0+10	-5+6	-15-40
120	0+7	0+8	0+10	0+10	0+10	-15-40

Table 4.2. Zeta potential change after EK treatment at 15 Am^{-2}

Time, h	5:5	5:10	5:15	5:20	Continuous	Control
0	-20-40	-20-40	-20-40	-20-40	-20-40	-15-40
24	-18-35	-15+15	-12+15	-5+5	-18+20	-15-40
48	-7+12	-12+18	-12+20	-5+5	-8+10	-15-40
72	0+7	-10+15	-10+12	-2+4	-5+5	-15-40
96	-3+6	-7+10	-10+15	0+11	-5+8	-15-40
120	0+10	-5+15	-5+10	0+9	0+18	-15-40

Table 4.3. Zeta potential change after EK treatment at 20 Am^{-2}

Time, h	5:5	5:10	5:15	5:20	Continuous	Control
0	-20-40	-20-40	-20-40	-20-40	-20-40	-15-40
24	-5+5	-5+5	-12+15	-5+5	-8+10	-15-40
48	-6+10	-5+10	-10+15	-3+5	-10+10	-15-40
72	0+5	-10+15	-10+15	-2+4	-5+5	-15-40
96	-6+8	-7+10	-10+15	0+10	-5+6	-15-40
120	0+8	0+12	0+14	0+6	0+10	-15-40

All current densities (12, 15 and 20 Am^{-2}) demonstrated substantial changes of zeta potential magnitude, whereas a current density 20 Am^{-2} showed the most significant destabilization of the system. Results demonstrate that the magnitude of zeta potential was reduced significantly

under different time cycles. Some essays demonstrated positive zeta potential as well. The mechanisms that contribute to such changes in zeta potentials under higher value of current density are related to the amount of the Al species in the solution generation of which leads to the neutralization of the negative charge on the particles surfaces until a positive zeta potential is reached.

4.1.8. Particles Size Distribution

The volume-based frequency distribution which represents a qualitative assessment demonstrated that EC resulted in substantial aggregation of particles that formed dense flocks. The mean particle size distribution (PSD) of floc size changed over the operating period based on the current density. Current density 12 Am^{-2} resulted in a significant increase of particles size compared to control sample (Figures 4.36 and 4.37). The highest impact was demonstrated by 5-On: 20-Off time cycle.

Current density 15 Am^{-2} also demonstrated a substantial increase of aggregates size for all time cycle modes, even with a higher outcome (Figures 4.38 and 4.39).

At 20 Am^{-2} particles size increased the most (Figures 4.40 and 4.41). For instance, the mean PSD increased for up to 25% at 5-On: 5-Off, 15% at 5-On: 10-Off, 20% at 5-On: 15-Off, 50% 5-On: 20-Off and 25% at continuous-On, respectively.

The collapse of smaller particles and formation of larger aggregates was attributed to the reduction of the repulsive forces between the particles as the magnitude of zeta potential approached to zero. This pattern of was observed as soon as the current was applied and the density was strong enough to cause the flocculation of particles.

The maximum PSD observed during this experiment was not necessarily the highest size produced in the reactor. It is probable that the aggregates were larger than represented as they might be broken to some extent by the mixing shear in the magnetically stirred cell of the particle size analyzer.

It should be also noted that once the maximum floc size is reached, the removal of bound water through electroosmosis is likely to cause subsequent reduction of flocs size [189, 272]. Since sampling for PSD measurements was taken once per day, there is not possible to know with certainty the maximum size of the particles. Furthermore, longer time-off modes demonstrated better results, which makes drawing relationship patterns more difficult. Nonetheless, it is

extremely important to confirm that direct current is able to cause particles collapse and flocculation, and improve overall treatment performance.
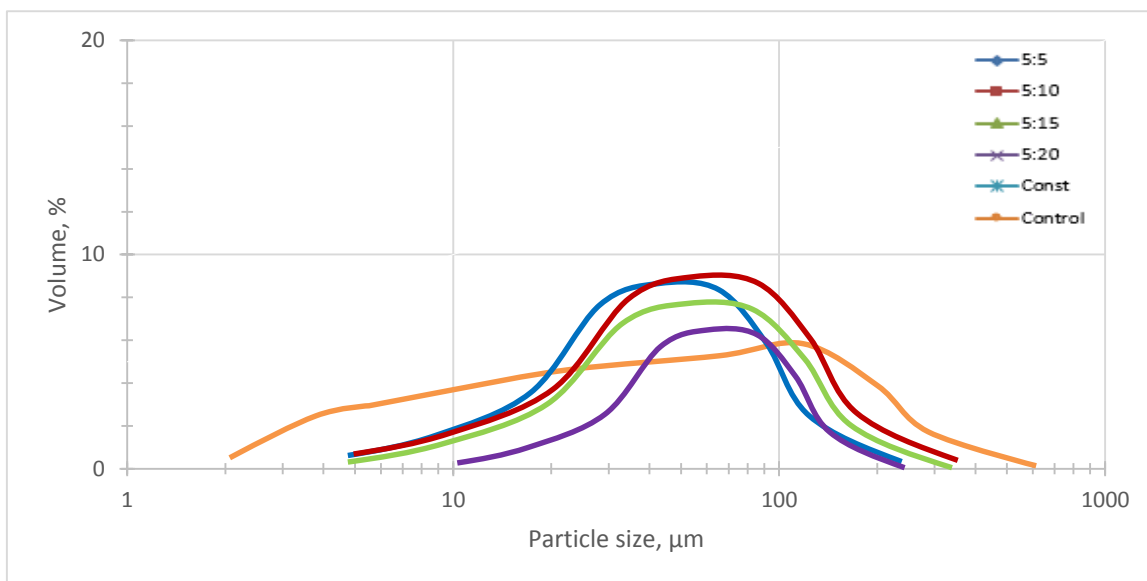
Figure 4.36. E1: PSD after 120 hours 12 Am^{-2} and 1.0 Vcm^{-1}
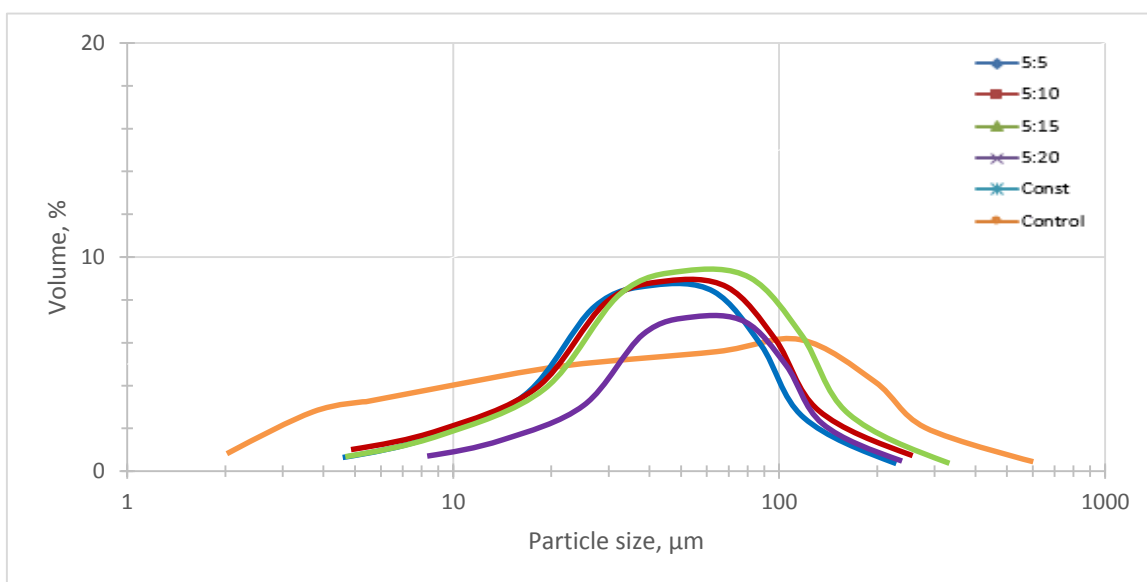
Figure 4.37. E2: PSD after 120 hours 12 Am^{-2} and 1.5 Vcm^{-1}
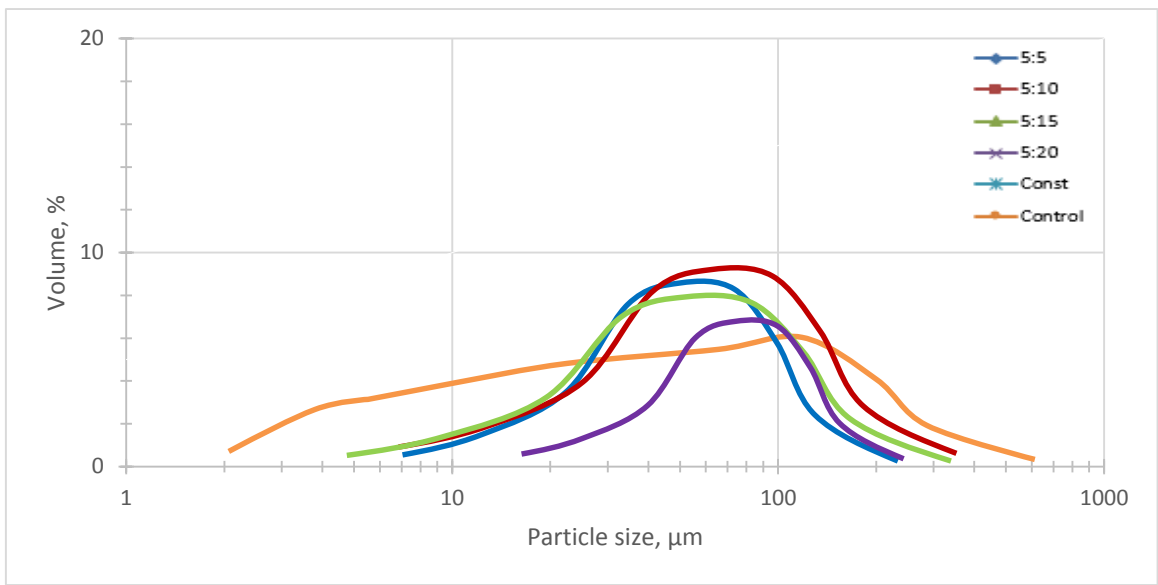
Figure 4.38. E3: PSD after 120 hours 15 Am^{-2} and 1.0 Vcm^{-1}
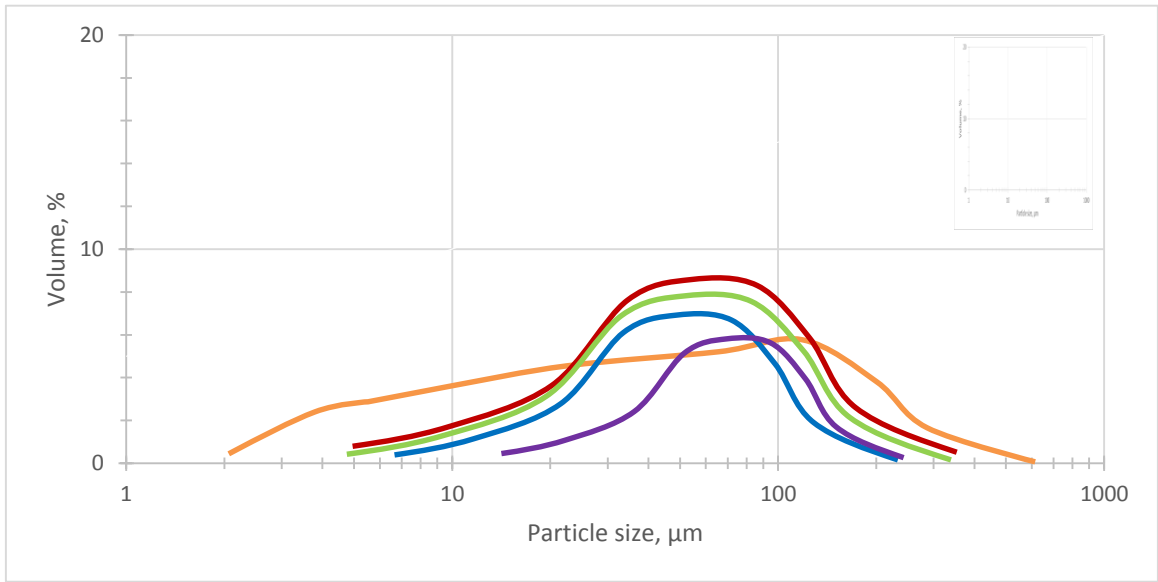
Figure 4.39. E4: PSD after 120 hours 15 Am^{-2} and 1.5 Vcm^{-1}
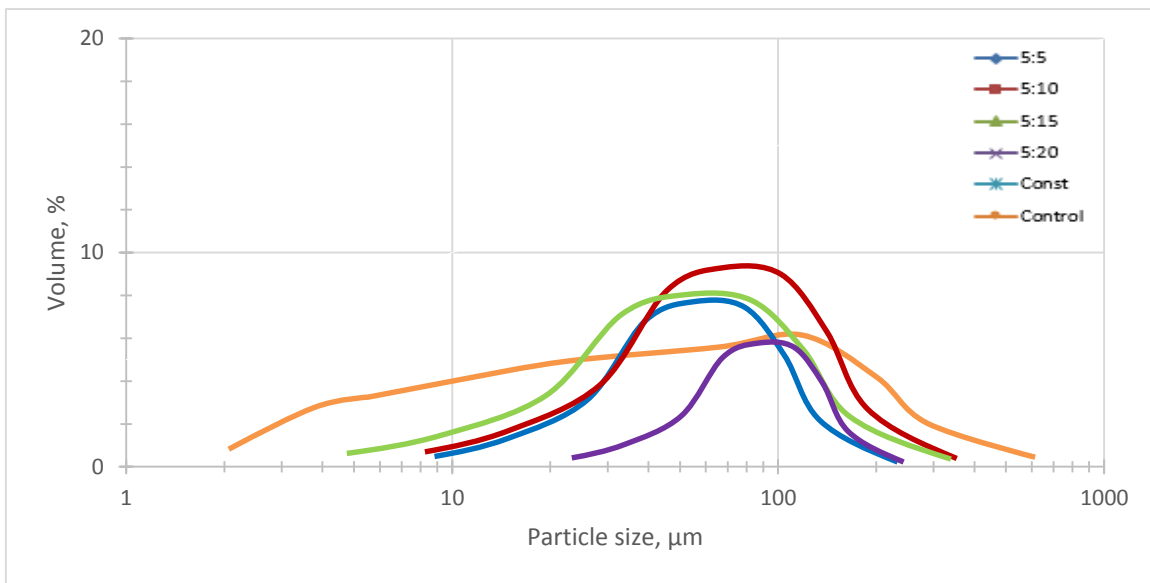
Figure 4.40. E5: PSD after 120 hours 20 Am^{-2} and 1.0 Vcm^{-1}
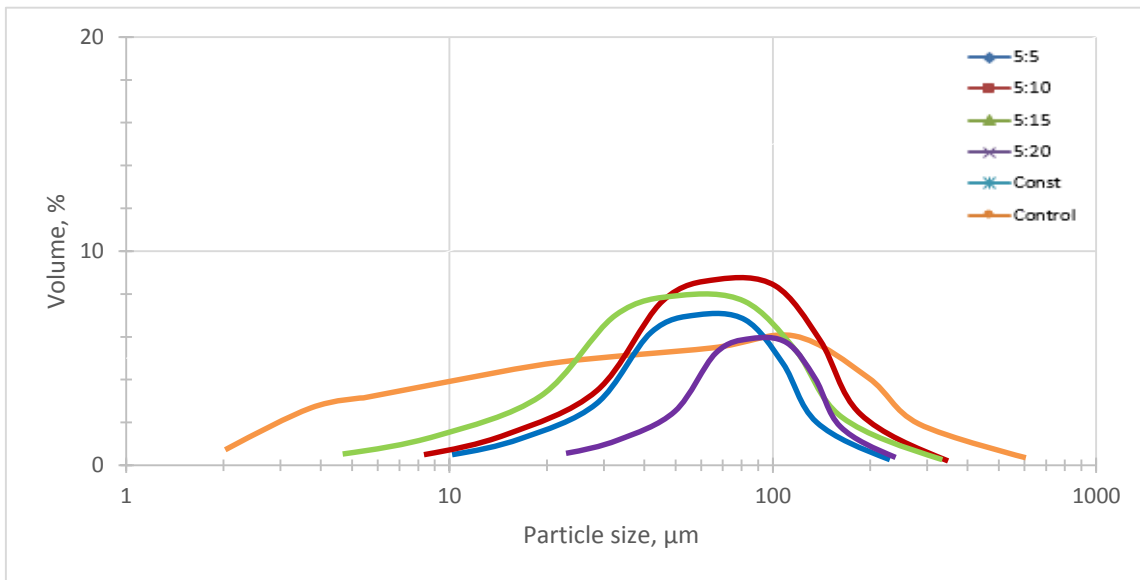
Figure 4.41. E6: PSD after 120 hours 20 Am^{-2} and 1.5 Vcm^{-1}

4.1.9. Phase I: Conclusions and Recommendations

The experimental phase demonstrated the changes to the waste water properties in terms of COD, TN, TP, and color as a result of applying direct current field. These changes are dependent on the current density and electrical switch-on: switch-off mode. All electrical

modes and CDs demonstrated significant improvement in the waste water effluent quality. Continuous-On mode did not show a significantly better performance compared to the other electrical modes, especially with short-On: long-Off regimes. Therefore, it is possible to reach the same treatment efficiency with lower energy consumption.

All current densities demonstrated significant performance in reduction of COD with up to 90% removal efficiency at 20 Am^{-2} with 5-On: 20-Off regime.

The removal efficiency of nitrogenous compounds in 120 min reached 59% for 12 Am^{-2}, 15 Am^{-2} and 80% for 20 Am^{-2}, respectively. Based on the experimental results, higher current densities were more effective in the removal of TN at all time cycles. However, longer time-on cycles were performing slightly better and substantially reduced TN concentration in the waste water, especially by the end of runs.

In terms of phosphorous removal, better results were achieved at current density 15 Am^{-2}, where the TP removal rate was up to 76% with the greater efficiency demonstrated by 5-On: 5-Off and 5-On: 20-Off modes. Current density 20 Am^{-2} was slightly less effective (up to 70%).

Maximum decolourisation of 96% was achieved after a run time of 120 min for essay E4 and E6 at 5-On:5-Off and 5-On:20-Off with better performance at 20 Am^{-2}.

Therefore, operation under these lower current densities is less effective and may result in underperformance of the system. Thus, selecting a current density at 20 Am^{-2} as an electrical operating parameter is recommended with 5-On: 20-Off period as it performed the best in terms of COD, TN, TP and color removal.

Particles size analysis suggested that at 20 Am^{-2} particles size increased the most forming dense flocks. For instance, the mean PSD increased for up to 25% at 5-On: 5-Off, 15% at 5-On: 10-Off, 20% at 5-On: 15-Off, 50% 5-On: 20-Off and 25% at continuous-On, respectively. These electrical modes and current densities are expected to improve the effluent quality. Thus, these parameters were carried forward for subsequent phases of experiments.

4.2. Phase II: Results and Discussion

This chapter represents state of the findings during the experimental Phase II. The results and discussion are structured and provided for Stage I and II, and a comparative analysis between the stages summarizes the chapter.

4.2.1. Stage I: Operation in the AnMBR Mode

In the Stage I of Phase II, the reactor was operated for 30 days as AnMBR without involvement of electrokinetic phenomena. This stage was designed as a reference for comparison purposes. Research of the electrokinetics phenomena impact on the physical, chemical and biological properties of the MLSS solution could not be achieved without this initial operation of the AnMBR system. This stage was extended for 30 days after allowing microbial community to acclimate and reach steady-state condition.

4.2.1.1. Impact of the AnMBR Operation on the Physico-chemical Properties

A research was undertaken to determine the role of physical and chemical properties in the treatment performance of AnMBR system. Monitoring changes in these properties permitted also improved prediction of the treatment potential of the novel system.

4.2.1.1.1. Changes in pH

The optimal range of bacterial growth in terms of pH depends on archaea, however in most cases is within limits in minimum and maximum range near 5 and 9 respectively. In Phase II, the pH values were measured daily. The variations of the pH values in the influent, the MLSS solution in the reactor and the treated effluent are presented in Figure 4.42.

For the first 10 days of Stage I, the pH values remained relatively stable in the AnMBR system (5.3-5.5), and were associated with changes of the pH in the influent from 5.5 to 5.2. These fluctuations were related to the changes of pH of the influent wastewater due to, a slow degradation process of organic materials in the feed storage tank. The same phenomenon was observed by other researchers, however in a greater magnitude [135].
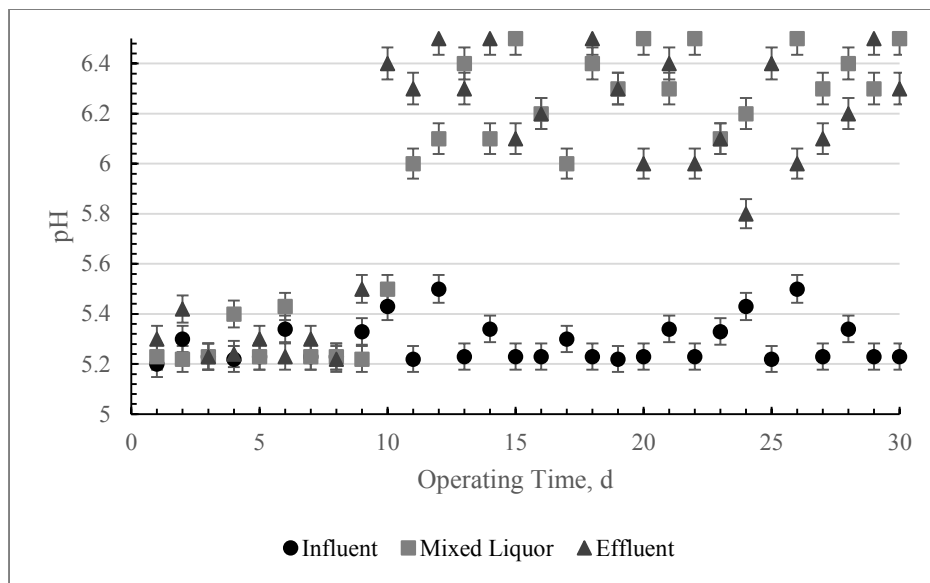
Figure 4.42. pH Changes during the Stage I of Phase II

The changes in the pH during the first stage of operation did not have a negative impact on the MLSS concentration, as well as on changes in nutrients species concentration as the microbial community had been adapted to pH of the system during the acclimation process. It was also observed that the influent pH did not have significant impact on the pH values in the EAnMBR system during the Stage I. The effluent pH was correlated with the system pH during the Stage I, when the DC was not applied to the system (Figure 4.42).

4.2.1.1.2. Temperature

Since temperature influences the rate of biochemical reactions, the changes in temperatures of the influent, the MLSS solution and the treated effluent were recorded and presented in Figure 4.43. The temperature of the influent was oscillating around ambient temperature (21 ± 2 ^{0}C). The heated blanked provided stable thermal conditions for mesophilic communities inside the reactor, therefore, the temperature of MLSS was 36 ± 1 ^{0}C and the effluent slightly lower (around 30 ± 1 ^{0}C). In general, the change in temperatures in the AnMBR was as following: Influent temperature < Effluent temperature < Temperature in the reactor. As it was shown in recent study, the higher temperature and longer duration of treatment affect organic matter solubilisation and lowering yield stress for longer duration of treatment [277]. As was found, regardless of sludge concentration, the ratio of yield stress measured at different treatment time to initial yield stress was linearly proportional to released soluble COD. Thus, at any sludge

concentrations, the longer the treatment time, the lower was yield stress and this yield stress reduction was proportional to the increase of released solubilised COD.
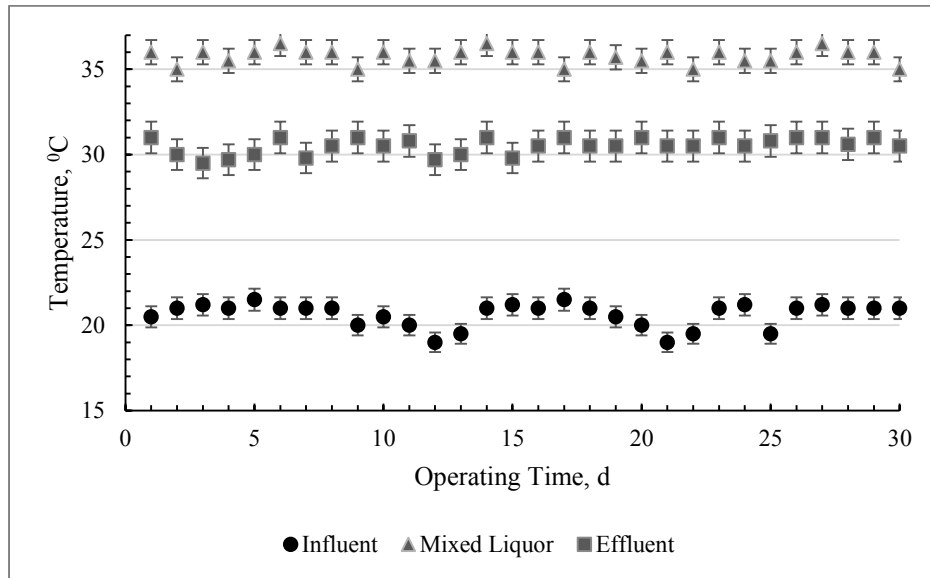
Figure 4.43. Changes in temperature during Stage I of Phase II

4.2.1.1.3. Impact of the AnMBR Operation on Specific Resistance to Filtration

During the operating period, the specific resistance to filtration (SRF) of the colloidal particles in the reactor was monitored every 10 days and at the end of the Stage I as shown in Figure 4.44. All the measurements were compared to the SRF of the MLSS solution at the beginning of the operation of the EAnMBR system. According to Carman-Kozeny [278], the specific SRF of the particles is inversely proportional to the square of particle diameter. Therefore, the SRF is a good indicator of the size fractions of the colloids.

After 10 days of operation, the results of the SRF analyses provided in Figure 4.44 during Stage I did not show significant changes in the SRF. This fact suggests that the particle size of the colloids remained relatively of the same size during the first ten days of operation as the microbial community was still adapting to the environment.

A small improvement was observed in the SRF on day 20 and day 30 of the Stage I which may be attributed to growing particle sizes and associated with an increase of the MLSS flocs size. This is in agreement with other studies [83, 279, 280]. Since the colloidal fraction of mixed

liquor plays significant role in the membrane fouling, the coagulation of colloids is a determining factor of a successful treatment process.
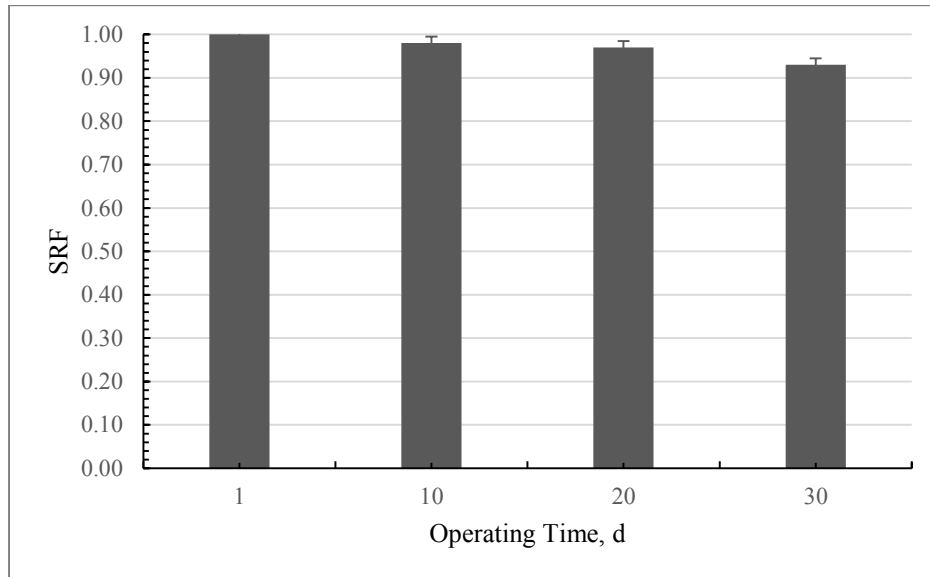
Figure 4.44. Changes of specific resistance to filtration of the MLSS solution Stage I

The relation between filterability and MLSS concentration can be explained by the characteristics of the activated sludge mass and the gel layer of membrane which accounts for pore plugging and is considered as irreversible membrane fouling due to the adsorption of foulants onto the membrane surface by colloids and solutes in the supernatant [281]. In sludge with an MLSS content below an apparent critical concentration, fouling particles are available in the free water of the activated sludge bulk. As opposed, in sludge with a high MLSS content, i.e. above a critical concentration, and moderate to good filterability, fouling particles become entrapped in the sludge matrix [282]. On day 30 (the end of Stage I), no significant improvement was observed and the SRF decreased by 4% compared to the initial phase of the operation.

4.2.1.1.4. Impact of the AnMBR Operation on Sludge Volume Index

SVI is one of the most important parameters for sludge flocculation and settling properties assessment. SVI is defined as the volume in millilitres occupied by 1 g of a suspension after 30 min of settling in a 1 L cylinder [271]. The lower the SVI, the denser the settled sludge,

and therefore better sludge settleability. For domestic wastewater, an activated sludge with a SVI below 70 mLg^{-1} indicates pin flocs, whereas over 150 mLg^{-1} is considered bulking [271]. However, industrial wastewater systems operating with SVIs of 300 mLg^{-1} consistently produce excellent effluent quality and are quite common. The results of SVI measurements taken every 5 days are presented on Figure 4.45.
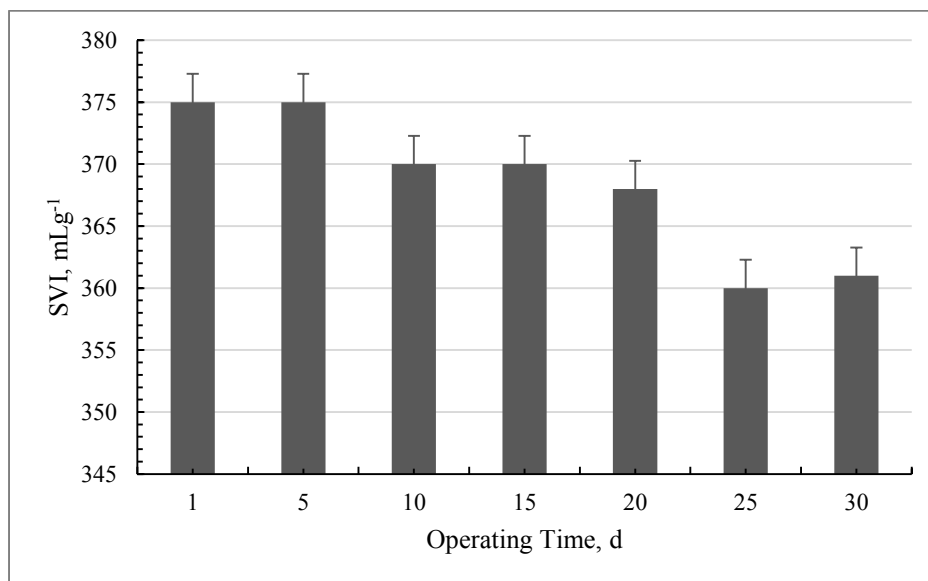
Figure 4.45. Changes of SVI during the Stage I of Phase II

It could be summarized that the SVI during the Stage I in AnMBR mode was within 360 - 375 mLg^{-1} range with better settling characteristics towards the end of the stage. The slight change could be observed on the day 10 of the study. This could be explained by the microbial communities starting activity inside the reactor and formation of denser flocs, respectively. However, the maximum reduction in SVI was 2.6% compared to initial state.

4.2.1.1.5. Role of Particles Size Distribution

During the Phase I, the wave cycles of floc PSD noticed with distinct peaks on day 4, 11, 19 and day 30. Each peak was followed by a decline as presented on Figure 4.46, suggesting a multistage-stage flocculation process was observed during this study. The peaks could be attributed to formation of larger flocs as a result of aggregation of bio flocs. And decline could be associated with soluble microbial product (SMP) release and break of aggregates. Changing of PSD was similar to that of Phase I during the preliminary study. The mean PSD in the

AnMBR mode reached its maximum value at 123.2 µm at the end of the stage on day 30 as biological process peaked as well. The particles PSD increase was 11% (from the mean 109.6 µm). The cyclical increase of PSD was related to the formation of larger EPS particles as a result of biological activity [136]. The magnitude of zeta potential in the AnMBR at the same time was between 22 and -38 mV, and, as can be seen in the following section, was not related to PSD.
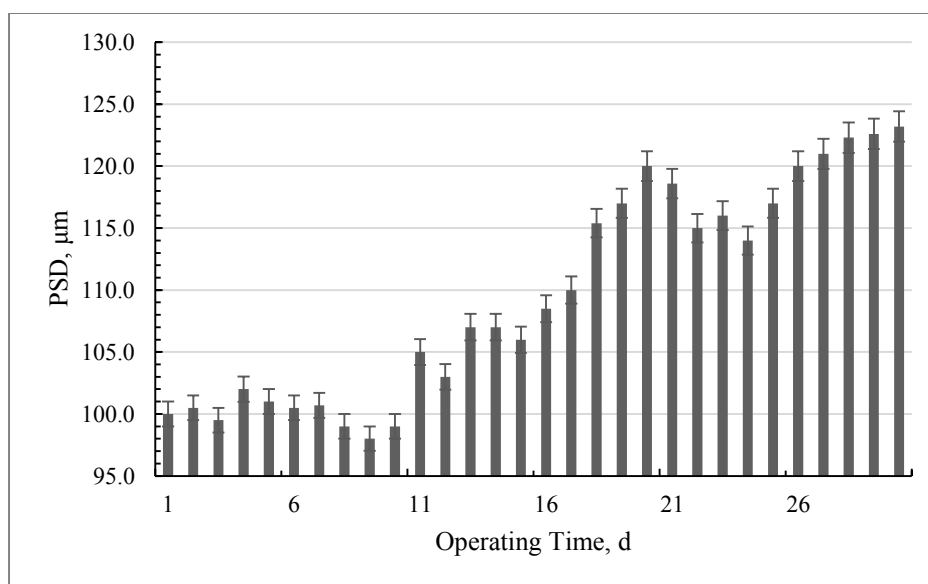
Figure 4.46. Changes in PSD in the AnMBR over time

4.2.1.1.6. Role of Zeta Potential

Zeta potential is a measure of the magnitude of the electric potential in the electric double layer, and the electrostatic repulsion/attraction forces between particles. The magnitude of particles aggregation in the electro-bioreactor was verified by measuring the zeta potential of colloids in the aqueous phase. In this research, zeta potential was used to estimate the mobility of particles affected by combined physicochemical and biological processes in the AnMBR system. The magnitude of the zeta potential provides an indication of the potential stability of the colloidal system. If particles have a large negative or positive zeta potential, the colloidal system is stable and the interaction between the particles is insignificant. When particles have low zeta potential values, the system shifts towards instability and the formation of aggregates

is more likely as there is no significant force to prevent the particles collapsing. The results of the zeta potential measurements during the Stage I are presented in Figure 4.47.
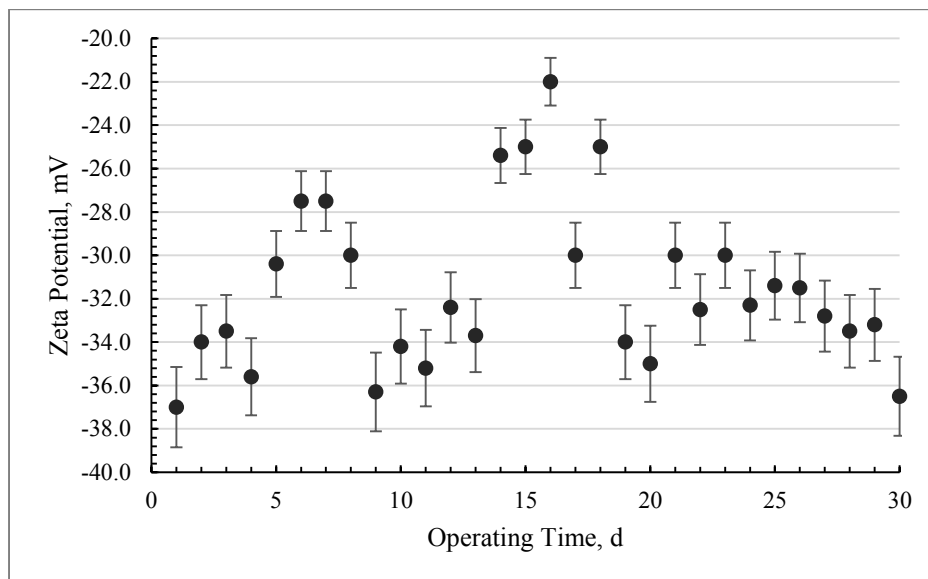
Figure 4.47. Changes in zeta potential in the system during the Stage I of Phase II

During the first stage of operation, the zeta potential oscillated within the range between -22 and -38 mV, with average value of -32 mV. Thus, this value was close enough to the zeta potential -30 mV which is required for interaction. Therefore, applying a DC potential into the colloidal system can reduce the Van der Waals forces that prevent the collision of colloids.

4.2.1.2. Impact of the AnMBR Operation on the Biomass Characteristics

Figure 4.48 provides results on the variations of the MLSS and the MLVSS concentrations in the reactor during the AnMBR operation. MLSS and MLVSS samples that were taken for analyses from the AnMBR did not demonstrate notable differences. This can be explained by the good mixing conditions inside the system and the uniform distribution of mixed liquor suspension in the AnMBR provided by a mechanical stirring and gases resulted from the anaerobic activity. During the first 14 days of the Stage I, a gradual increase of the MLSS concentration was observed- the sludge concentration slowly increased from initial concentration 5,000 mgL^{-1} and reached an average of 5,500 mgL^{-1}. An explanation for the phenomenon of the relatively constant sludge concentration during this period of the Phase I

might be due to the long HRT and SRT, and slow activity of anaerobic process as well. At a relatively constant concentration of the substrate in the influent 4 days HRT, food to microorganism ratio (F/M) also was stable during the operating period and equal to 0.20 g CODg^{-1} MLSSday^{-1} on average. From day 14 until the end of the Stage I, the MLSS concentration in the vessel was relatively stable and remained 5,500 mgL^{-1}. This was confirmed by the stable MLVSS/MLSS ratio during Stage I. MLVSS/MLSS ratio during the entire Stage was around 84%, indicating that little inorganic matter accumulated in the AnMBR.
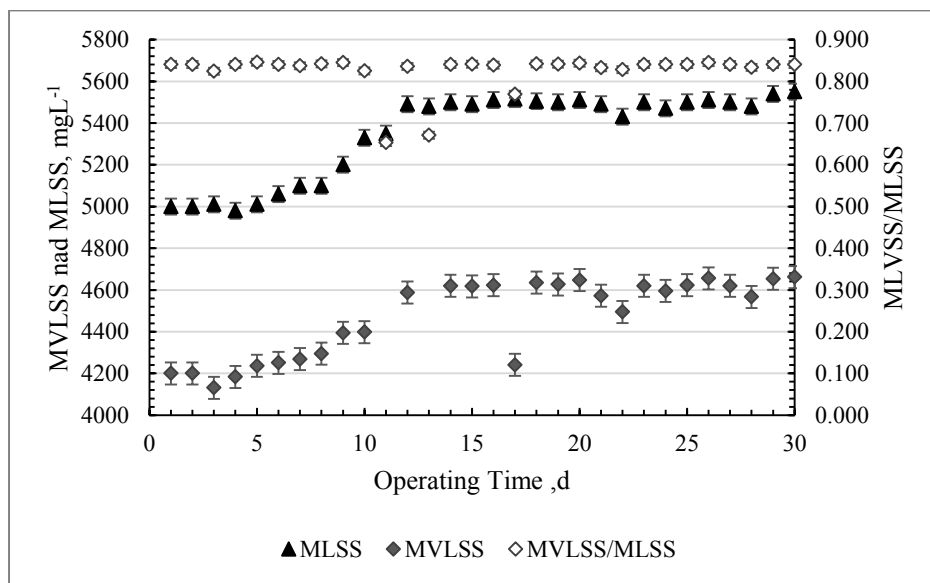
Figure 4.48. Changes of the biomass characteristics during the Stage I

4.2.1.3. Impact of the AnMBR Operation on the Wastewater Quality Properties

To calculate the wastewater treatment efficiency and quality parameters, the input and the output streams to/from the reactor and the membrane module were taken into account. The efficiency of membrane filtration process was measured in terms of pollutants concentrations. The removal efficiency (%R) is given by the following equation:

$$\%R = \frac{C_F - C_P}{C_F} \times 100\% \tag{4.1}$$

where C_F is the concentration of the pollutant in feed stream (mgL^{-1}) and C_P is the

concentration of the pollutant in permeate stream (mgL^{-1}). Because the EAnMBR consists of the electro-bioreactor vessel and membrane module, the removal efficiency of the bioreactor alone was calculated as follows:

$$\%R_{vessel} = \frac{C_F - C_R}{C_F} \times 100\% \tag{4.2}$$

where C_R the concentration of a pollutant (COD, ammonia, nitrate, nitrite etc.) in the supernatant in the reactor (mgL^{-1}).

4.2.1.3.1. COD Removal Mechanism

Figure 4.49 illustrates the changes of the COD concentration in the influent, in the reactor and the treated effluent during the Stage I. The removal efficiency of the COD in the electro-bioreactor and of the whole system is expressed by equations (4.1) and (4.2) respectively. The removal efficiency varied between 79.20% and 89.46% with average 85.51% during Stage I, which indicates that the system was able to provide consistently high removal rate throughout the entire Stage I. The concentration of COD in the effluent was reduced from 4,793±200 mgL^{-1} to 719±100 mgL^{-1} (on average).

The total COD removal efficiency of the system was maintained at a constantly high level due to the combination of anaerobic biological treatment with efficient membrane filtration. The data obtained during the investigation confirmed that the membrane module played significant role in the AnMBR processes. During Stage I, degradation due to microbial activity increased from 3% at the beginning to 75% towards the end. Microorganisms, adapted to the electron donor, might broke long-changed and larger organic molecules to smaller-size ones that could be transferred through the cell membrane and used as a source of energy for metabolic activity. The membrane system contributed from 15% to 50% towards the overall removal efficiency. The membrane contribution increase could be associated with the biological process of removal of particles which could block membrane pores and form cake layer on the surface. As the rate of biological activity increased, the interfacial shear stress induced by anaerobically-produced gas bubbles might prevent formation of the cake layer on the membrane surface as well. Contribution of the biological processes and membrane module towards the removal process is presented on Figure 4.50.
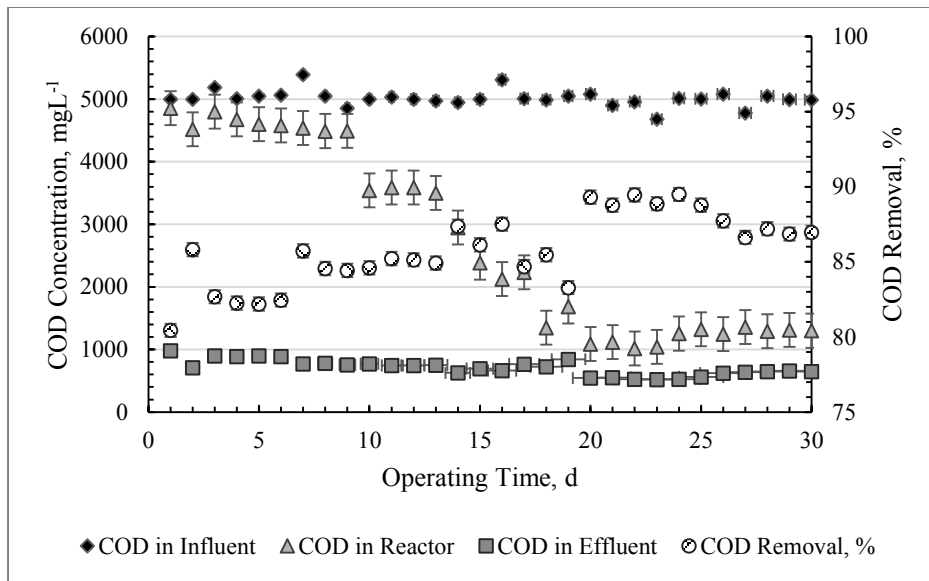
Figure 4.49. Changes in COD concentrations and percentage removal in Stage I
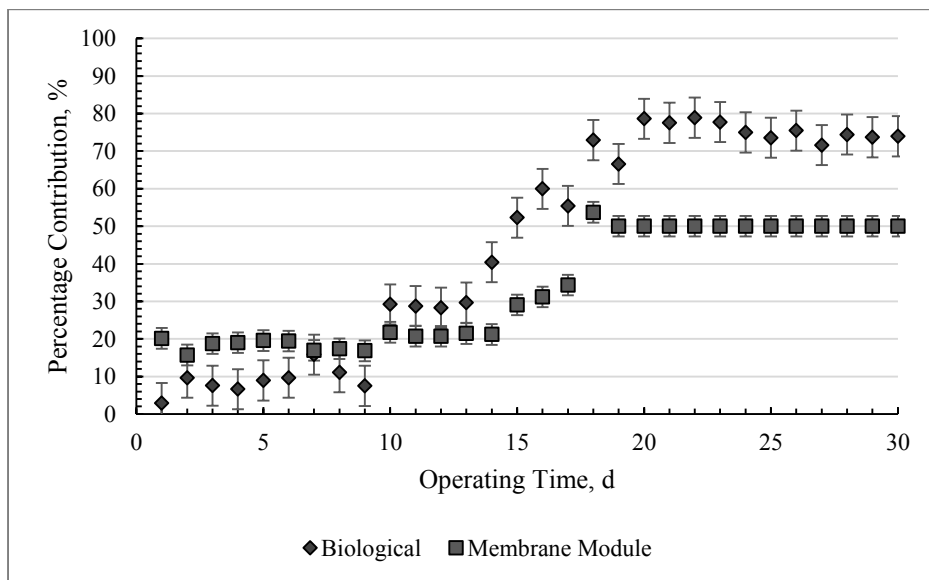
Figure 4.50. Contribution of membrane module and biological activities to COD removal in Stage I

4.2.1.3.2. Nitrogen Removal Mechanism

In anaerobic conditions, members of the *Planctomycetes phylum* group of bacteria, are capable of oxidizing ammonium using nitrite instead of oxygen and producing N_2 instead of nitrite [102]. This metabolism is strictly anoxic and the process is known as anaerobic ammonia

oxidation, or anammox. Anammox organisms are unique in many of ways; the pathway for oxidation of ammonium involves hydrazine, as an intermediate. Anammox organisms are strict autotrophs and utilize the acetyl-CoA pathway for CO_2 fixation. Nitrifying bacteria convert ammonia nitrogen (NH_3-N) to nitrate nitrogen (NO_3-N) in a nitrification reaction according to following reactions [102]:

$$NH_4^+ + NO_2^- \rightarrow N_2 + 2H_2O \tag{4.3}$$

This process requires nitrite which is generated by nitrification of ammonia:

$$NH_4^+ + 1.5O_2^- \rightarrow NO_2^- + H_2O + 2H^+ \tag{4.4}$$

And by denitratation of nitrate:

$$NO_3^- + 2e^- + 2H^+ \rightarrow NO_2^- + H_2O \tag{4.5}$$

In carbon and sulfide rich environment, anammox process is combined autotrophic denitratation using sulphide and/or acetate as an electron donor and known as deamox:

$$NO_3^- + 0.25HS^- \rightarrow NO_2^- + 0.25SO_4^{2-} + 0.25H^+ \tag{4.6}$$

$$NO_3^- + 0.25CH_3COO^- \rightarrow NO_2^- + 0.5HCO_3^- + 0.25H^+ \tag{4.7}$$

$$NO_3^- + 0.25CH_3COO^- + NH_4^+ \rightarrow N_2 + 0.5HCO_3^- + 0.25H^+ + H_2O \tag{4.8}$$
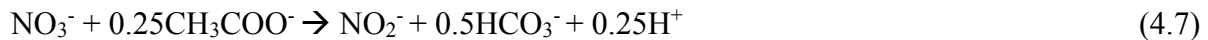
Consequently, the change in ammonia concentration can be used as an indirect measurement in the changes in the nitrification process. In Phase II of this research, the fluctuations of the nitrogen concentration in the influent, the supernatant of the reactor and in the treated effluent along with the corresponding removal performance of the AnMBR system are represented on Figure 4.51. The average concentration influent was 939 ± 3 mgL^{-1}. The concentrations in the effluent fluctuated in Stage I it decreased from 58 mgL^{-1} during the first day of operation to below 41 mgL^{-1} at the end of Stage I.
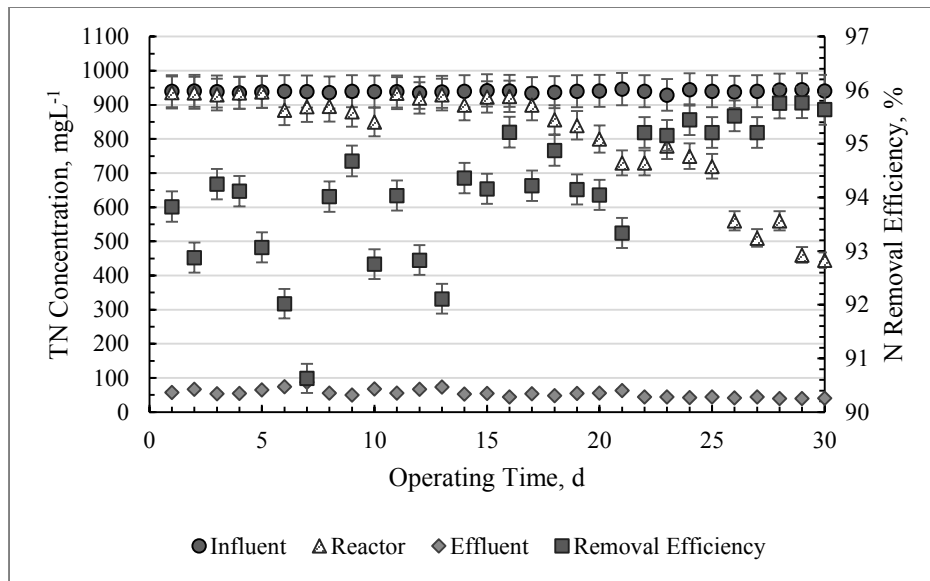
Figure 4.51. Changes in nitrogen concentrations in the system during the Stage I

The removal rate of total nitrogen in the effluent started with 94±1 % and was around 95±1 % at the end of the Stage I indicating relatively stable and high removal efficiency. The concentration of TN in the reactor was 936 mgL^{-1} at the day 1 and reached 445 mgL^{-1} at the day 30. Noticeable increase of removal rate in the reactor, however, was achieved after day 20 and reached about 53% at the end of the Stage I. The low removal efficiency of nitrogen during the first days of the Phase II in the vessel was attributed to the low growth rate of anaerobic nitrifying bacteria and, consequently, a slow anaerobic ammonium oxidation process, as these bacteria require more time to reach sufficient concentrations [101]. The removal efficiency comparison by biological process and by the membrane module is presented on Figure 4.52. Analysis of the data presented on Figure 4.52, suggests that gradual increase in ammonia oxidation performance started only after 20 days of the Stage I, however the removal performance of the membrane module was constant during the entire Stage I operation. Therefore, both the anaerobic nitrification process and the filtration through the membrane module were primary mechanisms responsible for major part of ammonia removal.
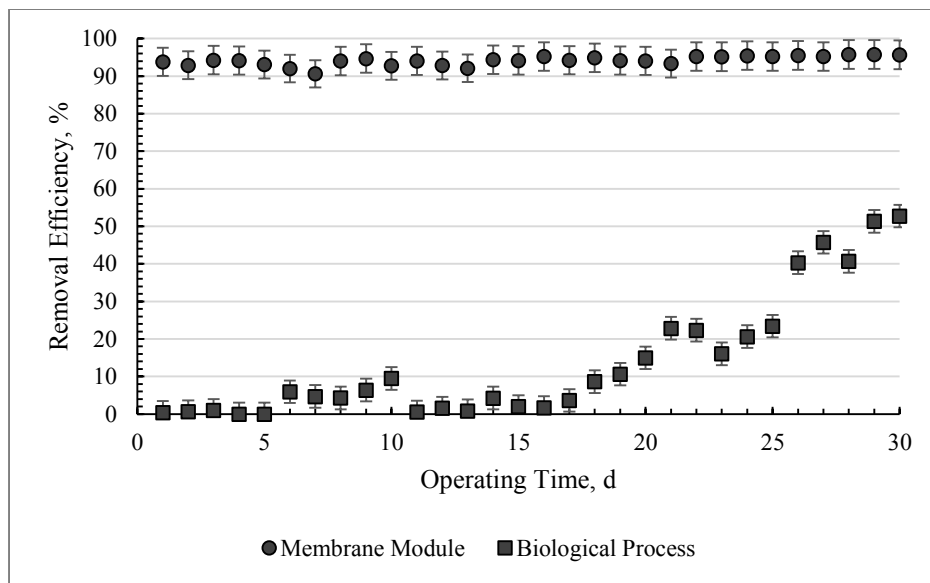
Figure 4.52. Removal efficiency comparison by biotic processes and membrane module

4.2.1.3.3. Phosphorous Removal Mechanism

Advanced biological phosphorous removal processes can lower the total phosphorous (TP) concentrations in the effluent to 0.1–0.2 mgL^{-1}, however, supplemental additions of Al or Fe(III) salts, polymeric coagulants such as poly-aluminum chloride (PACl), and/or lime for coagulation purposes are often required to maintain acceptable effluent TP concentrations [106]. Chemical coagulation decreases filtration time due to removal of soluble and particulate materials that could deposit onto membrane surface and into the membrane pores. However, chemical coagulation inevitably increases amount of produced sludge in case of MBRs which is a significant problem. One of the main objectives of designing the proposed AnMBR system was to enhance phosphorous removal from industrial wastewater.

The main phosphorus compounds in wastewater are generally orthophosphate (PO_4-P) forms along with smaller amounts of organic phosphate [135]. TP which is defined as the sum of all phosphorus compounds that occur in various forms was measured as a performance metric in phosphorus removal efficiency. The variations of total phosphorus concentration in the influent, the supernatant in the bioreactor and the treated effluent are presented in Figure 4.52. Figure 4.53 presents the corresponding removal efficiency of TP of the bioreactor and for the overall AnMBR during the Stage I.
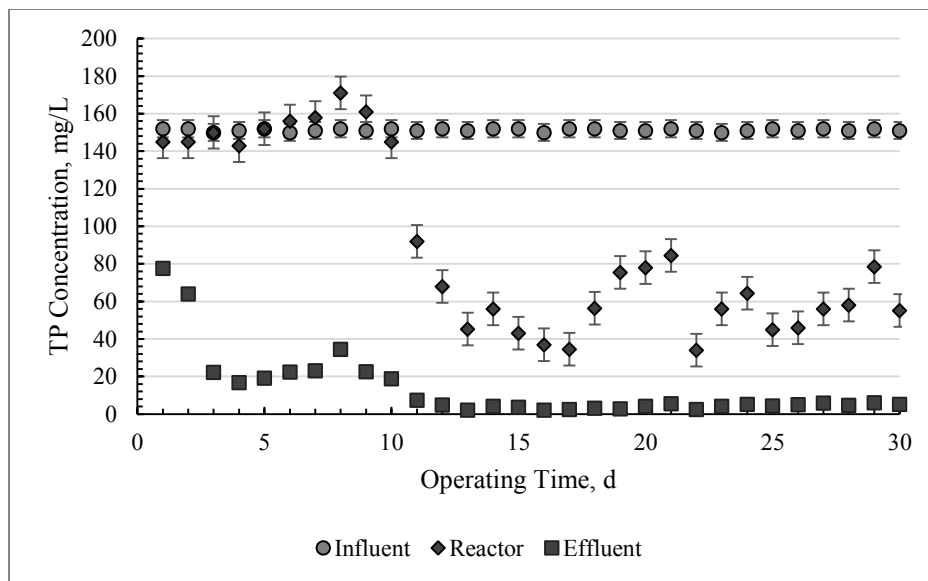
Figure 4.52. Changes in TP concentrations during the Stage I

The influent concentration of phosphorus measured as TP in the feed was 151 ± 1 mgL^{-1}. The concentrations of TP in the reactor was 145-150 mgL^{-1} at the beginning of the Stage I and reduced to 55.2 mgL^{-1} at day 30 (last day of Stage I) which represented 63.4% efficiency towards the end of the experiment. However, increase of phosphorus concentration was observed from day 5 to day10 in the reactor (peaked at 171 mgL^{-1}) and the effluent as well (34.6 mgL^{-1}). The TP concentration in the reactor during this period exceeded the concentration of TP in the influent. This increase can be attributed to the release of phosphorus by microorganisms in the process of hydrolysis of the phosphate groups in adenosine triphosphate. The concentration of TP in the effluent varied between 16.8 and 77.6 mgL^{-1} in the first days and reached less than 4.5 mgL^{-1} during the last days with minimum value of 1.84 mgL^{-1} during the Stage I. Further increase in the MLSS concentration in the bioreactor enhanced the phosphorus uptake in Stage I which peaked at 77% removal. Although the phosphorus uptake was lower during the initial period of Stage I, Figure 4.53 demonstrates that the AnMBR system had an excellent removal performance in terms of TP removal also due to the contribution of the membrane module to the overall performance. The membrane contributed up to 47% during the first day of operation and reached maximum 96 % at day 19. The overall performance of the system (combined biological and membrane module) was recorded as low as 49% on the first day and progressed up to 97% at the day 30 with maximum during the days 16-22 (98.3%). In general the lowering in TP concentrations were attributed

to membrane filtration during the first phase of Stage I. However, the contribution of the membrane module decreased over the time, and the primary removal mechanism in the second phase was biological activity (MLSS increased from initial 5,000 mgL^{-1} to 5,600-5,700 mgL^{-1}) and raise in pH from 5.3 initially to 6.0-6.7 at the same time.
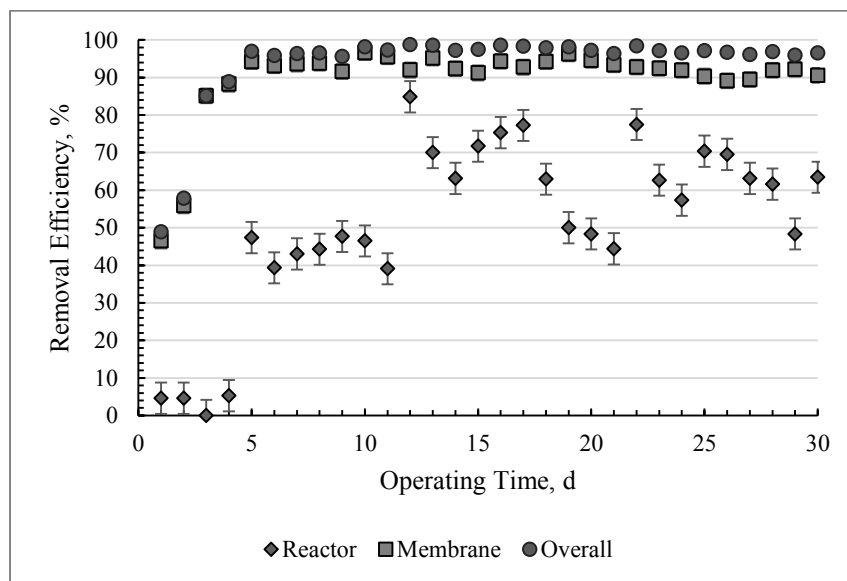
Figure 4.53. Removal efficiency of TP concentration during the Stage I

4.2.2. Stage II: Operation in the EAnMBR Mode

The Stage II was conducted to research the performance of the EAnMBR system when the DC is applied to the MLSS solution in conjunction with the operation of the membrane module. In the Stage II of Phase II of this study, the reactor was operated for 30 days as EAnMBR with DC of 20 Am^{-2} supplied with operational mode 5-On: 20-Off. Research of the electrokinetics phenomena impact on the physical, chemical and biological properties of the MLSS solution was conducted in EAnMBR system for 30 days in order to gather sufficient data for analysis.

4.2.2.1. Impact of the EAnMBR Operation on the Physico-chemical Properties

A research was undertaken to determine the role of physical and chemical properties in the treatment performance of EAnMBR. Monitoring changes in these properties permitted improved prediction of the treatment potential of the novel system for future research. The results presented in this chapter combine outcome from both Stages I and II, i.e. both reactors

AnMBR (1st – 30th day) and EAnMBR (31st – 60th day). Electrical field was applied to AnMBR on day 31st and switched it into EAnMBR.

4.2.2.1.1. Changes in pH

The pH of the mixed liquor after introducing a voltage gradient in the activated sludge was an important parameter for the study of the impact of DC on microbial activities and overall behaviour of the system.

Figure 4.54 shows changes in the pH after applying the voltage gradient. The significant changes began immediately after the beginning of the Stage II, when the pH increased as a result of the electrokinetic phenomena. The increase in the pH solution after applying DC field into wastewater was also observed in other studies and it was attributed to production of hydroxyls at the cathodes associated with hydrogen evolution [134, 140, 283].

 After the first days of operation, a sharp increase in the pH values was observed in the MLSS solutions and in the treated effluent. The pH value of the MLSS solution increased from 6.5 at the end of Stage I to 7.1 at beginning of Stage II and to 8.4 after 3 days of operation, while the effluent pH increased from 7.1 to 8.2.
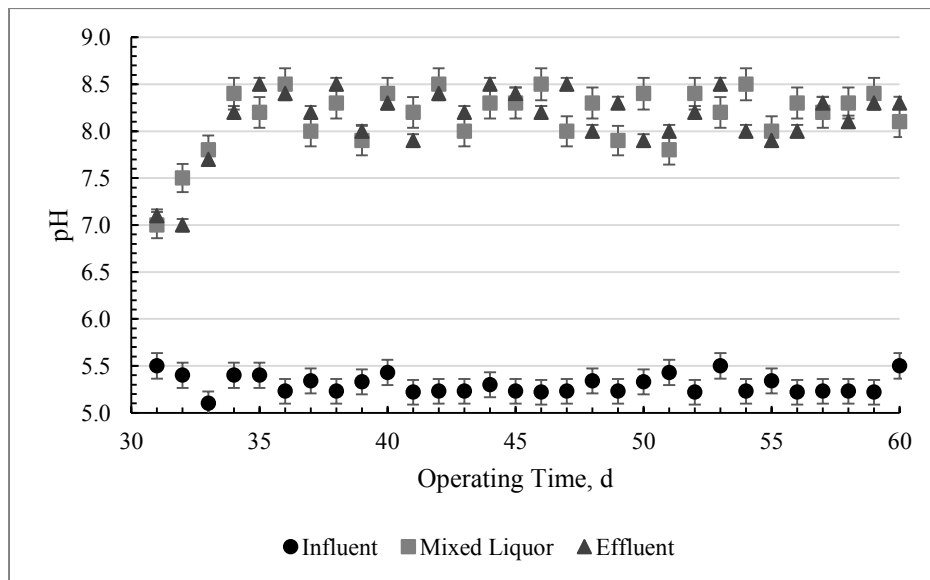
Figure 4.54. pH Changes during the Stage II of Phase II

During the application of the voltage gradient, the changes in the pH of the treated effluent were within the range of 7.0 to 8.3, with the average value of 7.8 which demonstrates that the effluent of the EAnMBR system does not need further adjustment for pH. The increase of pH can be attributed to the design of the EAnMBR system. Equations 4.9 to Equation 4.14 provide the insight into anodic aluminium corrosion in the electrolysis in dilute electrolytes.

Direct electrolytic corrosion of an aluminium anode occurs according to Equation 4.9. $Al(OH)_3$ is formed according to Equation 4.10 at the isoelectric point, however the equilibria shown in Equation 4.11 and Equation 4.12 are more general. Equation 4.12 shows hydrolysis at the isoelectric point [284].

$$Al \rightarrow Al^{3+} + 3e^- \tag{4.9}$$
$$3Al^{3+} + 3OH^- \rightarrow 3Al(OH)_3 \tag{4.10}$$
$$xAl^{3+} + yH_2O \rightarrow Al_x(OH)_y^{(3x-y)+} \tag{4.11}$$
$$Al + 3H_2O \rightarrow Al(OH)_3 + 3/2H_2 \tag{4.12}$$

Reaction of aluminum with electrolytically formed chlorine as shown in the sequence of Equation 4.13 to Equation 4.14 will result in a further hydrolysis similar to Equation 4.10.

$$3Cl^- \rightarrow 3/2Cl_2 + 3e^- \tag{4.13}$$
$$3/2Cl_2 + Al \rightarrow Al^{3+} + 3Cl^- \tag{4.14}$$

Electrolysis of water produces oxygen at the anode in basic conditions, according to Equation 4.15, that could attack the aluminum (Equation 4.16) with the resulting oxide then hydrolysis, albeit slowly (Equation 4.17), to the usual hydroxide at the isoelectric point.

$$3OH^- \rightarrow 3/2O_2 + 3/2H_2O + 3e^- \tag{4.15}$$
$$3/2O_2 + Al \rightarrow 1/2Al_2O_3 \tag{4.16}$$
$$1/2Al_2O_3 + 3/2H_2O \rightarrow Al(OH)_3 \tag{4.17}$$
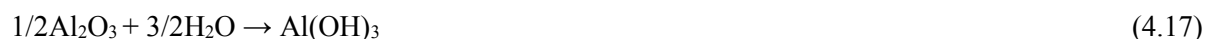
The proportions of current (the current fractions) going into the primary reactions Equation 4.9, Equation 4.13 and Equation 4.15 area. b and c respectively, the secondary and tertiary reactions go virtually to completion, and the overall anodic reaction is represented by Equation 4.18.

$$(a+b+c)Al^{+3}(a+b+c)OH^- \rightarrow (a+b+c)Al(OH)_3 + 3e^- \tag{4.18}$$
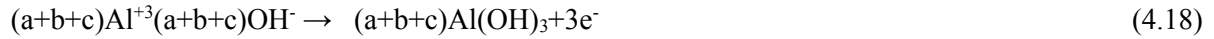
If a+b+c=1, the above equations predict that 1 net mol of acid is added at the anode per mol of electrons transferred, irrespective of the individual current fractions. The cathodic reaction (at a non-corroding cathode) is shown in Equation 4.19 [284].

$$xM^{n+} + yH_2O \leftrightarrow M_x(OH)_y^{n-y} + yH^+ \tag{4.19}$$

Equation 4.19 indicates that 1 mol of acid is consumed per mol of electrons transferred.

In EAnMBR the anodic reactants and products were kept separate from the cathodic versions by a plastic circular baffle as discussed in previous chapter, which was also a support for the electrodes, and the bulk of the flow went through the Anode Zone as anolyte. On the other compartment- Cathode Zone, catholyte, the separately formed and outflew with of different pH. Equation 4.11 suggests that if the anolyte and catholyte are mixed then the outflow will have the same pH as the inflow. When gaseous products of electrolysis were removed from the system and any neither the secondary nor tertiary reactions might not went to completion, then a net pH increase would be expected as it was observed in the Stage II.

Simple chemical corrosion of aluminum by water according to Equation 4.10 and further dissolution in alkaline conditions according to Equation 4.13, produces 1 net mol of acid and 1.5 mol of hydrogen per mol of aluminum consumed [285].

At the isoelectric point of $Al(OH)_3$, by definition, the resulting $Al(OH)_3$ remains uncharged and will precipitate, as in Equation 4.20. At a pH more alkaline than the isoelectric point net hydroxide is absorbed, producing a negatively charged aluminium species and lowering the pH, as shown in Equation 4.21. A series of $Al(OH)_2^+$, $Al(OH)_3$, $Al(OH)_4^-$ is produced by removal or addition of either H^+ or OH^- at appropriate conditions. This hydrolysis series is represented in Equation 4.22.

$$Al(OH)_3 \rightarrow Al(OH)_3 \downarrow \tag{4.20}$$
$$Al(OH)_3 + OH^- \rightarrow Al(OH)_4^- \tag{4.21}$$
$$Al(OH)_4^- + H^+ \leftrightarrow OH^- + Al(OH)_3 + H^+ \leftrightarrow OH^- + Al(OH)_2^+ + H^+ \leftrightarrow OH^- +$$
$$Al(OH)_2^+ + H^+ \leftrightarrow OH^- - Al_3^+ \tag{4.22}$$
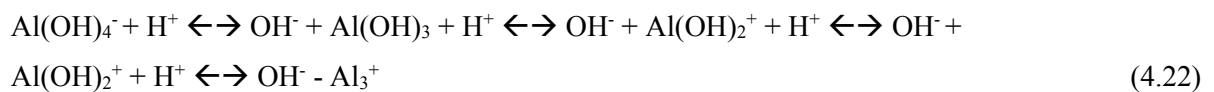
Therefore, the influent pH is an important operating parameter affecting the electrokinetic process in the EAnMBR system, however the most significant change of pH is dependent on the amount of the $Al(OH)_2^+$, $Al(OH)_2^+$, $Al(OH)_3$, $Al(OH)_4^-$ species released into the aqueous phase which is directly proportional to the period of electrolysis.

4.2.2.1.2. Temperature

Results of temperature changes in the system are represented on Figure 4.55. The EAnMBR kept the temperature of 36±1 ^0C degree during the entire experimental period.

Therefore, according to the results analysis of temperature changes, it can be concluded that effect of electrokinetic process on the temperature of aqueous phase was not observable in the EAnMBR during the duration of the entire Phase II. Such conditions provided ideal conditions for anaerobic microbial community growth. Based on the analysis, the order of change in temperatures in the EAnMBR system was as follows:

Influent temperature < Effluent temperature < Temperature in the reactor
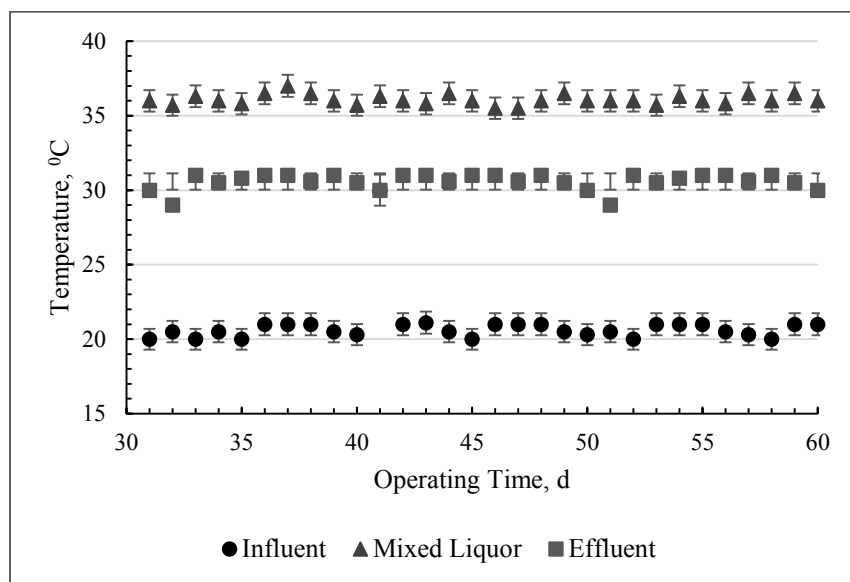
Figure 4.55. Changes in temperature during Stage II of Phase II

4.2.2.1.3. Impact of the EAnMBR Operation on Specific Resistance to Filtration

The SRF of the MLSS solution particles in the EAnMBR was monitored every 10 days and at the end of the Stage II during the operating time as presented in Figure 4.56.

According to a recent study, the electroosmotic dewatering mechanism is principally based on the interplay between the applied electric field and the electric charge density of ions existing in the liquid close to the particle surface [286]. In other words, under the electric current, water displacement is ensured by propagation of ionized mobile liquid on a solid-liquid interface, which drives the neutral liquid in the central channel through viscous momentum transfer. Capillary forces tend also to retain the water [287]. Despite this fact, water can still be released from inner colloids at slow rate even after extended drainage time. The dewatering rate was also influenced by electrochemical reactions at the electrodes, which affect the cake morphology and the chemistry of sludge.
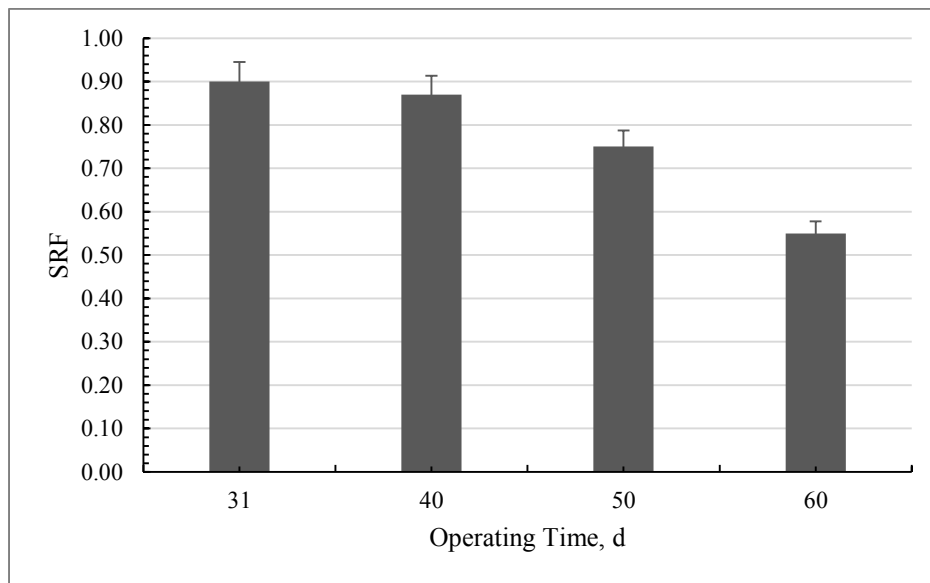
Figure 4.56. Changes of specific resistance to filtration of the MLSS solution Stage II

The possible electrochemical reactions occurring at electrodes made of aluminum are based on the electrolysis of water, producing notably hydronium and hydroxide electrolytic ions and gases [286]:

At the anode: $2H_2O_{(l)} \rightarrow 4H^+ + O_{2(g)} + 4e^-$ (4.23)

At the cathode: $2H_2O_{(l)} + 2e^- \rightarrow 2OH^-_{(aq)} + H_{2(g)}$ (4.24)
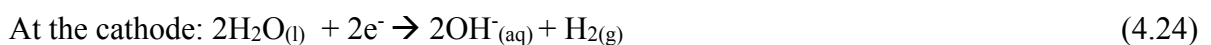
Therefore, the flocs formed by the EC process are relatively large and contain less bound water. They are also more stable thus, amenable to filtration due to formation around inorganic polymers of aluminum hydroxides [135].

The interaction of inorganic aluminum hydroxides with the organic solids created different sludge properties in the EAnMBR comparing to sludge in the MBR. It can be speculated that the process of organic-inorganic particles interactions was enhanced by the direct current (DC) field.

Starting from Stage II, the results demonstrated that the electrokinetic processes in the EAnMBR system, significantly affected the floc size of the MLSS solution. After day 31 of the Stage II, large and dense flocs started to appear which enhanced the overall performance of the solid-liquid separation processes. The effect was observed visually during the preparation the samples for the SRF analyses. The effect of aggregation was also reflected in the sedimentation velocity which increased dramatically after applying the DC field to the system.

A considerable improvement in the SRF was observed after day 31. The SRF decreased by 7% compared to initial phase by day 40 and by 32% at the end of Stage II. A reasonable explanation of the results of Stage II is that the EPS produced by well-developed microbial community and larger aggregates formed by microorganisms. In addition, electrokinetic phenomena might also significantly contributed in dewatering. The results are in agreement with the report about the significant role of the smaller size particles in the activated sludge on the membrane fouling phenomenon [134].

4.2.2.1.4. Impact of the EAnMBR Operation on Sludge Volume Index

Figure 4.57 represents the SVI at current density 20 Am^{-2} while the system was operating in EAnMBR configuration.
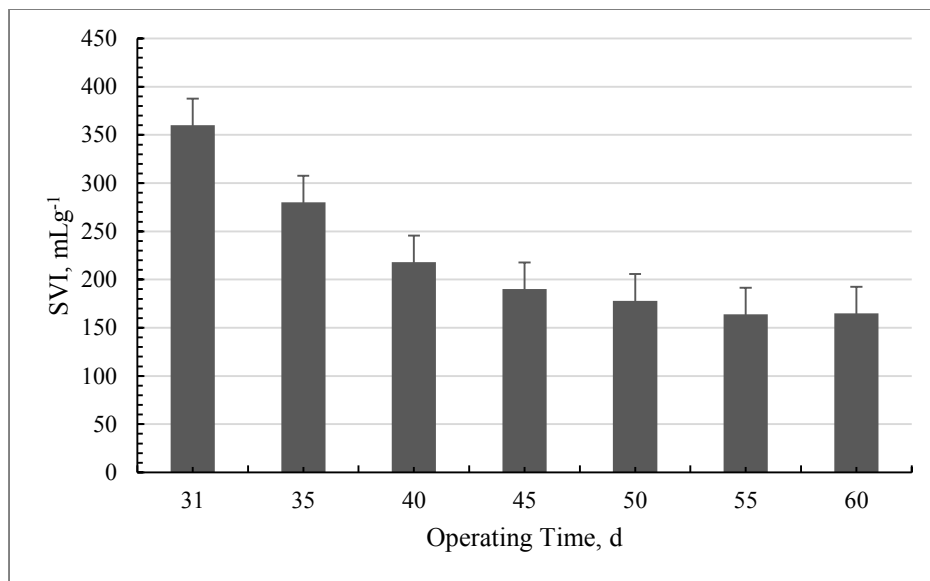
Figure 4.57. Changes of SVI during the Stage II of Phase II

As can be seen, the SVI in EAnMBR reached 164 mLg^{-1} which was significantly lower than in the AnMBR. This could be explained by the application of current density, and, as a result-involvement of electrokinetics. The conductance of current through the electrical double layer causes water molecules to move towards the electrodes through electroosmosis phenomena. Since pH of the sludge liquor observed in this study was alkaline, the solid surfaces were negatively charged and the electrical double layer was dominated by cations. Under a DC field, these cations have a tendency to move towards the cathode simultaneously prompting the movement of bound water molecules. At a current density 20 Am^{-2}, denser colloids were generated and better settleability was achieved after day 35. Similar findings were reported by other researchers for conventional and electro-bioreactors [273, 288]. Reported SVI were 65.8 and 121.5 mLg^{-1} at 47%, and 24%, respectively. During the Stage II, 218 mLg^{-1} was the maximum achieved, which was 54.29% reduction compared to AnMBR.

Based the visual observations and the results of the experiment, it could be concluded that the sludge at 54% reduction had good settleability and no bulky sludge was produced in EAnMBR configuration.

4.2.2.1.5. Role of Particles Size Distribution

The variation of colloids mean particle size diameter (PSD) over the operating time during the Stage II is depicted on Figure 4.58. The data analysis suggests that the increase in floc size

136

was 23.8% (from the mean value 168.5 µm) at CD of 20 Am^{-2} during the period from day 31 to day 49. This suggests that the forces of attraction dominated over the electroosmosis phenomenon during this period of the EAnMBR operation. However, after day 49, gradual decrease was observed until day 60. This can be explained by the formation of electric double layer as the negative charged particles of the sludge were surrounded by a layer of the positive ions. When a DC was applied to the MLSS solution, the positive counterions started migrating towards the cathode. As they moved, they would repel water molecules resulting in a total transport of water out of the sludge particles. Electroosmosis phenomenon enhanced the extraction of bound water from the sludge colloids, minimized their attachment to the surface of the membrane, and hence improved membrane fouling characteristics. This was a completely different behavior from conventional coagulants. A research focused on addition of polyacrylamides reported an increase in the flocs size while adding different coagulants [288]. The results of this study, however, were in line with other researches [272-274]. Therefore, the EAnMBR employs a different mechanism from chemical coagulation in enhancing the sludge filterability and thus minimizing the overall sludge management cost.
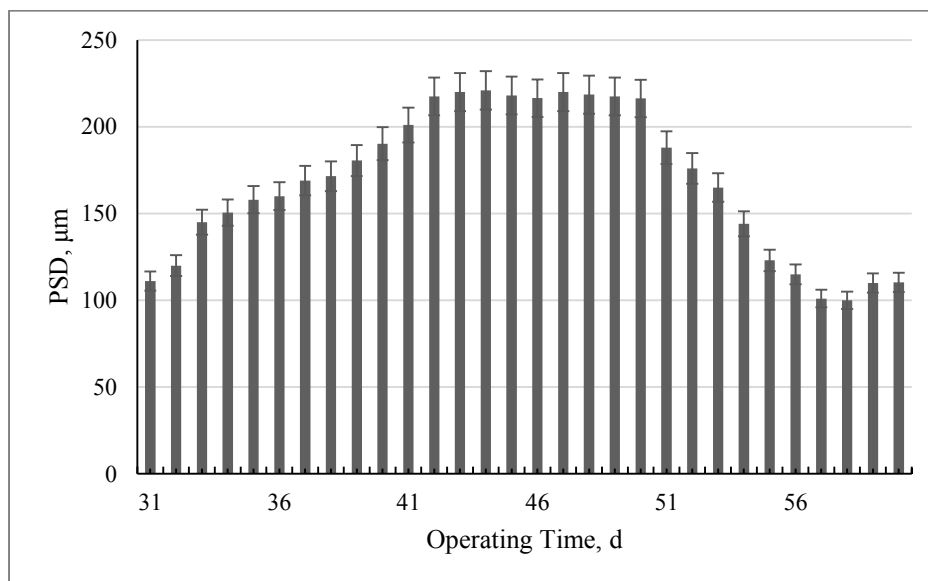
Figure 4.58. Changes of the floc mean PSD in the EAnMBR over time

4.2.2.1.6. Role of Zeta Potential

The improvement in membrane permeability within the EAnMBR system was confirmed by measuring the zeta potential of the sludge flocs (Figure 4.59).

Starting from the Stage II, the zeta potential of the particles in the supernatant shifted from -30 to -18.3 mV within first days of operation. Involvement of electrokinetics significantly improved the aggregation of particles and the overall treatment process. By the end of Stage II, zeta potential decreased from -18.3 to -10.0 mV with average -13.1 mV and maximum value of -8.0 mV toward the end of the Stage II. In Stage II, a gradual decrease in negative direction was observed in zeta potential values between the days 31 and 45 due to stable release of aluminum ions and formation of polymers in the aqueous phase. However, zeta potential stabilized after day 46 at around -8 -10 mV in the reactor until the end of the Stage II. The results of the study demonstrate that the colloidal particles of the mixed liquor solution approached close to isoelectric point. These values can explain the significant improvement of the treatment efficiency as explained later in the chapter.
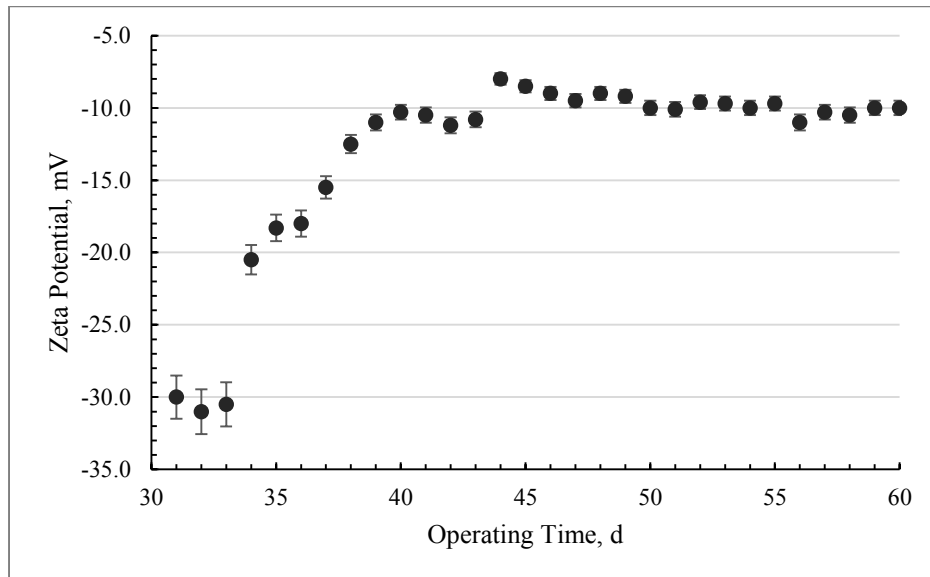
Figure 4.59. Changes in zeta potential in the system during the Stage II of Phase II

4.2.2.2. Impact of the EAnMBR Operation on the Biomass Characteristics

The impact of electrokinetic processes on the biomass characteristics in the EAnMBR system during Phase II was monitored by measuring the MLSS and the MLVSS concentrations in the

138

vessel. Figure 4.60 shows the changes of the mixed liquor concentration in the EAnMBR. During the first two days of Stage II, the MLSS concentration remained relatively stable and ranged between 5,500 mgL^{-1} to 5,700 mgL^{-1}. This stagnation was related to an increase in the pH of aqueous phase from 7.0 to 7.8 due to the release of Al^{3+} into the solution. The pH change might affect sensitive to pH changes anaerobic microorganisms and transition from acetogenesis to methanogenesis. Ten days after application of DC, the microorganisms began to adapt to the new conditions, including pH increase, and the MLSS stabilized around 5,670 – 5,850 mgL^{-1}. After day 41 of the Phase II (day 11 of Stage II) the mixed liquor concentration increased gradually and peaked 7,500 mgL^{-1} (average 6,721 mgL^{-1}) at the end of Stage II.
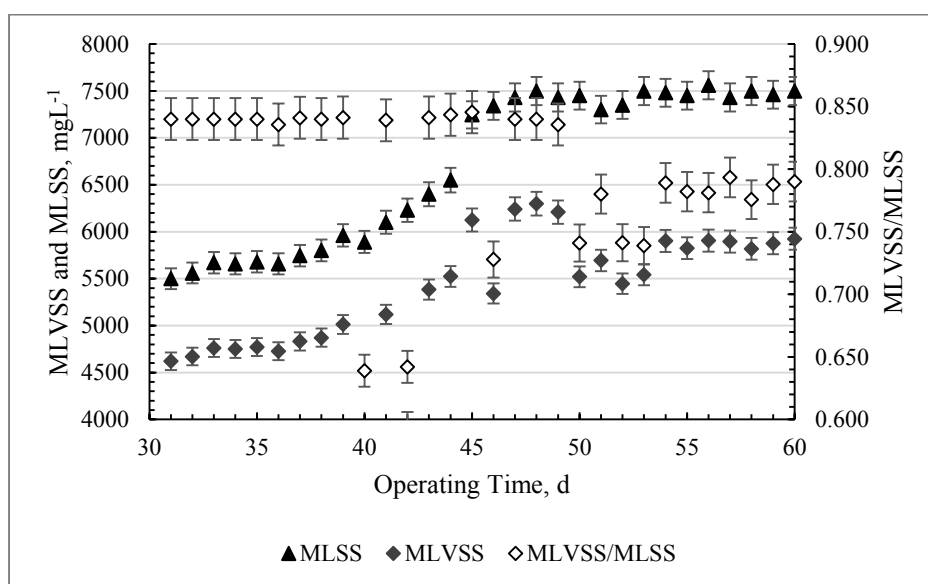
Figure 4.60. Changes of the biomass characteristics during the Stage II

Increase of MLSS concentration after introducing the DC field indicated the ability of microbial consortia to adapt quickly and start the biodegradation processes as a result of their metabolic activities. The study of biomass characteristics revealed that the volatile fraction of total suspended solids was relatively stable throughout the entire experiment as MLVSS/MLSS ratio remained within the range 0.65 to 0.84 during Stage II, which might suggest that inorganic particulate compounds accumulated in the bioreactor enmeshed in the biomass. This finding is in an agreement with other study conducted on anaerobic membrane bioreactor treating molasses containing wastewater [289]. More aluminum ions generated by the electrokinetic process were dissolved in the aqueous phase resulted in an increase in the overall total suspended solids by the end of the Stage II. However, MLVSS/MLSS ratio

decreased over the time which suggests that aluminum produced after the DC application contributed to inorganic particulates in the MLSS. In order to distinct between the amounts of the MLSS produced from biodegradation process and contributed by electrokinetic phenomena, a separate experiment was conducted as described below.

Four 1L batch bioreactors, having 0.8L effective volume each were used in this experiment. Three bioreactors operated under current densities 12, 15, and 20 Am^{-2} along with a control reactor without DC application. MLSS and MLVSS were determined on a daily basis for 10 days. The difference between MLSS and MLVSS in the control and MLSS and MLVSS in the EAnMBR represented the inorganic fraction due to electrokinetics. Figure. 4.61. provides detailed information on the increase in the suspended solids (in kgm^{-3} wastewater) in terms of the fixed suspended solids (inorganic fraction) generated in the EAnMBR due to the electrokinetic phenomena. From the Stage II, it could be concluded that the EAnMBR showed insignificant negative impact on biomass characteristics during the initial stage of operation compared to the AnMBR operation and ensured excellent performance in the treatment of the synthetic wastewater.
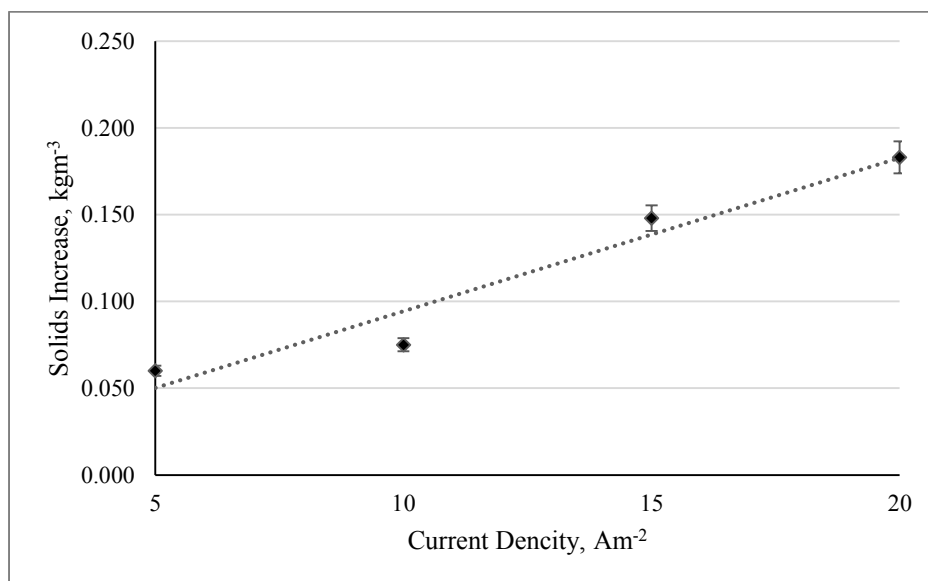
Figure 4.61. Daily solid increase in EAnMBR due to electrokinetic phenomena

4.2.2.3. Impact of the EAnMBR Operation on the Wastewater Quality Properties

This section of the study assessed EAnMBR operation influence on wastewater quality parameters and removal efficiency in terms of carbon and nutrients when electrokinetic processes became involved.

4.2.2.3.1. COD Removal Mechanism

The variations of the COD concentrations in the influent, the reactor and the effluent during the Stage II are presented on Figure 4.62. The total efficiency of COD removal in the EAnMBR was calculated according to equations (4.10) and (4.12) respectively. Considering difficult to treat nature of influent, the results generated by the EAnMBR show consistently high COD removal during the Stage II. The COD concentration in the reactor varied between 1,318 mgL^{-1} at the beginning and 78-105 mgL^{-1} towards the end of the experiment (280 mgL^{-1} on average). The COD concentration in the effluent was in the range between 609 mgL^{-1} at the beginning and 45 mgL^{-1} towards the end of the stage achieving the removal efficiency between 96-99%.
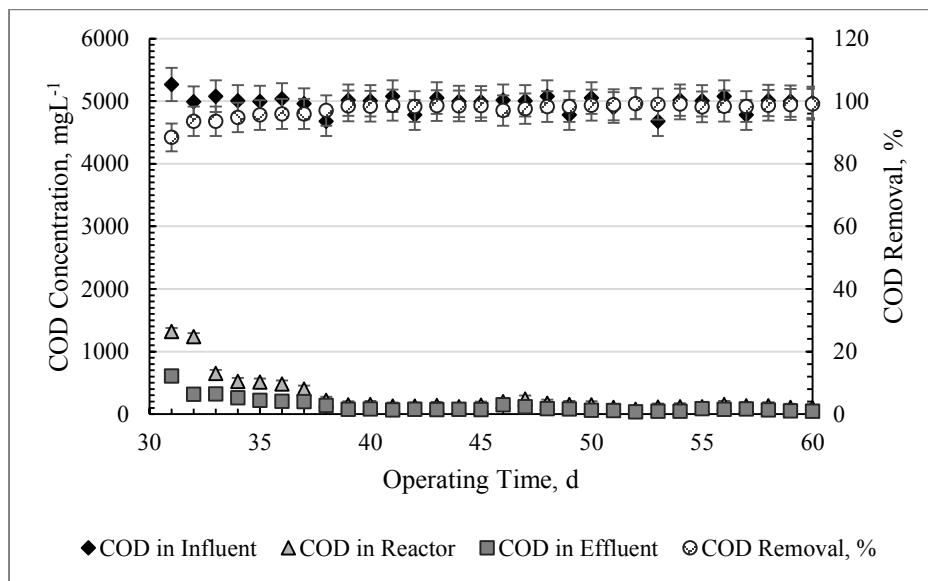
Figure 4.62. Changes in COD concentrations and percentage removal in Stage II

Figure 4.63 demonstrates the involvement of combined biological, electrokinetic processes and the membrane module in COD removal efficiency during Stage II. It is clear that he

electrokinetic phenomena enhanced contribution to the higher percentage of COD removed as the maximum removal efficiency of the COD in the EAnMBR reached more than 99%. Several phenomena such as electrocoagulation, electrochemical oxidation and adsorption by electrostatic attraction, electroflotation and physical entrapment could contribute significantly to improvement of the COD removal in EAnMBR after applying DC.

The data acquired during the Stage II proved that the electrokinetics acted as an important contributor in the enhancement of COD removal in AnMBR processes.

The substantial reduction of organic fraction in sludge colloids from the liquid phase resulted through the formation of complexes with aluminum hydroxides.

During Stage II, combined degradation due to microbial activity and electrokinetic was increased from 75% (at the beginning of day 31) to more than 97% (at day 60). The membrane system contributed from 46% to 53% maximum towards overall removal efficiency. Contribution of the electrokinetics, biological processes and the membrane module towards the overall removal process is presented on Figure 4.63.
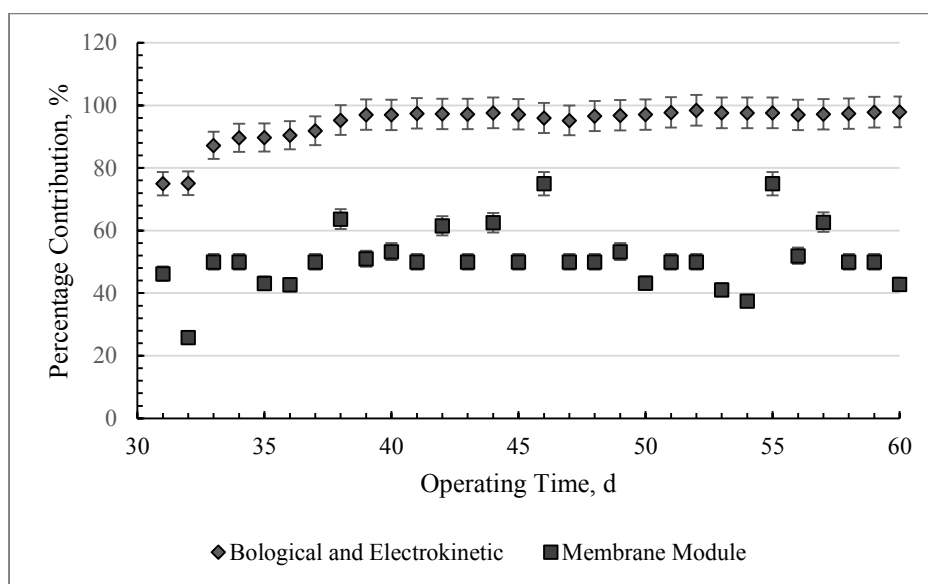
Figure 4.63. Contribution of membrane module and electrokinetic/biological activities to COD removal in Stage II

The biopolymers such as polysaccharides and proteins and humic-like substances were found to be the predominant fractions responsible for MF and UF hollow fibre membranes fouling

[290]. Molecular weight (MW) fingerprint profiles showed that a majority of fragments in anaerobic soluble microbial products (SMP) were retained by the membrane and some fragments were present in both SMP and in soluble extracellular polymeric substances (EPS), suggesting that the physical retention of SMP components might contribute to the AnMBR membrane fouling [291]. The EPS and SMP do not represent specific molecules with specific structure or configuration, however are operationally defined. Any molecules, colloids, or particles can be detected as EPS or SMP as long as they are qualified by the method used by reacting with the reagents used.

Electrokinetic processes affect stability of colloidal system and, therefore, reduce the contribution of the dissolved organics on membrane fouling. The results demonstrated that the application of the DC field played a significant role in providing dramatic reduction of COD and improving the effluent quality.

4.2.2.3.2. Nitrogen Removal Mechanism

The variations of the total nitrogen concentrations in the influent, EAnMBR supernatant and the treated effluent are presented in Figure 4.64.
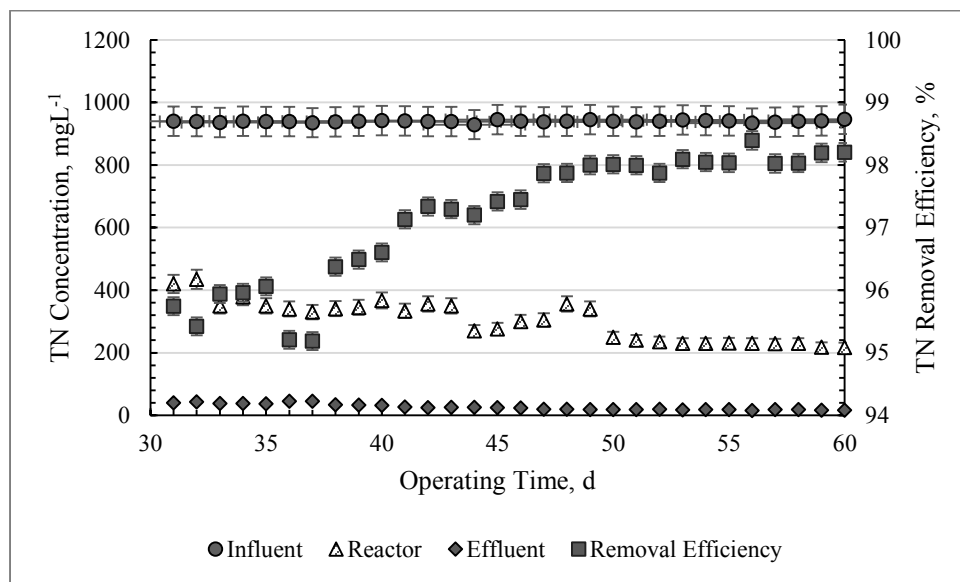
Figure 4.64. Changes in the TN concentrations and removal in EAnMBR during the Stage II

The overall removal efficiency of the EAnMBR system is also provided in Figure 4.65. The influent TN concentration was 940±3 mgL^{-1}. An initial concentration of nitrogen in the EAnMBR was 420 mgL^{-1} at the day 1. Slight increase of TN can be attributed most likely to the microbial biomass initial response to the electrical current by secreting enzymes of protein nature. Then, noticeable changes were observed after 3 days; the concentration gradually decreased in the reactor after application of the DC. During the first 5 days of the Stage I, removal of TN in the reactor was 59±3%, and up to day 50 oscillated around 65±1% reaching 77±1% by the end of the Stage II. The overall removal efficiency (by the combination of biological, electrokinetic and membrane processes) was 95% at the beginning and increased up to 98% by day 60. This result could be attributed to a significant involvement of electrokinetic phenomena at this stage in decomposition of nitrogen in combination with the microbial activity as can be seen from Figure 4.65.
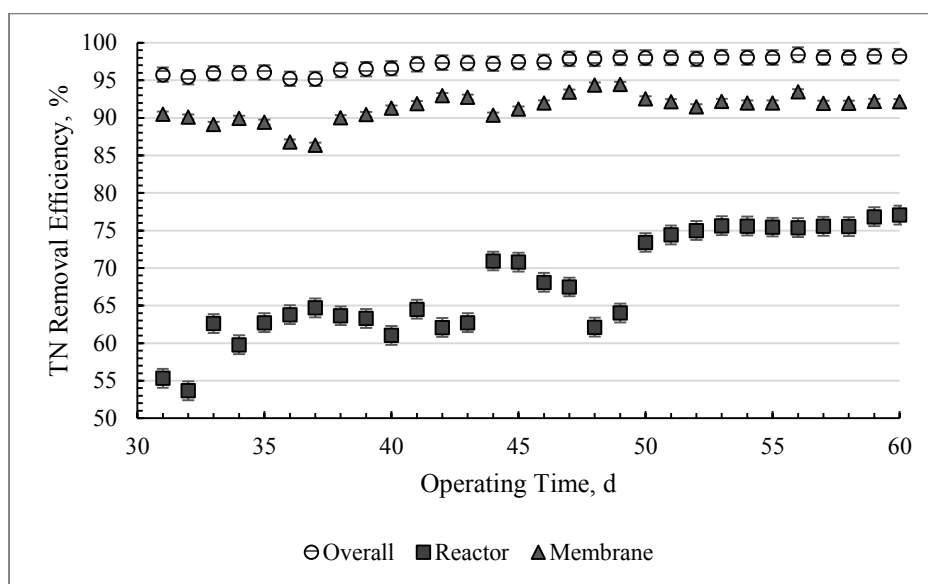
Figure 4.65. Removal efficiency comparison by biological process and membrane module in Stage II

The concentration of total nitrogen slightly increased at the first days after application of voltage gradient. This could be related to the sensitivity of the MLSS solution to the DC field in Stage II. It is probable that the microbial biomass initially responded to the electrical current by secreting enzymes of protein nature and degradation of proteins into ammonia. This

observation was also confirmed by other research [135, 136, 274]. During the operating period, some difference in TN concentration between the supernatant and the membrane effluent was observed, which suggests that the nitrogen removal was achieved by the combination of the membrane filtration, electrokinetic phenomena and microbial community, especially at the later stage of experiment when sludge well developed.

4.2.2.3.3. Phosphorous Removal Mechanism

Figure 4.66 provides details on the variations of the TP concentration of the influent, the supernatant liquors in the EAnMBR, and the treated effluent during the Stage II period of 30 days. Figure 4.67 demonstrates the corresponding TP removal efficiency by the reactor (combined anaerobic biological and electrokinetic), the membrane module and the overall by the entire EAnMBR system. The influent TP concentration was 151 ± 1 mgL^{-1}. During the first days of Stage II, when the electrokinetic phenomena became involved in the combined treatment, the removal efficiency of TP by the reactor increased from about 60% to 84.5% and the removal efficiency in the effluent was about 98% which provided an increase approximately by 38% compared to day one of the Stage II. The decline in the TP removal in the reactor from 20 mgL^{-1} to 40 mgL^{-1} and, as a consequence, the insignificant increase of the TP in the effluent noticed between day 30 and 50 was attributed to the temporary reduction of MLSS concentration during that period as a result of the system adjustment to the DC. However, shortly after, the removal efficiency sharply increased due to combined effect of the increased MLSS concentration (as uptake increased by microorganisms) and electrokinetic phenomena (coagulation) in the EAnMBR. It is likely that at the newly-formed after DC application oxic-anoxic interface near the anode, facultative microorganisms' started oxidation process which involves the regeneration of adenosine triphosphate by combining adenosine diphosphate with inorganic phosphates present in the wastewater.
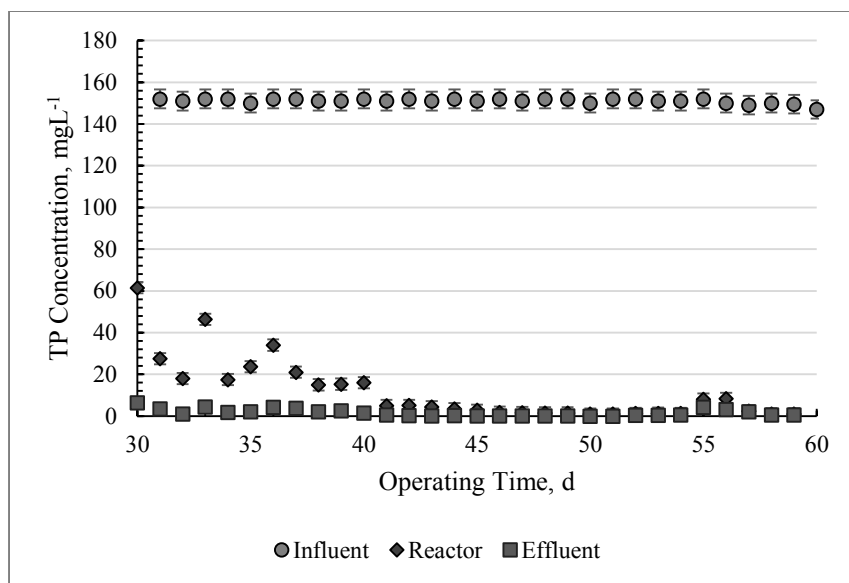
Figure 4.66. Changes in TP concentrations during the Stage II

The phosphorus concentration steadily reduced also due to release of Al^{3+} into the aqueous phase and formation of aluminum hydroxide inorganic polymers. The phosphorous molecules reacted with aluminum ions to produce $AlPO_4$ and precipitated out of the sludge with some (as observed after the experiment) deposited on the surface of the cathode and the membrane which resulted in decrease of the membrane performance after day 50 (Figure 4.67). In another pathway, the aluminum ions reacted with the hydroxyl ions OH^- produced at the cathode to form centers of gravitation in general form of $Al(OH)_3$. In this case, the phosphorous species could be adsorbed by the sweep flocs and removed from the aqueous phase by electrocoagulation.
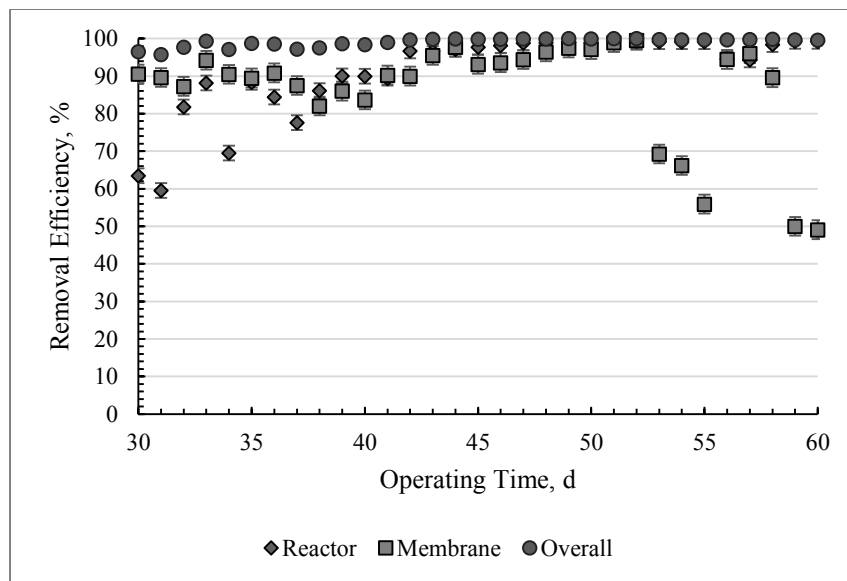
Figure 4.67. Removal efficiency of TP concentration during the Stage II

4.2.3. Comparison between AnMBR and EAnMBR performance Stage I and Stage II respectively

Comparative research between Stages I and II was necessary to present a more complete picture of the process and aimed to make comparisons across different physical, chemical and biological properties in order to assess the efficiency of EAnMBR.

4.2.3.1. Comparison of the Physico-chemical Properties

This section provides a comparison of physicochemical properties between Stage I and II in order to determine the role electrokinetic phenomena in changes of physical and chemical properties of the EAnMBR. Assessment of changes in these properties allowed to assess the treatment potential of the novel system compared to the AnMBR process.

4.2.3.1.1. Comparison of Changes in pH

The effluent pH was dependent on the influent pH in the AnMBR without the DC in Stage I (Figure 4.42). However, there was a different pattern after applying the DC field during the Stages II as shown in Figure 4.68.

During Stage II, the change in pH values in the EAnMBR system did not demonstrate a systematic trend with the influent pH. A possible reason for this behavior could the effect of

the DC operating mode, which reflects release of OH- into the solution, thus increasing the pH and the exposure time of the MLSS to the DC field. In Stage II, the operating mode was 5 minutes On and 20 minutes Off which is equivalent to an effective operational time for electrokinetic phenomena in the system of 25%. This draws a conclusion that the application of DC for 25% out the total operating time, increases substantially the effects of the electrokinetic processes on the pH of solution and microbial community; similarly, when the time for electrokinetic processes is reduced, the EAnMBR system operation will be similar to the AnMBR bioreactor in addition to benefitting from electrokinetic phenomena.
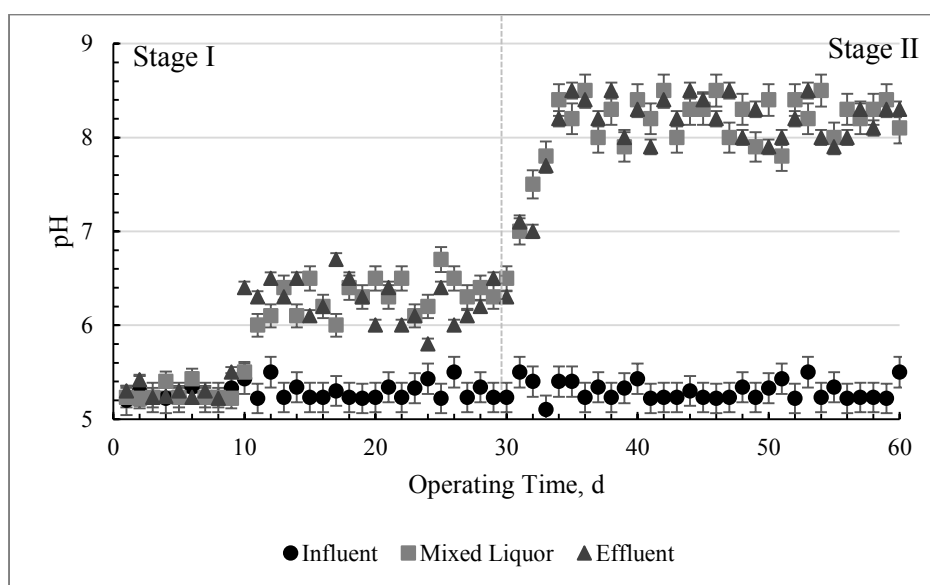
Figure 4.68. pH changes during the Stage I and II of Phase II

This indicates the importance of the exposure time of EAnMBR to DC fields as the key operation parameters. Thus, optimization of operating conditions for higher treatment efficiency with respect to a particulate pollutant depend on pH. These findings lay out basis for the process of optimization, which is discussed in the Phase IV of the research. Study showed that in AnMBR biodegradation dominated wastewater treatment process and the pH values of the MLSS in the bioreactor as well the pH of the effluent were slightly affected by pH of the influent. However, when the system operates as EAnMBR with the DC power supply providing voltage gradient to the reactor, the electrokinetic processes dominated and the pH

values of the EAnMBR system was be less dependent on the influent pH, but rather to the electro-coagulation process.

4.2.3.1.2. Comparison of Changes in Temperature

Comparative results in the variations of temperatures of the feed wastewater, the MLSS solutions and the treated effluent in the Stage I and Stage II are presented in Figure 4.69. The temperature of the influent was (21 ± 2 ^{0}C), while temperatures of the MLSS and the effluent were closer to each other (36 ± 1 ^{0}C and 30 ± 1 ^{0}C respectively). The temperatures in the electro-bioreactor zones were approximately the same in the Stage I and Stage II which suggests that the electrokinetic phenomena have an insignificant impact on the temperature. The order of change in temperatures in the Stage I and Stage II was as following:

Influent temperature < Effluent temperature < Temperature in the reactor

It should be noted that the temperature of the effluent dropped rapidly in the effluent storage tank ambient, therefore its discharge should not be a concern.
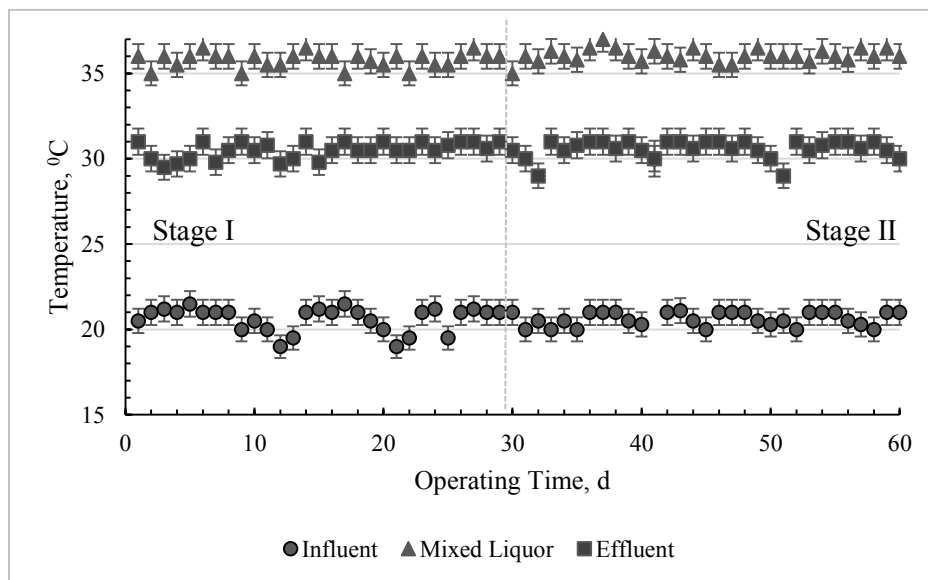
Figure 4.69. Temperature changes during the Stage I and II of Phase II

4.2.3.1.3. Impact of Electrokinetic Phenomena on Specific Resistance to Filtration

Form the results obtained during the Stage I and II operation (Figure 4.70), it can be concluded that the involvement of electrokinetic processes significantly improved the overall performance of the system in terms of SRF. The conductance of charge through the electrical double layer transfers the momentum to water molecules to move towards the electrodes (electroosmosis). This study demonstrated that 20 Am^{-2} was adequate to provide the driving force to remove bound water from the inside of the flocs. Current density 20 Am^{-2} was found to cause a substantial removal of bound water, thus increasing sludge dewaterability by decreasing the SRF. A reduction of SRF (up to 59%) was observed during the Stage II (EAnMBR configuration) compared to 7% achieved in the Stage I (AnMBR configuration). The magnitude of reduction was due to quality of the initial properties, mostly floc size and SMP concentrations [189, 272]. The electroosmosis process was evident through the reduction of the floc size over the operating period. The impact of electrokinetic on enhancement of sludge dewaterability is not only limited to the extraction of bound water. The formation of aluminum hydroxides that reduce the concentrations of SMP in the aqueous phase is another factor contributing in improvement of dewaterability. Furthermore, electrokinetic phenomena change the structural and morphological characteristics of the flocs through changing their size and decreasing the ratio of the organic to the inorganic matter concentrations. In addition, the application of an aluminum anode seemed to give an overall better prevention of the membrane fouling. This results agrees with the results from research conducted on electrokinetic aerobic systems [135, 136].
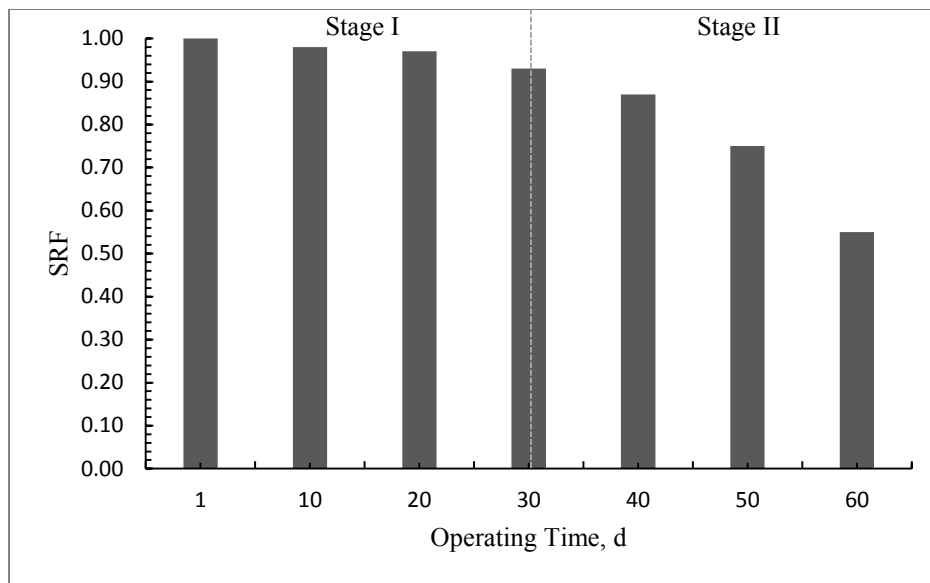
Figure 4.70. SRF changes during the Stage I and II of Phase II

4.2.3.1.4. Impact of Electrokinetic Phenomena on Sludge Volume Index

The results showed that sludge volume index (SVI), which represents the settleability of the sludge reached 360 mLg^{-1} (4% reduction) in AnMBR configuration, while 164 mLg^{-1} (54% reduction) was found in EAnMBR. The electroosmosis which draws charged particles out of the pores significantly contributed to the improvement of settling properties and reduction of SVI compared to the conventional operations (Figure 4.71).

The conductance of current through the electrical double layer causes water molecules to move towards the electrodes through electroosmosis phenomena. Since pH of the sludge liquor observed in this study was around 8, the solid surfaces were negatively charged and the electrical double layer was dominated by cations. Under a DC field, these cations have a tendency to move towards the cathode simultaneously prompting the movement of bound water molecules.

Several other factors may have contributed to the better sludge dewaterability in the EAnMBR over the AnMBR, namely: the reduction of SMP, the reduction of flocs' bound water, the reduction of MLVSS/MLSS ratio and the enhancement of bio-flocculation.
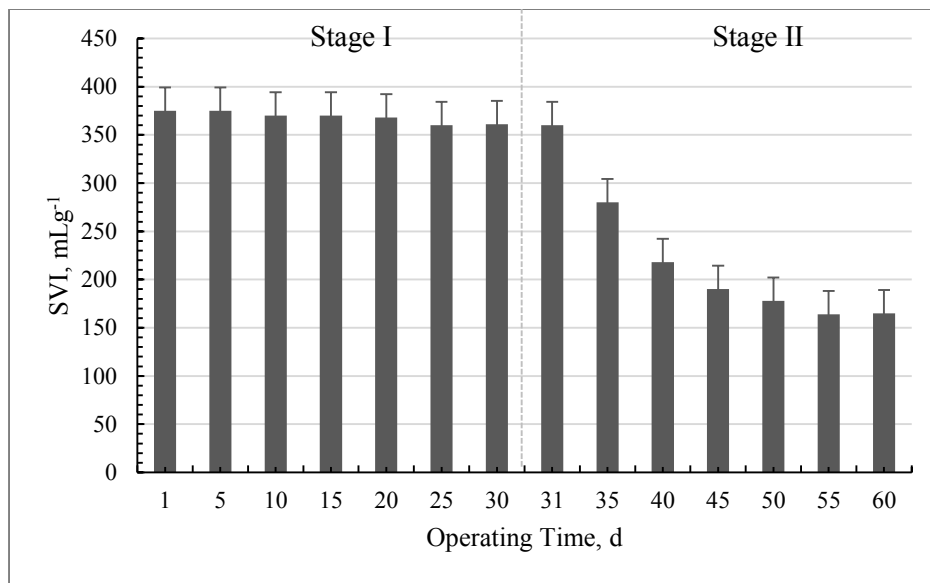
Figure 4.71. Changes of SVI during the Stage I and Stage II of Phase II

4.2.3.1.5. Impact of Electrokinetic Phenomena on Particles Size Distribution

The change in the PSD in the AnMBR was insignificant, indicating a comparatively slow coagulation rate. Therefore, the mechanism of dewatering in the AnMBR was different from the EAnMBR (Figure 4.72). However, towards the day 30 particles started to grow in size due to increased biological activity in AnMBR. In Stage II, however, PSD of colloids exhibited similar trend as in preliminary study in Phase I, i.e. initial wave pattern with gradual increase of PSD. However, the magnitude of the increase was different due to the different nature of the influent. Starting from the day 31, after the DC was applied to the system, the mean floc PSD increased from 111 μm to nearly 221 μm after by the day 41 of operation. The peak size was observed from day 41 to 49, and then the PSD slightly declined. The decline was caused by electroosmosis phenomenon and the extraction of bound water from the sludge colloids which led to a reduction of colloids size. These changes in particles size distribution size reflected the dynamics of the EAnMBR system over the period of time. The PSD increase can be also attributed to an electro-flocculation process during which the organic particles formed larger flocs mainly as a result of reducing the repulsive forces between the particles surfaces as the zeta potential decline. It was observed in subsequent stages some flocs size decline due to the removal of bounded water by the electroosmosis. This trend of increasing and decreasing of the flocs size was observed whenever the current density was strong enough to cause electro-flocculation and electro-extraction of the bound water. This observation was in line

152

with another study [189]. Thus, colloids size increased as the forces of attraction-repulsion and decreased when electroosmotic mechanism dominated and the extraction of the tightly bound water from the pores of the colloids reduced their size. Another important factor contributed in reducing the floc size over the time was the production of aluminum hydroxide polymers. The hydrated polymers became centers of gravitation for flocs which, in turn, combined with the other solids in the system. These aggregates formed suspended solids in the EAnMBR of smaller size compared to the microbial aggregates and reduced the measured mean PSD. Towards the end of the Stage II, the floc size started to stabilize at about 100 μm based on the average size of the aluminum hydroxide polymers produced [136]. The longer time required to develop larger particles can be attributed to a longer time necessary to develop long-chained inorganic polymers formed by aluminum hydroxide species. New particles composed of inorganic aluminum hydroxides or particles of organic/inorganic nature might also be formed.
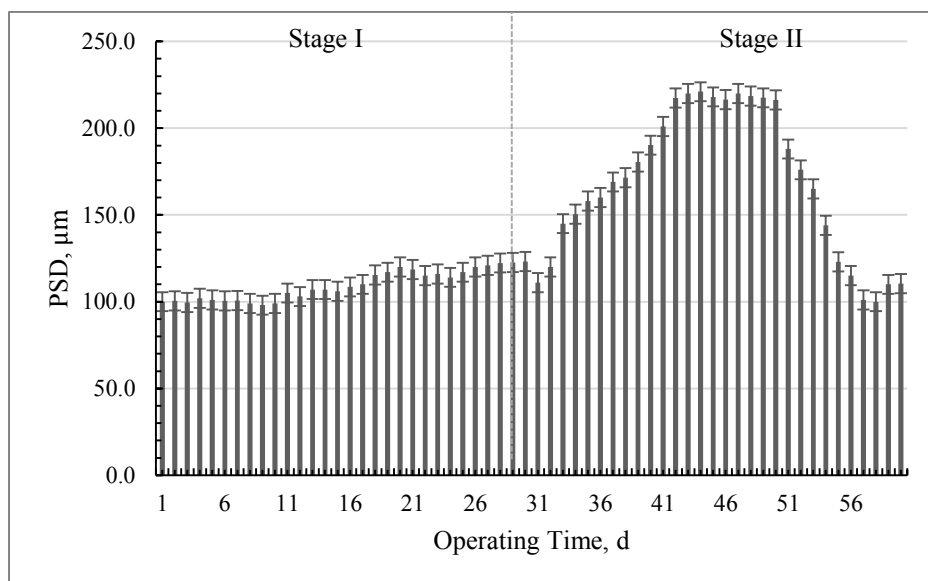
Figure 4.72. Changes of the floc mean PSD in the AnMBR and EAnMBR over time

4.2.3.1.6. Impact of Electrokinetic Phenomena on Zeta Potential

The results of zeta potential measurements (Fig. 4.73) demonstrated that EAnMBR enhanced flocs formation resulted from the electrokinetics phenomena involvement in physico-chemical and biological processes as well as membrane filtration. The destabilization of suspension in AnMBR was going at a slower rate according to the changes in the magnitude of zeta potential

153

(average -32 mV). However, the magnitude of zeta potential reduction (from -30.5 to -8.2 mV) in the Stage II indicated a significant enhancement of the aggregation of the colloids in the sludge flocs due to the presence of sufficient aluminum ions in the aqueous phase.
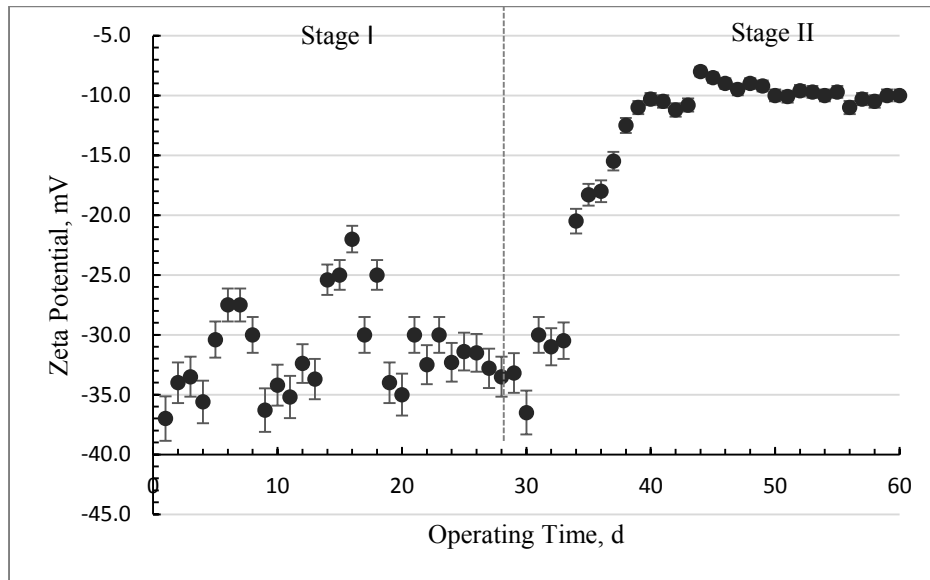
Figure 4.73. Changes in zeta potential in the system during the Stage I and II of Phase II

Decrease of zeta potential magnitude can be explained by the release of positive aluminum ions into aqueous phase which were absorbed by the negatively charged particles in the sludge suspension; creating electrostatic attraction forces and better coagulation.

DLVO theory described the force between charged surfaces in a liquid medium, and combined the effects of van der Waals attraction and electrostatic repulsion. The aluminum ions generated from the anodic electrooxidation (eq. 4.12-4.14) destabilized the negatively charged colloids and according to the DLVO theory changed net energy permitting van der Waals attraction forces to dominate, and thus the colloids to coagulate. According to the Smoluchowski's equation (eq. 4.25), the electrophoretic mobility of the particles was proportional to the electrophoretic velocity which was dependent on the strength of electric field. Therefore, particles moved relatively faster under EAnMBR operation mode when they carried a larger charge:

$$v = \frac{\varepsilon_r \varepsilon_0 (ZP) E}{\mu} \qquad (4.25)$$

154

Where, v is the particle velocity, ε_r is the media dielectric constant, ε_o is the permittivity of free space, ZP is zeta potential, E is the applied electric field, and μ is the medium viscosity.

It was concluded that the electrooxidation of the aluminum anode in EAnMBR caused breaking the repulsive forces between the negatively charged sludge colloids, and permitting the van der Waals forces to predominate and therefore flocs to aggregate as was demonstrated in Phases I and II. Overall, electrokinetics in EAnMBR enhanced the coagulation process and similar results were expected in subsequent study of industrial wastewater treatment.

4.2.3.2. Impact on the Biomass Characteristics

Figure 4.74 represents the changes of the MLSS and the MLVSS concentrations during the entire Phase II.
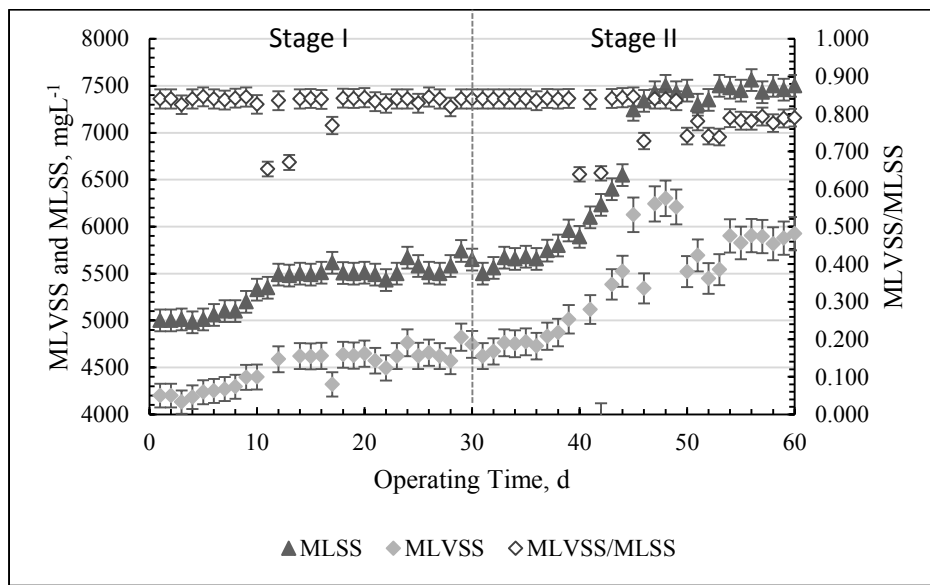
Figure 4.74. Changes of the biomass characteristics during the Phase II

There was a clear distinction between a gradual increase of the MLSS concentration during the first 14 days of the Stage I and steady grow in the Stage II. During the Stage I, the sludge concentration slowly increased from initial concentration 5,000 mgL^{-1} fluctuated around average value of 5,500 mgL^{-1}. A relatively constant concentration from day 11 to 30 might be related to the long HRT of 4 days and slow activity of anaerobic process. At a relatively constant concentration of the substrate in the influent, longer 4 days HRT, F/M 0.20 was stable

155

during the operating period; therefore, the available source of carbon did not limit growth of the microorganisms in Phase II. From 14 day of experiment until the end of the Stage I, the MLSS concentration in the vessel was relatively stable- the sludge concentration remained 5,500 mgL^{-1}. MLVSS/MLSS ratio during Stage I was around 84%, indicating that no inorganic matter accumulated in the EAnMBR.

The impact of electrokinetic processes on the biomass sludge characteristics in the EAnMBR system during Phase II, however, was more obvious (Figure 4.75), at the beginning of Stage II, the MLSS concentration remained relatively stable and comparable to Stage I, and ranged between 5,500 mgL^{-1} to 5,700 mgL^{-1}. This stagnation was related to an increase in the pH of aqueous phase of the system from 7.0 to 7.8 due to the release of Al^{3+} cations into the solution. The pH change could affect microorganisms sensitive to pH change. Ten days after application of DC, the microorganisms began to adapt to new conditions, including pH increase. The MLSS measured during this period was found to be around 5,670-5850 mgL^{-1}. After day 41 of the Phase II the mixed liquor concentration increased gradually and reached maximum about 7,500 mgL^{-1} (average 6,721 mgL^{-1}) at the end of Stage II.

Increase of MLSS concentration after introducing the DC field indicated the ability of microbial consortia to accommodate changes relatively fast and to start the biodegradation processes because of the metabolic activities. The study of biomass characteristics revealed that the volatile fraction of total suspended solids was relatively stable throughout the Stage I suggesting that there was no accumulation of fixed solids inside the vessel. However, as the DC was applied, MLVSS/MLSS ratio decreased from 84% to approximately 65% during Stage II, which might suggest that inorganic solids started to build-up in the reactor. This can be explained by increase of aluminum ions concentration generated by the electrokinetic process compared to Stage I where practically no aluminum were in the aqueous phase. Electrokinetics resulted in an increase in the overall total suspended solids by the end of the Stage II. However, MLVSS/MLSS ratio decreased over the time of the Stage II, which might suggests that aluminum produced after the DC application contributed to inorganic particulates in the MLSS. To distinct between the amounts of the MLSS produced from microbial activity and contributed by the electrokinetic processes, a separate experiment was conducted which confirmed a complex interaction of physical, chemical and biological process in the EAnMBR.

4.2.3.3. Impact of Electrokinetic Phenomena on the Wastewater Quality Properties

Impact of electrokinetic processes such as electrooxidation, electrocoagulation, electroflotation, electrosedimentation etc., on the wastewater quality was assessed in terms of COD, nitrogen, phosphorous removal and sludge properties.

4.2.3.3.1. Impact of Electrokinetic Phenomena on COD Removal Performance

Although the overall COD removal efficiency during the Stage I varied between 79% and 89% with average 86% and the concentration of COD was reduced from 4,793±200 mgL^{-1} to 719±100 mgL^{-1} (on average), the application of the DC field through the MLSS solution further increased the COD removal efficiency in the EAnMBR to more than 99%. When the electrokinetic processes started acting on the system, the COD removal rate improved quality of the effluent and achieved around 87% at beginning of Stage II reaching 95% in 5 days of the experiment. This fact can be directly attributed to the effect of the combination of electrokinetic phenomena (electrocoagulation, electrophoresis, electroosmosis, and electroflotation) with biological and physical-chemical processes (Figure 4.75).
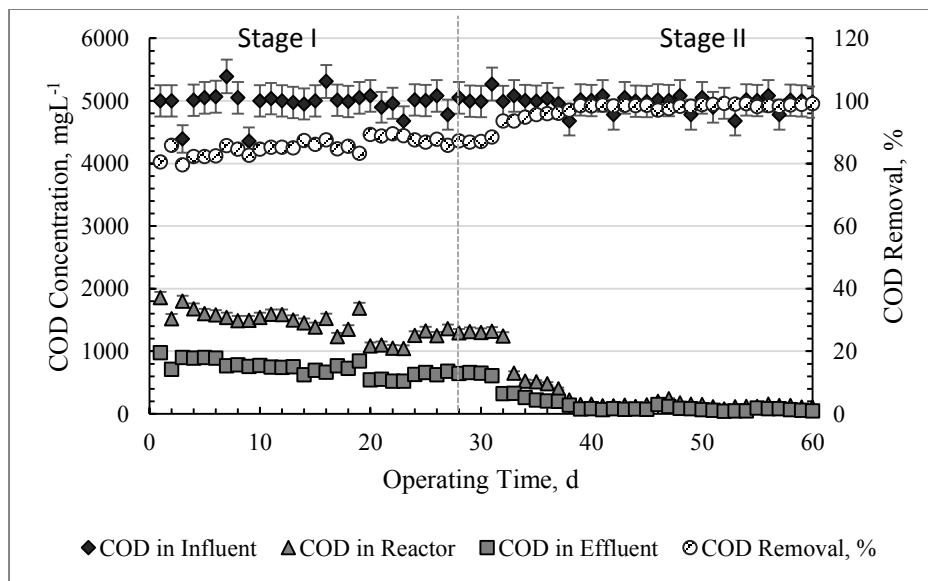
Figure 4.75. Changes in the COD concentrations and percentage removal in Phase II

Due to a complex interaction between biological, physico-chemical and electrokinetic processes in the EAnMBR, a combined effect of anaerobic processes and electrokinetics contribution to COD removal was assessed in the Stage II. Indirect evaluation was conducted (Figure 4.76). Without membrane contribution, the average COD removed by AnMBR during the last 5 days of the Stage I (74±3%) was compared to the COD percentage removal during the first 5 days of the Stage II (83±3%). Assuming there was no biological growth during the first days of the Stage II due to microbial community adjustment, the designed EAnMBR system contributed minimum 6 % to the COD removal performance. Some fractions of carbon in the mixed liquor have higher affinities to the membrane and may cause greater irreversible fouling [290]. Researchers found that the membrane fouling is caused not only by the microbial colloids but also by the organic and inorganic colloids [291].

Membrane module contributed from 46 % to 53% COD removal during the Stage II, which was an increase up to 13% compared to Stage I. According to a study conducted on aerobic membrane system, the removal rate increase was attributed to the removal of the materials that have high fouling potential (SMP and colloids) and to the extraction of the tightly bound water from the suspended solids as a result of electrophoresis [272]. MLVSS, EPS and SMP were interrelated in their effect on membrane fouling, therefore the reduction potential of membrane fouling and, as a result, increase in membrane performance in the EAnMBR was a complex process, i.e. larger particles forming cake layer had less bound water due to electrophoresis and electroosmosis phenomena. Electroflotation could also increase shear force and reduce EPS and inorganic cake formation on the surface of the membrane by washing out the particles.

Therefore, electrokinetic coagulation had a significant impact on the mixed liquor and could dramatically reduce amount of carbon in the wastewater due to increase of biodegradable fraction.
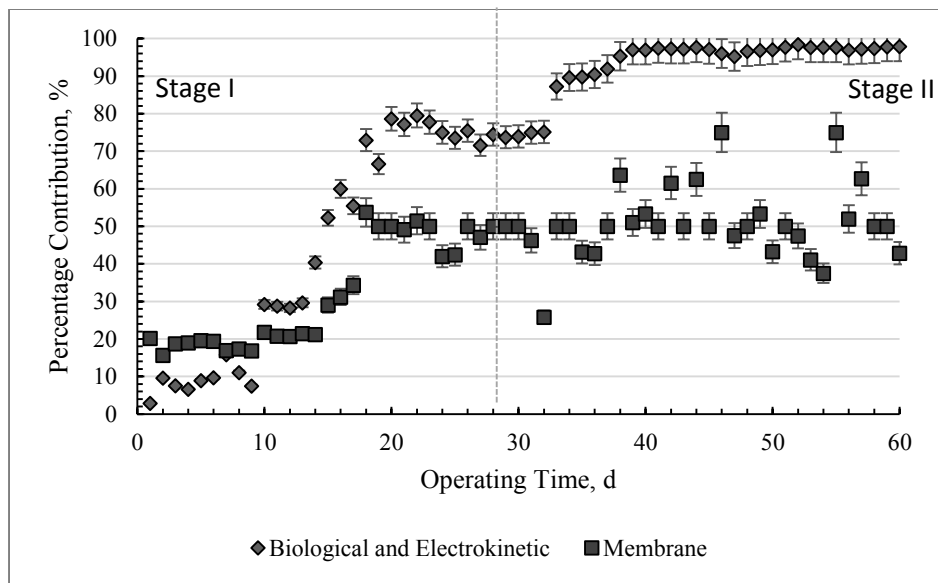
Figure 4.76. Contribution of membrane module and electrokinetic/biological activities to COD removal in Phase II

4.2.3.3.2. Impact of Electrokinetic Phenomena on Nitrogen Removal Performance

Changes in the TN concentration during the Phase II in the feed, the supernatant of the EAnMBR and in the membrane effluent are represented on Figure 4.77. The average concentration in influent during the Phase II was 940 ± 3 mgL^{-1}. The concentrations in the effluent decreased from 58 mgL^{-1} of TN at the start of operation in AnMBR to below 41 mgL^{-1} of TN at the end of Stage I, which corresponded to removal efficiency of total nitrogen $95\pm1\%$ by the end of the Stage I. The concentration in the effluent steadily decreased after electrokinetic phenomena involvement in the Stage II after 31 day of the experiment. The concentration of TN after application of the DC was 40 mgL^{-1} and the noticeable decrease was observed from the third day of operation, when concentration of Al^{3+} ions saturated the phases in the system - 35 mgL^{-1} and reached minimum 17 mgL^{-1} by the end of the experiment.

Analysis of TN concentration in the reactor presented on Figure 4.77 indicated slow anaerobic process of biodegradation. The concentration in the reactor was 936 mgL^{-1} at the day 1 and reached 445 mgL^{-1} at the day 30 (Stage I). Increase in ammonia oxidation was started only after 20 days of the Stage I During the first 20 days of the Stage I, removal by anaerobic process in the reactor was in the range from 0.43% to 8.64% (day 18). Noticeable increase of efficiency reactor was achieved after day 20 and reached about 53% at the end of the Stage I when microbial consortium well adapted to the new environment. The process of TN removal

159

started increasing gradually and reached maximum 52±1% by the end of Stage I. Significant performance increase in EAnMBR was observer after application of electrokinetics. Concentration of TN in the reactor was reduced from 420 mgL^{-1} to 217 mgL^{-1} which was 21.75% increase in removal efficiency compared to day one of the Stage II (and 77% overall from day 1 to 60 during Phase II).

The removal performance of the membrane module was constant during the entire duration of the Stage I operation. Therefore, a major part of TN was removed through the conversion to organic fraction, i.e. proteins. The overall removal efficiency (by the combination of biological, electrokinetic and membrane processes) was 95% at the beginning and increased up to 98% by day 60. This result could be attributed to a significant involvement of electrokinetic processes at this stage in decomposition of nitrogen at electrodes surface in combination with the microbial activity. The low removal efficiency of nitrogen, however, during the first Stage of the Phase II in the vessel was attributed to the low growth rate of anaerobic nitrifying bacteria and, consequently, a slow anaerobic ammonium oxidation process, as these bacteria require more time to reach sufficient concentrations [101]. In addition, conversion of ammonia on electrode surface is a reversible process. This could explain the slow rate of ammonia removal. The removal efficiency comparison by combination of biological process, electrokinetic phenomena and by the membrane module is presented on Figure 4.78.
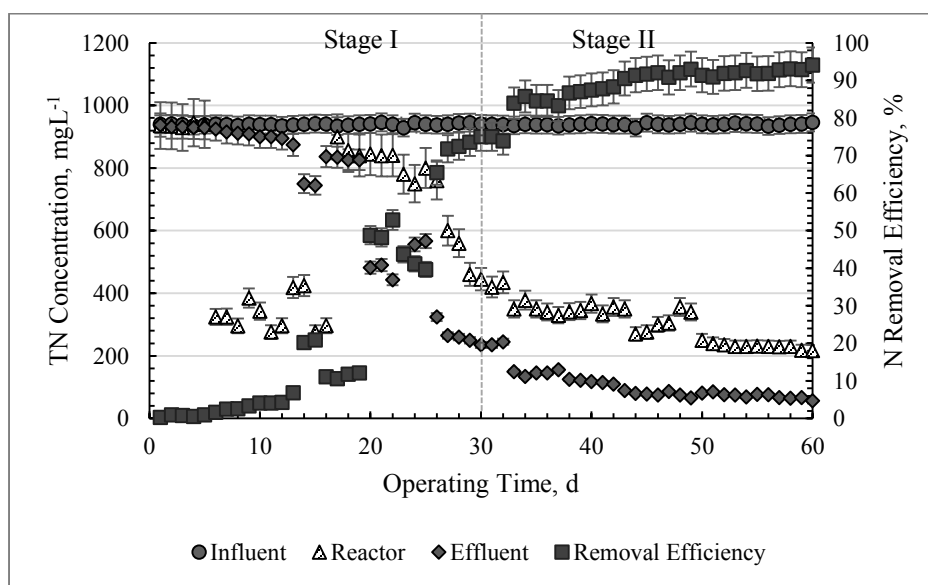
Figure 4.77. Changes in total nitrogen concentrations and percentage removal during the Phase II
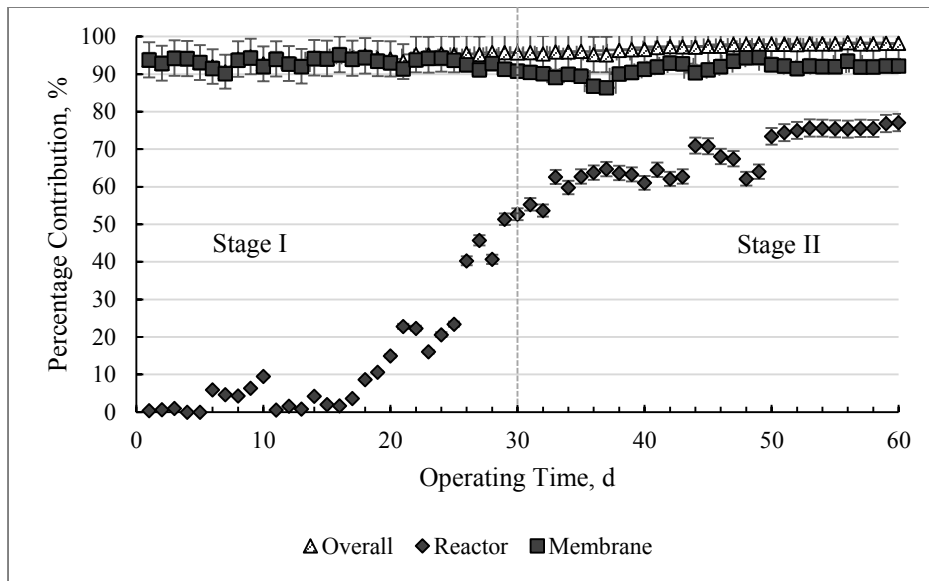
Figure 4.78. Contribution of membrane module and electrokinetic/biological activities to nitrogen removal during the Phase II

4.2.3.3.3. Impact of Electrokinetic Phenomena on Phosphorous Removal Performance

Comparative results of phosphorous removal between the two stages (AnMBR and EAnMBR) are presented on Figure 4.79.
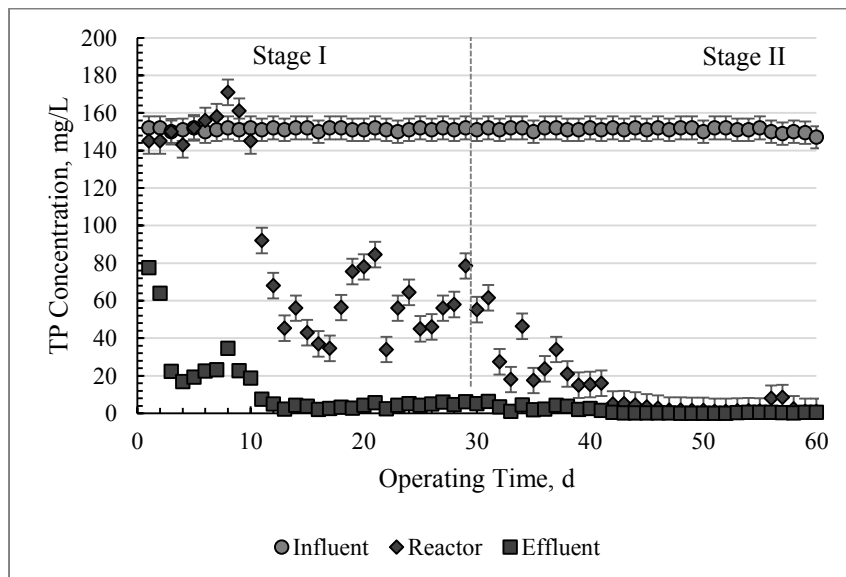
Figure 4.79. Changes in TP concentrations during the Phase II

Figure 4.80 presents the corresponding removal efficiency of TP of the electro-bioreactor and for the overall EAnMBR of operation during the Phase II. The concentration of phosphorus in the feed measured as TP was 151 ± 1 mgL^{-1}. the concentrations of TP in the reactor was 145-150 mgL^{-1} at the beginning of the Stage I and was reduced to 55.2 mgL^{-1} at day 30 which represented 63.4% efficiency by biological treatment alone towards the end of the Stage I. The concentration in the effluent was between 16.8 and 77.6 mgL^{-1} in the first days and reached less than 4.5 mgL^{-1} during the last days of Stage I with minimum reached 1.84 mgL^{-1}. The lower removal rate of phosphorus from the stream during the initial period of operation was due to the low reproduction rate of the anaerobic microbial community and release of phosphorus into the system by the community itself. Further increase in MLSS concentration in the vessel enhanced the phosphorus uptake in Stage I with maximum about 77%. Although the phosphorus uptake was lower during the initial period of Stage I, Figure 4.80 demonstrates that the AnMBR had an excellent removal performance in terms of TP removal also due to the contribution of the electrocoagulation to the overall performance. The process contributed up to 47% during the first day of operation and the efficiency reached maximum 96% on day 19. The overall performance of the system (combined biological and membrane module) was between 49% on the first day and 97% on the day 30 with maximum removal performance during the days 16-22 (98.3%). In general the lowering in TP concentrations were attributed to membrane filtration during the first phase of Stage I, while anaerobic biological treatment did not reach its full capacity (day 1-20). The primary removal mechanism in the later period of the Stage I was the biological absorption by bio flocks (MLSS increased from initial 5,000 mgL^{-1} to 5,600-5,700 mgL^{-1}).

During the first days of Stage II, when the electrokinetic phenomena became involved in the combined treatment, the removal efficiency of TP by the reactor increased from about 60% to 84.5% and the removal efficiency in the effluent was about 98% which provided an increase approximately by 38% compared to day one of the Stage II. The decline in the TP removal in the reactor from 20 mgL^{-1} to 40 mgL^{-1} and, as a consequence, the insignificant increase of the (TP) in the effluent noticed between day 30 and 50 was attributed to the temporary reduction of MLSS concentration during that period as a result of the system adjustment to the DC. However, shortly after, the removal efficiency sharply increased due to synergetic effect of the increased MLSS concentration consuming inorganic phosphorus from the aqueous phase and

electrokinetic phenomena in the EAnMBR which likely produced complex aluminum-phosphate minerals.
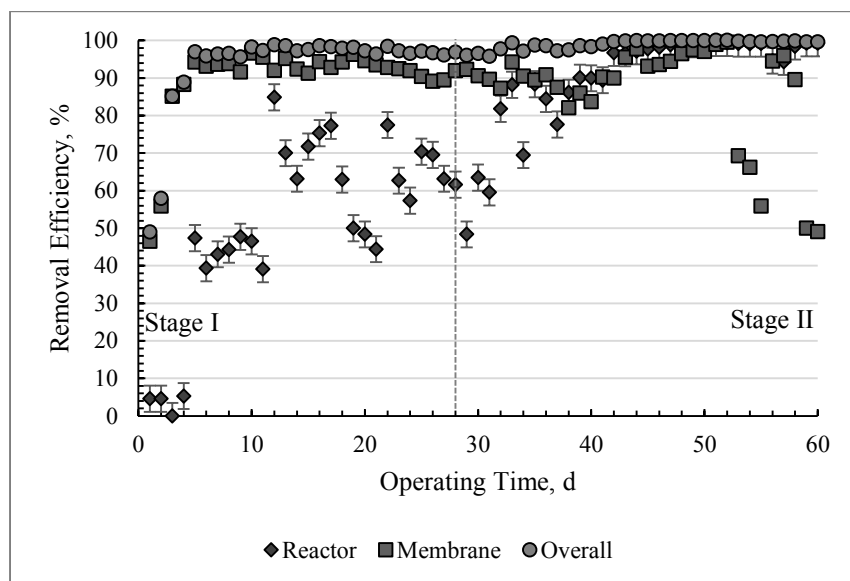
Figure 4.80. Removal efficiency of TP concentration during the Phase II

The phosphorus concentration steadily reduced after the anaerobic microorganisms' readjustment and, especially, release of Al^{3+} into the aqueous phase and formation of aluminum hydroxide inorganic polymers. The phosphorous molecules interacted with aluminum ions to produce alumophosphate species which precipitated out of the sludge with some depositions on the surface of the cathode and the membrane which resulted in the decrease of the membrane performance after day 50 of the Stage II. In another pathway, the aluminum ions reacted with the hydroxyl ions OH- produced at the cathode(as a result of the DC application) to form centers of gravitation in general form of $Al(OH)_x$. In this case, the phosphorous species could be adsorbed by the sweep flocs and removed from the aqueous phase by electrocoagulation.

Similarly, as a result of the electrokinetics, phosphorus might have created bonds with other cations in the aqueous phase such as magnesium, ammonium and potassium to form several complexes such as calcium phosphate (eq. 4.26), struvite (magnesium, ammonium and phosphate), and K-struvite (magnesium, potassium and phosphate). Calcium and phosphate constituted the synthetic wastewater supplied to EAnMBR system and, therefore, might have

been presented in forms of calcium phosphates such as dicalcium phosphate CaHPO4·2H2O, tricalcium phosphate $Ca_3(PO4)_2$, octocalcium phosphate $Ca_4H(PO_4)_3$·2.5H_2O, Monetite $CaHPO_4$, Brushite $CaHPO_4$·2H_2O, and hydroxyapatite $Ca_5(PO_4)_3OH$. These species could have been formed and deposit on the surface of the cathode and the membrane. Moreover, dicalcium phosphate, tricalcium phosphate, octocalcium phosphate, Monetite and Brushite might be the precursor phase where they would precipitate and eventually recrystallize to form hydroxyapatite [273]. Calcium phosphates might definitely be presented in EAnMBR system as it created alkaline conditions (pH > 8) because of applied electrical field (Equation 4.26).

$$Ca_3(PO_4)_2 \longleftrightarrow 3Ca^{2+} + 2PO_4^{3-} \tag{4.26}$$

Phosphate might have also reacted also with magnesium and ammonium forming magnesium-ammonium phosphate (struvite-$MgNH4PO4^.6H_2O$) which is formed according to equation 4.27.

$$Mg^{2+} + NH_4^+ + HPO_4^{2-} + OH^- + 6H_2O \rightarrow MgNH_4PO_4 \cdot 6H_2O + H_2O \tag{4.27}$$

Pearson's Crystal Data software was used to model the possible complexes in the solid phase such as lazulite $MgAl_2(PO_4)_2(OH)_2$, grandallite $CaAl_3(PO_4)_2(OH)\cdot5H_2O$, scorzalite $Fe^{2+}_{0.75}Mg_{0.25}Al_2(PO_4)_2(OH)_2$, bearthite $Ca_2Al(PO_4)_2(OH)$, variscite $AlPO_4\cdot2H_2O$, brazilianite$NaAl_3(PO_4)_2(OH)_4$,wavellite$Al_3(PO_4)(OH)_3\cdot5H_2O$, $Al_4Ca_4[H_2O]_{12}Mg[OH]_4[PO_4]_6$ and $Al_{0.18}Ca_2Fe_{4.26}[H_2O]_2Mg_{0.96}Mn_{0.6}Na[PO_4]_6$. The generated compounds could be major contributors to membrane fouling in AnMBR through forming a white precipitate on the surface. However, the negative impact was minimized by EAnMBR operating with electrokinetics since generated species might be removed from aqueous phase and deposited on the electrode surface and settled with sludge preventing the migration of colloids and complexes towards the membrane module. Therefore, the removal mechanism of phosphorous could be attributed to the biological activity, precipitation in form of the inorganic complexes, absorption to organic colloids and deposition on the surface of the electrodes, mainly on the surface of the cathode as a result of electrokinetic phenomena.

4.2.4. Phase II: Conclusions and Recommendations

In Phase II of this research, the treatment system was operated in AnMBR (Stage I) and in EAnMBR (Stage II) configuration for 30 days each. The conclusions of Phase II can be summarized as follows:

- The AnMBR system produced effluent of superior quality in terms of carbon, TN, TP removal by > 99%, > 98%, and up to 100% respectively.
- The system produced effluent of excellent quality in terms of carbon (> 99%) and nutrients removal (> 98% for nitrogen and up to 100% of phosphorus) in EAnMBR mode.
- pH of the liquid phase increased from 5.5 to 8.3-8.5 as a result of electrokinetics involvement.
- Electrokinetic process significantly affected the particle size distribution of the MLSS solution producing large and dense colloids, which increased the overall removal efficiency.
- Biological, physico-chemical and electrokinetic processes played significant positive role in each stage of operation.

The conclusions for each stage are summarized as follows:

- **Stage I (1-30 days):** The system was operated in AnMBR configuration without a DC field. The HRT was kept constant at 4 days to increase the sheer and sludge concentration. The average COD removal of the system was > 89%, nitrogen removal efficiency reached > 95% and the phosphorus removal performance was > 98%. SRF reduced by 7% and SVI reached 360 mLg^{-1} (4% reduction) in AnMBR configuration.

- **Stage II (31-60 days):** The system was operated in EAnMBR configuration with a DC field and an operational mode of 5 minutes On: 20 minutes Off. The electrokinetics in EAnMBR system produced a significant positive impact in terms of COD, nitrogen and phosphorus removal (> 99%, > 95%, > 98% respectively). COD removal mechanism was a combination of biological carbon removal, membrane filtration and electrokinetic formation of the nucleoids. A major part of nitrogen was removed by the membrane module and biological conversion. The phosphorous removal efficiency was attributed not only to biological consumption, but interaction with aluminum cations released into the aqueous phase as a result of electrokinetic processes. Thus, alumophosphate species were produced and precipitated out of the sludge with some depositions on the surface of the cathode and the membrane. SRF

reduced by 45% compared to reference AnMBR state and SVI reached 54% reduction in EAnMBR configuration.

Although AnMBR demonstrated very good treatment of high-strength wastewater, EAnMBR outperformed conventional advanced anaerobic membrane system and provided superior effluent quality due to involvement of electrokinetic processes.

4.3. Phase III Results and Discussion

This chapter represents state of the findings during Phase III, where real industrial wastewater was used in AnMBR and EAnMBR. The results and discussion are structured and provided for Stage I and II, a comparative analysis between the stages summarizes this chapter.

4.3.1. Stage I: Operation and Performance of the AnMBR in Treating Industrial Wastewater

The continuous AnMBR operation during the Stage I was conducted under constant temperature of 36 ± 1 ^{0}C for 60 days at SRT 21 days and HRT 4 days. The AnMBR was fed with the high-strength industrial wastewater at a food to microorganism ratio (F/M) of 0.25 g COD/g MLSS/day. Consequently, the feed concentration increased accordingly with MLSS concentration.

4.3.1.1. Carbon Removal Efficiency in AnMBR

The maximum COD removal efficiency in AnMBR reached 93 % after 60 days of continuous operation (Figure 4.81, Table 4.4). The influent concentration was $53\pm1.3gL^{-1}$ during the duration of Phase III. After 20 days of operation, a sharp spike in COD removal rate was observed. This suggested that the anaerobic microbial community was adapted to conditions in the AnMBR and entered to exponential phase of growth. That allowed to start the conversion of organic compounds gradually, increasing to the maximum level by the end of the operating cycle (the concentration in the effluent reduced from 9.78 gL^{-1} at day 1 to 3.5 gL^{-1} at day 60). Part of the carbonaceous content of the molasses wastewater is glucose, which may be attributed to the high removal rate of COD.

The summary reactions of possible fermentative hydrogen production from glucose at pH of the aqueous phase 5.2 ± 0.2 demonstrate that the acetate predominantly can be transformed to

hydrogen at these conditions (Figure 2.3), with a theoretical production rate of 4 mol hydrogen mol/L glucose [292]:

$$C_6H_{12}O_6 + 12H_2O \rightarrow 6HCO_3^- \; 12H_2 + 6H^+; \; \Delta G^0 = 241 \text{ kJ mol}^{-1} \tag{4.28}$$

$$C_6H_{12}O_6 + 4H_2O \rightarrow 2CH_3COO^- + 2HCO_3^- + 4H_2 + 4H^+; \; \Delta G^0 = 48 \text{ kJ mol}^{-1} \tag{4.29}$$

$$C_6H_{12}O_6 + 2H_2O \rightarrow 2CH_3CH_2CH_2 \; COO^- + 2HCO_3^- + 2H_2 + 3H^+; \; \Delta G^0 = -137 \text{kJ mol}^{-1} \tag{4.30}$$

$$C_6H_{12}O_6 + 3H_2O \rightarrow 2CH_3CH_2OH + CH_3COO^- + 2HCO_3^- + 2H_2 + 3H^+; \; \Delta G^0 = -97 \text{kJ mol}^{-1} \tag{4.31}$$
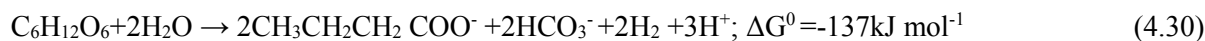
Another expected carbon conversion pathway- fermentation with butyrate as the major product is considered to be the most effective hydrogen-producing pathway. This type of fermentation is carried out by *Clostridium sp.*, with a maximum hydrogen yield, demonstrated experimentally, of 2.9 mol H_2 mol $^{-1}$ glucose. In contrast, production of propionate decreases the production of hydrogen.

$$C_6H_{12}O_6 + 3H_2O \rightarrow 2H_2 + 2CH_3CH_2COO^- + 2H_2O + 2H^+ \tag{4.32}$$
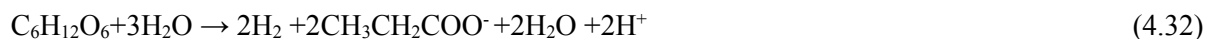
The activity of acetogen *Clostridium aceticum* may increase consumption of hydrogen or glucose [292].

$$2HCO_3^- + 4H_2 + H^+ \rightarrow 2CH_3COO^- + 4H_2O \tag{4.33}$$

$$C_6H_{12}O_6 \rightarrow 2CH_3CH_2 \; COO^- + 2H^+ \tag{4.34}$$
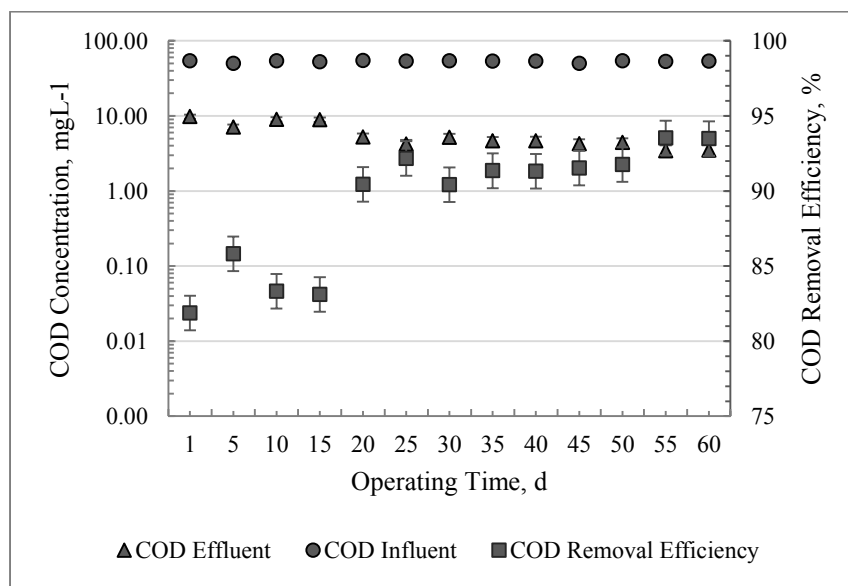
Figure 4.81. Phase III Stage I: Dynamics of COD removal over the time in the AnMBR

Despite the advantages of high rate anaerobic systems discussed in Chapter 2, the presence of sulfate (SO_4^{2-}) concentration in the molasses wastewater can represent a serious risk for the system and inhibit carbon removal [108]. COD/SO_4^{2-} relationship is one of the major factors that was assessed to evaluate the efficiency of the combined treatment in AnMBR.
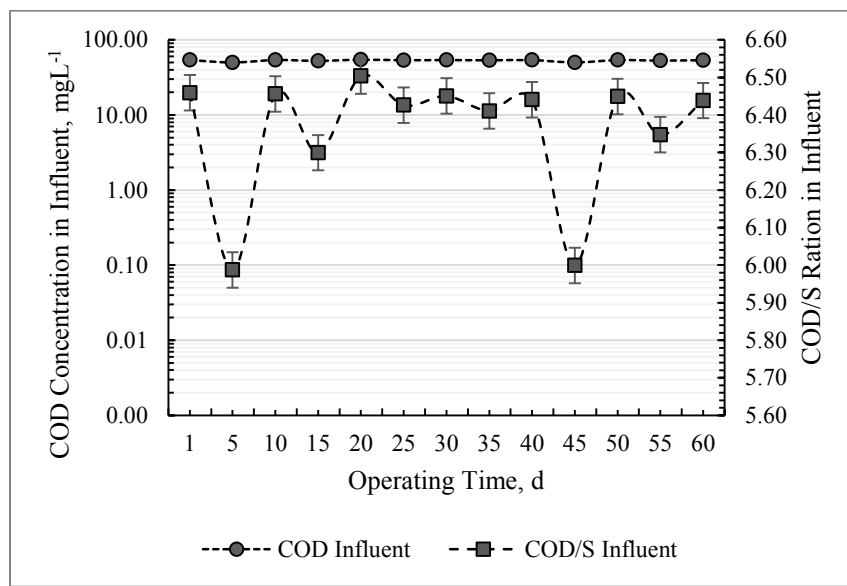
Figure 4.82. Phase III Stage I: Relationship between COD in the influent and the amount of sulfur in the aqueous phase

In conventional anaerobic reactors, for successful anaerobic treatment, the ratio COD/SO_4^{2-} should be > 10, although according to some research, this ratio can be as low as 5 to 8 [293]. In this research, COD/SO_4^{2-} in the influent was found to be in the range from 5.99 to 6.50 (Figure 4.82) with the minimums at the day 5 and 45 and peaks at the day 20 and 50.

In the treated effluent, the ratio was gradually increasing in the course of the operation ranging from 2.04 to 4.26 starting from the day 5 and reaching the maximum at the day 50 (Figure 4.83). Based on the data presented in Figure 4.83, it can be concluded that the decrease of COD/SO_4^{2-} ratio had no any adverse effect COD removal efficiency in the AnMBR as SO_4^{2-} was, probably, reduced by sulphate-reducing bacteria in the reactor as an electron donor to H_2S in the presence of organic carbon sources, which provided the necessary energy according with the following equation [108]:

$$2CH_3CHOHCOO- + SO_4^{2-} \rightarrow 2CH_3COO- + 2HCO_3^- + H_2S \tag{4.35}$$
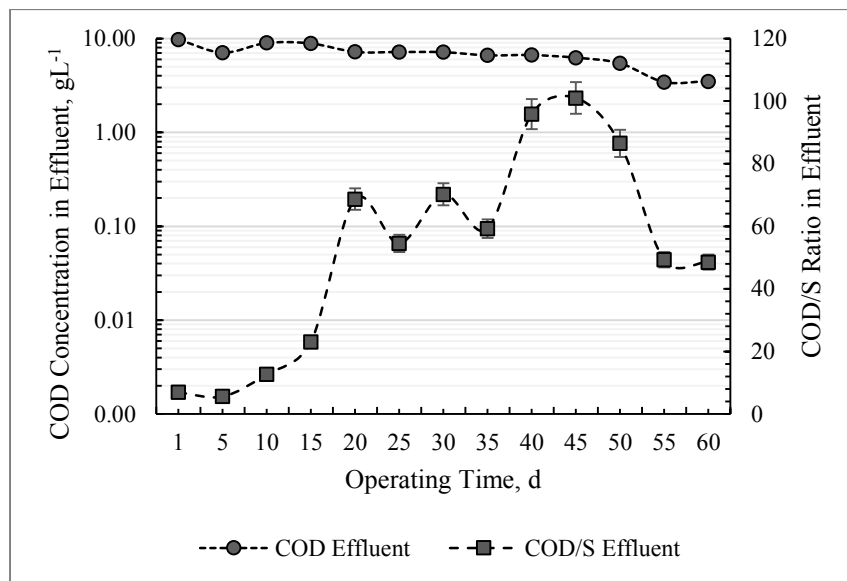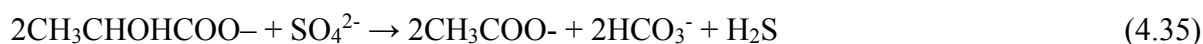
Figure 4.83. Phase III Stage I: Relationship between COD in the effluent and the amount of sulfur in the aqueous phase

4.3.1.2. VFAs

The VFA (expressed as acetate in milligrams per liter) concentration in the feed was stable during the Stage I and equal to $8,736\pm1.73$ mgL^{-1}. After the start-up period, the VFA concentration of the AnMBR effluent decreased from 1,688 to 74.7 mgHAcL^{-1} on days 1 to 60 (Figure 4.84) with stabilization at around $103-113$ mgHAcL^{-1} starting from day 40 and beyond. VFA rejection was also observed throughout the stage, which caused a decrease in the VFA and an increase in the pH from the final permeate.

The COD and the total VFA concentrations are presented in Figure 4.85. The results demonstrate that only a small part of the COD concentration comprises VFA, indicating that the significant part of the VFA concentration was utilised for biological nutrients and sulfur reduction. It can also be observed that the VFAs concentration fluctuations follow the pattern of the COD concentration over the time, showing that the VFA generation and utilisation are related to the COD production and consumption. It was observed that, initially, both the COD and the VFA concentrations increased but sharply decreased from day 5. This observation also indicated that part of the residual COD comprised propionate, oxidation of which might be the rate-limiting factor in the reduction of COD [294].

169
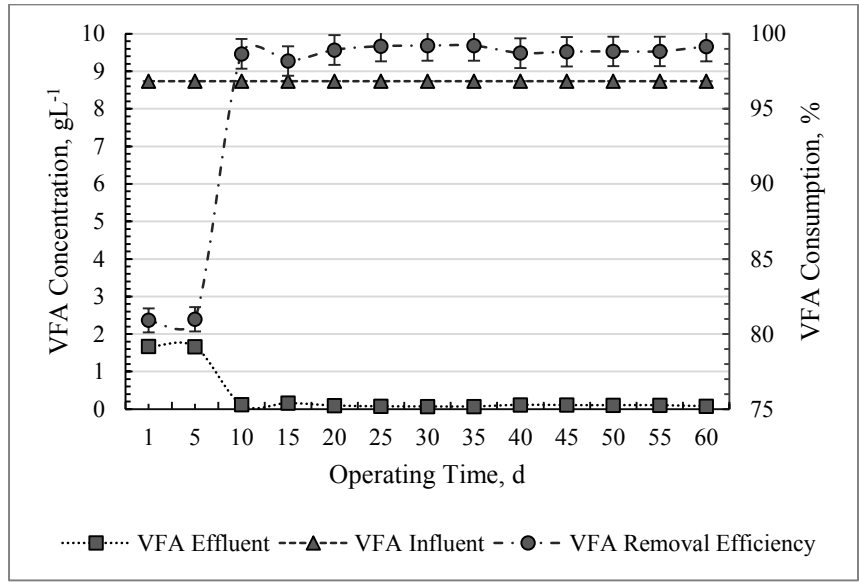
Figure 4.84. Phase III Stage I: VFAs concentration and consumption in the AnMBR
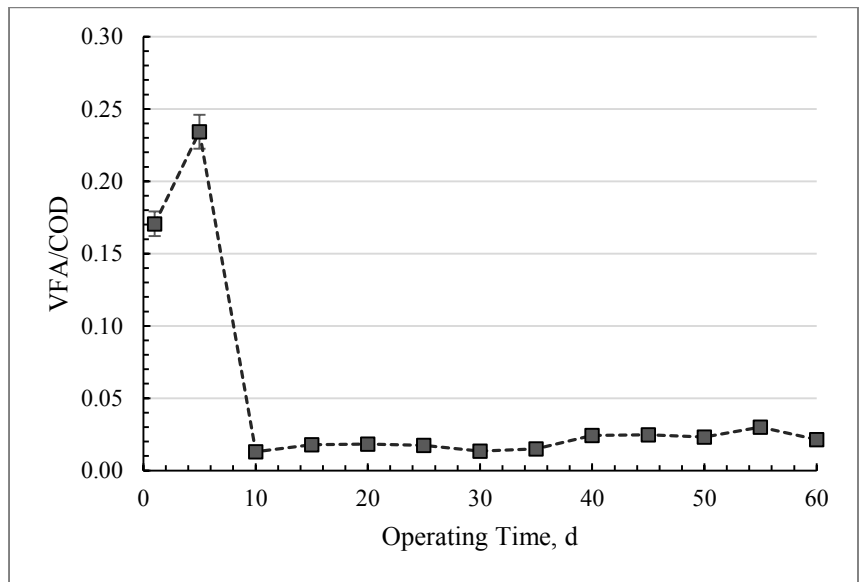
Figure 4.85. Phase III Stage I: VFA/COD ratio in the effluent from the AnMBR

4.3.1.3. Nitrogen Removal Performance in the AnMBR

In EAnMBR operating as AnMBR (without electrical field), the overall denitrification process was performed in three different biological processes. The first process was the heterotrophic

denitrification in which carbon was extracted from the organic materials and nitrate served as an electron acceptor (Equation 4.36).

$$5CH_3OH + 6NO^{3-} \rightarrow 3N_2 + 7H_2O + 5CO_2 + 6OH^- \qquad (4.36)$$

In single heterotrophic denitrification, as shown in Equation 4.36, the theoretical C/N ratio for complete denitrification was established as 0.71 according to theoretical stoichiometric equations when the carbon source was methanol [295].

The second denitrification process in EAnMBR was performed by the autotrophic hydrogen denitrification path (anammox) in which the hydrogen was produced as a result of acetogenesis and acted as an electron donor, whereas nitrate as an electron acceptor (Equation 4.3-4.8).

As the wastewater contained high concentration of sulfur, it was reasonable to speculate that the third process was the sulphate reduction in which sulphate ion served as an electron donor and ammonia as an electron acceptor. The sulphide ion can donate two electrons, and thus, can be converted into elemental sulphur which was visually confirmed. Considering the stoichiometric ratio in the chemical reaction between ammonia and the sulphide ion (sulphate ion), the nitrogen can be decreased according to Equation 4.37 (overall) and 4.38-4.40 [64]:

$$SO_2^{4-} + 2NH_4^+ \rightarrow S^0 + N_2 + 4H_2O \qquad (4.37)$$

$$3SO_2^{4-} + 4NH_4^+ \rightarrow 3S^{2-} + 4NO_2^- + 4H_2O + 8H^+ \qquad (4.38)$$

$$3S^- + 2NO_2^- + 8H^+ \rightarrow 3S^{2-} + N_2 + 3S^0 + 4H_2O \qquad (4.39)$$

$$2NO_2^- + 2NH_4^+ \rightarrow N_2 + 4H_2O \qquad (4.40)$$

Therefore, the COD/N ratio was one of the most important factors determining the denitrification efficiency during the Phase III.

Stage I was operated at influent TN concentration of $2,342\pm146$ mgL^{-1} and sulphate $8,736\pm1.73$ mgL^{-1}. During the first 15 days of operation, the AnMBR reduced ammonium in the effluent from 1,050 mgL^{-1} to 118 mgL^{-1} (Figure 4.86). When the nitrification potential of the reactors increased due to the growth of the denitrifying and sulfur-reducing bacteria and the conditions achieved the steady state, the denitrification performance in the reactor was constantly higher than 95% with the rate as high as up to 98%. Sulphate reduction increased from $1440\pm$ mgL^{-1} at the beginning to $72.1\pm$ mgL^{-1} in the end (99.14 % removal efficiency).

On the other hand, nitrate and nitrite concentration in the AnMBR also declined from 9.9 mgL^{-1} to 2.08 mgL^{-1} (97% reduction) during the entire operating period due to the high denitrification rate. The highest removal efficiency was achieved on days 45 and 60, when the effluent concentrations of ammonium (33.4 mg NH$_3^+$L^{-1}), nitrate and nitrite (2.08 mgL^{-1}), TN (63.6 mg NL^{-1}) and DON (28.10 mg NL^{-1}) with the highest removal efficiency of 98.06%, 98.27%, 97.77%, and 97.22% respectively (Figure 4.87). The EAnMBR proved again the possibility of achieving practically complete denitrification of ammonium and complete denitrification of nitrate if the loading of ammonium into the reactor was lower than the nitrification capacity of the system, which was the case in the Stage I.

The COD/TN ratio increased from 5.53 to 55.03 and high denitrification rate during the course of the experiment supported the fact that high C/N ratios could accelerate the growth of heterotrophic denitrifying bacteria in the reactor and thus promote the denitrification rate. Despite antioxidant properties of the melanoidin, the substantial reduction of nitrate/nitrite concentration in the significant predominance of organic carbon (Figure 4.88) and sulfur sources indicates the role of the heterotrophic and sulfur-reducing denitrification, where electron donors were taken from organic compounds and sulphate. However, the anammox process using nitrite from the incomplete nitrification as electron acceptor helped in reducing the production of nitrate in the reactor as well (Figure 4.86, 4.87).
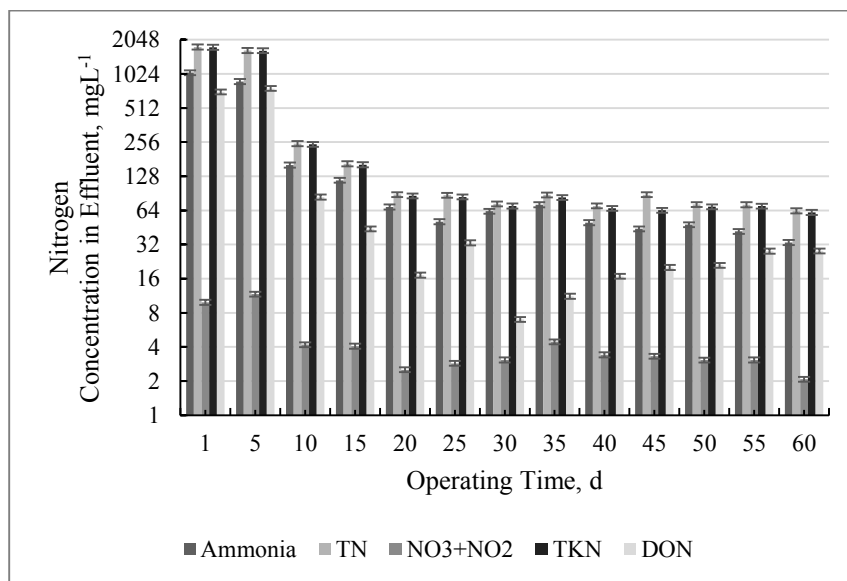
Figure 4.86. Phase III Stage I: Nitrogen fractions concentration in the effluent from the AnMBR

Therefore, anammox with the other two denitrification processes acting simultaneously in the reactor ensured an effluent with a very low nitrogen species concentration compared to the influent, which was the case in this study.
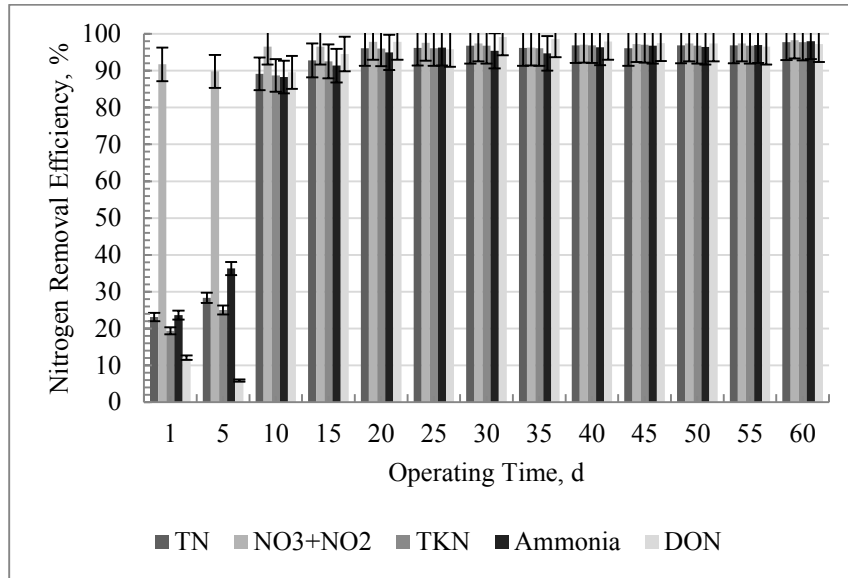
Figure 4.87. Phase III Stage I: Nitrogen fractions removal dynamics in the AnMBR
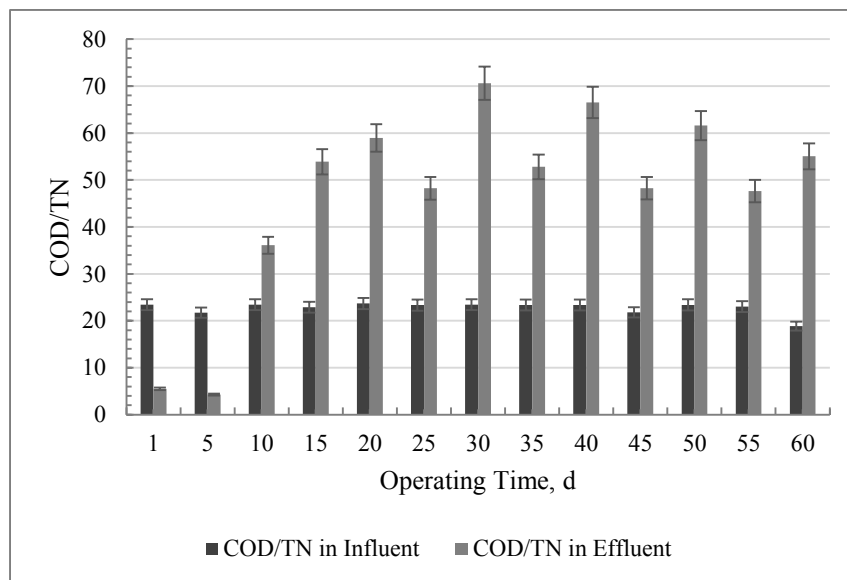
Figure 4.88. Phase III Stage I: COD and TN relationship in the aqueous phase

4.3.1.4. Phosphorous Removal Performance in the AnMBR

The effluent TP concentration decreased in the system operated as AnMBR from around 77.6 mgL^{-1} at the day 1 up to 1.84-2.17 mgL^{-1} of TP with the maximum removal efficiency in the MBR achieved up to 98.79% (Figure 4.89). The COD/TP ratio was gradually increased in the same time from 126.03 to 1,612.90 with peak periods at day 20, 30-35, 45, and 50 (Figure 4.90).
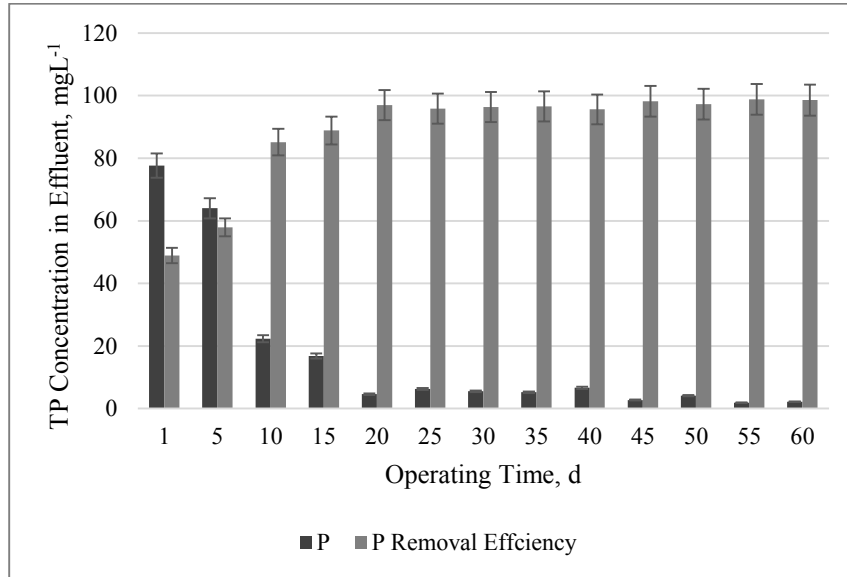
Figure 4.89. Phase III Stage I: Phosphorous concentration in the effluent and phosphorous removal efficiency in the AnMBR
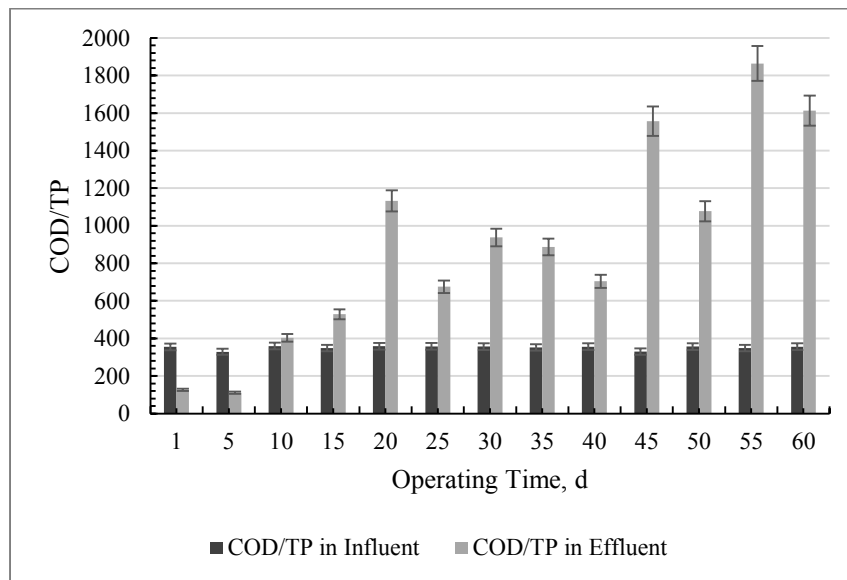
Figure 4.90. Phase III Stage I: COD and TP relationship in the aqueous phase

174

The influent concentration of phosphorus measured as TP in the feed was 151.30 ± 0.72 mgL^{-1}. The concentration in the effluent sharply decreased during the first 10 days of the study (from 77.6 mgL^{-1} to 22.3 mgL^{-1}). On day 15, the TP concentration reached 16.8 mgL^{-1} whereas 5 days later it was 4.6 mgL^{-1} only. Starting from day 20, it reduced relatively constantly and reached 1.84–2.17 mgL^{-1} during the last days. The lower removal rate of phosphorus during the initial period of operation can be attributed to the slow adjustment of the anaerobic microbial community to the changes in the feed stream (significantly higher concentration of COD and nutrients compared to Phase II). Biological phosphorus removal was performed by mechanism described in Section 4.2.1.3.3. Increase in MLSS concentration in the electro-bioreactor boosted the phosphorus uptake and therefore, contributed to the overall performance.

The experimental results demonstrated that the AnMBR system developed in this research was highly effective over the long-term experimental operation and evidenced the stable performance of the AnMBR treatment process.

4.3.1.5. Mechanism of Discoloration in the AnMBR

Food-producing industries utilizing beet molasses as raw material generate highly recalcitrant wastewaters [67]. Before disposal, the wastewater undergoes biological sequential anaerobic/aerobic treatment in order to minimize environmental impact. The resultant effluent remains highly colored. As discussed in Chapter 2, color presence in the effluent is a result of high melanoidins concentration- acidic polymers with a complex structure, mainly built up from sugar degradation products formed in the early stages of the Maillard reaction, polymerized and linked by amino compounds. These chromophores are recalcitrant to biodegradation processes and remain in the biologically and chemically treated effluents [95]. Therefore, the color changes were assessed during the continuous 60 days experiment with the industrial wastewater in order to evaluate the practical application of AnMBR. Figure 4.91 shows the color changes in influent and the membrane effluent. Figure 4.92 demonstrates color removal efficiency by the AnMBR during the Stage I of the Phase III.

The concentration of color substances in the feed wastewater was $19,969\pm114$ mgL^{-1} Pt-Co that corresponded to the dark-brown color of the liquid phase. The color in the effluent however was reduced to 1,200 mgL^{-1} in the first day of operation, which corresponded to 94%

of removal performance. After 5 days, the concentration was further reduced to 600 mgL^{-1} (97%).
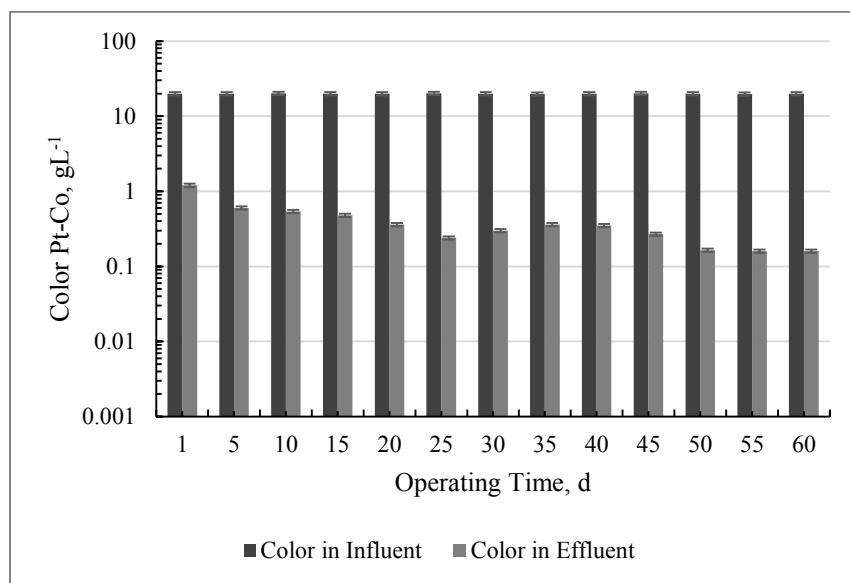
Figure 4.91. Phase III Stage I: Color in the influent vs in the effluent over the time
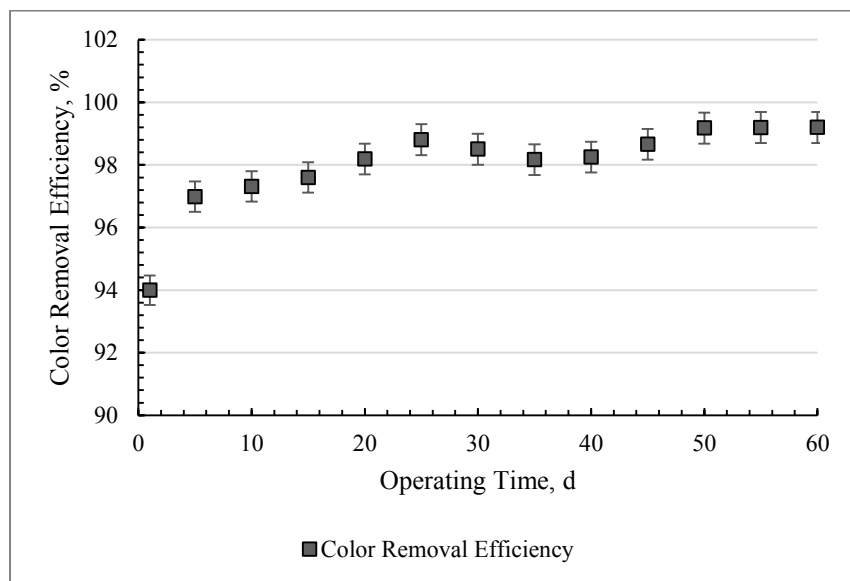
Figure 4.92. Phase III Stage I: Color removal efficiency

These results suggested that the primary removal mechanism of the chromophores was the membrane filtration since the biological decomposition is a slow process and could not

contribute to the performance at this point. After significant drop in concentration during the first days, the removal rate was consistently high during the course of the study and reached 160 mgL^{-1} by day 60, or 99.20% of removal. Figures 4.93 and 4.94 show COD/Color and DON/Color ratio.
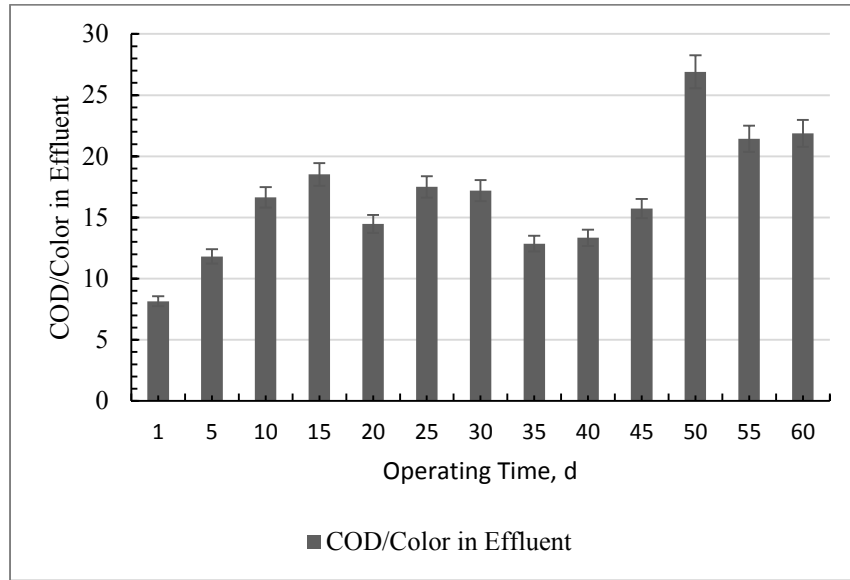
Figure 4.93. Phase III Stage I: Effect of COD on the color in the AnMBR
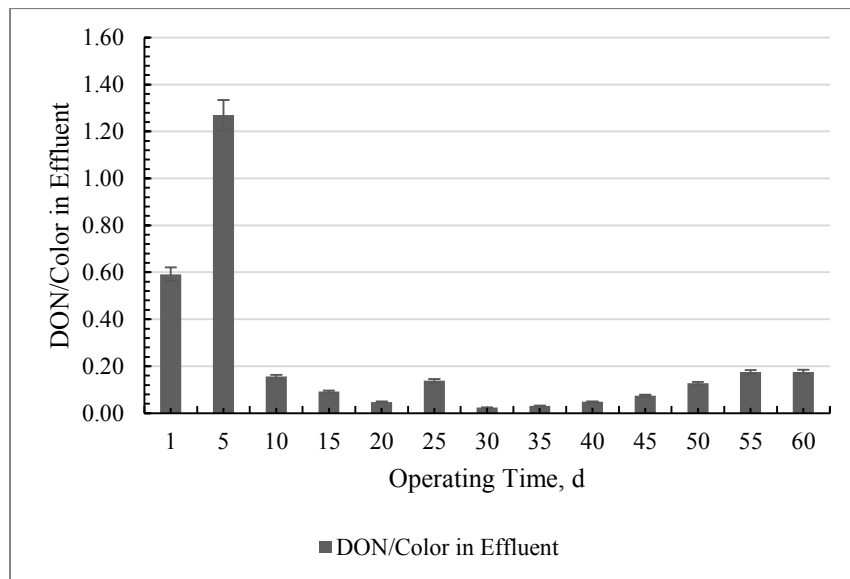
Figure 4.94. Phase III Stage I: Effect of DON on the color in the AnMBR

A fairly strong positive trend in COD/Color relationship could be observed suggesting that the fraction of organic chelates was reduced over the course of the experiment, especially during the periods from day 1 to 15 and day 40 to 55. The maximum of COD/Color ratio was observed on day 55 and the minimum at the beginning of the run. COD/Color ratio strongly correlated with carbon removal efficiency depicted on Figure 4.93. Minima and maxima in color removal efficiencies corresponded to minima and maxima of COD/Color ratios. Therefore, it can be concluded, that the significant portion of carbon-containing particles included chromophores as structural components, and organic fraction was represented by colored humic acids and phenolic compounds.

Color-forming substances were also partially represented by DON as the correlation between nitrogen particles and color was observed as well. DON/Color ratio demonstrated changes in color with respect to changes in DON concentration in the effluent. The mass of nitrogenous compounds removed relative to the mass of colour removal was also obvious. Significant decrease of color components in the DON fraction during the first days of operation can be explained by the rejection of significant part of DON by the membrane module. After 10 days of operation, nitrogenous chromophores represented only small fraction of DON. DON/Color continued to decrease after day 10 to day 45 (from 1.27 to 0.05) with small spikes at day 25 (0.13). Starting from day 45 until the end of the run, presence of organic fraction in DON slightly increased to 0.17 due to the membrane fouling.

The wastewater quality parameters in the feed and in the treated effluent along with overall performance of the system in Stage I is summarized in Table 4.4. pH changed from 5.2±0.20 to 6.3±0.20 from the beginning to the end of the experiment respectively. The overall removal efficiency of COD, total nitrogen, total phosphorus and color was 89.24, 97, 98.52, 99.20% respectively. These results demonstrated a significant improvement of effluent quality compared to other studies conducted previously in MBR [117]. They reported the overall COD removal efficiency of the two-stage system 87±2%.

Table 4.4. The influent and effluent concentrations and the performance of the AnMBR

Parameter	Influent, mgL^{-1}		Effluent, mgL^{-1}		Average Removal Efficiency, %
	Average	Standard Deviation	Average at the End of Stage I	Standard Deviation	
pH	5.2	±0.20	6.3	±0.20	-
COD	53,114	±1380	3790	±35.00	89.24
N$_{tot}$	2,300	±2.00	69	±4.00	97.00
P$_{tot}$	151	±0.72	2.24	±0.37	98.52
Color	19,969	±113.58	160	±2.35	99.20

4.3.2. Stage II: Operation and Performance of the EAnMBR Treating Industrial Wastewater

The EAnMBR was continuously operated during the Stage II under constant temperature of 36±1ºC for 60 days at SRT 21 days and HRT 4 days similar to Stage I. The EAnMBR was fed with the high-strength industrial wastewater at a food to microorganism ratio (F/M) of 0.25.

4.3.2.1. Carbon Removal Performance in the EAnMBR

Figure 4.95 illustrates the variations of the COD concentration in the influent and the membrane effluent throughout Stage II of Phase III; whereas Figure 4.96 illustrates the corresponding overall performance of the EAnMBR system. The removal efficiency of the COD of the whole system is expressed by Equation (4.2). While the removal efficiency varied between 81.87% and 93.53% during Stage I, Figure 4.96 demonstrates that the overall system can provide consistently higher COD removal when electrokinetic processes are involved. The total COD removal efficiency of the system was maintained at a high level surpassing 99% because of the combined effect of electrokinetic phenomena, biological processes and efficient filtration of the membrane module. The results obtained during the run confirmed that the electrokinetics played an important role in providing an excellent and stable effluent quality

during the EAnMBR process. The removal mechanism of organics is related to organics conversion to negatively charged SMP and EPS in the EAnMBR and attraction to the long chains of aluminum hydroxides with net positive charge [136]. These hydroxides are able to remove SMP and EPS by making organic/inorganic solid complexes by means of electrostatic forces and adsorption. Since the pH in the reactors was always between 7 and 8, the surfaces of microbial products carry a net negative charge due to the broken edges of hydroxyl groups in alkaline medium. This negative charge enables SMP to get attracted to the aluminum hydroxides. However, this process is likely to be facilitated under the influence of the direct current field. During Stage I of Phase II, most of the COD was degraded by the microbial activity in the bioreactor and rejected by the membrane module as some of the larger EPS particles migrated towards membrane did not block the pores and were washed out by biological gases, as it was discussed in details earlier. Similar result was obtained during Phase II of this research. Although the overall COD removal efficiency remained stable at around 81 - 90% during the Stage I, from the beginning of Stage II until the end, the application of a DC field through the MLSS solution increased the COD removal efficiency by more than 10 % compared to Stage I. This observation can be attributed to the effect of the electro-coagulation phenomenon. That is very important conclusion because as it was reported previously, some fractions of organic matter in the mixed liquor have higher affinities with the membrane than do other fractions and consequently cause greater irreversible fouling [272, 274]. Consequently, applying a DC field to the mixed liquor can reduce the load contributed by the organic matter on membrane fouling, i.e. formation of complexes with aluminum hydroxides and removal from membrane surface by synergetic effect of bio and electrolytic gases movement. This conclusion may explain the good performance of the EAnMBR system during Stage II where the concentration of COD decreased dramatically despite the high concentration of organics in the wastewater.
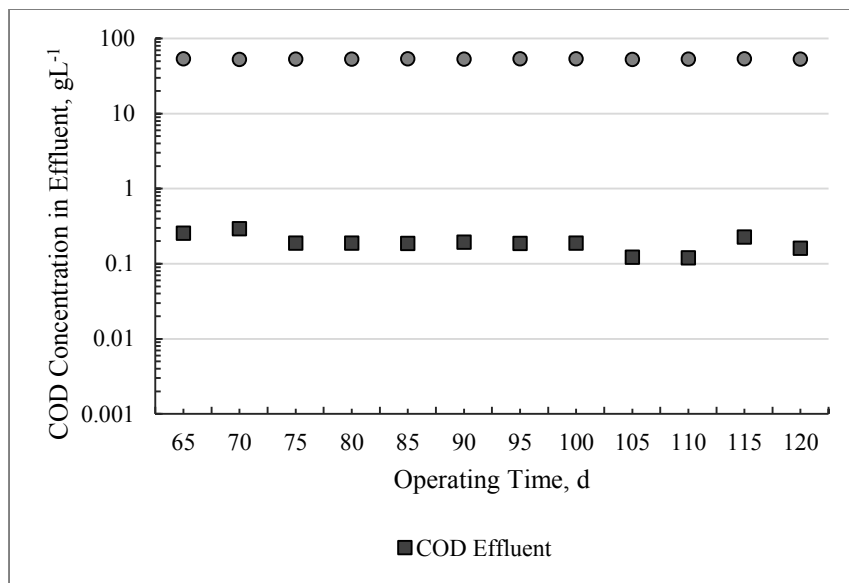
Figure 4.95. Phase III Stage II: Dynamics of COD removal over the time in EAnMBR

The presence of sulfate (SO_4^{2-}) ions in the molasses wastewater can represent a serious risk for the system and inhibit biological activity for carbon removal [108]. COD/SO_4^{2-} relationship in Stage II was assessed to evaluate the efficiency of the combined treatment in EAnMBR and compared to Stage I. In the Stage II, COD/SO_4^{2-} in the influent was found to be in the range 6.41±0.05 (Figure 4.97) with the minimums at the day 70 and 105 and peaks at the day 85, 100 and 115 (similar pattern to Stage I).
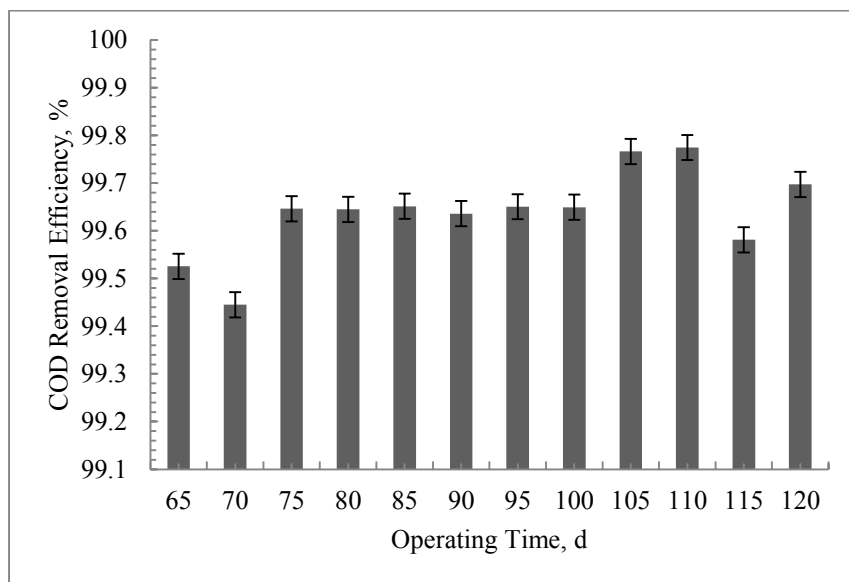
Figure 4.96. Phase III Stage II: COD removal efficiency in the EAnMBR

In the treated effluent, however, the picture was completely different to Stage I (Figure 4.59). The ratio was dramatically decreased from 48.54 on the last day of Stage I (day 60) to 3.45 at the beginning of the Stage II (day 65). Afterwards, the ratio remained relatively constant in the course of the operation ranging from 2.01 to 4.26. The COD/S ratio started decreasing slightly on day 100 up to day 105-110 when it reached its minimum of 2.01-2.04 and then gradually increased once again up to the end of the experimental Stage II. Based on the data presented in Figure 4.98, it can be concluded that the increase of COD/SO_4^{2-} ratio had no any adverse effect on COD removal efficiency in the EAnMBR as sulfur was, reduced by sulphate-reducing bacteria in the reactor as an electron donor to H_2S in the presence of organic carbon sources, which provided the necessary energy according to eq. 4.35. However, majority of sulphur was removed by electrokinetic phenomena involved in this stage of operation. Trivalent Al^{3+} ions cannot combine with H_2S and sulfide ions (HS^- and S^{2-}) in aqueous phase to form insoluble precipitates like does iron, however, aluminium sulfate $Al_2(SO_4)_3$ is formed as a result of interaction of $Al3^+$ released from anode and SO_4^{2-} ions in aqueous phase. This is a chemical compound soluble in water and is a flocculating agent. The aluminum sulphate was formed according to reaction 4.41:

$$2Al^{3+} + 9SO_4^{2-} \rightarrow 3Al_2(SO_4)_3 \tag{4.41}$$

Aluminum sulphate further reacted with alkalinity to form aluminum hydroxide, calcium sulphate and carbon dioxide according to the formula 4.42:

$$Al_2(SO_4)_3 + 3Ca(HCO_3)_2 \rightarrow 2Al(OH)_3 + 3CaSO_4 + 6 CO_2 \tag{4.42}$$

The formation of soluble aluminum sulphates and little soluble calcium sulphate in the EAnMBR had a positive multiplication effect on the overall removal efficiency of EAnMBR.
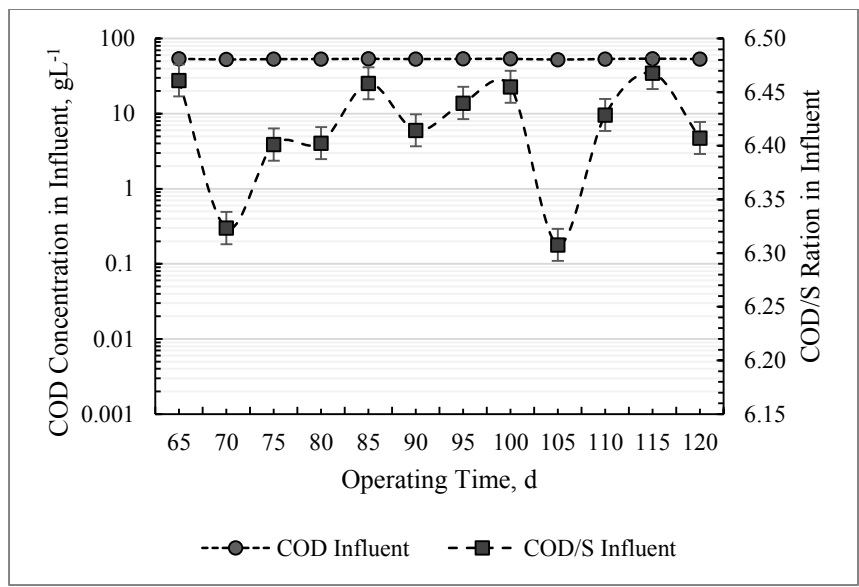
Figure 4.97. Phase III Stage II: Relationship between COD in the influent and the amount of sulfur in the aqueous phase
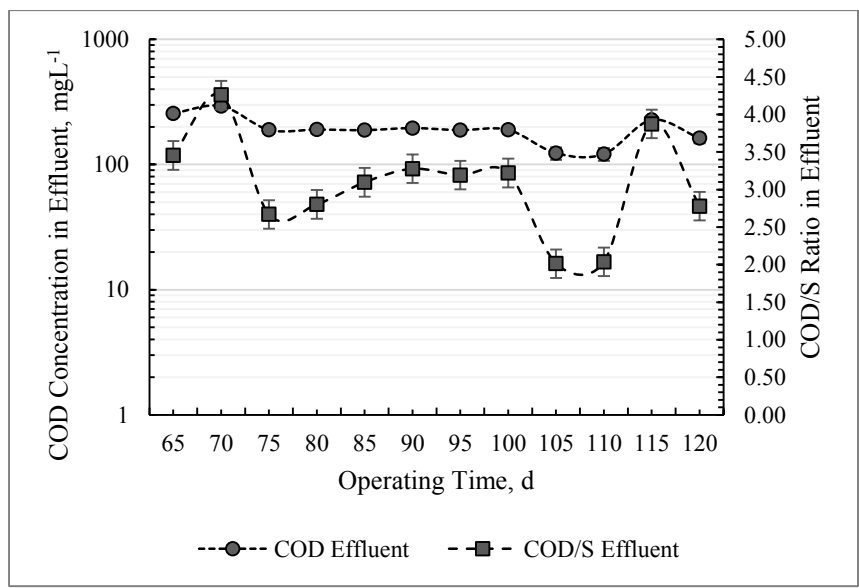
Figure 4.98. Phase III Stage II: Relationship between COD in the effluent and the amount of sulfur in the aqueous phase

4.3.2.2. VFAs

The molasses-containing wastewater undergoes biological sequential anaerobic/aerobic treatment before disposal to water bodies in order to minimize environmental impact, as a result, it contains a high amount of VFAs. [154].

The VFA concentration in the feed was similar to the Stage I and equal to $8{,}736 \pm 1.73$ mgL^{-1}. After application of the DC field, the VFA concentration of the EAnMBR effluent decreased from 57.2 at the beginning of Stage II (day 65 of Phase III) to 38.6 mgHAcL^{-1} on day 80 (Figure 4.99) which corresponded to removal efficiency increase from 99.35% to 99.56%. However, starting from day 85, an increase was observed up to 67.5 mgHAcL^{-1} which stabilized at around 67.5–73.7 mgHAcL^{-1} during the following 15 days of the experiment. Further increase of VFA content was observed until the end of the stage (167 mgHAcL^{-1} on day 105 to 259 mgHAcL^{-1} on day 120). This observation is best explained by the H_2 generation during the process of electrolysis as a result of the current application to the system. This, in turn, boosted the acidogenesis of the residual components left after hydrolysis, to then produce a highly concentrated mixture of VFAs.
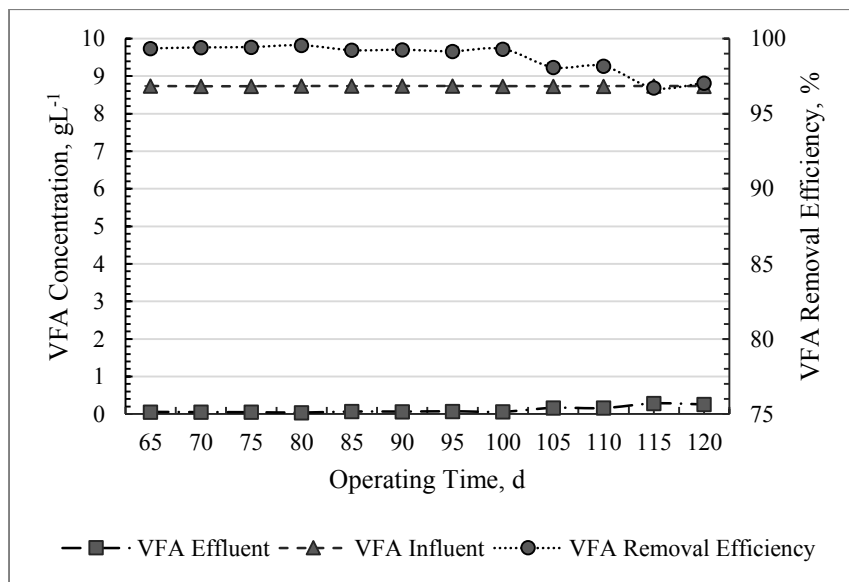
Figure 4.99. Phase III Stage II: VFAs concentration and consumption in the EAnMBR

The COD/VFA relationship is presented in Figure 4.100. It can be observed that the ratio remained small from day 1 of the Stage II until day 100. During this period only a small part of the COD concentration comprised VFA, indicating that the significant part of the VFA concentration was utilised for biological nutrients and sulfur reduction. However, electrokinetic phenomena boosted generation of VFAs production and COD/VFA ratio increased accordingly. It can also be observed that the VFAs concentration fluctuations followed the pattern of the COD concentration over the time, showing that the VFA generation and utilisation were related to the COD production and consumption. Initially, both the COD and the VFA concentrations fluctuated in accordance before a sharp increase of VFA on day 100. Overall performance in VFA reduction was 98.73±0.95%, which was 2.61% better compared to 96.12±0.95% obtained during the Stage I.
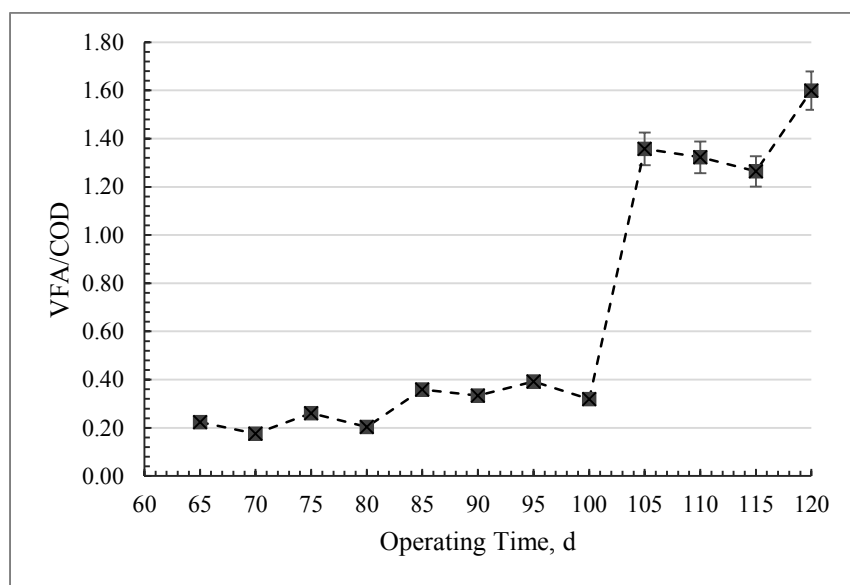
Figure 4.100. Phase III Stage II: VFA/COD ratio in the effluent from the EAnMBR

4.3.2.3. Nitrogen Removal Performance in the EAnMBR

Stage II was operated at influent content of TN 2,298±4 mg NH_3-NL^{-1} and ammonia concentration 1,372.51±2.90 NH_3-NL^{-1}. In this run, the EAnMBR exhibited excellent denitrification from day1 (Figure 4.101). Most of the ammonium was denitrified in EAnMBR from the beginning of the stage and the removal efficiency remained > 99%

until the end of the experiment. Initial increase of TN The nitrate and nitrite concentration was extremely high in the influent (119.5±1.38 mgL^{-1}), however in the effluent of the EAnMBR, it was reduced to 1.3±0.18 mgL^{-1} on average (> 99% reduction). The removal efficiency of nitrate and nitrite remained constantly high throughout the entire run. The effluent concentrations of ammonium were 6.37-7.27 mg NH$_3$-NL^{-1}), TN (32.51±7.76 mg NL^{-1}) and DON (17.53±8.23 mg NL^{-1}) with the highest removal efficiency of 99.53%, 99.98, and 99.43% respectively (Figure 4.102). The DC applied to the system increased removal efficiency of ammonia by 1.47%, nitrate and nitrite by 1.7%, TN and DON by 2.21% compared to Stage I.
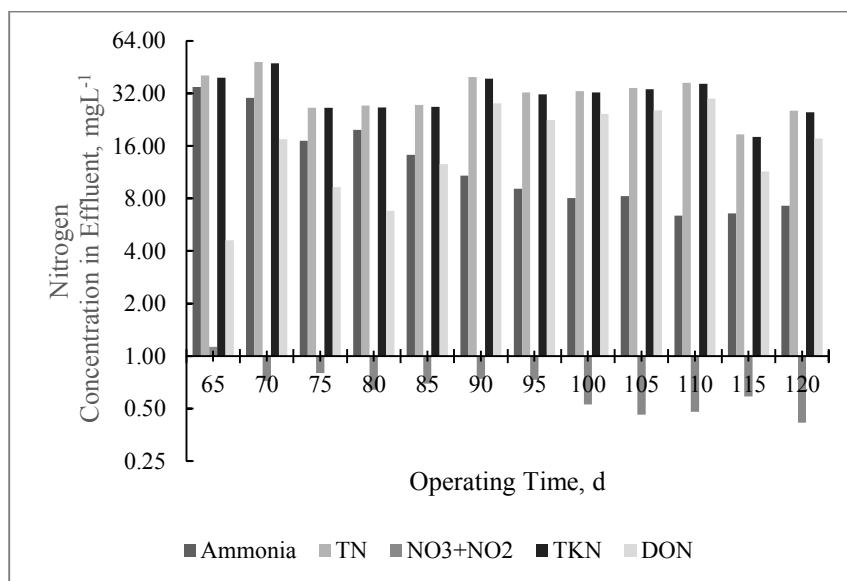
Figure 4.101. Phase III Stage II: Nitrogen fractions concentration in the effluent from the EAnMBR
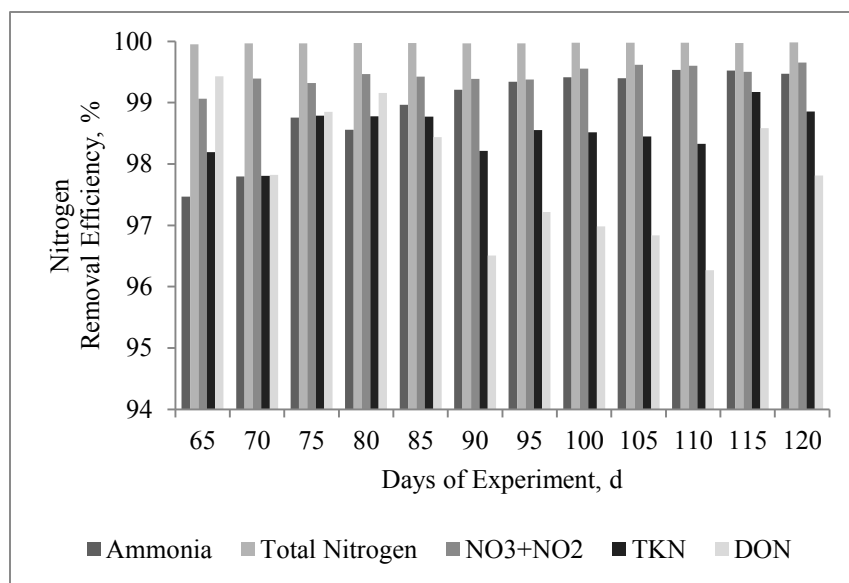
Figure 4.102. Phase III Stage II: Nitrogen fractions removal dynamics in the EAnMBR
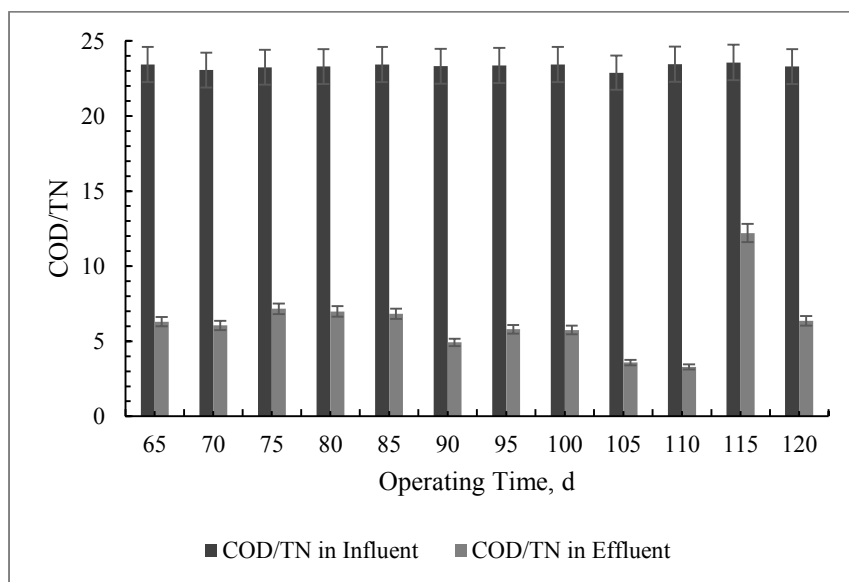
Figure 4.103. Phase III Stage II: COD and TN relationship in the aqueous phase

The concentration of nitrogen fractions in the effluent was clearly attributed to the electrokinetic processes after application of the DC field. On days 110 and 120, the effluent concentrations of ammonia (6.37 mg NH_4^+-L^{-1}), nitrate and nitrite (0.48 mg N-L^{-1}), and TN (118 mg N-L^{-1}) were the lowest with the highest removal efficiency of more than 99%. The

EAnMBR (Figure 4.102) proved again the possibility of achieving almost complete removal of ammonium and other fractions compared to the influent concentration.

In EAnMBR, the same biological processes carried out denitrification as in the Stage I- The anammox with the other two denitrification processes (heterotrophic and denitrification) was working simultaneously with electrokinetics and membrane filtration in one reactor ensuring an effluent with a very low nitrate concentration of nitrogenous compounds.

The COD/TN ratio reduced from 55.03 at the end of Stage I to 6.31 at the beginning of the Stage II after applying the DC field and then further up to the minimum of 3.29 (Figure 4.103). These data suggested that the amount of nitrogen was substantially reduced in the system and the electrokinetic phenomena were jointly responsible for denitrification during the course of the experiment in Stage II compared to the growth of heterotrophic denitrifying bacteria in the AnMBR process.

4.3.2.4. Phosphorous Removal Performance in the EAnMBR

The exposure mode 5-On:20-Off allowed to reach nearly complete removal of phosphorus at the current density of 20 Am^{-2}. The application of the DC resulted in release of Al^{+3} into the aqueous phase, and the concentration was suffice to form aluminum sulphate complexes and bonds, and to extract phosphorous from the liquid phase of the activated sludge in the reactor. Removal efficiency was constantly > 99% when the EAnMBR operated at HRT of 4 and SRT of 21 days respectively (Figure 4.104).

Long HRT led to less loading of dissolved salts into the EAnMBR. At this level of current density, the 5-On:20-Off exposure mode provided enough Al^{+3} ions responsible for P removal. The current density 20 Am^{-2} increased the voltage gradient to compensate for the reduction of the soluble ion concentration due to the HRT. These results confirm that CD and electrical exposure mode were critical to produce the required concentration of Al^{+3} in order to remove phosphorus from the wastewater effectively.
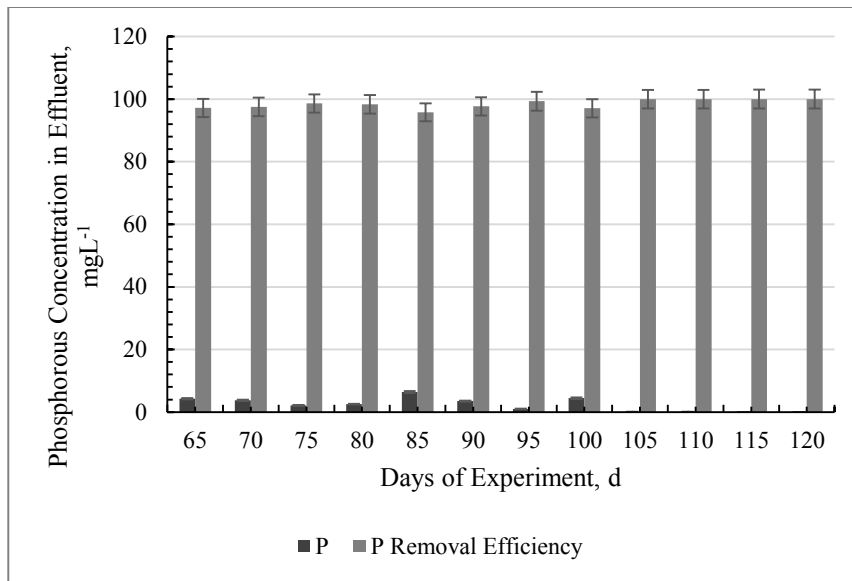
Figure 4.104. Phase III Stage II: Phosphorous concentration in the effluent and phosphorous removal efficiency in the EAnMBR

COD/TP ratio was significantly reduced from 1613 to 60 during the first days of Stage II with small increase on days 70 – 75, reduction from day 80 to 85 and then drastic increase of COD/TP ratio starting from day 105 (Figure 4.105).
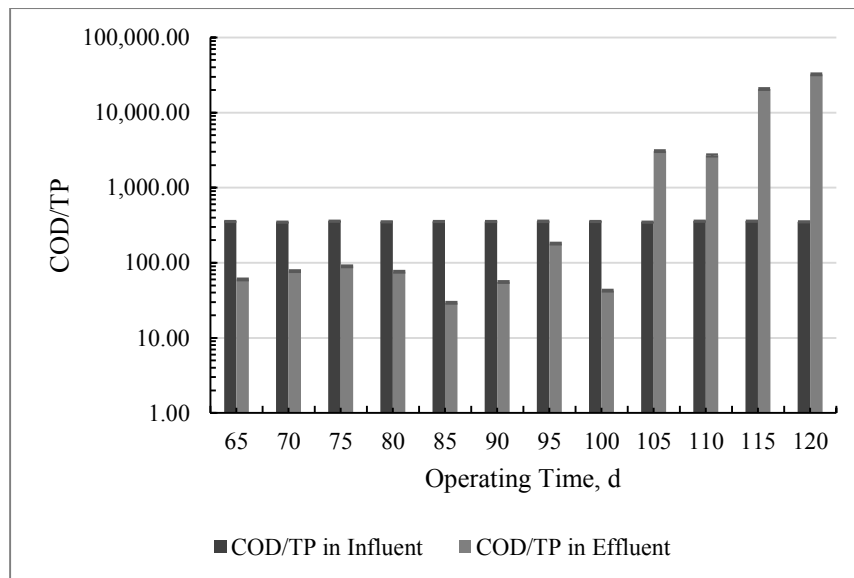
Figure 4.105. Phase III Stage II: COD and TP relationship in the wastewater

This increase coincided with the removal significant efficiency increase (up to 99.99%). The sludge was examined in order to determine the fate of phosphorus in the EAnMBR. For this purpose, the supernatant from EAnMBR was extracted by centrifugation at 2700 g for 20 minutes. The supernatant then was filtered through 0.45 µm glass paper to separate the insoluble and soluble fractions of phosphorous. The results demonstrated that the majority of phosphorous in the EAnMBR was in the soluble form, which explained why it was removed almost entirely from the supernatant and the effluent of EAnMBR; only an insignificant amount of phosphorous still existed in the particulate form.

Since phosphorus in the EAnMBR was not a part of the liquid phase of the sludge, it became a part of the suspended solids of the sludge liquor. In order to confirm this hypothesis, a 1 ml sample of MLSS from the reactor was taken to measure the TP concentration bounded with the solid phase of the sludge liquor. The concentration of phosphorus embedded within the suspended solids was much higher after 14 days of operation. This proves that the influent orthophosphate precipitated in the form of aluminum phosphate complexes. In AnMBR operation, the biological activity was primarily responsible for the phosphorus removal.

The experimental results demonstrated by the EAnMBR system developed in this research suggested that involvement electrokinetics and appearance of oxic interface in the anode zone was highly effective over the long-term experimental operation and evidenced the stable performance of the EAnMBR treatment process.

4.3.2.5. Mechanism of Discoloration in the EAnMBR

Melanoidins behave as anionic hydrophilic polymers, which can form stable complexes with metal cations. It was reported that ketone or hydroxyl groups of pyranone or pyridone residues act as donor groups in melanoidins and participate in the chelation with metals as melanoidins have net negative charge [83, 123, 129, 291]. Therefore, different heavy metals (Cu^{2+}, Cr^{3+}, Fe^{3+}, Zn^{2+}, Pb^{2+}, etc.) form large complex molecules with melanoidins, amino acids, proteins and sugars in acidic medium and get precipitated.
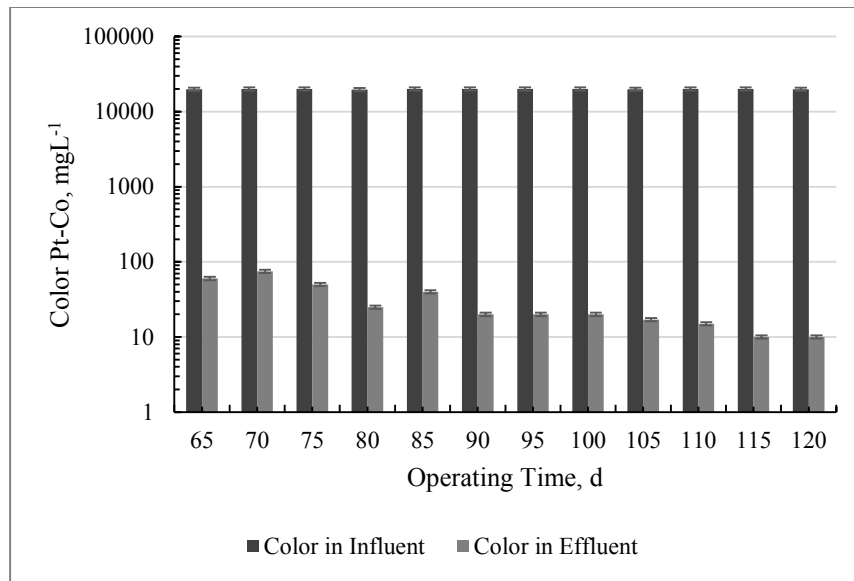
Figure 4.106. Phase III Stage II: Color in the influent vs in the effluent over the time in EAnMBR
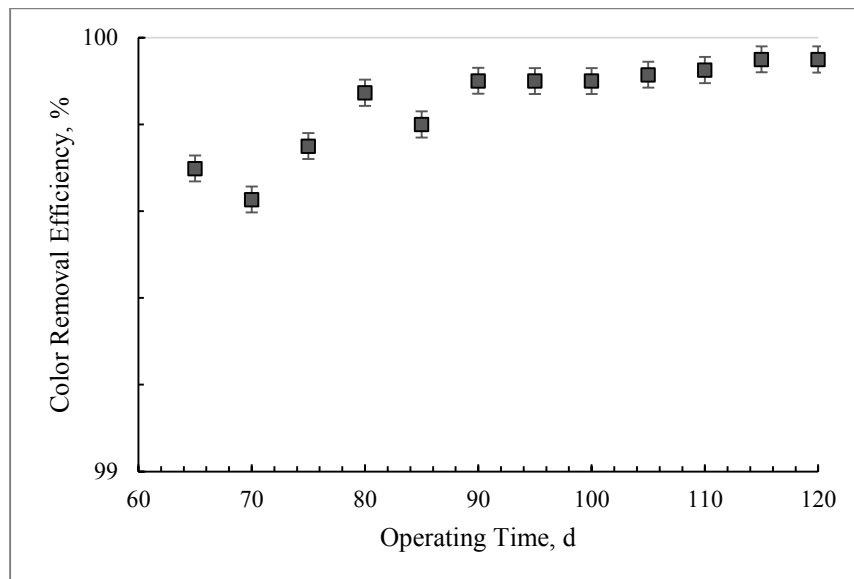
Figure 4.107. Phase III Stage II: Color removal efficiency in the EAnMBR

In this Stage, the color changes were studied during the continuous 60 days experiment with the industrial wastewater under electrical field applied in order to evaluate the practical application of EAnMBR. Figure 4.106 shows the color changes in influent and the membrane effluent during the course of the experiment. Figure 4.107 demonstrates color removal efficiency by the EAnMBR during the Stage II of the Phase III.

The concentration of color substances in the feed wastewater was 19,975±109 mgL^{-1} Pt-Co units that corresponded to the dark-brown color of the wastewater influent, similar to Stage I. However, the color content in the effluent was reduced to 60 mgL^{-1} in the first five days of operation, which corresponded to 99.70% of removal efficiency. The removal of color remained constantly high up to the end of the stage from maximum 75 mgL^{-1} Pt-Co during the first 10 days to 10 mgL^{-1} Pt-Co towards the end (average 99.85±0.1%). The effluent changed color from dark-brown to practically clear in the end of the Stage II.

These results suggested that the primary removal mechanism in the EAnMBR process of the chromophores was electrokinetic mechanism in addition to the membrane filtration. Comparing the result obtained by EAnMBR to AnMBR during the Stage I, the improvement was significant and obvious. A significant drop in the concentration from 160 mgL^{-1} Pt-Co during the last day of Stage I to 60 mgL^{-1} Pt-Co at the beginning of Stage II and further to 10 mgL^{-1} Pt-Co provided additional gain of 100 mgL^{-1} Pt-Co removal, or practically complete removal of color from the effluent from the EAnMBR.

Figures 4.108 and 4.109 provide relationship between the COD and color and DON and color in terms of COD/Color and DON/Color ratios. Similar to AnMBR, a strong relationship between COD and color relationship was observed, suggesting that the fraction of organic chelates was reduced over the course of the experiment starting from day 1. However, magnitude of the ratio was significantly lower compared to Stage I for obvious reasons- the organic content in EAnMBR was also lower as a result of the DC field applied. The maximum of COD/Color ratio was observed towards the end of the experiment- day 115, and the minimum at the beginning of the run, when the concentration of organic substances in the reactor was the highest. COD/Color ratio strongly correlated with carbon removal efficiency depicted on Figure 4.107. Minima and maxima in color removal efficiency corresponded to minima and maxima of COD/Color ratios. Therefore, it can be concluded, that the significant portion of carbon-containing particles included chromophores as structural components, and colored humic acids and phenolic compounds represented organic fraction. Some of them could form colorless chelates with Al^{3+} ions in the aqueous phase in addition to other mechanisms of removal.

Figure 4.109 provides relationship between color-forming substances and DON. The correlation between nitrogen particles and color was observed as for COD/Color. This correlation might suggest that DON also contained color-forming substances as color changed

with respect to DON concentration in the effluent. The higher concentration of nitrogenous compounds removed by EAnMBR relative to the concentration of colour removed by AnMBR was also observed. DON/Color of 0.1756 was observed at the end of AnMBR operation, whereas it dropped to 0.0767 during the first days of Stage II (Figure 4.109). Significant decrease of color components in the DON fraction during the first days of operation can be explained by the rejection of significant part of DON by the membrane module. However, electrokinetic processes involved at this stage significantly improved the quality of the effluent. Nitrogenous chromophores represented only small fraction of DON during the experiment and DON/Color continued to decrease after day until day 45 (from 0.0767 to 0.3150). However, starting from day 45 until the end of the run, presence of organic fraction in DON slightly increased to 1.7630 – 1.9953 due to the membrane fouling which did not, however, affect visual quality of the effluent.

The parameters of wastewater in the feed and in treated effluent along with overall performance of the system in Stage II are summarized in Table 4.5. pH changed from 5.2±0.20 in the influent (6.3±0.20 in the effluent) from the beginning of the experiment to 8.4±0.20 towards the end respectively due to electrolysis in the EAnMBR. The overall removal efficiency of COD, TN, TP and color was 99.68%, 99.04%, 99.98%, 99.94%, respectively, showing increase in performance over AnMBR by 10.44%, 2.04%, 1.46%, and 0.74%.
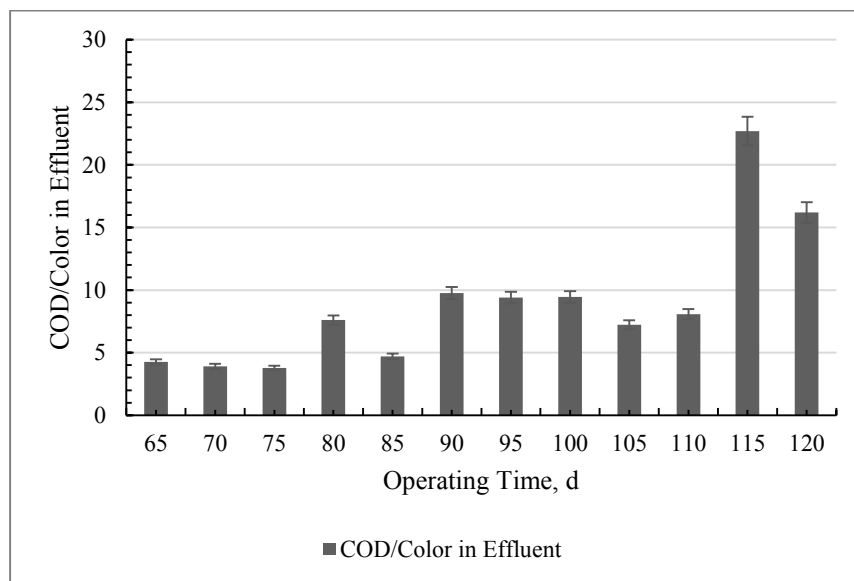
Figure 4.108. Phase III Stage II: Effect of COD on the color of the EAnMBR
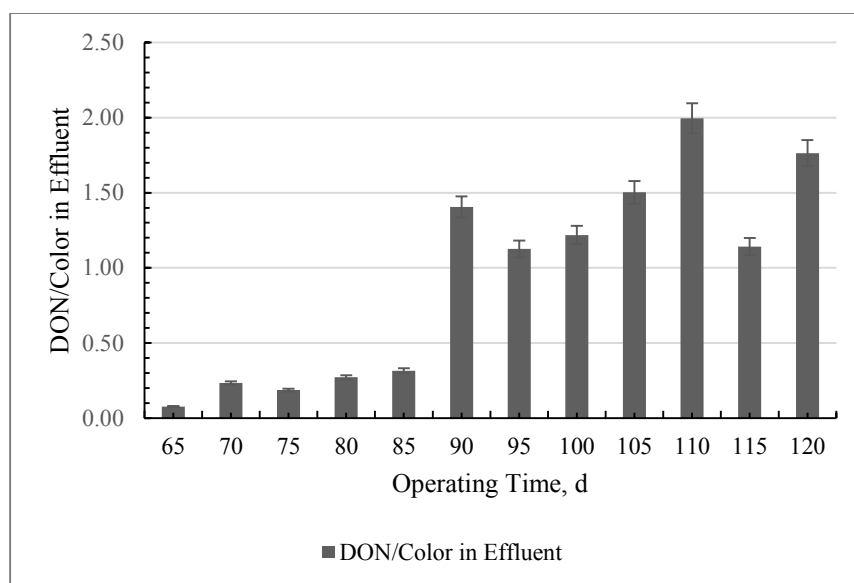
Figure 4.109. Phase III Stage II: Effect of DON on the color in the EAnMBR

Table 4.5. The influent and effluent concentrations and the performance of the EAnMBR.

Parameter	Influent, mgL^{-1}		Effluent, mgL^{-1}		Average Removal Efficiency, %
	Average	Standard Deviation	Average at the End of Stage II	Standard Deviation	
pH	5.2	±0.20	8.4	±0.20	-
COD	53,574	±432	170	±43.64	>99
N$_{tot}$	2,298	±4.03	22.05	±3.45	>99
P$_{tot}$	151	±0.82	0.02	±0.02	>99
Color	19,975	±81	11.66	±2.36	>99

Figure 4.110 present color-changing dynamic during the Phase III.

| Day 1-20 | Day 20-40 | Day 45-60 |
| Day 70-90 | Day 95-115 | Day 170-180 |
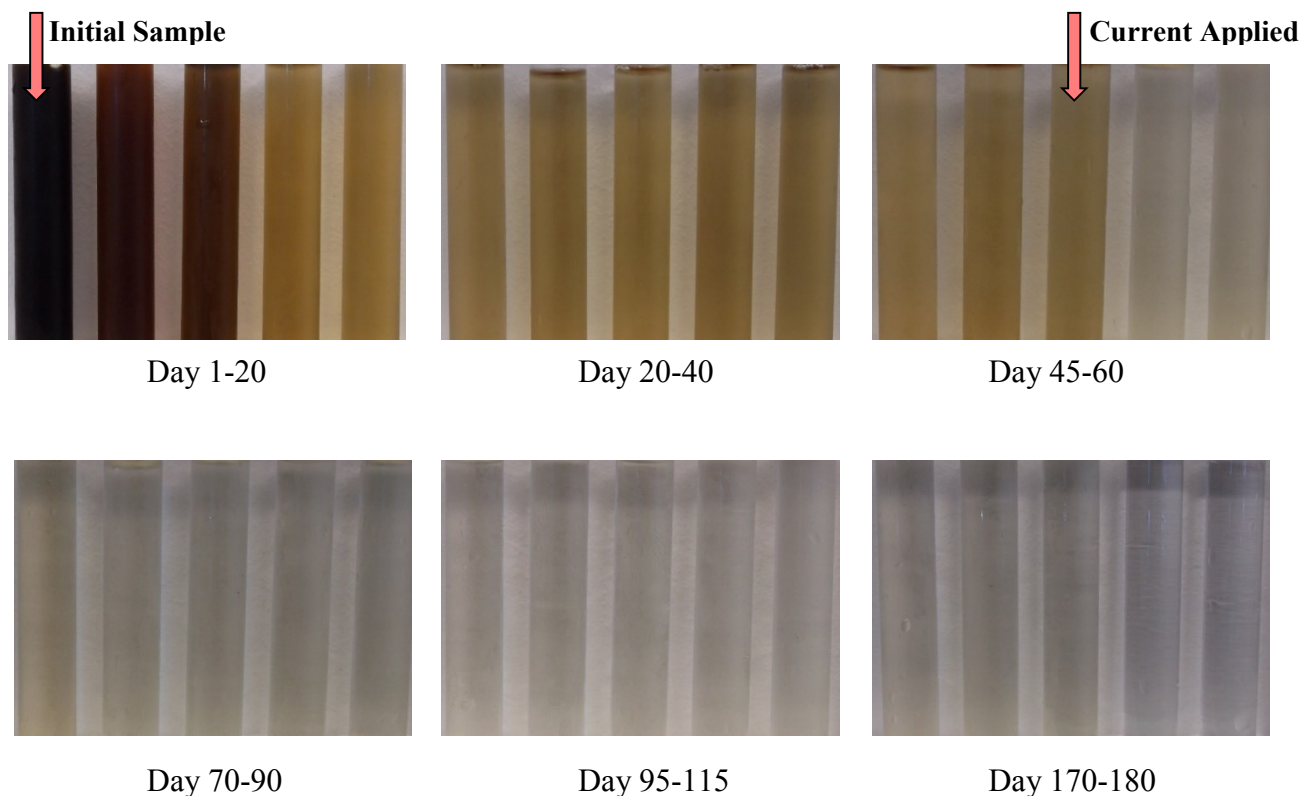
Figure 4.110. Color-changing dynamic during the Phase III

4.3.3. Cost Analysis

The specific energy demand of electro-anaerobic membrane bioreactor was mainly due to the electrical power related to the applied voltage for maintaining the exposure time. The aeration was not required and liquid pumping had low contribution to the energy demand. Detailed calculations were summarized as follows. For AnMBR calculation, it was assumed that for pilot and/or full-scale operation a coagulant addition and rapid mixing are required. Aluminum dose and power consumption are strongly dependent on conductivity; therefore, calculations were made based on the previous study [273]. The specific energy consumption of EAnMBR system could be reduced to less than 1 kWhm^{-3} taking into considerations the operating conditions were related to the exposure time to electrical field and heating. Based on the results of the research, change of electrodes was required after six month of exploitation.

Anaerobic Membrane Bioreactor (AnMBR)

1. Aeration of biomass: not required
2. Aeration of Membrane: not required
3. Coagulation Rapid Mixing/Agitation: **0.05** CADm^{-3}
4. Coagulation Chemicals:

a. Aluminium sulphate (solid) 6.5 CADkg^{-1} of Al
   Dose: 0.06 Al kgm^{-3}
   Cost (6.5 CADkg^{-1} x 0.06 Al kgm^{-3}): **0.39** CADm^{-3}
b. Aluminium polychloride (liquid) 4.0 CADkg^{-1} of Al
   Dose: 0.06 Al kgm^{-3}
   Cost (4.0 CADkg^{-1} x 0.06 Al kgm^{-3}): **0.24** CADm^{-3}
5. Electrokinetic: N/A

Total Cost of AnMBR Operation (Aluminium sulphate): 0.05 CADm^{-3} + 0.39 CADm^{-3} = **0.44** CADm^{-3}

Total Cost of AnMBR Operation (Aluminium polychloride): 0.05 CADm^{-3} + 0.24 CADm^{-3} = **0.29** CADm^{-3}

TOTAL for AnMBR:

0.44 CADm^{-3} using Aluminium sulphate

0.29 CADm^{-3} using Aluminium polychloride

Electro Anaerobic Membrane Bioreactor (EAnMBR)

1. Aeration of biomass: not required
2. Aeration of Membrane: not required
3. Coagulation Rapid Mixing/Agitation: not required
4. Coagulation Chemicals: not required
5. Electrokinetic:
a. the price of metal sheet (used as anode):

Aluminium (3003 H14) of size 2m × 1m with 1 mm thickness is **6.0** CAD per Piece

Open Area 23%

Metric Density of Al: 2.80 gcm^{-3}

Weight of Al sheet: 2m × 1m with x 1 mm x 2.80 gcm^{-3} = 5.6 kg x 0.77 = 4.3 kg

Surface Area of Circular Anode: S=2πrh

The present electricity cost for high power customers in Canada is 0.048CAD per kWh.

b. aluminum dissolved: 0.06 Al kgm^{-3}

c. energy costs: **0.566** CADkg^{-1} Al

TOTAL for EAnMBR: 0.06 Al kgm^{-3} x 0.566 CADkg^{-1} Al = **0.03** CADm^{-3}

4.3.4. Phase III: Summary and Conclusions

Based on this research, the electro-bioreactor has proven its capability for high removal efficiency of the carbon, nutrients and color in one single operation unit. The studies showed removal efficiency up to more than 99% for all nutrients when the electrical parameters and the other operating conditions (HRT, SRT and organic loading) were adjusted to that purpose. Carbon was removed primarily through biomass oxidation; phosphorus was removed through the formation of aluminum phosphate complexes, while nitrogenous compounds were transformed through denitrification processes in the reactor. Nitrification potential was enhanced up to 25% in the EAnMBR due to the activation of anammox while autotrophic nitrification took place in the AnMBR only.

In Phase III of this research, the system was operated in AnMBR (Stage I) and in EAnMBR (Stage II) configuration for treatment of industrial wastewater containing molasses. In AnMBR configuration, the system was operated from day 1 to 60 as advanced anaerobic membrane bioreactor. In EAnMBR mode of operation from day 61 to 120, aluminum was used as an anode and iron as a cathode similar to Phase II. The conclusions of Phase III can be summarized as follows:

- The AnMBR system produced effluents of excellent quality (> 89%) in terms of carbon, nitrogen, phosphorus, and color, where the removal reached more than 89, 97, 98, and 99%, respectively.

- The EAnMBR system demonstrated excellent results in terms of carbon, nutrients and color removal (more than 99% each).

- pH of the liquid phase increased from 6.3 to 8.3-8.5 due to electrolysis and electrokinetic processes involvement.

- Combination of biological, physico-chemical and electrokinetic processes played significant and positive role in each stage of operation.

The conclusions for each stage are summarized as follows:

- Stage I (1-60 days): The system was operated in AnMBR configuration without an electrical field. The HRT was kept constant at 4 days to increase sheer and reduce fouling of the membrane module. The average COD removal of the system was > 89%, nitrogen removal efficiency demonstrated > 97% and the phosphorus removal performance was > 98 %.

- Stage II (61-120 days): The system was operated in EAnMBR configuration with a DC field applied and an operational mode of 5'On: 20'Off. The electrokinetic phenomena in EAnMBR system produced a significant positive impact in terms of COD, nitrogen, phosphorus and color removal (> 99%). COD removal mechanism was a combination of biological carbon removal and electrokinetic formation of nucleoids for negatively charged colloids which were removed from the aqueous phase by the forces of gravity. Due to the slow rate of the anaerobic nitrification process, a major part of nitrogen was removed by the biological decomposition and electrokinetically induced denitrification. The phosphorous removal efficiency was attributed not only to biological degradation, but interaction with aluminum cations released into the aqueous phase as a result of electrokinetic processes. Alumophosphate species were produced and precipitated out of the sludge with some depositions on the surface of the cathode and the membrane as product of Al^{3+} interaction with PO_4^{3-}.

Although AnMBR demonstrated very good treatment of high-strength industrial wastewater, EAnMBR outperformed conventional advanced anaerobic membrane system and provided superior effluent quality due to involvement of electrokinetic processes.

5. Phase IV: Modeling and Optimization

The Box–Behnken statistical experimental design was employed to determine the effects of environmental, electrical and biological operating variables on COD, nitrogen, phosphorus and color removal efficiency. Furthermore, finding of the combination of variables resulting in maximum removal performance was also considered. As environmental, electrical and biological parameters, pH, current density and MLSS were selected, respectively.

The response surface methodology or RSM is an empirical modeling technique, used for the evaluation of the relationship of a set of controlled experimental factors and observed results. The results of RSM were statistically analyzed using one-way ANOVA to determine the major properties which had significant influence, and to analyze the differences among group means and their associated procedures.

The RSM generates empirical model which can describe the process and analyze the influence of independent variables on a specific dependent variable (response). The independent variables denoted by x_1, x_2, …… x_k are assumed as continuous and can be controlled with negligible error. The response (y) is assumed to be a random variable. The individual variables (x_1, x_2, …, x_k) and the response (y) can be related as follows:

$$y = f(x_1, x_2, x_3 \dots x_k) + \varepsilon \tag{5.1}$$

where y is the response of the system, f the unknown function of response, x_1, x_2, x_3 …… x_k the independent variables, k the number of independent variables, and ε the statistical error. RSM postulates the functional relationship between the response (y) and the independent variables. A first order RSM can be expressed as follows:

$$y = \beta_0 + \sum_{i=1}^{k}(\beta_i x_i + \varepsilon) \tag{5.2}$$

For maximization problem, experiments are conducted along the path of steepest ascent until no further increase in the response is observed. The set of values of independent variables where no further increase in response is observed is known as optimal region. In most of the cases a second order response surface model is used which can be given as:

$$y = \beta_0 + \sum_{i=1}^{k}\beta_i x_i^1 + \sum_{i=1}^{k}\beta_{ii}x_i^2 + \sum_{i=1}^{k-1}\sum_{j=2}^{k}\beta_{ij}x_i x_j + \varepsilon \tag{5.3}$$

where x_i, x_j - independent variables and

$$\beta_0, \beta_i, \beta_{ii}, \beta_{ij}(i = 1,2, \dots k), \beta_{ij}(i = 1,2 \dots k; j = 1,2, \dots k)$$

regression coefficients for intercept, linear, quadratic and interaction terms respectively; and ε- statistical error. In the present study, the RSM has been used to determine the relationship between COD, TP, TN and color removal with operating parameters such as pH and applied current density. The variables are converted to coded variables using the following equation:

$$x = \frac{X - [X_{max} + X_{min}]/2}{[X_{max} - X_{min}]/2} \qquad (5.4)$$

where, X = natural variable and x = coded variable. The dimensional coded variables x_1, x_2, x_3, x_k vary between -1 and +1, while the variables are designated as $-$ 1, 0 and +1. The mathematical representation of the response Y and the variables is given as:

$$Y = \beta_0 + \beta_1 x_1 + \beta_2 x_2 + \beta_3 x_3 + \beta_4 x_4 + \beta_{11} x_1^2 + \beta_{22} x_2^2 + \beta_{33} x_3^2 + \beta_{12} x_1 x_2 + \beta_{13} x_1 x_3 + \beta_{23} x_2 x_3 \qquad (5.5)$$

and

$$\beta_{ij} = 0,1,2,3 \qquad (5.6)$$

where β and x are regression coefficients and variables. In the present study, the Box–Behnken experimental design was selected to find the relationship between the response functions and variables. A 15-run Box-Behnken design with three center points was conducted using Minitab software and a full quadratic model was fitted to the data. Using this model, the optimal settings that provided the highest reduction of COD, nitrogen, phosphorous and color were found. The parameters and their ranges covered in the present investigation are listed in Table 5.1. Randomized design table (Table 5.2) for 3 center points provides the design matrix.

The electrolyte pH, applied current density and MLSS concentration are referred by variables as A, B, C respectively. The variables were designated as -1, 0 and +1. Experiments were carried out according to the experimental conditions designed by RSM and the responses are summarized in Table 5.3. Correlations were considered statistically significant when their p-values were less than 0.05.

Table 5.1. The level and range of independent variables

Factor	Variable	Unit	Levels		
			-1	**0**	**+1**
A	pH	-	6	7	8
B	CD	Am^{-2}	15.0	17.5	20.0
C	MLSS	gL^{-1}	5.0	6.5	8.0

Table 5.2. Randomized design table

Run	Block	Factors		
		A	**B**	**C**
1	1	0	-1	1
2	1	0	0	0
3	1	-1	0	1
4	1	0	-1	-1
5	1	1	-1	0
6	1	0	1	1
7	1	-1	-1	0
8	1	0	0	0
9	1	1	1	0
10	1	1	0	1
11	1	-1	1	0
12	1	0	0	0
13	1	-1	0	-1
14	1	1	0	-1
15	1	0	1	-1

Table 5.3. Observed and predicted removal efficiency

Run	pH	CD, Am^{-2}	MLVSS, gL^{-1}	Experimental				Predicted			
				COD	TN	TP	Color	COD	TN	TP	Color
1	7	15.0	8.0	97.64	93.00	99.33	99.48	97.25	93.55	99.54	99.57
2	7	17.5	6.5	94.22	93.72	96.85	99.65	94.97	92.72	96.60	99.64
3	6	17.5	8.0	95.99	95.03	95.19	99.27	96.26	93.90	95.72	99.21
4	7	15.0	5.0	87.85	82.60	97.80	99.51	87.75	82.86	97.86	99.56
5	8	15.0	6.5	89.15	83.75	98.85	99.67	89.52	82.36	99.32	99.73
6	7	20.0	8.0	99.67	98.85	99.98	99.51	99.77	98.59	99.93	99.48
7	6	15.0	6.5	89.87	85.25	97.61	99.67	90.00	85.83	96.88	99.57
8	7	17.5	6.5	95.20	93.72	96.50	99.79	94.97	92.72	96.60	99.82
9	8	20.0	6.5	96.12	94.79	98.95	99.75	95.99	94.21	99.68	99.66
10	8	17.5	8.0	97.15	92.40	98.87	99.77	97.18	93.24	98.20	99.72
11	6	20.0	6.5	98.50	92.18	98.88	99.57	98.13	93.57	98.41	99.57
12	7	17.5	6.5	95.50	90.70	96.45	99.20	94.97	92.72	96.60	99.29
13	6	17.5	5.0	93.80	89.55	94.54	99.45	93.77	88.71	95.22	99.46
14	8	17.5	5.0	90.50	85.40	96.97	99.96	90.23	86.53	96.45	99.92
15	7	20.0	5.0	99.45	97.95	99.56	99.90	99.84	97.40	99.36	99.90

The mathematical relationship between the independent variables and their responses and optimization for each pollutant are provided in the following sections.

5.1. Optimization for COD Removal

The mathematical relationship between the independent variables and COD removal efficiency responses in uncoded units:

$$\% \text{ COD} = -51.9 + 20.91 \text{ pH} + 6.13 \text{ CD} + 1.38 \text{ MLVSS} - 1.678 \text{ pH*pH} + 0.0183 \text{ CD*CD}$$
$$+ 0.473 \text{ MLVSS*MLVSS} - 0.166 \text{ pH*CD} + 0.743 \text{ pH*MLVSS} - 0.6380 \text{ CD*MLVSS} \qquad (5.7)$$

The predictions of percentage COD removal using the Equation 5.7 was compared with the experimental observations (Figure 5.1). It can be observed that the predictions using above equation fit with the experimental observations with the acceptable error range.
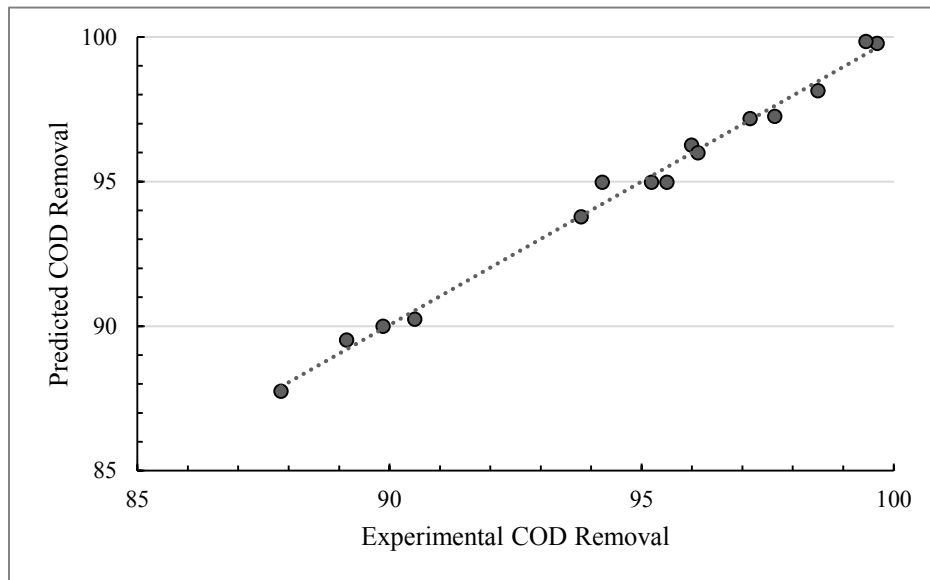
Figure 5.1. Model prediction comparison to experimental data for COD removal efficiency

Figure 5.2 demonstrate the response surface effect of current density and pH on the COD removal. The carbon removal increased with increase of applied current density. The effect of pH also influenced removal efficiency. In order to reach the maximum removal efficiency, the CD and pH must be in the range of 19.5 Am^{-2} and 6.0 - 7.5 accordingly.
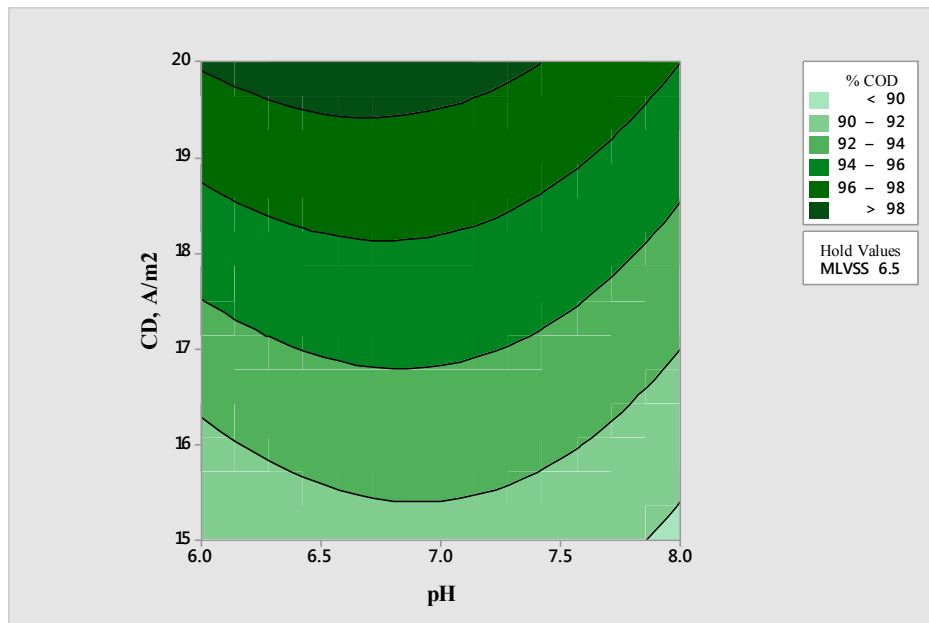
Figure 5.2. Effect of current density and pH on COD removal
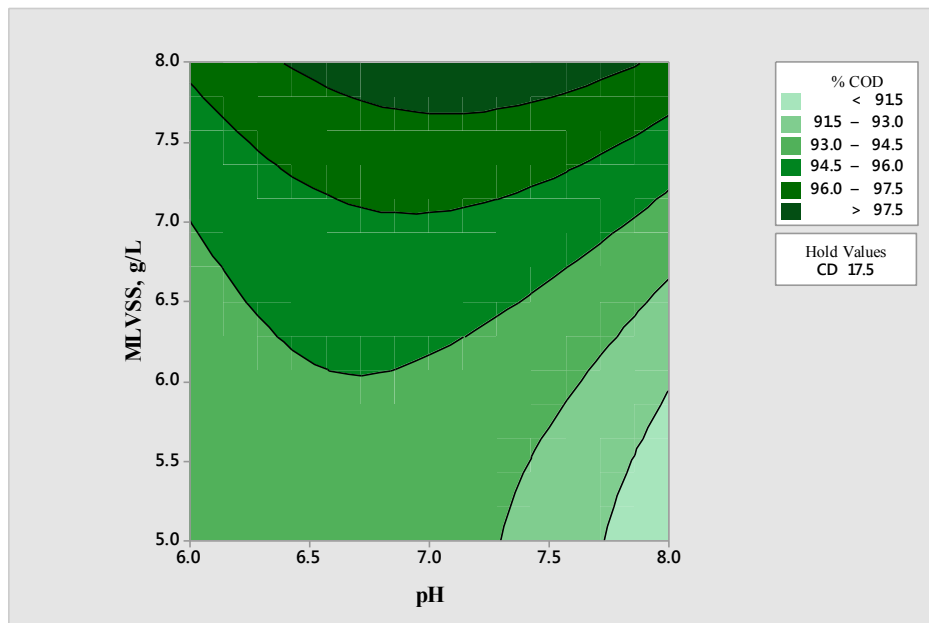
Figure 5.3. Effect of MLVSS concentration and pH on COD removal

Figure 5.3 represents the effect of the biomass concentration and pH on COD removal. The COD removal was strongly influenced by the MLVSS concentration and the pH of electrolyte. In order to reach the best performance in terms of carbon removal, the higher MLVSS and pH values in the range between 6.5 and 7.8 should be maintained. Figure 5.4 provides information

on response surface effects of the MLVSS concentration and the CD on percentage of COD removal. The graphical model showed the similar trends for COD removal efficiency- higher current density and MLVSS led to higher percent removal. To reach the COD removal more than 98%, MLVSS concentration should be maintained at 8 gL^{-1} and CD should be ranged from 19 to 20 Am^{-2}.
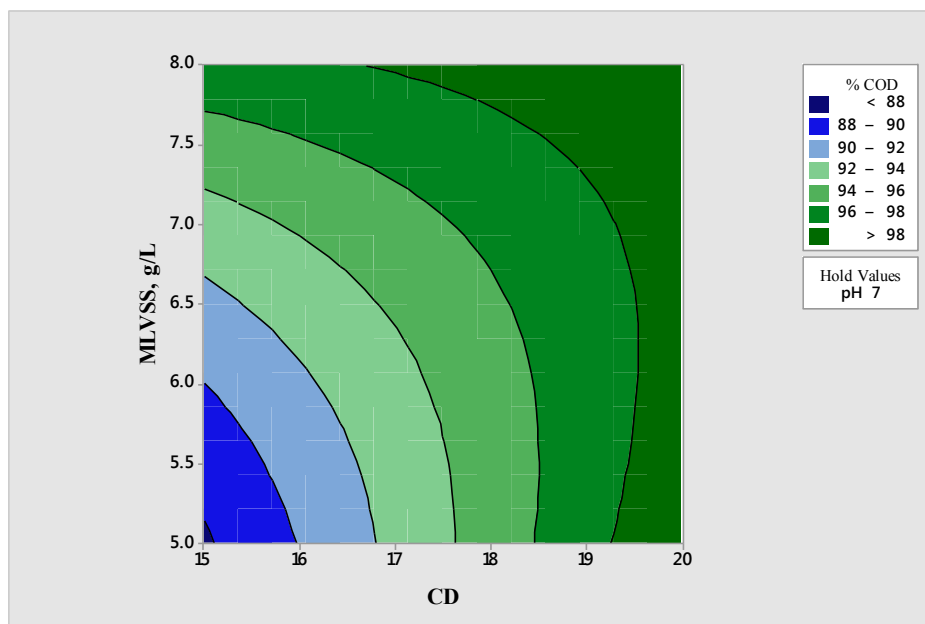
Figure 5.4. Effect of current density and MLVSS concentration on COD removal

The actual and predicted values of the response shown in Table 5.3 as well as the model regression (eq. 5.7) were used to construct graphical models and statistical parameter for the ANOVA as shown in Table 5.4 and Table 5.5. The adequacy of the responses was evaluated by ANOVA and Tables 5.4 – 5.5 show statistical data for validating the precision of the model.

Table 5.4. Analysis of variance for COD removal optimization

Source	DF	Seq SS	Contribution	Adj SS	Adj MS	f-Value	p-Value
Model	9	198.986	99.17%	198.986	22.11	66.29	< 0.0001
Linear	3	154.647	77.07%	154.647	51.549	154.55	< 0.0001
pH	1	3.432	1.71%	3.432	3.432	10.29	0.024
CD	1	106.799	53.23%	106.799	106.799	320.2	< 0.0001
MLVSS	1	44.415	22.14%	44.415	44.415	133.16	< 0.0001
Square	3	15.781	7.86%	15.781	5.26	15.77	0.006

pH*pH	1	11.593	5.78%	10.395	10.395	31.17	0.003
CD*CD	1	0.004	0.00%	0.048	0.048	0.15	0.719
MLVSS*MLVSS	1	4.185	2.09%	4.185	4.185	12.55	0.017
2-Way Interaction	3	28.558	14.23%	28.558	9.519	28.54	0.001
pH*CD	1	0.689	0.34%	0.689	0.689	2.07	0.21
pH*MLVSS	1	4.973	2.48%	4.973	4.973	14.91	0.012
CD*MLVSS	1	22.896	11.41%	22.896	22.896	68.65	< 0.0001
Error	5	1.668	0.83%	1.668	0.334		
Lack-of-Fit	3	0.771	0.38%	0.771	0.257	0.57	0.685
Pure Error	2	0.896	0.45%	0.896	0.448		
Total	14	200.653	100.00%				

DF represents the total degree of freedom; **Seq SS** is sequential sums of squares; **Contribution**- is the % contribution of the parameter; **Adj SS**- adjusted sum of squares; **Adj MS**- adjusted mean squares.

Table 5.5. Coded coefficients COD removal optimization

Term	Effect	Coef	SE Coef	95%	CI	t-Value	p-Value	VIF
Constant		94.973	0.333	(94.116,	95.83)	284.83	0	
pH	-1.31	-0.655	0.204	(-1.180,	-0.130)	-3.21	0.024	1
CD	7.307	3.654	0.204	(3.129,	4.179)	17.89	0	1
MLVSS	4.713	2.356	0.204	(1.831,	2.881)	11.54	0	1
pH*pH	-3.356	-1.678	0.301	(-2.451,	-0.905)	-5.58	0.003	1.01
CD*CD	0.229	0.115	0.301	(-0.658,	0.887)	0.38	0.719	1.01
MLVSS*MLVSS	2.129	1.065	0.301	(0.292,	1.837)	3.54	0.017	1.01
pH*CD	-0.83	-0.415	0.289	(-1.157,	0.327)	-1.44	0.21	1
pH*MLVSS	2.23	1.115	0.289	(0.373,	1.857)	3.86	0.012	1
CD*MLVSS	-4.785	-2.393	0.289	(-3.135,	-1.650)	-8.29	0	1

Coef and **SE Coef** are coefficients and standard error coefficients respectively;
CI- is the confidence interval;
t-Value is the measurement of the size of the difference relative to the variation in the sample data;
VIF- Variance Inflation Factor.

Model summary:

S = 0.577528, R-sq = 99.17%, R-sq(adj) = 97.67%, PRESS = 14.3594

The significance of the regression was determined by f-value and p-value. The f-value of COD removal model is indicated in Table 5.5. The large number of f-value indicates that the regression models well included variations of the response range. Moreover, the relation

between p-value and f-value was used to analyse whether f-value was large enough to include the model variations. The p-value less than 0.05 can indicate that the model terms are significant at the 95% level of significance. Furthermore, the value of model coefficient of determination showed that R-sq and R-sq(adj) values were 99.17% and 97.67% for COD removal model. The values of R-sq and R-sq(adj) more than 80% indicated good fit of COD removal model points. Good ness of fit test was run in order to determine the best distribution model for COD removal. The results are presented in Table 5.6 and 5.7 and show that the best suitable distribution model is 3-Parameter Weibull. The graphical results of goodness of fit test are also presented in Figure 5.7 and confirm the best fit for 3-Parameter Weibull distribution. The residual plots for COD removal model are represented in Figure 5.5 and optimal range of all three values (pH, CD, MLVSS) for optimal COD removal is depicted on Figure 5.6.
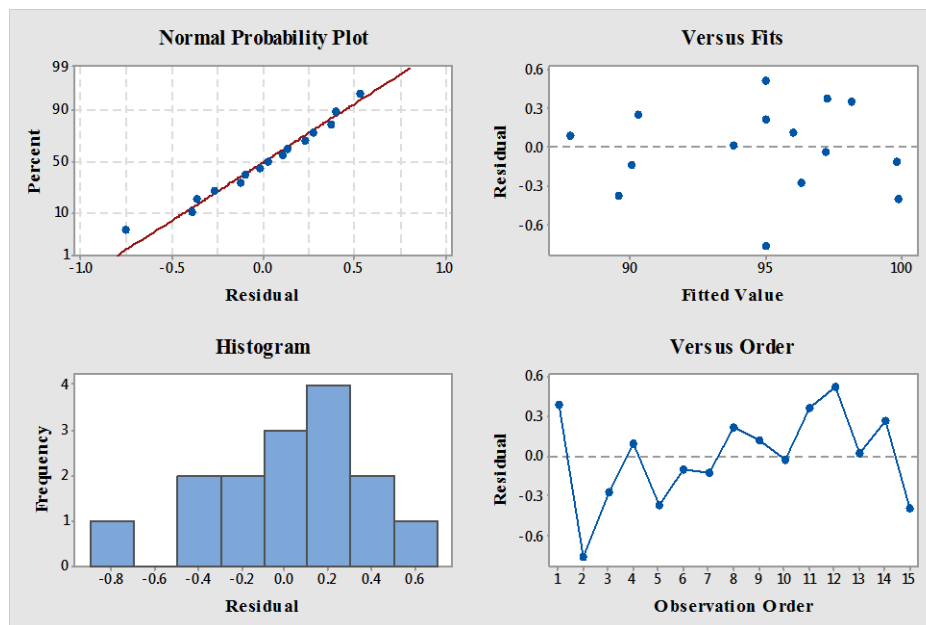
Figure 5.5. Residual plots for COD removal
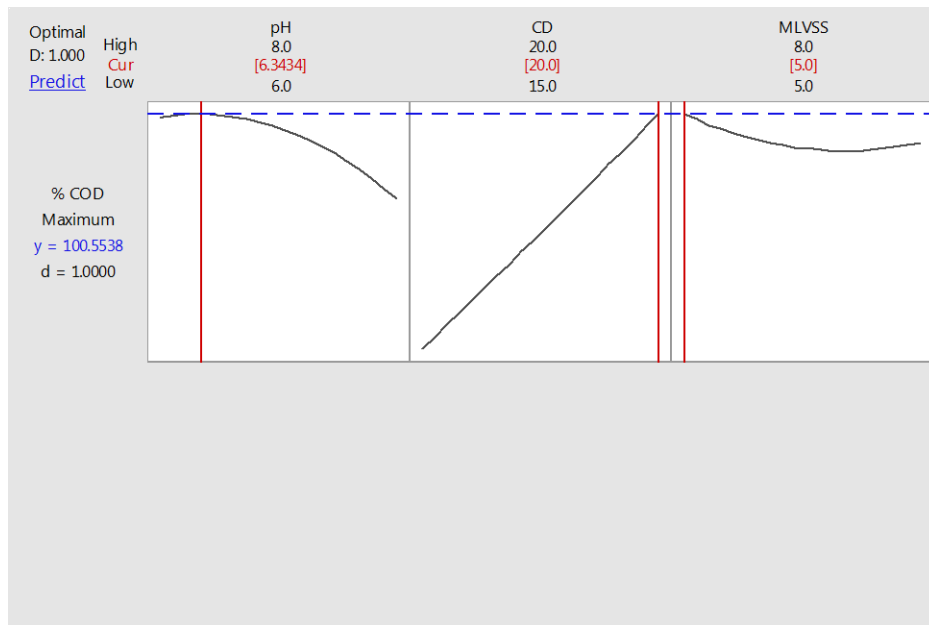
Figure 5.6. Optimum range for COD removal

Table 5.6. Goodness of fit test percent COD removal

Distribution	AD	P	LRT P
Normal	0.428	0.271	
Box-Cox Transformation	0.316	0.507	
Lognormal	0.462	0.221	
3-Parameter Lognormal	0.462	*	0.59
Exponential	6.374	<0.003	
2-Parameter Exponential	1.601	<0.010	0
Weibull	0.275	>0.250	
3-Parameter Weibull	0.262	>0.500	0.919
Smallest Extreme Value	0.262	>0.250	
Largest Extreme Value	0.714	0.053	
Gamma	0.485	0.236	
3-Parameter Gamma	1.58	*	1
Logistic	0.421	0.248	
Loglogistic	0.45	0.215	
3-Parameter Loglogistic	0.421	*	0.618

Table 5.7. Estimates of distribution parameters for COD removal

Distribution	Location	Shape	Scale	Threshold
Normal*	94.71		3.79	
Box-Cox Transformation*	7.73E+09		1.48E+09	
Lognormal*	4.55		0.04	
3-Parameter Lognormal	10.72		0.01	-4.49E+04
Exponential			94.71	
2-Parameter Exponential			7.35	87.36019
Weibull		32.34	96.38	
3-Parameter Weibull		15298.78	44983.63	-4.49E+04
Smallest Extreme Value	96.43		2.94	
Largest Extreme Value	92.80		3.68	
Gamma		661.44	0.14	
3-Parameter Gamma		1323.63	0.101	-40.24954
Logistic	95.01		2.16	
Loglogistic	4.55		0.023	
3-Parameter Loglogistic	10.71		0.00005	-4.49E+04

* Scale: Adjusted ML estimate

AD: Anderson-Darling statistic (AD): Lower AD values indicate a better fit;
P: p-value;
LRT P: For 3-parameter distributions only, a low value indicates that adding the third parameter is a significant improvement over the 2-Parameter version.

As the best-fitting distribution was identified, the best estimate graph for the model (3-Parameter Weibull with Shape 15298.78327, Scale 44983.62826, and Threshold -4.49E+04) and probabilities for minimum (87.85%) and maximum (99.67%) COD removal efficiency values (from Table 5.3) that fall in the range were plotted and is represented in Figure 5.7. The distribution shown in Figure 5.8 seemed reasonable as the particles distribution in the aqueous phase also followed similar pattern.
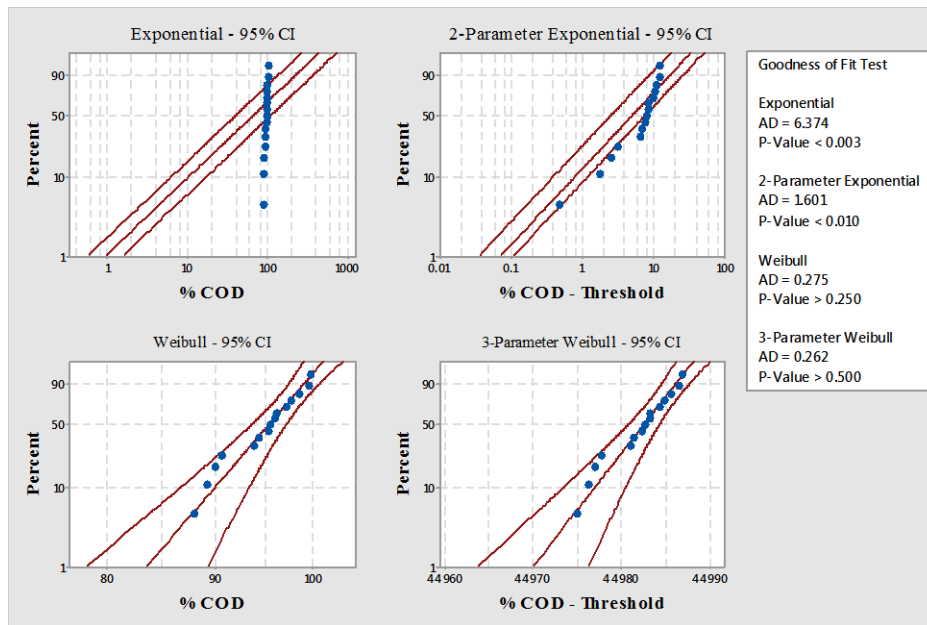
Figure 5.7. Probability plot for COD removal
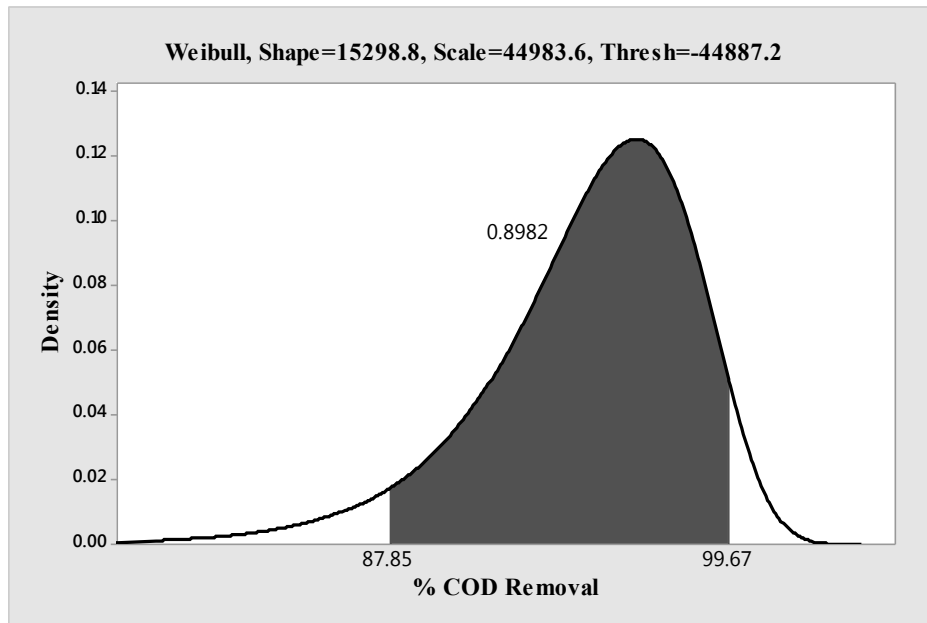
Figure 5.8. Distribution plot for COD removal

5.2. Optimization for Nitrogen Removal

The mathematical relationship between the independent variables and nitrogen removal efficiency responses in uncoded units is represented by Equation 5.8:

% TN = -123.3 + 34.0 pH + 6.60 CD + 5.56 MLVSS - 3.114 pH*pH - 0.097 CD*CD

+ 0.441 MLVSS*MLVSS + 0.411 pH*CD + 0.253 pH*MLVSS - 0.633 CD*MLVSS   (5.8)

The predicted values of percentage TN removal using the Equation 5.8 were compared with the experimental results (Figure 5.9). It can be observed that the predictions using above equation fit with the experimental observations.
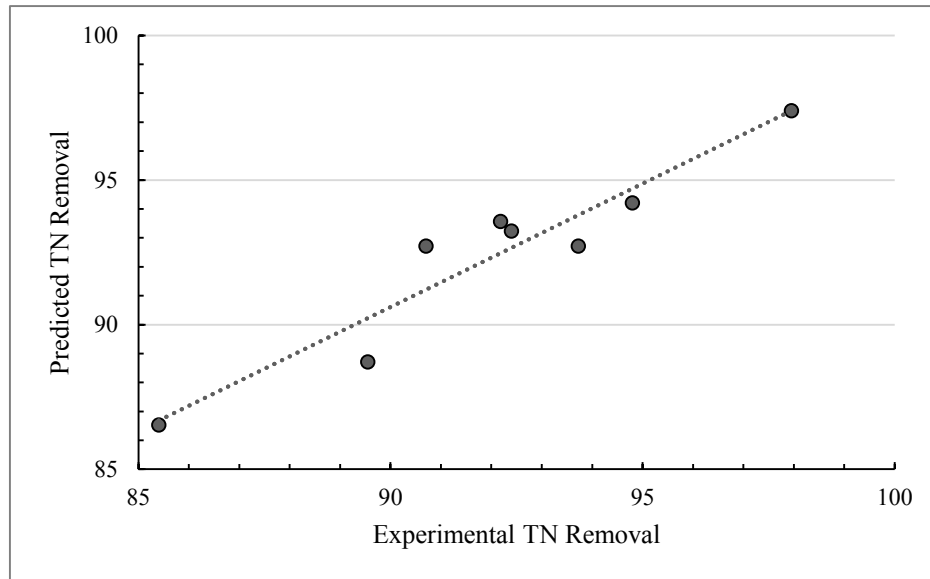
Figure 5.9. Model prediction comparison to experimental data for TN removal efficiency

Figure 5.10 provides the response surface effect of current density and pH on the TN removal efficiency. Similar to COD, the nitrogen removal efficiency increased with rise of applied current density. The pH also influenced removal efficiency with optimal range for the best performance within 6.5 – 7.5. In order to provide the maximum removal performance for TN, the CD must be in the range of 19.5 – 20.0 Am^{-2}.

Figure 5.11 represents the effect of MLVSS and pH on percent nitrogen removal. The TN removal was strongly influenced by the biomass concentration and the pH of the aqueous phase. To reach the best performance in terms of TN removal, the higher MLVSS and pH values in the range between 6.5 and 7.3 are recommended. Figure 5.12 provides information on the effect of the MLVSS concentration and the current density on % TN removal. The model presented on Figure 5.12 demonstrated the similar pattern for TN removal efficiency-the higher current density and MLVSS provided higher performance. To reach the nitrogen

removal higher than 98%, MLVSS concentration should be maintained similar to COD removal model for the same parameters- at 8 gL^{-1} and CD should be ranged from 19 to 20 Am^{-2}.
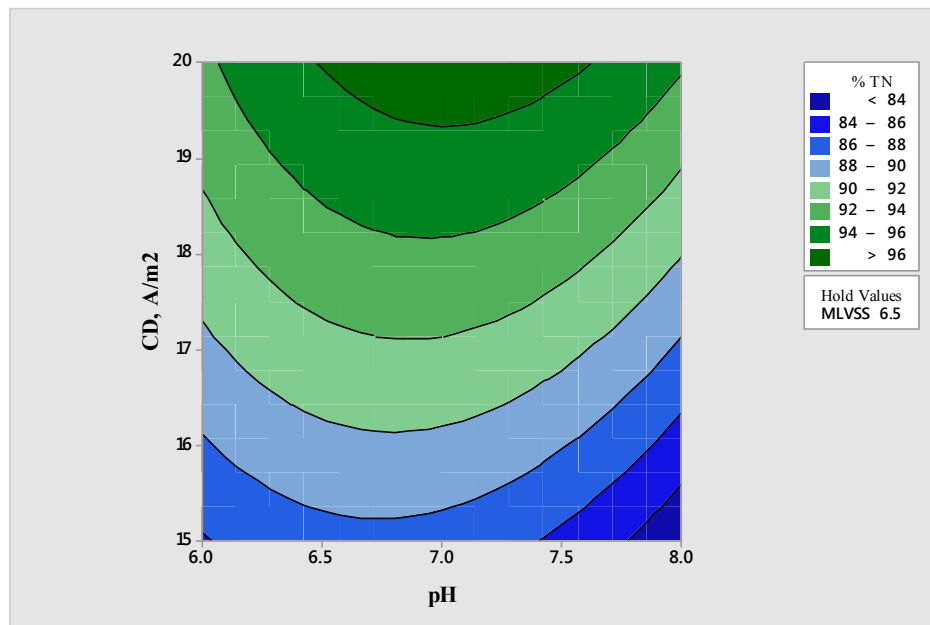
Figure 5.10. Effect of current density and pH on TN removal
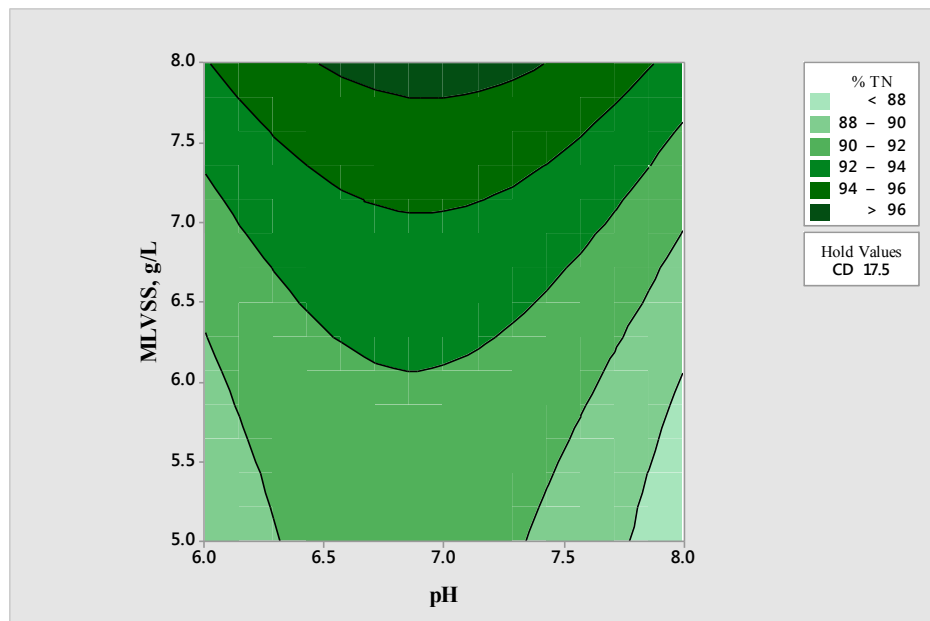
Figure 5.11. Effect of MLVSS concentration and pH on TN removal
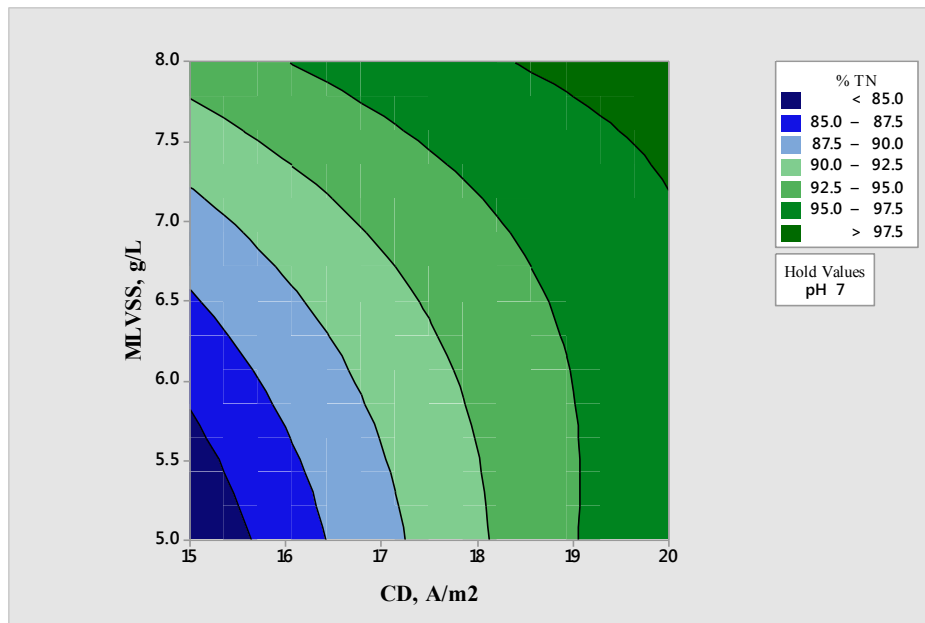
Figure 5.12. Effect of current denscity and MLSS concentration on TN removal

The experimental and predicted values of the surface responses that presented in Table 5.3 and by the model regression equation 5.8 were employed to build the graphical models and statistical parameters for the ANOVA as presented in Table 5.8. Table 5.9 summarizes the coded coefficients for the total nitrogen removal optimization. The adequacy of the surface responses was checked by ANOVA. The results are presented in Tables 5.10 – 5.11 and show statistical data for validating the model for TN removal.

Table 5.8. Analysis of variance nitrogen removal optimization

Source	DF	Seq SS	Contribution	Adj SS	Adj MS	f-Value	p-Value
Model	9	336.119	95.63%	336.119	37.347	12.16	0.007
Linear	3	266.532	75.83%	266.532	88.844	28.92	0.001
pH	1	4.013	1.14%	4.013	4.013	1.31	0.305
CD	1	191.829	54.58%	191.829	191.829	62.44	0.001
MLVSS	1	70.69	20.11%	70.69	70.69	23.01	0.005
Square	3	42.215	12.01%	42.215	14.072	4.58	0.067
pH*pH	1	36.832	10.48%	35.794	35.794	11.65	0.019
CD*CD	1	1.743	0.50%	1.368	1.368	0.45	0.534
MLVSS*MLVSS	1	3.64	1.04%	3.64	3.64	1.18	0.326
2-Way Interaction	3	27.372	7.79%	27.372	9.124	2.97	0.136
pH*CD	1	4.232	1.20%	4.232	4.232	1.38	0.293
pH*MLVSS	1	0.577	0.16%	0.577	0.577	0.19	0.683

CD*MLVSS	1	22.563	6.42%	22.563	22.563	7.34	0.042
Error	5	15.362	4.37%	15.362	3.072		
Lack-of-Fit	3	9.266	2.64%	9.266	3.089	1.01	0.532
Pure Error	2	6.095	1.73%	6.095	3.048		
Total	14	351.481	100.00%				

DF represents the total degree of freedom; **Seq SS** is sequential sums of squares; **Contribution**- is the % contribution of the parameter; **Adj SS**- adjusted sum of squares; **Adj MS**- adjusted mean squares.

Table 5.9. Coded coefficients nitrogen removal optimization

Term	Effect	Coef	SE Coef	95%	CI	t-Value	p-Value	VIF
Constant		92.72	1.01	(90.11,	95.32)	91.62	0	
pH	-1.417	-0.708	0.62	(-2.301,	0.885)	-1.14	0.305	1
CD	9.794	4.897	0.62	(3.304,	6.490)	7.9	0.001	1
MLVSS	5.945	2.973	0.62	(1.380,	4.566)	4.8	0.005	1
pH*pH	-6.227	-3.114	0.912	(-5.458,	-0.769)	-3.41	0.019	1.01
CD*CD	-1.217	-0.609	0.912	(-2.954,	1.736)	-0.67	0.534	1.01
MLVSS*MLVSS	1.986	0.993	0.912	(-1.352,	3.338)	1.09	0.326	1.01
pH*CD	2.057	1.029	0.876	(-1.224,	3.281)	1.17	0.293	1
pH*MLVSS	0.76	0.38	0.876	(-1.873,	2.633)	0.43	0.683	1
CD*MLVSS	-4.75	-2.375	0.876	(-4.628,	-0.122)	-2.71	0.042	1

Coef and **SE Coef** are coefficients and standard error coefficients respectively;
CI- is the confidence interval;
t-Value is the measurement of the size of the difference relative to the variation in the sample data;
VIF- Variance Inflation Factor.

Model summary:

S = 1.75280, R-sq = 95.63%, R-sq(adj) = 87.76%, PRESS = 161.974

As in the previous assessment, the significance of the regression was determined by f-value and p-value. The higher numbers of f-value suggested that the regression models well comprised ranges of the response values. The relation between p-value and f-value was used to analyse if f-value was adequate to include the model variations. The value of model coefficient of determination showed that R-sq and R-sq(adj) values were 95.63% and 87.76%, respectively, for TN removal model. The values of R-sq and R-sq(adj) are higher than than 80% which indicates a good fit of TN removal model points. Goodness of fit test was used to determine the best distribution model for TN removal. The results are provided in Tables 5.10

and 5.11 and demonstrate that the suitable distribution model is 3-Parameter Weibull. The graphical results of goodness of fit test are presented in Figure 5.14 and confirm the best fit for 3-Parameter Weibull distribution. The residual plots for TN removal model are presented in Figure 5.12 and optimal range of all three values (pH, CD, MLVSS) for optimal TN removal is depicted on Figure 5.13.
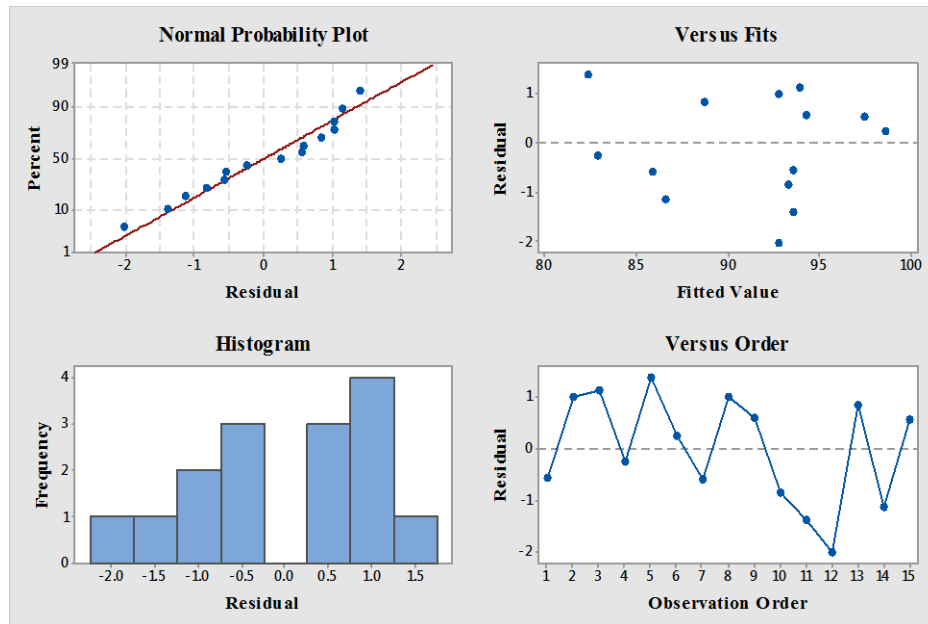
Figure 5.12. Residual plots for TN removal
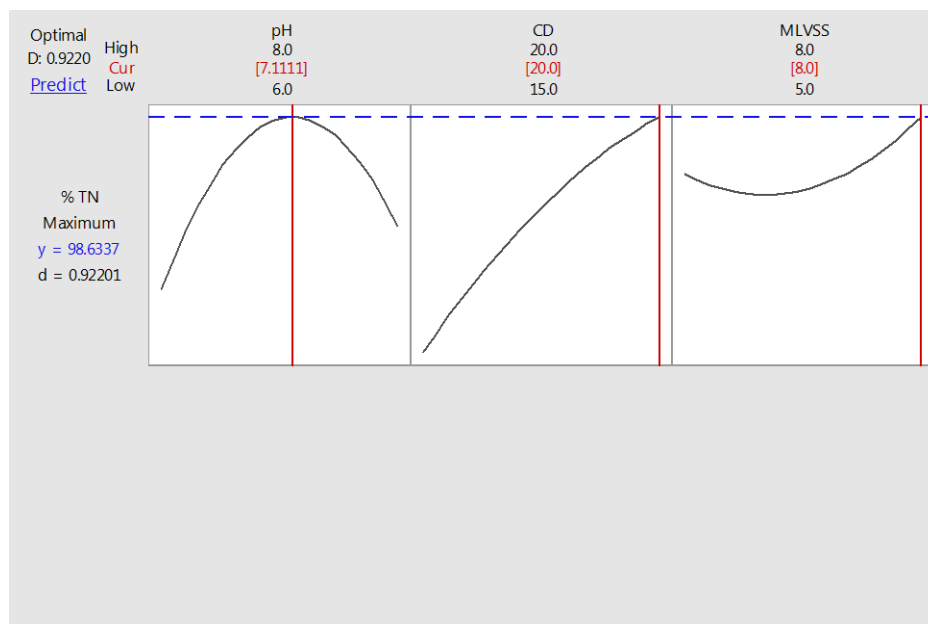
Figure 5.13. Optimum range for TN removal

Table 5.10. Goodness of fit test TN removal

Distribution	AD	P	LRT P
Normal	0.433	0.263	
Box-Cox Transformation	0.317	0.506	
Lognormal	0.478	0.201	
3-Parameter Lognormal	0.465	*	0.574
Exponential	6.192	<0.003	
2-Parameter Exponential	1.471	0.011	0
Weibull	0.302	>0.250	
3-Parameter Weibull	0.346	0.392	0.73
Smallest Extreme Value	0.294	>0.250	
Largest Extreme Value	0.719	0.05	
Gamma	0.495	0.226	
3-Parameter Gamma	1.135	*	1
Logistic	0.438	0.228	
Loglogistic	0.477	0.185	
3-Parameter Loglogistic	0.439	*	0.59

AD: Anderson-Darling statistic (AD): Lower AD values indicate a better fit;
P: p-value;
LRT P: For 3-parameter distributions only, a low value indicates that adding the third parameter is a significant improvement over the 2-Parameter version.

Table 5.11. Estimates of distribution parameters for TN removal

Distribution	Location	Shape	Scale	Threshold
Normal*	91.26		5.01	
Box-Cox Transformation*	1.04E+09		2.52E+08	
Lognormal*	4.51		0.06	
3-Parameter Lognormal	10.65		0.01	-4.23E+04
Exponential			91.26	
2-Parameter Exponential			9.28	81.98
Weibull		22.54	93.48	
3-Parameter Weibull		7.27	31.17	62.10
Smallest Extreme Value	93.58		4.10	
Largest Extreme Value	88.76		4.78	
Gamma		350.01	0.26	
3-Parameter Gamma		819.95	0.17	-49.29

Logistic	91.60	2.86	
Loglogistic	4.52	0.03	
3-Parameter Loglogistic	10.66	0.00007	-4.22E+04

*** Scale: Adjusted ML estimate**

As the best distribution was determined, the graph for the estimated model (3-Parameter Weibull with Shape 7.27, Scale 31.17, and Threshold 62.10) and probabilities for removal efficiency values (minimum and maximum from Table 5.3) that fall in the range of 88.76 – 93.58% TN was constructed and is presented in Figure 5.15. The distribution represented in Figure 5.15 seems adequate as the nitrogen particles distribution in the aqueous phase also might follow similar pattern to those of carbon. The distribution is, however, narrower as the concentration of nitrogen is much less than of carbon.
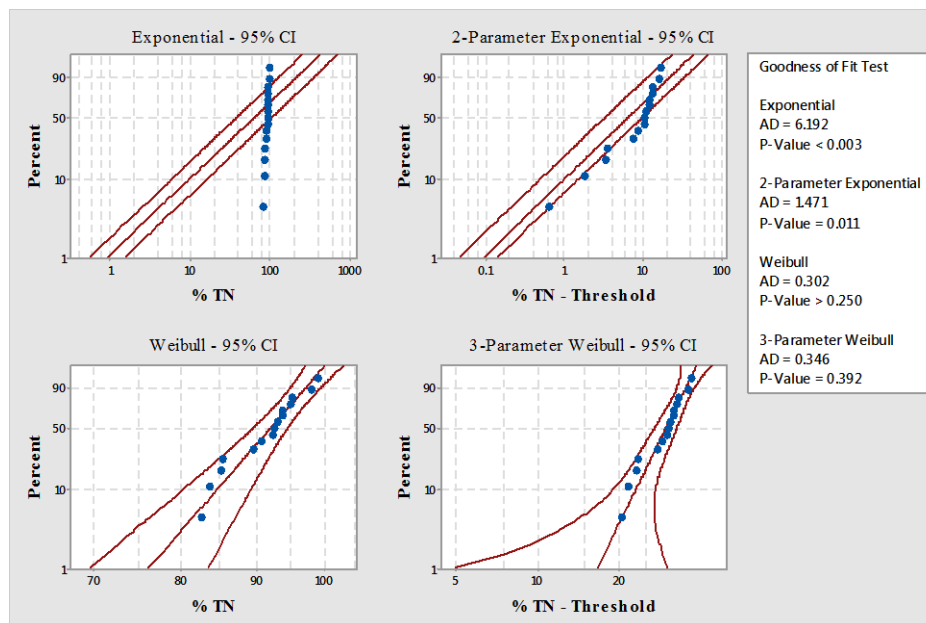
Figure 5.14. Probability plot for TN removal
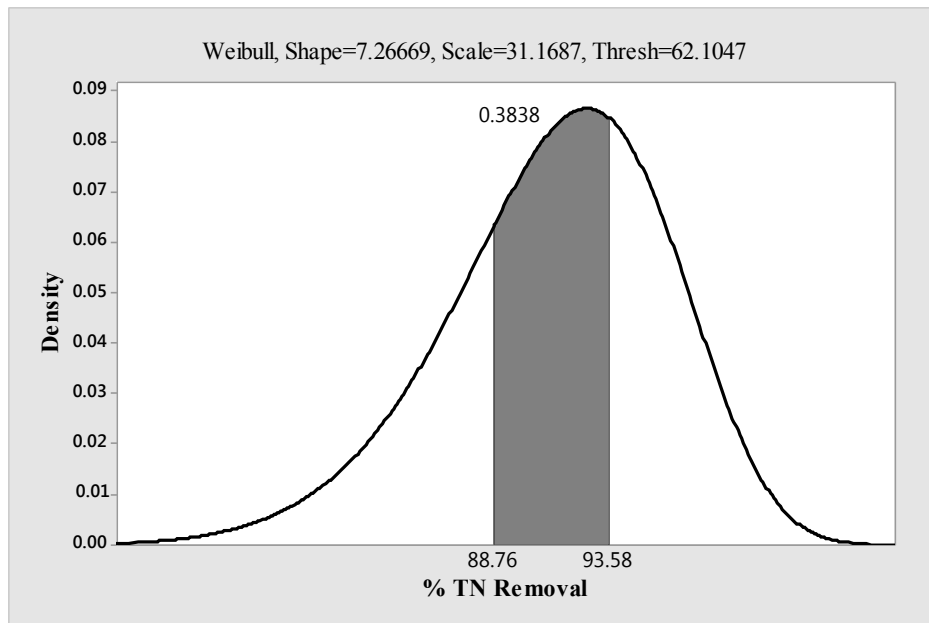
Figure 5.15. Distribution plot for TN removal

5.3. Optimization for Phosphorous Removal

The relationship between the independent variables and TP removal efficiency responses in uncoded units is reflected by Equation 5.9:

% TP = 171.4 + 7.24 pH - 11.80 CD - 0.91 MLVSS - 0.401 pH*pH + 0.3798 CD*CD
+ 0.086 MLVSS*MLVSS - 0.117 pH*CD + 0.208 pH*MLVSS - 0.074 CD*MLVSS   (5.9)

The predictions of percentage TP removal using the equation 5.9 was compared with the experimental results (Figure 5.16). The model described by the equation 5.9 fit with the experimental observations quite well.
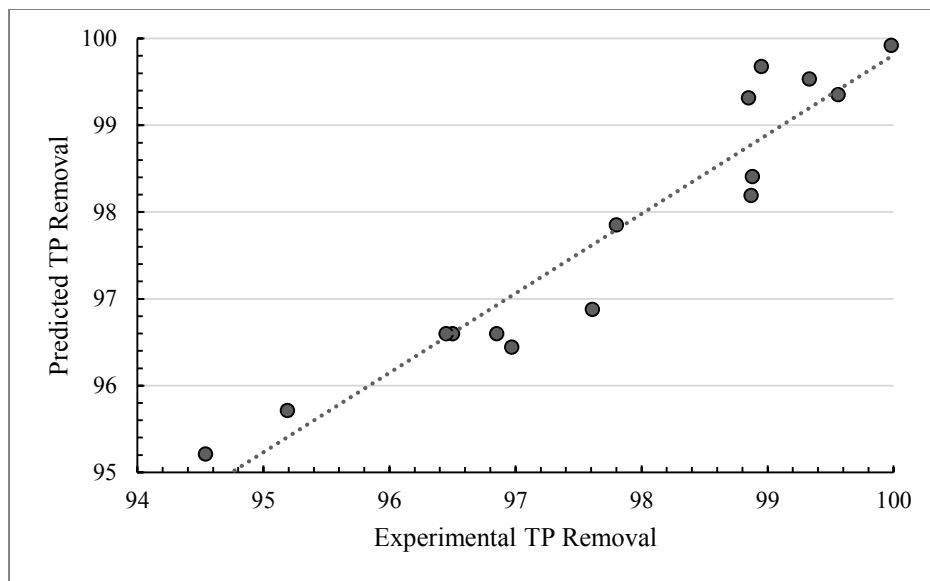
Figure 5.16. Model prediction comparison to experimental data for TP removal efficiency

The effect of current density and pH on the phosphorus removal is depicted on Figure 5.17. The graphical model exhibits the same trend for each fixed value as in previously discussed models for COD and TN. Figure 5.18 represents the effect of MLVSS concentration and pH on TP removal. The concentration of MLVSS affected phosphorus removal. Furthermore, pH increase also affected TP removal, which is reasonable as the precipitation of phosphorus increases at higher pH levels (optimal value according to the graph > 7.5). Figure 5.19 presents the effect of MLVSS and current density on phosphorus removal. The graphical model representation demonstrates a complex trend as the TP removal increases at lower and higher current density, while, the best performance could be achieved at MLVSS > 7 gL^{-1} and CD > 19.2 Am^{-2}. Figure 5.19 shows that applied current density has little impact on phosphorus removal between 16.2 Am^{-2} and 18.0 Am^{-2} (dark blue region).
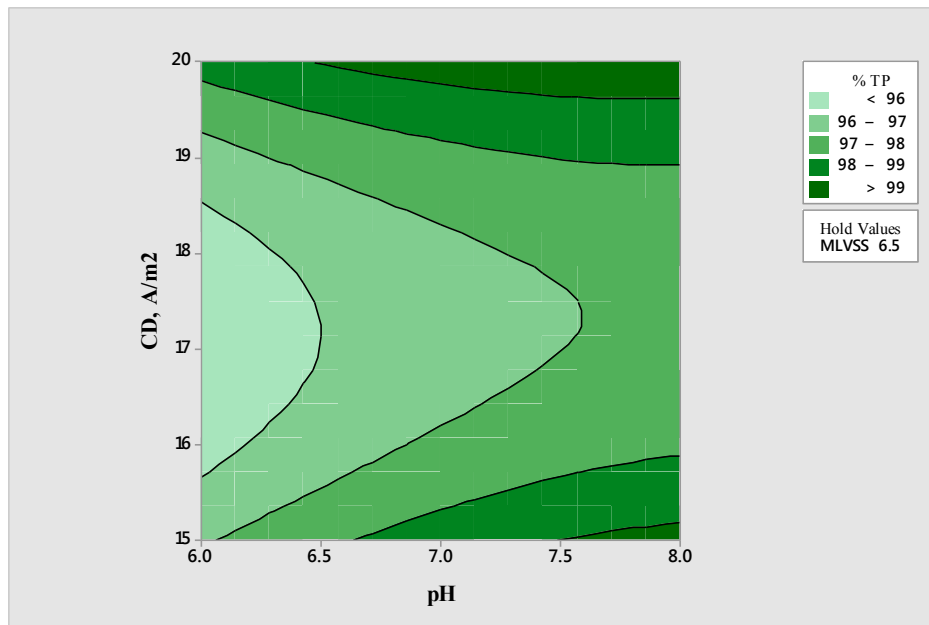
Figure 5.17. Effect of current denscity and pH on TP removal
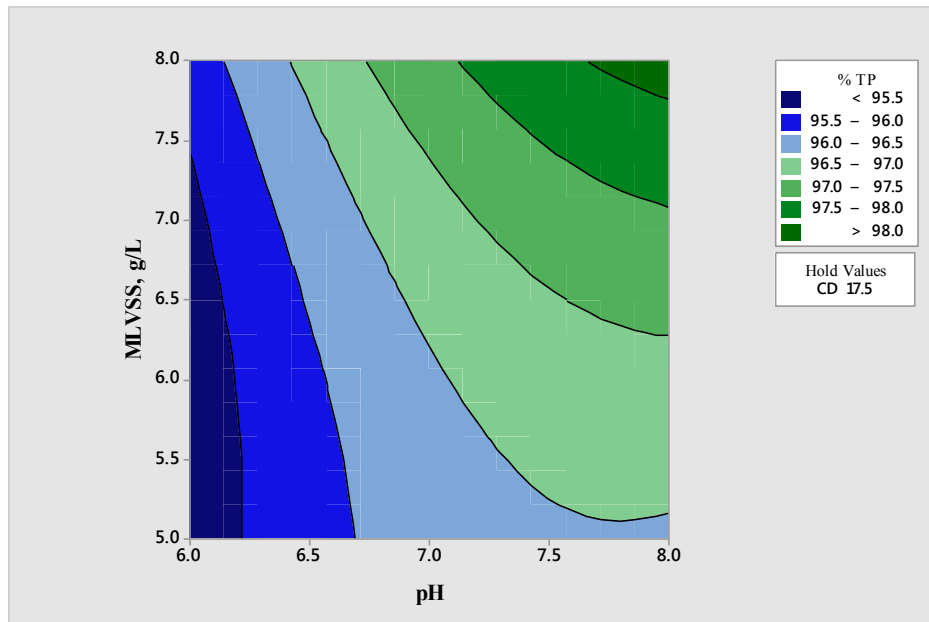
Figure 4.18. Effect of MLVSS concentration and pH on TP removal
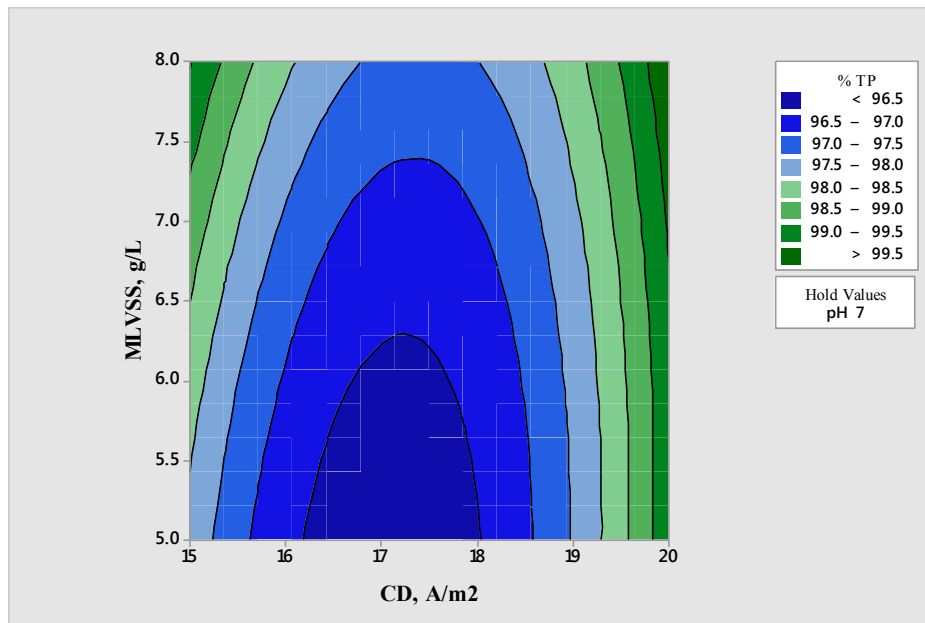
Figure 4.19. Effect of current dencity and MLVSS concentration on TP removal

To build graphical models and statistical parameters for the ANOVA as presented in Table 5.12, the actual and predicted values of the surface responses provided in Table 5.3 and the model regression equation 5.9 were employed. The Table 5.13 provides the coded coefficients for phosphorus removal optimization. The adequacy of the surface responses was evaluated by ANOVA. The results presented in Tables 5.12 – 5.13 provide statistical data for validating the model for total phosphorus removal.

Table 5.12. Analysis of variance for phosphorus removal optimization

Source	DF	Seq SS	Contribution	Adj SS	Adj MS	F-Value	P-Value
Model	9	34.3218	91.58%	34.3218	3.8135	6.04	0.031
Linear	3	11.1994	29.88%	11.1994	3.7331	5.92	0.042
pH	1	6.8821	18.36%	6.8821	6.8821	10.91	0.021
CD	1	1.7861	4.77%	1.7861	1.7861	2.83	0.153
MLVSS	1	2.5312	6.75%	2.5312	2.5312	4.01	0.102
Square	3	22.0815	58.92%	22.0815	7.3605	11.66	0.011
pH*pH	1	1.2761	3.40%	0.5945	0.5945	0.94	0.376
CD*CD	1	20.6669	55.15%	20.805	20.805	32.97	0.002
MLVSS*MLVSS	1	0.1386	0.37%	0.1386	0.1386	0.22	0.659
2-Way Interaction	3	1.0409	2.78%	1.0409	0.347	0.55	0.67

pH*CD	1	0.3422	0.91%	0.3422	0.3422	0.54	0.495
pH*MLVSS	1	0.3906	1.04%	0.3906	0.3906	0.62	0.467
CD*MLVSS	1	0.308	0.82%	0.308	0.308	0.49	0.516
Error	5	3.1552	8.42%	3.1552	0.631		
Lack-of-Fit	3	3.0602	8.17%	3.0602	1.0201	21.48	0.045
Pure Error	2	0.095	0.25%	0.095	0.0475		
Total	14	37.477	100.00%				

DF represents the total degree of freedom; **Seq SS** is sequential sums of squares; **Contribution**- is the % contribution of the parameter; **Adj SS**- adjusted sum of squares; **Adj MS**- adjusted mean squares.

Table 5.13. Coded coefficients for phosphorus removal optimization

Term	Effect	Coef	SE Coef	95%	CI	T-Value	P-Value	VIF
Constant		96.6	0.459	(95.421,	97.779)	210.62	0	
pH	1.855	0.928	0.281	(0.206,	1.649)	3.3	0.021	1
CD	0.945	0.473	0.281	(-0.249,	1.194)	1.68	0.153	1
MLVSS	1.125	0.562	0.281	(-0.159,	1.284)	2	0.102	1
pH*pH	-0.803	-0.401	0.413	(-1.464,	0.661)	-0.97	0.376	1.01
CD*CD	4.747	2.374	0.413	(1.311,	3.436)	5.74	0.002	1.01
MLVSS*MLVSS	0.388	0.194	0.413	(-0.869,	1.256)	0.47	0.659	1.01
pH*CD	-0.585	-0.292	0.397	(-1.314,	0.729)	-0.74	0.495	1
pH*MLVSS	0.625	0.313	0.397	(-0.709,	1.334)	0.79	0.467	1
CD*MLVSS	-0.555	-0.278	0.397	(-1.299,	0.744)	-0.7	0.516	1

Coef and **SE Coef** are coefficients and standard error coefficients respectively;
CI- is the confidence interval;
t-Value is the measurement of the size of the difference relative to the variation in the sample data;
VIF- Variance Inflation Factor.

Model summary:

S = 0.794380, R-sq = 91.58%, R-sq(adj) = 76.43%, PRESS = 49.1769

Higher values of f-value suggested that the regression models included wide range of the surface response values. The relationship between p- and f-values was used to for f-value analysis and to check if it was adequate to include the model variations for TP. The value of model coefficient of determination demonstrated that R-sq and R-sq(adj) values were 91.58%

and 76.43% for TP removal model. The values of R-sq and R-sq(adj) are higher enough and indicate a good fit of TP removal model points. In order to determine the best distribution model for TP removal, the goodness of fit test was employed similarly to the COD and TN models. The results are provided in Tables 5.14 and 5.15 and show that the suitable distribution model is 3-Parameter Weibull. The graphical results of goodness of fit test are presented in Figure 5.20 and confirm the best fit for 3-Parameter Weibull distribution. The residual plots for TP removal model are represented in Figure 5.21 and optimal range of all three parameters (pH, CD, MLVSS) for optimal phosphorus removal is depicted in Figure 5.20.
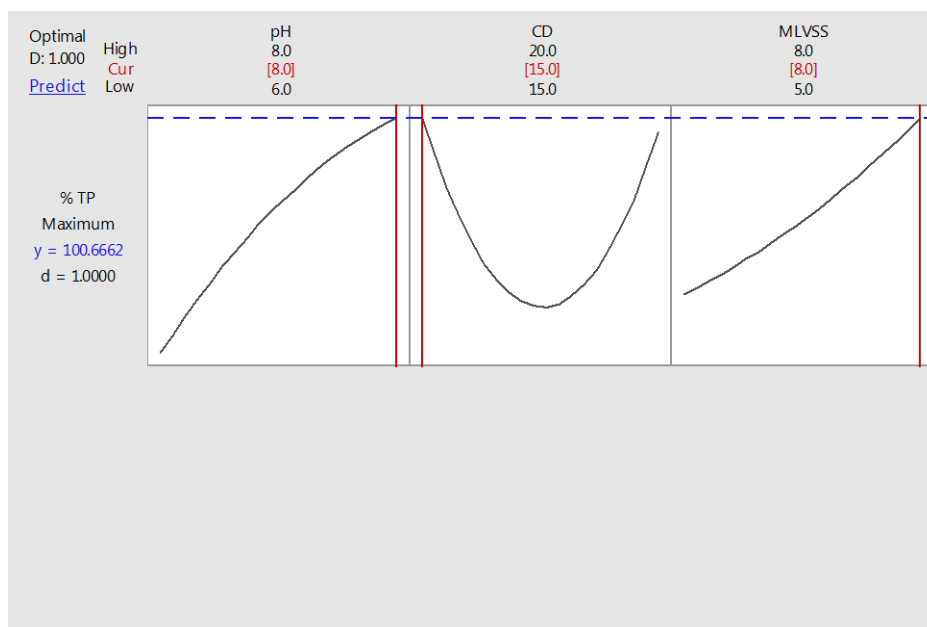
Figure 5.20. Optimum range for TP removal
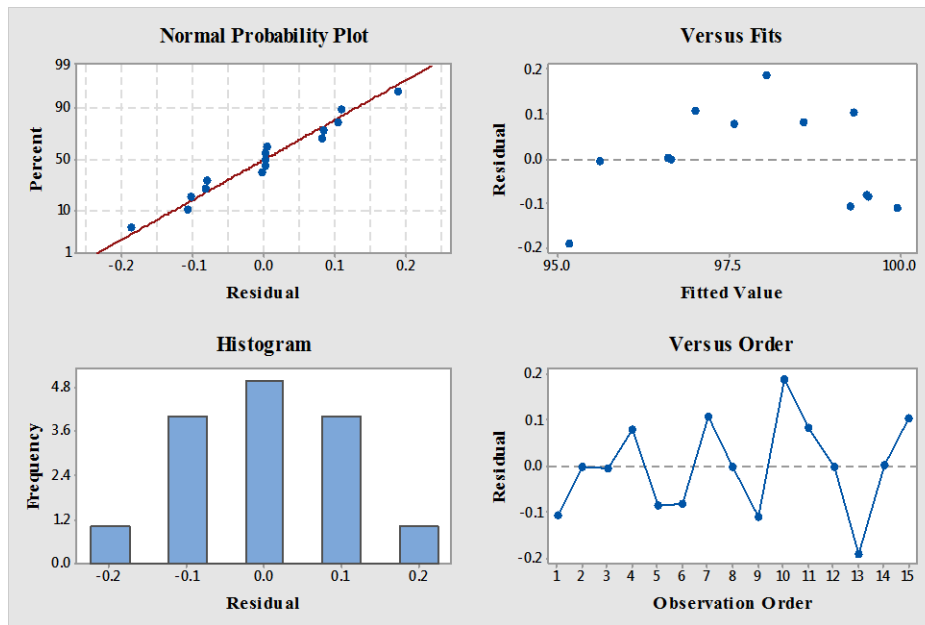
Figure 5.21. Residual plots for TP removal

Table 5.14. Goodness of fit test TP removal

Distribution	AD	P	LRT P
Normal	0.413	0.295	
Box-Cox Transformation	0.388	0.341	
Lognormal	0.421	0.282	
3-Parameter Lognormal	0.445	*	0.728
Exponential	6.667	<0.003	
2-Parameter Exponential	1.887	<0.010	0
Weibull	0.376	>0.250	
3-Parameter Weibull	0.374	0.301	0.945
Smallest Extreme Value	0.374	>0.250	
Largest Extreme Value	0.612	0.097	
Gamma	0.449	>0.250	
3-Parameter Gamma	2.603	*	1
Logistic	0.436	0.231	
Loglogistic	0.44	0.227	
3-Parameter Loglogistic	0.436	*	0.769

AD: Anderson-Darling statistic (AD): Lower AD values indicate a better fit;
P: p-value;
LRT P: For 3-parameter distributions only, a low value indicates that adding the third parameter is a significant improvement over the 2-Parameter version.

Table 5.15. Estimates of distribution parameters for TP removal

Distribution	Location	Shape	Scale	Threshold
Normal*	97.76		1.64	
Box-Cox Transformation*	8.95E+09		7.36E+08	
Lognormal*	4.58		0.02	
3-Parameter Lognormal	10.79		0.00003	-4.83E+04
Exponential			97.76	
2-Parameter Exponential			3.45	94.31033
Weibull		77.09	98.49	
3-Parameter Weibull		38739.33	49199.46	-4.91E+04
Smallest Extreme Value	98.50		1.27	
Largest Extreme Value	96.93		1.62	
Gamma		3803.82	0.03	
3-Parameter Gamma		2680.23	0.03	14.8567
Logistic	97.86		0.94	
Loglogistic	4.58		0.01	
3-Parameter Loglogistic	10.79		0.00002	-4.83E+04

* Scale: Adjusted ML estimate

The graph was built for the best distribution model (3-Parameter Weibull with Shape 38739.33, Scale 49199.46, and Threshold -4.91E+04). The probabilities for removal efficiency values (minimum and maximum from Table 5.3) in the range of 96.93 – 98.50% TP are presented in Figure 5.22. The distribution depicted in Figure 5.23 follows the same pattern as for nitrogen: the range is narrow, as the variation in concentration of phosphorus removal lied in between 96.93 – 98.50%.
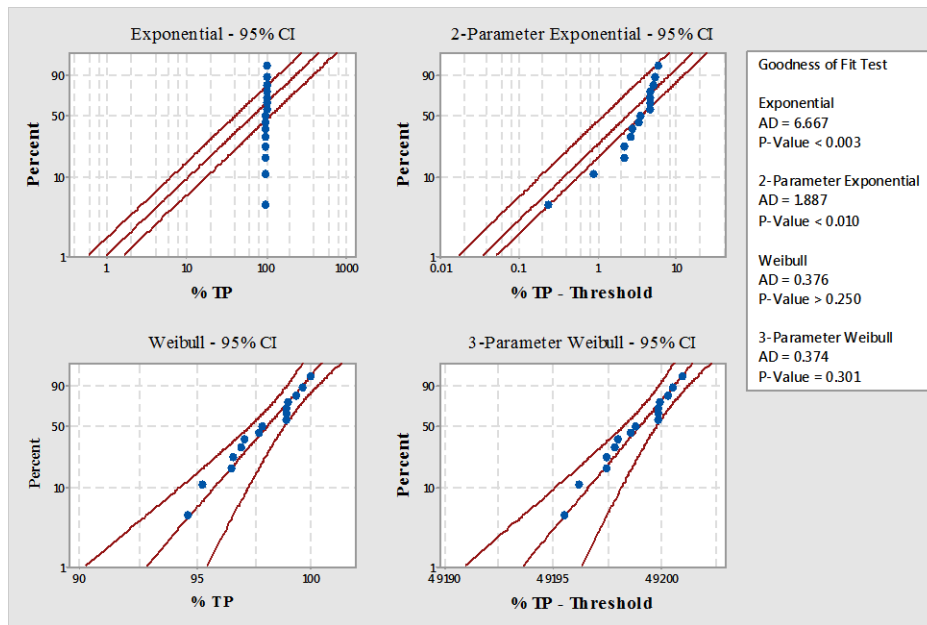
Figure 5.22. Probability plot for TP removal
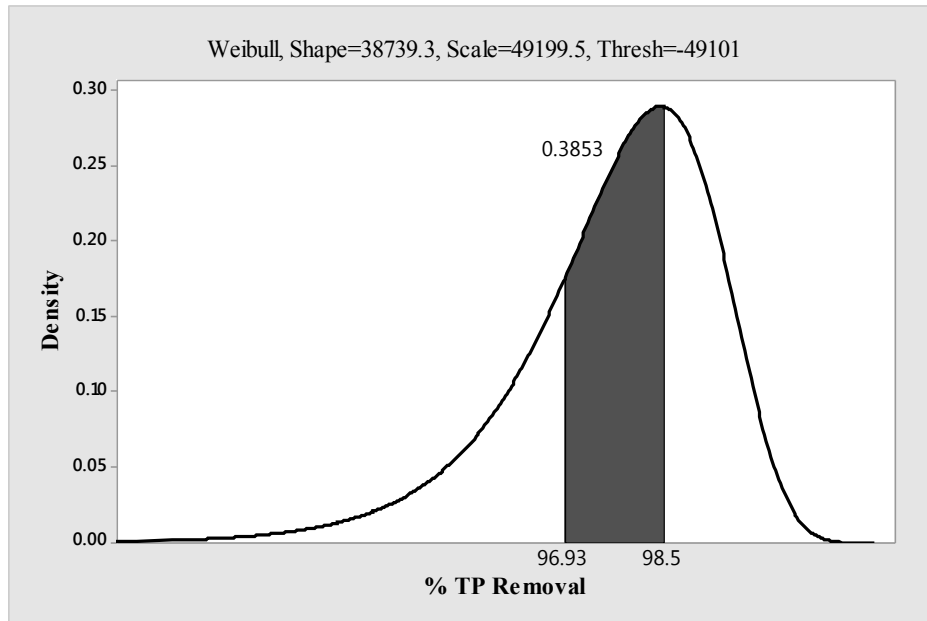
Figure 5.23. Distribution plot for TP removal

5.4. Optimization for Discoloration

The mathematical relationship between the independent variables and color removal efficiency responses in uncoded units is represented by equation 5.10:

% Color = 93.27 + 1.020 pH - 0.297 CD + 1.367 MLVSS - 0.0604 pH*pH + 0.02113 CD*CD

- 0.0002 MLVSS*MLVSS + 0.0020 pH*CD - 0.0250 pH*MLVSS - 0.0627 CD*MLVSS   (5.10)

The predictions of the color removal efficiency, using the eq. 5.10, were compared with the experimental observations (Figure 5.24). It can be observed that the predictions using above equation fit with the experimental data with the acceptable error range.
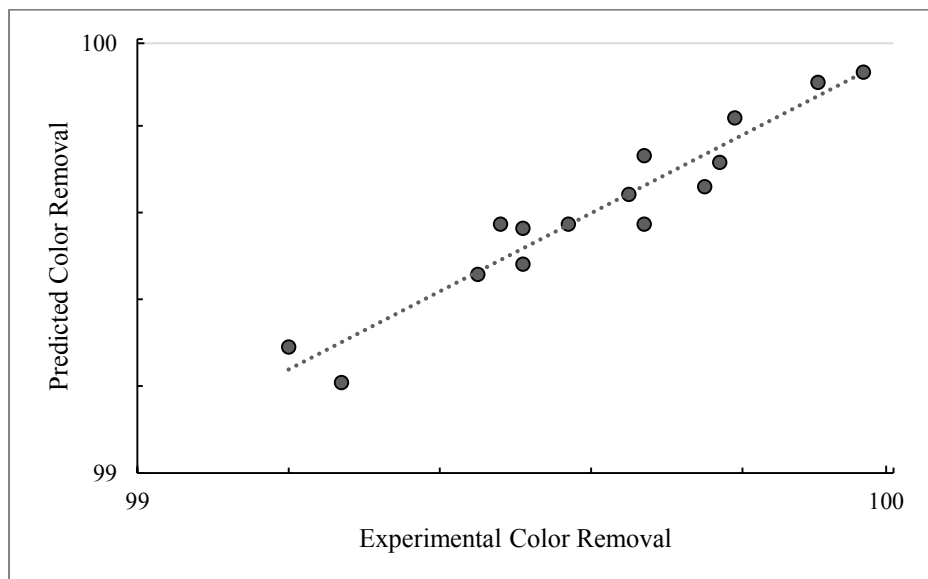
Figure 5.24. Model prediction comparison to experimental data for color removal efficiency

The effect of current density and pH on the discoloration of wastewater is presented in Figure 5.25. The graphical model demonstrates the same trend for each fixed value as in previously discussed models for COD and TN- the higher CD leads to the better performance within pH 6.7 – 8.0. Figure 5.26 presents the effect of MLVSS concentration and pH on color removal performance. The MLVSS concentration of microorganisms affected color presence in pH range between 6.7 and 7.5. According to the model, increase of MLVSS should positively affect the process of discoloration (dark-green field) which is in accordance with experimental observations. Figure 5.27 represents the effect of MLVSS and current density on color removal. The graphically-represented model demonstrates a complex relationship between the parameters. The color removal is increased at lower and higher applied current density and MLVSS concentration and the best performance is observed at 15 Am^{-2} and 8 gL^{-1}; 20 Am^{-2} and 5 gL^{-1} for CD and MLVSS respectively. Figure 5.27 demonstrates that applied current

density has little impact on color removal between 15.0 Am^{-2} and 16.2 Am^{-2} (dark blue region) which is in agreement with experimental observations.
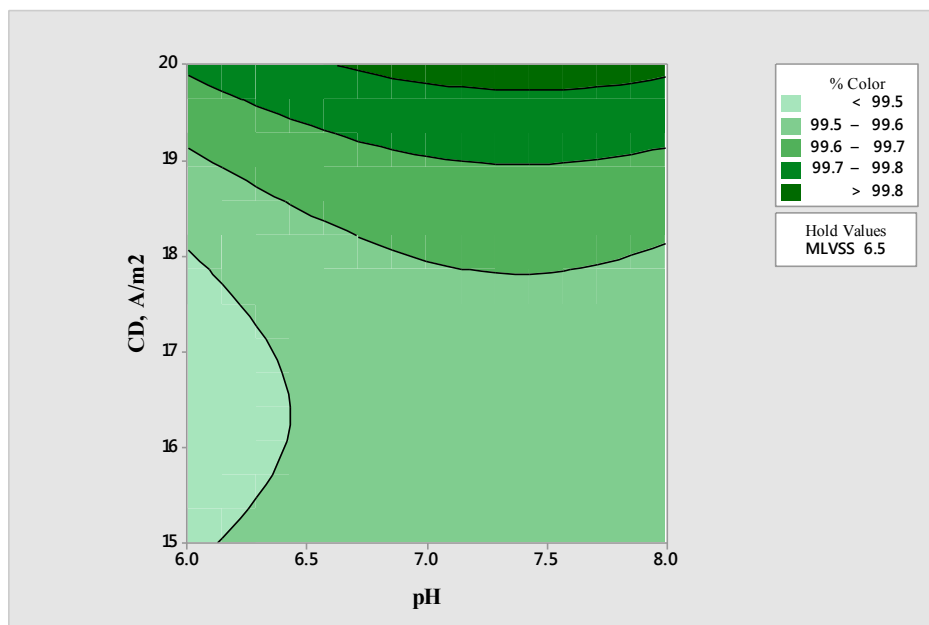
Figure 5.25. Effect of current density and pH on color removal
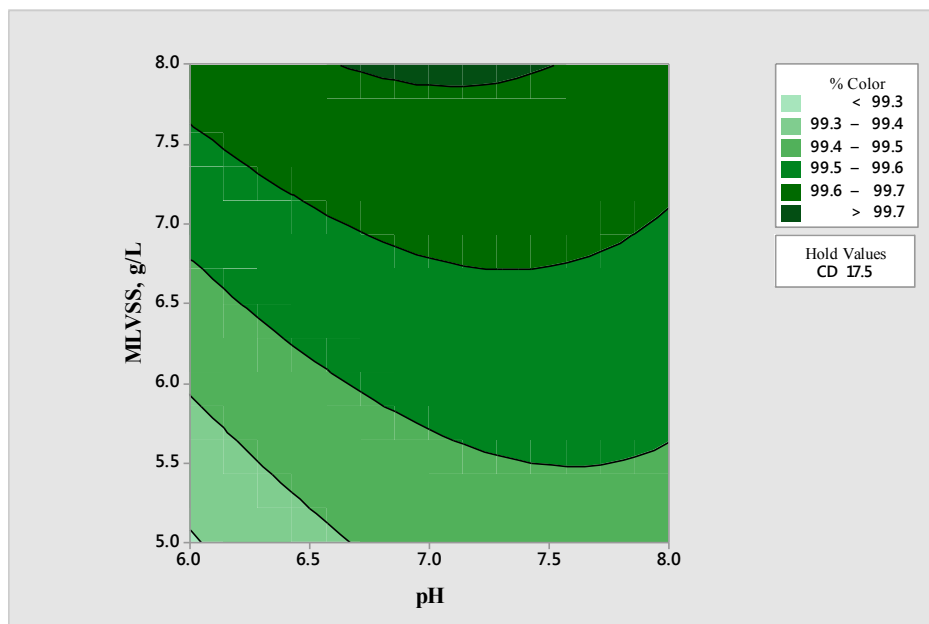
Figure 5.26. Effect of MLVSS concentration and pH on color removal
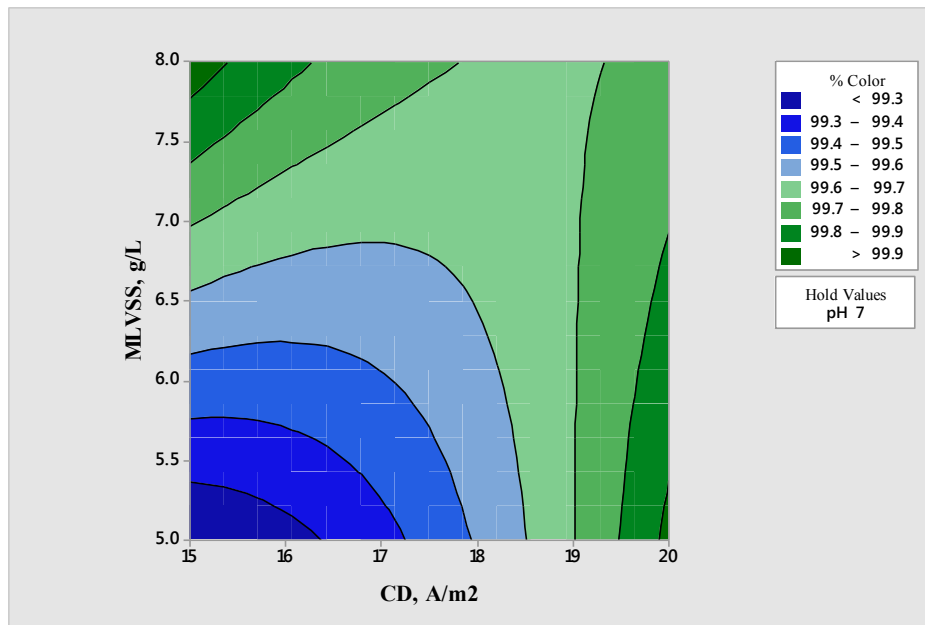
Figure 5.27. Effect of current denscity and MLVSS concentration on color removal

To construct graphical models and statistical parameters for the ANOVA as presented in Table 5.16, the experimental and predicted values of the surface responses provided in Table 5.3 and the model regression equation 5.10 were used. The Table 5.17 provides the coded coefficients for color removal optimization. The adequacy of the surface responses was evaluated by ANOVA. The results presented in Tables 5.16 – 5.17 provide a summary of statistical data for validating the model for discoloration of the wastewater.

Table 5.16. Analysis of variance for color removal optimization

Source	DF	Seq SS	Contribution	Adj SS	Adj MS	F-Value	P-Value
Model	9	0.600832	92.04%	0.600832	0.066759	6.43	0.027
Linear	3	0.291175	44.61%	0.291175	0.097058	9.34	0.017
pH	1	0.017113	2.62%	0.017112	0.017112	1.65	0.256
CD	1	0.12005	18.39%	0.12005	0.12005	11.56	0.019
MLVSS	1	0.154013	23.59%	0.154012	0.154012	14.83	0.012
Square	3	0.083032	12.72%	0.083032	0.027677	2.66	0.159
pH*pH	1	0.0182	2.79%	0.013478	0.013478	1.3	0.306
CD*CD	1	0.064831	9.93%	0.064416	0.064416	6.2	0.055
MLVSS*MLVSS	1	0.000001	0.00%	0.000001	0.000001	0	0.994
2-Way Interaction	3	0.226625	34.72%	0.226625	0.075542	7.27	0.028
pH*CD	1	0.0001	0.02%	0.0001	0.0001	0.01	0.926

pH*MLVSS	1	0.005625	0.86%	0.005625	0.005625	0.54	0.495
CD*MLVSS	1	0.2209	33.84%	0.2209	0.2209	21.26	0.006
Error	5	0.051942	7.96%	0.051942	0.010388		
Lack-of-Fit	3	0.033875	5.19%	0.033875	0.011292	1.25	0.473
Pure Error	2	0.018067	2.77%	0.018067	0.009033		
Total	14	0.652773	100.00%				

DF represents the total degree of freedom; **Seq SS** is sequential sums of squares; **Contribution**- is the % contribution of the parameter; **Adj SS**- adjusted sum of squares; **Adj MS**- adjusted mean squares.

Table 5.17. Coded coefficients color removal optimization

Term	Effect	Coef	SE Coef	95% CI		T-Value	P-Value	VIF
Constant		99.5733	0.0588	(99.4221,	99.7246)	1692.12	0	
pH	0.0925	0.0463	0.036	(-0.0464,	0.1389)	1.28	0.256	1
CD	0.245	0.1225	0.036	(0.0299,	0.2151)	3.4	0.019	1
MLVSS	0.2775	0.1388	0.036	(0.0461,	0.2314)	3.85	0.012	1
pH*pH	-0.1208	-0.0604	0.053	(-0.1968,	0.0759)	-1.14	0.306	1.01
CD*CD	0.2642	0.1321	0.053	(-0.0043,	0.2684)	2.49	0.055	1.01
MLVSS*MLVSS	-0.0008	-0.0004	0.053	(-0.1368,	0.1359)	-0.01	0.994	1.01
pH*CD	0.01	0.005	0.051	(-0.1260,	0.1360)	0.1	0.926	1
pH*MLVSS	-0.075	-0.0375	0.051	(-0.1685,	0.0935)	-0.74	0.495	1
CD*MLVSS	-0.47	-0.235	0.051	(-0.3660,	-0.1040)	-4.61	0.006	1

Coef and **SE Coef** are coefficients and standard error coefficients respectively;
CI- is the confidence interval;
t-Value is the measurement of the size of the difference relative to the variation in the sample data;
VIF- Variance Inflation Factor.

Model summary:

S = 0.101923, R-sq = 92.04%, R-sq(adj) = 77.72%, PRESS = 0.58265

f-value and p-value were assessed in details in order to evaluate the significance of the regression. The higher numbers of f-value implied that the regression models included acceptable range of the surface response values. p-value and f-value interrelationship was employed for f-value analysis and to evaluate if the model included required number of variations. The value of model coefficient of determination demonstrated that R-sq and R-sq(adj) values were 92.04% and 77.72% for color removal model. The values of R-sq and R-

sq(adj) are high which indicates a good fit of color removal model points. In order to establish the best distribution model for discoloration, the goodness of fit test was used similarly to the previous models for COD, TN and TP. The results are provided in Tables 5.18 and 5.19 and demonstrate that the suitable distribution model is 3-Parameter Weibull, similar to the previously designed models for carbon and nutrients. The residual plots for color removal model are represented in Figure 5.27. Optimal range of all three parameters (pH, CD, MLVSS) for optimal phosphorus removal is provided in Figure 5.27. The graphical results of goodness of fit evaluation are presented in Figure 5.29 and confirm the best fit for 3-Parameter Weibull distribution.
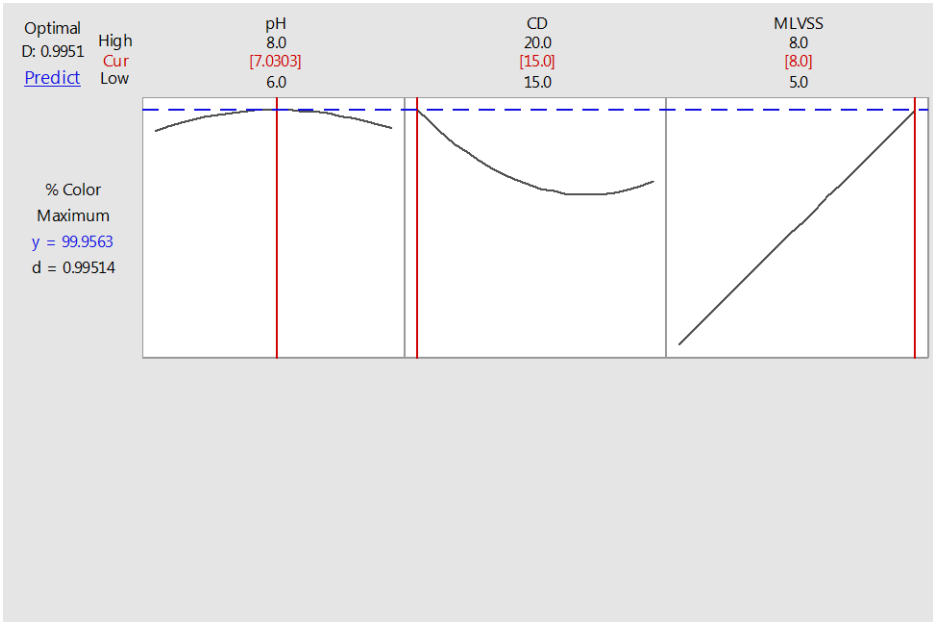
Figure 5.27. Optimum range for color removal
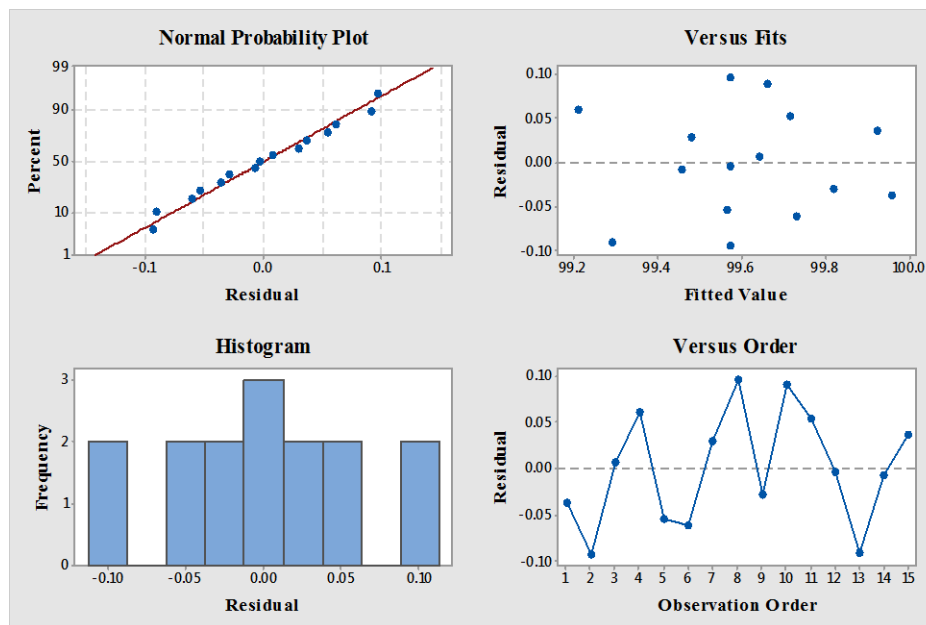
Figure 5.28. Residual plots for color removal

Table 5.18. Goodness of fit test color removal

Distribution	AD	P	LRT P
Normal	0.19	0.88	
Box-Cox Transformation	0.188	0.886	
Lognormal	0.191	0.878	
3-Parameter Lognormal	0.202	*	0.93
Exponential	6.852	<0.003	
2-Parameter Exponential	1.773	<0.010	0
Weibull	0.239	>0.250	
3-Parameter Weibull	0.189	>0.500	0.357
Smallest Extreme Value	0.241	>0.250	
Largest Extreme Value	0.444	>0.250	
Gamma	0.202	>0.250	
3-Parameter Gamma	1.763	*	1
Logistic	0.193	>0.250	
Loglogistic	0.193	>0.250	
3-Parameter Loglogistic	0.193	*	0.943

AD: Anderson-Darling statistic (AD): Lower AD values indicate a better fit;
P: p-value;
LRT P: For 3-parameter distributions only, a low value indicates that adding the third parameter is a significant improvement over the 2-Parameter version.

Table 5.19. Estimates of distribution parameters for color removal

Distribution	Location	Shape	Scale	Threshold
Normal*	99.61		0.22	
Box-Cox Transformation*	9.81E+09		1.06E+08	
Lognormal*	4.60		0.01	
3-Parameter Lognormal	10.84		0	-5.07E+04
Exponential			99.61	
2-Parameter Exponential			0.44	99.17
Weibull		534.40	99.71	
3-Parameter Weibull		4.57	0.90	98.79
Smallest Extreme Value	99.71		0.19	
Largest Extreme Value	99.50		0.21	
Gamma		2.28E+05	0.01	
3-Parameter Gamma		2159.07	0.0045	89.81
Logistic	99.62		0.12	
Loglogistic	4.60		0.001	
3-Parameter Loglogistic	10.84		0	-5.07E+04

* Scale: Adjusted ML estimate

The graph was constructed for the 3-Parameter Weibull distribution model with Shape 4.57, Scale 0.90, and Threshold 98.79). The probabilities for the removal efficiency values (minimum and maximum taken from Table 5.3) that fall in the range of 95.50 – 99.71% are presented in Figure 5.29. The distribution represented in Figure 5.30 follows the same pattern as other pollutants of interest. The removal performance of color was very high, therefore the range of observed values is narrow as the variation in color-forming substances removal lied in between 95.50 – 99.71%.
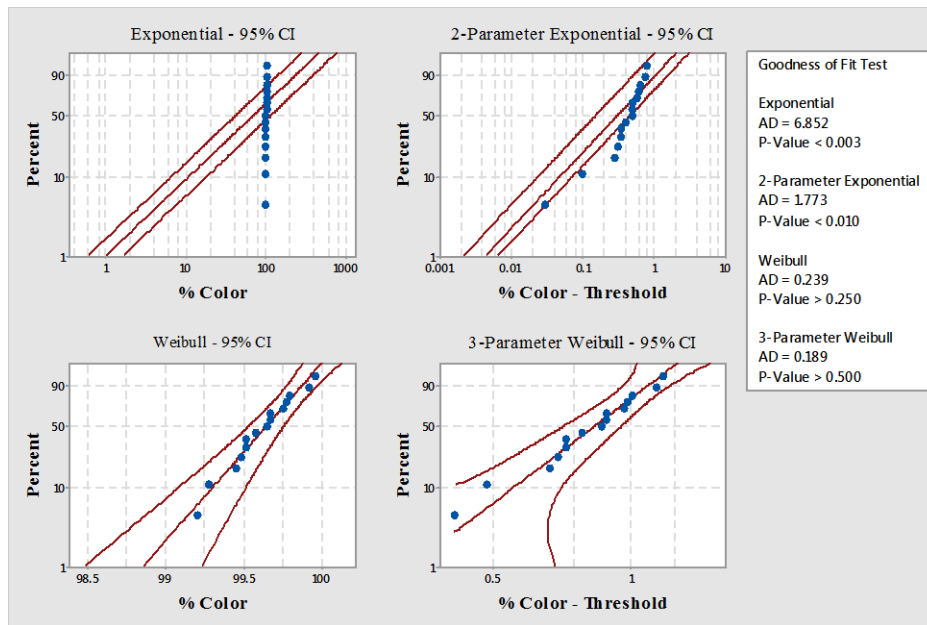
Figure 5.29. Probability plot for color removal
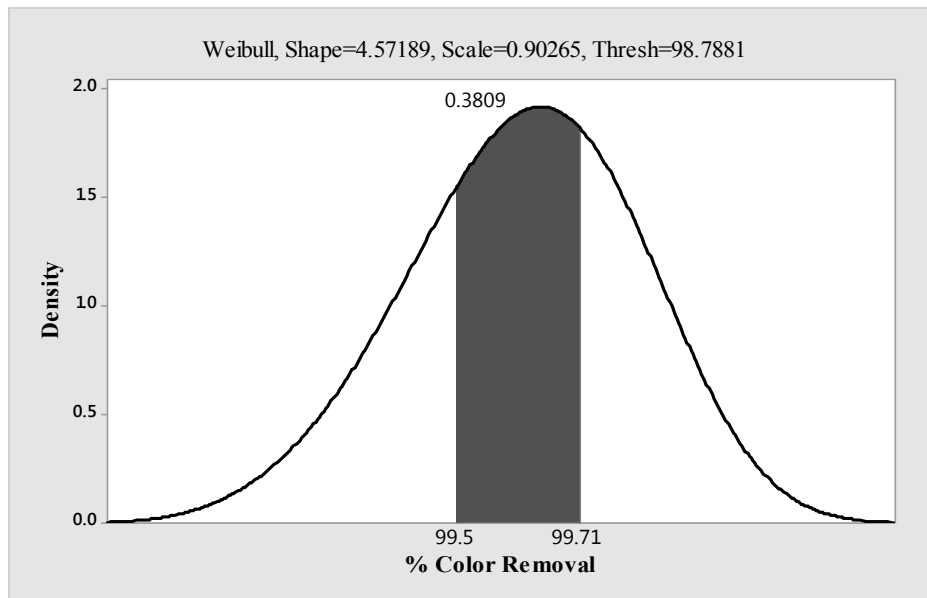
Figure 5.30. Distribution plot for color removal

5.5. Phase IV: Summary and Conclusions

Experiments were carried out to investigate degree of influence of pH, current density and concentration of mixed liquor on removal efficiency of COD, nitrogen, phosphorus and color removal from molasses-containing industrial effluent covering wide range of operating conditions in EAnMBR. The percentage of carbon, nutrients and color removal demonstrated

233

various degree of influence by technological parameters such as pH, current density and MLVSS concentration. The experimental data obtained during 60 days of phase IV were analyzed using response surface methodology to find out optimal values of pH, CD and MLVSS to maximize percent removal. Three-level three factorial Box–Behnken experimental designs were applied in the present study in order to determine optimal variations. Regression equations were developed for the percentage COD, TN, TP and color removal.

Table 5.20. Optimal values correlations between pH, CD, MLVSS concentration and removal efficiencies

Variable	Unit	Value	Parameter	Degree of Significance
pH	-	6.34		insignificant
CD	Am^{-2}	20.00	COD	highly significant
MLVSS	gL^{-1}	5.00		insignificant
pH	-	7.11		insignificant
CD	Am^{-2}	20.00	Nitrogen	highly significant
MLVSS	gL^{-1}	8.00		highly significant
pH	-	8.00		highly significant
CD	Am^{-2}	15.00	Phosphorus	significant
MLVSS	gL^{-1}	8.00		highly significant
pH	-	7.03		insignificant
CD	Am^{-2}	15.00	Color	significant
MLVSS	gL^{-1}	8.00		highly significant

The degree of significance was assessed based on the developed models (P-value for linear, square and two-way interaction) for each regression equation and the levels of operating parameter required to maximize the removal performance- low, high and midpoint (Figure 4.134, 4.142, 4.149, 4.157). Optimal values correlations between the pH, CD, MLVSS concentration and removal efficiencies are summarized in Table 5.20.

The results of the study demonstrated that the removal performance of COD removal was very high (in the range between 87.85% and 99.67%) and the process was significantly affected by the current density, whereas pH and biological activity were less important for COD removal. The optimal operating parameters are as follows: pH= 6.34, CD= 20 Am^{-2}, and MLVSS= 5 gL^{-1}.

With RSM it was determined that nitrogenous compounds removal performance depends mostly on level of current density and biological treatment (20 Am^{-2} and 8 gL^{-1} required for optimal performance), while pH could be maintained at 7.11. With the parameters at these levels, the maximum removal performance achieved could be between 88.76–93.58%.

The research demonstrated that the removal performance of phosphorous was very high (95.50 – 99.71%), and highly-dependant on pH of the electrolyte and biological activity in the EAnMBR. by combination of biological processes and the current density, whereas pH plays a minor role in color-forming substances removal. The optimal parameters are: pH= 7.03, CD= 15 Am^{-2}, and MLVSS= 8 gL^{-1}.

The results of the study demonstrated that the removal performance of color-forming substances was very high (95.50 – 99.71%), and the significant role is played by combination of biological processes and the current density, whereas pH plays a minor role in color-forming substances removal. The optimal parameters are: pH= 7.03, CD= 15 Am^{-2}, and MLVSS= 8 gL^{-1}.

Based on the results obtained during the Phase IV, it can be concluded that different operating parameters and their combination in the EAnMBR affect particular pollutants to a different extent. The operating parameters can be adjusted accordingly to maximize the desired pollutant removal depending on the nature of wastewater fed into the system.

6. Final Conclusion. Research Contributions. Future Work

This chapter presents final conclusion, research contributions and future work.

6.1. Final Conclusion

This work permitted to develop a sustainable novel advanced wastewater treatment system for industrial wastewater. The novel treatment system developed and studied in this research is unique and the first of its kind and, therefore, provides a novel hybrid wastewater treatment method by integrating anaerobic biological process, membrane treatment and electrochemical phenomena into a single compact unit called the electro-anaerobic membrane bioreactor-EAnMBR. Results demonstrated the removal by 99% of carbon, nitrogen and phosphorus from high-strength industrial wastewater. It also permitted a full complete discoloration of the effluent and improving sludge properties. Comparative study with anaerobic membrane bioreactor (AnMBR) showed superiority of a newly developed system. This work also used response surface design to optimize the laboratory tests outcomes.

The significant improvement in nitrogen and phosphorus removal by the novel design of the EAnMBR system may be utilized in a number of environmentally-sustainable technologies, for example- phosphorus-reach solids can serve as an excellent fertilizer in agriculture.

During the research, the novel system proved the favourable interactions between three main processes: physico-chemical, biological and electrokinetic phenomena. The electrical field, applied in order to introduce electrokinetics in addition to physico-chemical and biological processes, did not adversely affect the biological activity in the electro-bioreactor to a significant extent.

The EAnMBR contributes to:

a) Environmental protection by increasing quality of the effluent in terms of carbon, nitrogen, phosphorus and color;

b) Sustainability, as a small footprint system that treats wastewater at a point of generation and produces less amount of sludge by omitting the chemicals addition for coagulation process in favor of electrokinetic processes. In addition, the system generates reusable non-greenhouse gases;

c) Initiating research in a novel type of anaerobic advanced systems for more efficient wastewater treatment.

One of the main advantages of the novel approach was the implementation of the electrokinetic phenomena in anaerobic conditions instead of conventional coagulation. As a result, increased size of the colloids further enhanced the membrane filtration process and improved the effluent quality and solid phase properties. Proved to be effective for molasses-containing recalcitrant wastewater, the novel system could be used for the treatment of variety of industrial wastewaters as well. The EAnMBR may also find use for treating wastewater coming from agricultural, military and naval facilities, and remote locations such as resorts and hotels.

6.2. Research Contributions

There are a several contributions made by this research to the current knowledge including:

a) Designing of a novel EAnMBR system for advanced treatment of high-strength wastewater;

b) Assessing relationship between combination of processes: physicochemical, anaerobic biological and electrokinetic in anaerobic system in presence of membranes;

c) Determining the optimal physicochemical, biological and electrical operating conditions of the EAnMBR that ensure high performance in terms of carbon, nutrients removal and discoloration of effluent;

d) Evaluating the performance of EAnMBR system with respect to quality of effluent, membrane fouling and the changes in the physical, chemical, and biological sludge properties by performing comparative study between EAnMBR and AnMBR operated under the same conditions.

e) Improving sludge dewatering characteristics by significantly reducing the specific resistance to filtration.

f) Providing mechanisms for a superior removal of carbon, nitrogen, phosphorous and color under anaerobic conditions in membrane electrobioreactor.

6.3. Future Work

In order to apply the system on full scale, the following future work is suggested:

a) Pilot Scale Investigation. Despite the fact that the novel system demonstrated excellent performance in a laboratory scale, a pilot scale investigation is suggested before application of the system on full scale.

b) Impact of Transmembrane Pressure. In this research, the flux was constant whereas the transmembrane pressure varied with time. The fouling mechanisms in constant flow applications and variable pressure applications should be investigated further to study impact of transmembrane pressure variation.

c) Optimization of Sludge Retention Time. In this work, a SRT was assumed arbitrary and was constant throughout the experimental phases. The optimization of SRT in the EAnMBR is suggested to conduct in order to optimize the quality of effluent.

d) Gas Production Intensity and Composition. Due to the complexity of the processes taking place in the EAnMBR system, the mixture of gases is heterogeneous, further work can focus on gas production and its efficient utilization.

References

[1] H.T.p.o. Orange, No Water No Future: A Water Focus for Johannesburg. Contribution to the Panel of the UN Secretary General in preparation for the Johannesburg Summit, in, 2002.

[2] UN/WWAP, Water. A shared responsability, The United Nations World Water Development Report 2 (2006).

[3] WHO/UNICEF, Global water supply and sanitation assessment 2000 report, in: WHO/Unicef Joint Water Supply Sanitation Monitoring, Programme, World Health Organization and United Nations Children's Fund, Switzerland, 2000.

[4] WHO/UNICEF, Progress on sanitation and drinking water: 2010 update, WHO/UNICEF Joint Monitoring Programme for Water Supply and Sanitation, (2010).

[5] UN, World Population to 2300, (2004).

[6] UN, Intergovernmental Panel on Climate Change, Climate Change 2007: Impacts, adaptation and vulnerability, Contribution of Working Group II to the Fourth Assessment Report of the Intergovernmental Panel on Climate Change, (2007) 42, 44, 48-49.

[7] UN, United Nations Framework Convention on Climate Change, (1992).

[8] O. Apaydin, U. Kurt, M.T. Gonullu, An investigation of the treatment of tannery wastewater by electrocoagulation, Glob. Nest. J., 11 (2009) 546-555.

[9] J.Q. Jiang, N.J.D. Graham, C.M. Andre, G.H. Kelsall, N.P. Brandon, M.J. Chipps, Comparative performance of an electrocoagulation/flotation system with chemical coagulation/dissolved air flotation: A pilot-scale trial, in, IWA Publishing, 2002, pp. 289-297.

[10] T.A. Kharlamova, L.T. Gorokhova, The use of electrocoagulation for the purification of phenol-containing effluents, Soviet Journal of Water Chemistry and Technology (English Translation of Khimiya i Tekhnologiya Vody), 4 (1982) 81-84.

[11] M.C. Marti, M. Roeckel, E. Aspe, M. Novoa, Fat removal from process waters of the fish-meal industry- A study of 3 flotation methods, Environmental Technology, 15 (1994) 29-39.

[12] J. Park, Y. Jung, M. Han, S. Lee, Simultaneous removal of cadmium and turbidity in contaminated soil-washing water by DAF and electroflotation, in, IWA Publishing, 2002, pp. 225-230.

[13] I. Arslan-Alaton, G. Turkoglu, I. Kabdasli, Chemical pretreatment of a spent disperse dyebath analogue by coagulation and electrocoagulation, Fresenius Environmental Bulletin, 17 (2008) 1809-1815.

[14] P. Canizares, C. Jimenez, F. Martinez, M.A. Rodrigo, C. Saez, The pH as a key parameter in the choice between coagulation and electrocoagulation for the treatment of wastewaters, Journal of Hazardous Materials, 163 (2009) 158-164.

[15] P. Canizares, F. Martinez, C. Jimenez, J. Lobato, M.A. Rodrigo, Coagulation and electrocoagulation of wastes polluted with dyes, Environ. Sci. Technol., 40 (2006) 6418-6424.

[16] P. Canizares, F. Martinez, C. Jimenez, J. Lobato, M.A. Rodrigo, Coagulation and electrocoagulation of wastes polluted with colloids, Separation Science and Technology, 42 (2007) 2157-2175.

[17] P. Canizares, F. Martinez, C. Jimenez, C. Saez, M.A. Rodrigo, Coagulation and electrocoagulation of oil-in-water emulsions, Journal of Hazardous Materials, 151 (2008) 44-51.

[18] A.I. Ivanishvili, V.I. Przhegorlinskii, T.D. Kalinichenko, A comparative evaluation of the efficiency of electrocoagulation and reagent methods of clarifying waste water, Soviet Journal of Water Chemistry and Technology (English Translation of Khimiya i Tekhnologiya Vo, 9 (1987) 118-119.

[19] P.K. Holt, G.W. Barton, C.A. Mitchell, The future for electrocoagulation as a localised water treatment technology, Chemosphere, 59 (2005) 355-367.

[20] L.E. De-Bashan, Y. Bashan, Recent advances in removing phosphorus from wastewater and its future use as fertilizer (1997-2003), Water Research, 38 (2004) 4222-4246.

[21] B.Y. Gao, H.H. Hahn, E. Hoffmann, Evaluation of aluminum-silicate polymer composite as a coagulant for water treatment, Water Research, 36 (2002) 3573-3581.

[22] P.R. Gogate, A.B. Pandit, A review of imperative technologies for wastewater treatment I: Oxidation technologies at ambient conditions, Advances in Environmental Research, 8 (2004) 501-551.

[23] J.K. Edzwald, Coagulation in drinking water treatment: Particles, organics and coagulants, in: Proceedings of the 2nd Conference of the IAWQ-IWSA Joint Specialist Group on Coagulation, Flocculation, Filtration, Sedimentation and Flotation, September 1, 1992 - September 3, 1992, Geneva, Switz, 1993, pp. 21-35.

[24] C. Volk, K. Bell, E. Ibrahim, D. Verges, G. Amy, M. Lechevallier, Impact of enhanced and optimized coagulation on removal of organic matter and its biodegradable fraction in drinking water, Water Research, 34 (2000) 3247-3257.

[25] B.A. Bolto, D.R. Dixon, S.R. Gray, H. Chee, P.J. Harbour, L. Ngoc, A.J. Ware, The use of soluble organic polymers in waste treatment, in: Proceedings of the 1996 18th Biennial Conference of the International Association on Water Quality. Part 5, June 23, 1996 - June 28, 1996, Elsevier Science Inc., Singapore, Singapore, 1996, pp. 117-124.

[26] J. Fettig, H. Ratnaweera, H. Odegaard, Synthetic organic polymers as primary coagulants in wastewater treatment, in: IWSA/IAWPRC Joint Specialized Conference on Coagulation, Flocculation, Filtration, Sedimentation and Flotation, April 24, 1990 - April 26, 1990, Jonkoping, Swed, 1991, pp. 19-26.

[27] B. Gao, Q. Yue, J. Miao, Evaluation of polyaluminium ferric chloride (PAFC) as a composite coagulant for water and wastewater treatment, in, IWA Publishing, 2003, pp. 127-132.

[28] D.J. Pernitsky, J.K. Edzwald, Solubility of polyaluminium coagulants, Journal of Water Supply: Research and Technology - AQUA, 52 (2003) 395-406.

[29] M. Rak, M. Swiderska-Broz, Efficiency of alum and prehydrolyzed polyaluminium chlorides as coagulating agents: A comparative study, Environmental Protection Engineering, 27 (2001) 5-15.

[30] N.D. Tzoupanos, A.I. Zouboulis, C.A. Tsoleridis, A systematic study for the characterization of a novel coagulant (polyaluminium silicate chloride), Colloids and Surfaces A: Physicochemical and Engineering Aspects, 342 (2009) 30-39.

[31] A.I. Zouboulis, N. Tzoupanos, Alternative cost-effective preparation method of polyaluminium chloride (PAC) coagulant agent: Characterization and comparative application for water/wastewater treatment, Desalination, 250 (2010) 339-344.

[32] R.G. Rice, Applications of ozone for industrial wastewater treatment - A review, Ozone: Science and Engineering, 18 (1997) 477-515.

[33] A. Aleboyeh, M.E. Olya, H. Aleboyeh, Oxidative treatment of azo dyes in aqueous solution by potassium permanganate, Journal of Hazardous Materials, 162 (2009) 1530-1535.

[34] X.-R. Xu, H.-B. Li, W.-H. Wang, J.-D. Gu, Decolorization of dyes and textile wastewater by potassium permanganate, Chemosphere, 59 (2005) 893-898.

[35] C.A. Martinez-Huitle, E. Brillas, Decontamination of wastewaters containing synthetic organic dyes by electrochemical methods: A general review, Applied Catalysis B: Environmental, 87 (2009) 105-145.

[36] C.G. Schmit, K. Jahan, K.H. Schmit, E. Debik, V. Mahendraker, Activated sludge and other aerobic suspended culture processes, Water Environment Research, 81 (2009) 1127-1193.

[37] S.W.H. Van Hulle, H.J.P. Vandeweyer, B.D. Meesschaert, P.A. Vanrolleghem, P. Dejans, A. Dumoulin, Engineering aspects and practical application of autotrophic nitrogen removal from nitrogen rich streams, Chemical Engineering Journal, 162 (2010) 1-20.

[38] W.P. Barber, D.C. Stuckey, The use of the anaerobic baffled reactor (ABR) for wastewater treatment: A review, Water Research, 33 (1999) 1559-1578.

[39] B. Demirel, O. Yenigun, T.T. Onay, Anaerobic treatment of dairy wastewaters: A review, Process Biochemistry, 40 (2005) 2583-2595.

[40] A.B. dos Santos, F.J. Cervantes, J.B. van Lier, Review paper on current technologies for decolourisation of textile wastewaters: Perspectives for anaerobic biotechnology, Bioresource Technology, 98 (2007) 2369-2385.

[41] W.W. Eckenfelder, Y. Argaman, E. Miller, Process selection criteria for the biological treatment of industrial wastewaters, Environmental Progress, 8 (1989) 40-45.

[42] S.R. Harper, F.G. Pohland, Recent developments in hydrogen management during anaerobic biological wastewater treatment, Biotechnology and Bioengineering, 28 (1986) 585-602.

[43] M. Henze, P. Harremoes, Anaerobic treatment of wastewater in fixed film reactors - A literature review, Water Science and Technology, 15 (1983) 1-101.

[44] J. Iza, Fluidized bed reactors for anaerobic wastewater treatment, in: Proceedings of the IAWPRC International Specialised Workshop, September 24, 1990 - September 26, 1990, Valladolid, Spain, 1991, pp. 109-132.

[45] R.C. Leitao, A.C. Van Haandel, G. Zeeman, G. Lettinga, The effects of operational and environmental variations on anaerobic wastewater treatment systems: A review, Bioresource Technology, 97 (2006) 1105-1118.

[46] K.V. Rajeshwari, M. Balakrishnan, A. Kansal, K. Lata, V.V.N. Kishore, State-of-the-art of anaerobic digestion technology for industrial wastewater treatment, Renewable & sustainable energy reviews, 4 (2000) 135-156.

[47] I.R. Ramsay, P.C. Pullammanappallil, Protein degradation during anaerobic wastewater treatment: Derivation of stoichiometry, Biodegradation, 12 (2001) 247-257.

[48] M.S. Switzenbaum, Anaerobic fixed film wastewater treatment, Enzyme and Microbial Technology, 5 (1983) 242-250.

[49] S. Ren, Assessing wastewater toxicity to activated sludge: Recent research and developments, Environment International, 30 (2004) 1151-1164.

[50] S. Yan, B. Subramanian, R.Y. Surampalli, S. Narasiah, R.D. Tyagi, Isolation, characterization, and identification of bacteria from activated sludge and soluble microbial products in wastewater treatment systems, Practice Periodical of Hazardous, Toxic, and Radioactive Waste Management, 11 (2007) 240-258.

[51] P. Canizares, F. Martinez, C. Jimenez, C. Saez, M.A. Rodrigo, Technical and economic comparison of conventional and electrochemical coagulation processes, Journal of Chemical Technology and Biotechnology, 84 (2009) 702-710.

[52] J.C. Donini, J. Kan, J. Szynkarczuk, T.A. Hassan, K.L. Kar, Operating cost of electrocoagulation, Can. J. Chem. Eng., 72 (1994) 1007-1012.

[53] H. Melcer, D.T. Merrill, M.B. Gerhardt, C. Van Maltby, Tappi, Technical and economic feasibility assessment of metals reduction in pulp and paper mill wastewaters, Tappi Press, Atlanta, 1998.

[54] M. Bayramoglu, M. Eyvaz, M. Kobya, Treatment of the textile wastewater by electrocoagulation Economical evaluation, Chemical Engineering Journal, 128 (2007) 155-161.

[55] N. Meunier, P. Drogui, C. Gourvenec, G. Mercier, R. Hausler, J.F. Blais, Removal of metals in leachate from sewage sludge using electrochemical technology, Environmental Technology, 25 (2004) 235-245.

[56] A.E. Yilmaz, R. Boncukcuoglu, M.M. Kocakerim, A quantitative comparison between electrocoagulation and chemical coagulation for boron removal from boron-containing solution, Journal of Hazardous Materials, 149 (2007) 475-481.

[57] S. Veli, T. Ozturk, A. Dimoglo, Treatment of municipal solid wastes leachate by means of chemical- and electro-coagulation, Separation and Purification Technology, 61 (2008) 82-88.

[58] G.H. Chen, Electrochemical technologies in wastewater treatment, Separation and Purification Technology, 38 (2004) 11-41.

[59] V. Blonskaja, S. Zub, Possible ways for post-treatment of biologically treated wastewater from yeast factory, Journal of Environmental Engineering and Landscape Management, 17 (2009) 189-197.

[60] M. Gladchenko, E. Starostina, S. Shcherbakov, B. Versprille, S. Kalyuzhnyi, Combined biological and physico-chemical treatment of baker's yeast wastewater including removal of coloured and recalcitrant to biodegradation pollutants, Water science and technology : a journal of the International Association on Water Pollution Research, 50 (2004) 67-72.

[61] V. Blonskaja, I. Kamenev, S. Zub, Possibilities of using ozone for the treatment of wastewater from the yeast industry, PROCEEDINGS- ESTONIAN ACADEMY OF SCIENCES CHEMISTRY, 55 (2006) 29-39.

[62] M. Coca, M. Pena, G. Gonzalez, Variables affecting efficiency of molasses fermentation wastewater ozonation, Chemosphere, 60 (2005) 1408-1415.

[63] S. Kalyuzhnyi, M. Gladchenko, E. Starostina, S. Shcherbakov, A. Versprille, Combined biological and physico-chemical treatment of baker's yeast wastewater, Water Science and Technology, 52 (2005) 175-181.

[64] S. Zub, T. Kurissoo, A. Menert, V. Blonskaja, Combined biological treatment of high-sulphate wastewater from yeast production, Water and Environment Journal, 22 (2008) 274-286.

[65] F. Tahar, R. Cheikh, J. Blais, Décoloration des eaux usées de levurerie par adsorption sur charbon, Journal of Environmental Engineering and Science, 3 (2004) 269-277.

[66] Y. Shi, H. Liu, X. Zhou, A. Xie, C. Hu, Mechanism on impact of internal-electrolysis pretreatment on biodegradability of yeast wastewater, Chinese Science Bulletin, 54 (2009) 2124-2130.

[67] M. Pena, M. Coca, G. Gonzalez, Continuous ozonation of biologically pretreated molasses fermentation effluents, Journal of Environmental Science and Health - Part A Toxic/Hazardous Substances and Environmental Engineering, 42 (2007) 777-783.

[68] K.-Y. Park, K.-H. Ahn, K.-P. Kim, J.H. Kweon, S.-K. Maeng, Characteristics and treatability of persistent colors in biologically treated wastewater effluents, Environmental Engineering Science, 22 (2005) 557-566.

[69] M. Koplimaa, A. Menert, V. Blonskaja, T. Kurissoo, S. Zub, M. Saareleht, E. Vaarmets, T. Menert, Liquid and gas chromatographic studies of the anaerobic degradation of baker's yeast wastewater, in: 5th Symposium by Nordic Separation Science Society, NoSSS 2009, August 26, 2009 - August 29, 2009, Elsevier, Tallinn, Estonia, 2010, pp. 120-129.

[70] S. Kalyuzhnyi, M. Gladchenko, A. Mulder, B. Versprille, Comparison of quasisteady-state performance of the DEAMOX process under intermittent and continuous feeding and different nitrogen loading rates, Biotechnol J, (2007).

[71] L. Fan, T. Nguyen, F.A. Roddick, Characterisation of the impact of coagulation and anaerobic bio-treatment on the removal of chromophores from molasses wastewater, Water Research, 45 (2011) 3933-3940.

[72] J. Dwyer, P. Griffiths, P. Lant, Simultaneous colour and DON removal from sewage treatment plant effluent: Alum coagulation of melanoidin, Water Research, 43 (2009) 553-561.

[73] A. Gadd, D. Ryan, J. Kavanagh, A.-L. Beaurain, S. Luxem, G. Barton, Electrocoagulation of fermentation wastewater by low carbon steel (Fe) and 5005 aluminium (Al) electrodes, Journal of Applied Electrochemistry, 40 (2010) 1511-1517.

[74] S. Figaro, S. Louisy-Louis, J. Lambert, J.J. Ehrhardt, A. Ouensanga, S. Gaspard, Adsorption studies of recalcitrant compounds of molasses spentwash on activated carbons, Water Research, 40 (2006) 3456-3466.

[75] M. Altinbas, A.F. Aydin, M.F. Sevimli, I. Ozturk, Advanced Oxidation of Biologically Pretreated Baker's Yeast Industry Effluents for High Recalcitrant COD and Color Removal, Journal of Environmental Science and Health, Part A, 38 (2003) 2229-2240.

[76] A. Battimelli, D. Loisel, D. Garcia-Bernet, H. Carrere, J.-P. Delgenes, Combined ozone pretreatment and biological processes for removal of colored and biorefractory compounds in wastewater from molasses fermentation industries, Journal of Chemical Technology and Biotechnology, 85 (2010) 968-975.

[77] H.-Y. Wang, H. Qian, W.-R. Yao, Melanoidins produced by the Maillard reaction: Structure and biological activity, Food Chemistry, 128 (2011) 573-584.

[78] K. De Vleeschouwer, I. Van der Plancken, A. Van Loey, M.E. Hendrickx, The Effect of High Pressure-High Temperature Processing Conditions on Acrylamide Formation and Other Maillard Reaction Compounds, Journal of Agricultural and Food Chemistry, 58 (2010) 11740-11748.

[79] J.K. Eun, S.L. Young, M. Murata, S. Homma, Effect of pH control on the intermediates and melanoidins of nonenzymatic browning reaction, LWT - Food Science and Technology, 38 (2005) 1-6.

[80] B. Cosovic, V. Vojvodic, N. Bokovic, M. Plavic, C. Lee, Characterization of natural and synthetic humic substances (melanoidins) by chemical composition and adsorption measurements, Organic Geochemistry, 41 (2010) 200-205.

[81] Z. Xuan, L. Hui, L. YuQian, Z. Miao, The main components of color and dissolved organic matter from yeast industry effluent, in: 2010 2nd Conference on Environmental Science and Information Application Technology (ESIAT 2010), 17-18 July 2010, IEEE, Piscataway, NJ, USA, 2010, pp. 833-836.

[82] A. Smaniotto, A. Bertazzo, S. Comai, P. Traldi, The role of peptides and proteins in melanoidinb formation, Journal of Mass Spectrometry, 44 (2009) 410-418.

[83] O.T. Iorhemen, R.A. Hamza, J.H. Tay, Membrane Bioreactor (MBR) Technology for Wastewater Treatment and Reclamation: Membrane Fouling, Membranes, 6 (2016) 1-29.

[84] L.W. Kroh, T. Fiedler, J. Wagner, alpha-dicarbonyl compounds - Key intermediates for the formation of carbohydrate-based melanoidins, in: E.S.V.S.P. Schleicher (Ed.) Maillard Reaction: Recent Advances in Food and Biomedical Sciences, 2008, pp. 210-215.

[85] D. Marko, M. Habermeyer, M. Kemeny, U. Weyand, E. Niederberger, O. Frank, T. Hofmann, Maillard reaction products modulating the growth of human tumor cells in vitro, Chemical Research in Toxicology, 16 (2003) 48-55.

[86] Y. Shirahashi, H. Watanabe, F. Hayase, Identification of Red Pigments Formed in a D-Xylose-glycine Reaction System, Bioscience Biotechnology and Biochemistry, 73 (2009) 2287-2292.

[87] F.J. Morales, C. Fernández-Fraguas, S. Jiménez-Pérez, Iron-binding ability of melanoidins from food and model systems, Food Chemistry, 90 (2005) 821-827.

[88] J. Herzfeld, D. Rand, Y. Matsuki, E. Daviso, M. Mak-Jurkauskas, I. Mamajanov, Molecular Structure of Humin and Melanoidin Via Solid state NMR, Journal of Physical Chemistry B, 115 (2011) 5741-5745.

[89] E. Venir, P. Pittia, S. Giavon, E. Maltini, Structure and water relations of melanoidins investigated by thermal, rheological, and microscopic analysis, International Journal of Food Properties, 12 (2009) 819-833.

[90] T. Fiedler, L.W. Kroh, Formation of discrete molecular size domains of melanoidins depending on the involvement of several -dicarbonyl compounds: Part 2, European Food Research and Technology, 225 (2007) 473-481.

[91] J.-S. Kim, Y.-S. Lee, Effect of reaction pH on enolization and racemization reactions of glucose and fructose on heating with amino acid enantiomers and formation of melanoidins as result of the Maillard reaction, Food Chemistry, 108 (2008) 582-592.

[92] J.A. Rufian-Henares, F.J. Morales, Antimicrobial activity of melanoidins against Escherichia coli is mediated by a membrane-damage mechanism, Journal of Agricultural and Food Chemistry, 56 (2008) 2357-2362.

[93] J.A. Rufian-Henares, F.J. Morales, A new application of a commercial microtiter plate-based assay for assessing the antimicrobial activity of Maillard reaction products, Food Research International, 39 (2006) 33-39.

[94] J.A. Rufian-Henares, F.J. Morales, Effect of in vitro enzymatic digestion on antioxidant activity of coffee melanoidins and fractions, Journal of Agricultural and Food Chemistry, 55 (2007) 10016-10021.

[95] J.A. Rufian-Henares, F.J. Morales, Functional properties of melanoidins: In vitro antioxidant, antimicrobial and antihypertensive activities, Food Research International, 40 (2007) 995-1002.

[96] J.A. Rufian-Henares, S.P. de la Cueva, Antimicrobial Activity of Coffee Melanoidins-A Study of Their Metal-Chelating Properties, Journal of Agricultural and Food Chemistry, 57 (2009) 432-438.

[97] G.K. Ziyatdinova, A.A. Gainetdinova, G.K. Budnikov, Reactions of synthetic phenolic antioxidants with electrogenerated titrants and their analytical applications, Journal of Analytical Chemistry, 65 (2010) 929-934.

[98] F.a.A.O. UN, Enzymatic browning, in, 2011, pp. Formation of melanins from a simple polyphenol.

[99] S. Kalyuzhnyi, M. Gladchenko, A. Mulder, B. Versprille, New anaerobic process of nitrogen removal, in: 5th World Water Congress: Wastewater Treatment Processes, IWA Publishing, 2006, pp. 163-170.

[100] S. Kalyuzhnyi, M. Gladchenko, A. Mulder, B. Versprille, DEAMOX-New biological nitrogen removal process based on anaerobic ammonia oxidation coupled to sulphide-driven conversion of nitrate into nitrite, Water Research, 40 (2006) 3637-3645.

[101] S.V. Kalyuzhnyi, M.A. Gladchenko, A.I. Trukhina, N.M. Shestakova, T.P. Tourova, T.N. Nazina, A.B. Poltaraus, Phylogenetic analysis of a microbial community involved in anaerobic oxidation of ammonium nitrogen, Microbiology Microbiology, 79 (2010) 237-246.

[102] S. Kalyuzhnyi, M. Gladchenko, DEAMOX - New microbiological process of nitrogen removal from strong nitrogenous wastewater, Desalination, 248 (2009) 783-793.

[103] S.V. Kalyuzhnyi, M.A. Gladchenko, H. Kang, A. Mulder, A. Versprille, Development and optimisation of VFA driven DEAMOX process for treatment of strong nitrogenous anaerobic effluents, Water Science and Technology, 57 (2008) 323-328.

[104] H.-G. Kim, H.-N. Jang, H.-M. Kim, D.-S. Lee, T.-H. Chung, Effect of an electro phosphorous removal process on phosphorous removal and membrane permeability in a pilot-scale MBR, Desalination, 250 (2010) 629-633.

[105] A.P. Buzzini, L.J. Patrizzi, A.J. Motheo, E.C. Pires, Preliminary evaluation of the electrochemical and chemical coagulation processes in the post-treatment of effluent from an upflow anaerobic sludge blanket (UASB) reactor, Journal of Environmental Management, 85 (2007) 847-857.

[106] H.G. Kim, H.N. Jang, H.M. Kim, D.S. Lee, T.H. Chung, Effect of an electro phosphorous removal process on phosphorous removal and membrane permeability in a pilot-scale MBR, Desalination, 250 (2010) 629-633.

[107] P.K. Gkotsis, E.L. Batsari, E.N. Peleka, A.K. Tolkou, A.I. Zouboulis, Fouling control in a lab-scale MBR system: Comparison of several commercially applied coagulants, Journal of Environmental Management.

[108] M. Krapivina, T. Kurissoo, V. Blonskaja, S. Zub, R. Vilu, Treatment of sulphate containing yeast wastewater in an anaerobic sequence batch reactor, Proceedings- Estonian Academy of Sciences Cchemistry, 56 (2007) 38-52.

[109] P.N.L. Lens, A. Visser, A.J.H. Janssen, L.W.H. Pol, G. Lettinga, Biotechnological treatment of sulfate-rich wastewaters, Critical Reviews in Environmental Science and Technology, 28 (1998) 41-88.

[110] W. Liamleam, A.P. Annachhatre, Electron donors for biological sulfate reduction, Biotechnology Advances, 25 (2007) 452-463.

[111] S. Tait, W.P. Clarke, J. Keller, D.J. Batstone, Removal of sulfate from high-strength wastewater by crystallisation, Water Research, 43 (2009) 762-772.

[112] A.J. Geldenhuys, J.P. Maree, M. de Beer, P. Hlabela, An integrated limestone/lime process for partial sulphate removal, Journal of the South African Institute of Mining and Metallurgy, 103 (2003) 345-353.

[113] A. Pala, G. Erden, Decolorization of a baker's yeast industry effluent by Fenton oxidation, Journal of Hazardous Materials, 127 (2005) 141-148.

[114] M.E. Ersahin, R.K. Dereli, H. Ozgun, B.G. Donmez, I. Koyuncu, M. Altinbas, I. Ozturk, Source Based Characterization and Pollution Profile of a Baker's Yeast Industry, Clean - Soil, Air, Water, 39 (2011) 543-548.

[115] A.S. Gadd, D.R. Ryan, J.M. Kavanagh, G.W. Barton, Design development of an electrocoagulation reactor for molasses process wastewater treatment, Water Science and Technology, 61 (2010) 3221-3227.

[116] K. Neira, D. Jeison, Anaerobic co-digestion of surplus yeast and wastewater to increase energy recovery in breweries, Water Science and Technology, 61 (2010) 1129-1135.

[117] Z.-y. Yan, J.-s. Wang, L. Xie, Anaerobic Treatment of Yeast Effluent in an Expanded Granular Sludge Bed Reactor, in: 2010 International Conference on Digital Manufacturing and Automation (ICDMA 2010), 18-20 Dec. 2010, IEEE Computer Society, Los Alamitos, CA, USA, 2010, pp. 219-222.

[118] S. Kahraman, O. Yesilada, Decolorization and bioremediation of molasses wastewater by white-rot fungi in a semi-solid-state condition, Folia microbiologica, 48 (2003) 525-528.

[119] W. Lee, P. Westerhoff, Dissolved organic nitrogen removal during water treatment by aluminum sulfate and cationic polymer coagulation, Water Research, 40 (2006) 3767-3774.

[120] T. Sreethawong, S. Chavadej, Color removal of distillery wastewater by ozonation in the absence and presence of immobilized iron oxide catalyst, Journal of Hazardous Materials, 155 (2008) 486-493.

[121] C.-H. Wei, Y.-P. Zhang, C.-F. Wu, C.-S. Hu, Decoloration and mineralization of yeast wastewater by using Ce-Fe/Al2O3 as heterogeneous photo-Fenton catalyst, Journal of Central South University of Technology (English Edition), 13 (2006) 481-485.

[122] S.H. Mutlu, U. Yetis, T. Gurkan, L. Yilmaz, Decolorization of wastewater of a baker's yeast plant by membrane processes, Water Research, 36 (2002) 609-616.

[123] T.I. Liakos, N.K. Lazaridis, Melanoidin removal from molasses effluents by adsorption, Journal of Water Process Engineering, 10 (2016) 156-164.

[124] Z. Liang, Y. Wang, Y. Zhou, H. Liu, Z. Wu, Stoichiometric relationship in the coagulation of melanoidins-dominated molasses wastewater, Desalination, 250 (2010) 42-48.

[125] Z. Liang, Y. Wang, Y. Zhou, H. Liu, Z. Wu, Variables affecting melanoidins removal from molasses wastewater by coagulation/flocculation, Separation and Purification Technology, 68 (2009) 382-389.

[126] D. Ryan, A. Gadd, J. Kavanagh, M. Zhou, G. Barton, A comparison of coagulant dosing options for the remediation of molasses process water, Separation and Purification Technology, 58 (2008) 347-352.

[127] Y. Zhou, Z. Liang, Y. Wang, Decolorization and COD removal of secondary yeast wastewater effluents by coagulation using aluminum sulfate, Desalination, 225 (2008) 301-311.

[128] S. Mohana, B.K. Acharya, D. Madamwar, Distillery spent wash: Treatment technologies and potential applications, Journal of Hazardous Materials, 163 (2009) 12-25.

[129] M. Mischopoulou, P. Naidis, S. Kalamaras, T.A. Kotsopoulos, P. Samaras, Effect of ultrasonic and ozonation pretreatment on methane production potential of raw molasses wastewater, Renewable Energy, 96, Part B (2016) 1078-1085.

[130] M. Hadavifar, H. Younesi, A.A. Zinatizadeh, F. Mahdad, Q. Li, Z. Ghasemi, Application of integrated ozone and granular activated carbon for decolorization and chemical oxygen demand reduction of vinasse from alcohol distilleries, Journal of Environmental Management, 170 (2016) 28-36.

[131] S. Zak, The Use of Fenton's System in the Yeast Industry Wastewater Treatment, Environmental Technology, 26 (2005) 11-19.

[132] N. Amaral-Silva, R.C. Martins, C. Paiva, S. Castro-Silva, R.M. Quinta-Ferreira, A new winery wastewater treatment approach during vintage periods integrating ferric coagulation, Fenton reaction and activated sludge, Journal of Environmental Chemical Engineering, 4 (2016) 2207-2215.

[133] J. Dwyer, L. Kavanagh, P. Lant, The degradation of dissolved organic nitrogen associated with melanoidin using a UV/H2O2 AOP, Chemosphere, 71 (2008) 1745-1753.

[134] K. Bani-Melhem, M. Elektorowicz, Development of a novel submerged membrane electro-bioreactor (SMEBR): Performance for fouling reduction, Environmental Science and Technology, 44 (2010) 3298-3304.

[135] K. Bani-Melhem, M. Elektorowicz, Performance of the submerged membrane electro-bioreactor (SMEBR) with iron electrodes for wastewater treatment and fouling reduction, Journal of Membrane Science, 379 (2011) 434-439.

[136] S. Ibeid, M. Elektorowicz, J.A. Oleszkiewicz, Impact of electro-coagulation on the fate of soluble microbial products (SMP) in submerged membrane electro-bioreactor (SMEBR), in: Annual

Conference of the Canadian Society for Civil Engineering 2010, CSCE 2010, June 9, 2010 - June 12, 2010, Canadian Society for Civil Engineering, Winnipeg, MB, Canada, 2010, pp. 634-640.

[137] F.J. Benitez, J.L. Acero, A.I. Leal, F.J. Real, Cork processing wastewaters purification by the application of microfiltration and ultrafiltration membranes and assessment of the membrane fouling, in: CHISA 2006 - 17th International Congress of Chemical and Process Engineering, August 27, 2006 - August 31, 2006, Czech Society of Chemical Engineering, Prague, Czech republic, 2006, pp. Hexion Specialty Chemicals; Mitsubishi Chemical Corporation; CS Cabot; Zentiva; BorsodChem MCHZ.

[138] M. Bernardo, A. Santos, P. Cantinho, M. Minhalma, Cork industry wastewater partition by ultra/nanofiltration: A biodegradation and valorisation study, Water Research, 45 (2011) 904-912.

[139] S. Kalyuzhnyi, M. Gladchenko, E. Starostina, S. Shcherbakov, B. Versprille, Integrated biological (anaerobic-aerobic) and physico-chemical treatment of baker's yeast wastewater, Water science and technology : a journal of the International Association on Water Pollution Research, 52 (2005) 10-11.

[140] M. Kobya, S. Delipinar, Treatment of the baker's yeast wastewater by electrocoagulation, Journal of Hazardous Materials, 154 (2008) 1133-1140.

[141] B. Tartakovsky, P. Mehta, J.S. Bourque, S.R. Guiot, Electrolysis-enhanced anaerobic digestion of wastewater, (2011).

[142] E.C. Catalkaya, F. Sengul, Application of Box-Wilson experimental design method for the photodegradation of bakery's yeast industry with UV/H2O2 and UV/H2O2/Fe(II) process, Journal of Hazardous Materials, 128 (2006) 201-207.

[143] S. Chaturvedi, R. Chandra, V. Rai, Isolation and characterization of Phragmites australis (L.) rhizosphere bacteria from contaminated site for bioremediation of colored distillery effluent, Ecological Engineering, 27 (2006) 202-207.

[144] P. Kumar, R. Chandra, Decolourisation and detoxification of synthetic molasses melanoidins by individual and mixed cultures of Bacillus spp, Bioresource Technology, 97 (2006) 2096-2102.

[145] S. Mohana, C. Desai, D. Madamwar, Biodegradation and decolourization of anaerobically treated distillery spent wash by a novel bacterial consortium, Bioresource Technology, 98 (2007) 333-339.

[146] P.J. Strong, J.E. Burgess, Treatment Methods for Wine-Related and Distillery Wastewaters: A Review, Bioremediation Journal, 12 (2008) 70-87.

[147] M.-C. Dictor, C. Joulian, S. Touze, I. Ignatiadis, D. Guyonnet, Electro-stimulated biological production of hydrogen from municipal solid waste, International Journal of Hydrogen Energy, 35 (2010) 10682-10692.

[148] J. Ditzig, H. Liu, B.E. Logan, Production of hydrogen from domestic wastewater using a bioelectrochemically assisted microbial reactor (BEAMR), International Journal of Hydrogen Energy, 32 (2007) 2296-2304.

[149] P.C. Hallenbeck, Fermentative hydrogen production: Principles, progress, and prognosis, International Journal of Hydrogen Energy, 34 (2009) 7379-7389.

[150] G. Luo, L. Xie, Q. Zhou, I. Angelidaki, Enhancement of bioenergy production from organic wastes by two-stage anaerobic hydrogen and methane production process, (2011).

[151] J.B. Van Lier, N. Mahmoud, G. Zeeman, Anaerobic wastewater treatment, (2008).

[152] D. Botheju, B. Lie, R. Bakke, Oxygen effects in anaerobic digestion, Modeling, Identification and Control, 30 (2009) 191-201.

[153] D. Botheju, B. Lie, R. Bakke, Oxygen effects in anaerobic digestion II, Modeling, Identification and Control, 31 (2010) 55-65.

[154] Y. Satyawali, M. Balakrishnan, Wastewater treatment in molasses-based alcohol distilleries for COD and color removal: A review, J. Environ. Manage. Journal of Environmental Management, 86 (2008) 481-497.

[155] S. Sirianuntapiboon, P. Phothilangka, S. Ohmomo, Decolorization of molasses wastewater by a strain No.BP103 of acetogenic bacteria, Bioresource Technology, 92 (2004) 31-39.

[156] S. Sirianuntapiboon, K. Prasertsong, Treatment of molasses wastewater by acetogenic bacteria BP103 in sequencing batch reactor (SBR) system, Bioresource Technology, 99 (2008) 1806-1815.

[157] D. Francisca Kalavathi, L. Uma, G. Subramanian, Degradation and metabolization of the pigment - Melanoidin in distillery effluent by the marine cyanobacterium Oscillatoria boryana BDU 92181, Enzyme and Microbial Technology, 29 (2001) 246-251.

[158] D. Ryan, A. Gadd, J. Kavanagh, G.W. Barton, Integrated biorefinery wastewater design, Chemical engineering research & design : transactions of the Institution of Chemical Engineers., 87 (2009) 1261.

[159] E.A. Vik, D.A. Carlson, A.S. Eikum, E.T. Gjessing, Electrocoagulation of potable water, Water Research, 18 (1984) 1355-1360.

[160] F.L. Antisell, U.S. Patent 1313246, in, 1919.

[161] J.T. Harris, Patent 937210, in, 1909.

[162] F.B. Hinkson, U.S. Patent 820113, in, 1906.

[163] H. Korten, U.S. Patent 913827, in, 1909.

[164] J.D. Kynaston, U.S. Patent 1219333, in, 1917.

[165] J.A.M. Lacomme, U.S. Patent 672231, in, 1901.

[166] D.W. Moody, U.S. Patent 1183753, in, 1916.

[167] H. Parker, U.S. Patent 1069169 in, 1913.

[168] A.T. Stuart, U.S. Patent 1269128, in, 1918.

[169] G.D. Van Arsdale, U.S. Patent 1449462, in, 1923.

[170] M. Merriman, Elements of sanitary engineering, Bibliolife, 2008.

[171] P.P. Strokach, Perspectives for the use of anodic dissolving of metals in water treatment technology, Elektronnaya Obrabotka Materialov, (1975) 52-57.

[172] L. Fassina, Purification of tannery effluents, Journal of the American Leather Chemists Association, 33 (1938) 380.

[173] B.M. Matov, Application of electrolysis in coagulation and flotation, Izvestiya Vysshikh Uchebnykh Zavedenii, Pishchevaya Tekhnologiya, 2 (1967) 84-86.

[174] G.A. Archakova, Purification of wastewaters by an electrochemical method, Vodootvedenie Ochistka Vod, (1969) 82-90.

[175] E.R. Ramirez, Comparative physicochemical study of industrial wastewater treatment by electrolytic, disspersed air and dissolved air flotation technologies, Proceedings of the Industrial Waste Conference, (1980) 699-709.

[176] F.E. Elmore, A process for separating certain constituents of subdivided ores and like substances, and apparatus therfor. B. P. Office. United Kingdom. British Patent 13578 (1905). , in, 1904.

[177] I.V. Gerasimov, Ivleva, M. G., Malyavko, M., Electroflotation purification of emulsified sewage from oil refineries, Novosti Neft. i Gaz. Tekhn., Neftepererabotka i Neftekhim, 12 (1962) 18-20.

[178] S. Zodi, O. Potier, F. Lapicque, J.P. Leclerc, Treatment of the industrial wastewaters by electrocoagulation: Optimization of coupled electrochemical and sedimentation processes, Desalination, 261 (2010) 186-190.

[179] E. Terrazas, A. Vazquez, R. Briones, I. Lazaro, I. Rodriguez, EC treatment for reuse of tissue paper wastewater: Aspects that affect energy consumption, Journal of Hazardous Materials, 181 (2010) 809-816.

[180] M. Ben Sasson, A. Adin, Fouling mitigation by iron-based electroflocculation in microfiltration: Mechanisms and energy minimization, Water Research, 44 (2010) 3973-3981.

[181] X.Y. Zheng, H.N. Kong, D.Y. Wu, C. Wang, Y. Li, H.R. Ye, Phosphate removal from source separated urine by electrocoagulation using iron plate electrodes, Water Science and Technology, 60 (2009) 2929-2938.

[182] P. Canizares, F. Martinez, C. Jimenez, J. Lobato, M.A. Rodrigo, Comparison of the aluminum speciation in chemical and electrochemical dosing processes, Ind. Eng. Chem. Res., 45 (2006) 8749-8756.

[183] P. Canizares, F. Martinez, M. Carmona, J. Lobato, M.A. Rodrigo, Continuous electrocoagulation of synthetic colloid-polluted wastes, Industrial and Engineering Chemistry Research, 44 (2005) 8171-8177.

[184] P. Canizares, M. Carmona, J. Lobato, F. Martinez, M.A. Rodrigo, Electrodissolution of aluminum electrodes in electrocoagulation processes, Ind. Eng. Chem. Res., 44 (2005) 4178-4185.
[185] P. Canizares, J. Lobato, J. Garcia-Gomez, M.A. Rodrigo, Combined adsorption and electrochemical processes for the treatment of acidic aqueous phenol wastes, Journal of Applied Electrochemistry, 34 (2004) 111-117.
[186] P. Canizares, J. Garcia-Gomez, J. Lobato, M.A. Rodrigo, Modeling of Wastewater Electro-oxidation Processes Part I. General Description and Application to Inactive Electrodes, Industrial and Engineering Chemistry Research, 43 (2004) 1915-1922.
[187] P. Canizares, J. Garcia-Gomez, J. Lobato, M.A. Rodrigo, Modeling of wastewater electro-oxidation processes part II. Application to active electrodes, Ind. Eng. Chem. Res., 43 (2004) 1923-1931.
[188] P.K. Holt, G.W. Barton, M. Wark, C.A. Mitchell, A quantitative comparison between chemical dosing and electrocoagulation, Colloids and Surfaces A: Physicochemical and Engineering Aspects, 211 (2002) 233-248.
[189] S. Ibeid, M. Elektorowicz, J.A. Oleszkiewicz, Modification of activated sludge properties caused by application of continuous and intermittent current, Water Research, 47 (2013) 903-910.
[190] V.Y. Baklan, I.P. Kolesnikova, Influence of electrode material on the electrocoagulation, Journal of Aerosol Science, 27, Supplement 1 (1996) S209-S210.
[191] M. Kobya, H. Hiz, E. Senturk, C. Aydiner, E. Demirbas, Treatment of potato chips manufacturing wastewater by electrocoagulation, Desalination, 190 (2006) 201-211.
[192] M.Y.A. Mollah, R. Schennach, J.R. Parga, D.L. Cocke, Electrocoagulation (EC) - Science and applications, Journal of Hazardous Materials, 84 (2001) 29-41.
[193] G. Chen, Electrochemical technologies in wastewater treatment, Separation and Purification Technology, 38 (2004) 11-41.
[194] O. Larue, E. Vorobiev, C. Vu, B. Durand, Electrocoagulation and coagulation by iron of latex particles in aqueous suspensions, Separation and Purification Technology, 31 (2003) 177-192.
[195] G. Mouedhen, M. Feki, M.D.P. Wery, H.F. Ayedi, Behavior of aluminum electrodes in electrocoagulation process, Journal of Hazardous Materials, 150 (2008) 124-135.
[196] M. Mechelhoff, G.H. Kelsall, N.J.D. Graham, Aluminium electrochemistry in electrocoagulation reactors, in: 213th ECS Meeting Abstracts 2008, May 18, 2008 - May 22, 2008, Electrochemical Society Inc., Phoenix, AZ, United states, 2008, pp. 875.
[197] H.K. Shon, S. Phuntsho, S. Vigneswaran, J. Kandasamy, L.D. Nghiem, G.J. Kim, J.B. Kim, J.H. Kim, Preparation of titanium dioxide nanoparticles from electrocoagulated sludge using sacrificial titanium electrodes, Environmental Science and Technology, 44 (2010) 5553-5557.
[198] P. Canizares, F. Martinez, C. Saez, M.A. Rodrigo, The electrocoagulation, an alternative to the conventional coagulation process of wastewater, Afinidad, 66 (2009) 27-37.
[199] C.J. Izquierdo, P. Canizares, M.A. Rodrigo, J.P. Leclerc, G. Valentin, F. Lapicque, Effect of the nature of the supporting electrolyte on the treatment of soluble oils by electrocoagulation, Desalination, 255 (2010) 15-20.
[200] M. Aoudjehane, M. Rezzouk, A. Kellil, Y. Aurelle, C. Guigui, Comparative study of electrocoagulation and coagulation-flocculation effects on the destabilization of cutting oil emulsion

Etude comparative de l'electrocoagulation et de la coagulation floculation vis-a-vis de la destabilisation d'une emulsion d'huile de coupe, Revue des Sciences de l'Eau, 23 (2010) 17-30.
[201] J.L. Trompette, H. Vergnes, On the crucial influence of some supporting electrolytes during electrocoagulation in the presence of aluminum electrodes, Journal of Hazardous Materials, 163 (2009) 1282-1288.
[202] M. Tir, N. Moulai-Mostefa, Electrochemical treatment of metal working emulsions using Box-Behnken design, Desalin. Water Treat., 7 (2009) 214-219.
[203] A.G. Merma, L.V. Gonzales, R.M. Rangel, R.J. de Carvalho, M.L. Torem, Fundamental aspects of electrocoagulation: removal of oily wastewaters from the mining industry, in: EPD Congress 2009, 15-19 Feb. 2009, Metals & Materials Society (TMS), Warrendale, PA, USA, 2009, pp. 963-968.

[204] E. GilPavas, K. Molina-Tirado, M.A. Gomez-Garcia, Treatment of automotive industry oily wastewater by electrocoagulation: Statistical optimization of the operational parameters, in, IWA Publishing, 12 Caxton Street, London, SW1H 0QS, United Kingdom, 2009, pp. 2581-2588.

[205] Y.O.A. Fouad, A.H. Konsowa, H.A. Farag, G.H. Sedahmed, Performance of an electrocoagulation cell with horizontally oriented electrodes in oil separation compared to a cell with vertical electrodes, Chemical Engineering Journal, 145 (2009) 436-440.

[206] S. Yoo, J.S. Hsieh, Advanced water recycling through electrochemical treatment of effluent from dissolved air flotation unit of food processing industry, Water Science and Technology, 61 (2010) 181-190.

[207] W.L. Chou, C.T. Wang, W.C. Chang, S.Y. Chang, Adsorption treatment of oxide chemical mechanical polishing wastewater from a semiconductor manufacturing plant by electrocoagulation, Journal of Hazardous Materials, 180 (2010) 217-224.

[208] J.H. Cho, J.E. Lee, C.S. Ra, Effects of electric voltage and sodium chloride level on electrolysis of swine wastewater, Journal of Hazardous Materials, 180 (2010) 535-541.

[209] P. Canizares, F. Martinez, M.A. Rodrigo, C. Jimenez, C. Saez, J. Lobato, Modelling of wastewater electrocoagulation processes Part I. General description and application to kaolin-polluted wastewaters, Separation and Purification Technology, 60 (2008) 155-161.

[210] P. Canizares, F. Martinez, M.A. Rodrigo, C. Jimenez, C. Saez, J. Lobato, Modelling of wastewater electrocoagulation processes Part II: Application to dye-polluted wastewaters and oil-in-water emulsions, Separation and Purification Technology, 60 (2008) 147-154.

[211] J. Nouri, A.H. Mahvi, E. Bazrafshan, Application of Electrocoagulation Process in Removal of Zinc and Copper From Aqueous Solutions by Aluminum Electrodes, Int. J. Environ. Res., 4 (2010) 201-208.

[212] S.S. Gao, M.A. Du, J.Y. Tian, J.Y. Yang, J.X. Yang, F. Ma, J. Nan, Effects of chloride ions on electro-coagulation-flotation process with aluminum electrodes for algae removal, Journal of Hazardous Materials, 182 (2010) 827-834.

[213] P.K. Holt, G.W. Barton, C.A. Mitchell, Deciphering the science behind electrocoagulation to remove suspended clay particles from water, Water Science and Technology, 50 (2004) 177-184.

[214] P.K. Holt, G.W. Barton, M. Wark, C.A. Mitchell, A quantitative comparison between chemical dosing and electrocoagulation, Colloids and Surfaces A: Physicochemical and Engineering Aspects, 211 (2002) 233-248.

[215] P.K. Holt, G.W. Barton, C.A. Mitchell, I.P.C.I.P. Iwa Programme Committee, Committee, Mathematical analysis of a batch electrocoagulation reactor, in: 3rd World Water Congress: Drinking Water Treatment, I W a Publishing, London, 2002, pp. 65-71.

[216] X.C. Ruan, M.Y. Liu, Q.F. Zeng, Y.H. Ding, Degradation and decolorization of reactive red X-3B aqueous solution by ozone integrated with internal micro-electrolysis, Separation and Purification Technology, 74 (2010) 195-201.

[217] C. Phalakornkule, S. Polgumhang, W. Tongdaung, B. Karakat, T. Nuyut, Electrocoagulation of blue reactive, red disperse and mixed dyes, and application in treating textile effluent, Journal of Environmental Management, 91 (2010) 918-926.

[218] M.Y.A. Mollah, J.A.G. Gomes, K.K. Das, D.L. Cocke, Electrochemical treatment of Orange II dye solution-Use of aluminum sacrificial electrodes and floc characterization, Journal of Hazardous Materials, 174 (2010) 851-858.

[219] A.I. Gladkij, E.Y. Sokol, M.Y. Gapunin, Estimation of batch and continuous electrocoagulants' operation efficiency, Khimiya i Tekhnologiya Vody, 13 (1991) 745-748.

[220] S.P. Novikova, T.L. Shkorbatova, E.Y. Sokol, G.V. Sleptsov, Electrochemical treatment of spent wash solutions at machine plants, Soviet Journal of Water Chemistry and Technology (English Translation of Khimiya i Tekhnologiya Vo, 9 (1987) 87-91.

[221] R.V. Drondina, T.M. Khmel'nitskaya, P.P. Strokach, A.M. Romanov, V.M. Bobrinskii, Combination methods of purifying underground waters polluted with Selenium and Strontium, Soviet surface engineering and applied electrochemistry, (1985) 84-86.

[222] R.V. Drondina, T.M. Khmel'nitskaya, P.P. Strokach, A.M. Romanov, Anode dissolution of iron in ground waters containing strontium, Soviet Journal of Water Chemistry and Technology (English Translation of Khimiya i Tekhnologiya Vo, 7 (1985) 67-70.

[223] I.A. Zolotukhin, V.A. Vasev, A.L. Lukin, Electroflotation purification of the pit waters of the Kuzbass, Soviet Journal of Water Chemistry and Technology (English Translation of Khimiya i Tekhnologiya Vo, 5 (1983) 85-89.

[224] A.N. Volkova, L.V. Ivanova, V.I. Yakovlev, Removal of protein and of suspended and ether-soluble substances from wastewaters by electrocoagulation, Journal of Applied Chemistry of the Ussr, 54 (1981) 970-972.

[225] V.N. Shilov, Polarization interaction and electrocoagulation1. Expression of the force of disperce interaction in an electric-field by away of an induced dipole-moment, Colloid Journal of the Ussr, 42 (1980) 963-967.

[226] A.F. Morozov, G.I. Konshina, V.P. Morozova, Electroflotation extraction of suspentions from waste thickeners, Soviet Mining Science Ussr, 16 (1980) 189-191.

[227] V.V. Vershinina, I.E. Rogovets, Purification of fluorine-containing effluent by electrochemical methods, 35 (1978) 511-512.

[228] V.D. Osipenko, P.I. Pogorelyi, Electrocoagulation neutralization of chromium containing effluent, Metallurgist, 21 (1977) 628-630.

[229] R.K. Alekseeva, A.P. Seligerskaya, Purifying Industrial Waste Water at the Severonikel' Combine, Tsvetnye Metally, (1977) 53-54.

[230] B.K. Korbahti, K. Artut, Electrochemical oil/water demulsification and purification of bilge water using Pt/Ir electrodes, Desalination, 258 (2010) 219-228.

[231] F. Zaviska, P. Drogui, J.F. Blais, G. Mercier, In situ active chlorine generation for the treatment of dye-containing effluents, Journal of Applied Electrochemistry, 39 (2009) 2397-2408.

[232] D. Rajkumar, B.J. Song, J.G. Kim, Electrochemical degradation of Reactive Blue 19 in chloride medium for the treatment of textile dyeing wastewater with identification of intermediate compounds, Dyes Pigment., 72 (2007) 1-7.

[233] S. Raghu, C.W. Lee, S. Chellammal, S. Palanichamy, C.A. Basha, Evaluation of electrochemical oxidation techniques for degradation of dye effluents-A comparative approach, Journal of Hazardous Materials, 171 (2009) 748-754.

[234] N.A. Maslennikov, Zhdanova, T. M., Concentration of excess activated sludge by electroflotation, Sbornik Nauchnih Rabot Akademii Kommunalnogo Khozyaystva, 6 (1961) 230-256.

[235] M. Belkacem, M. Khodir, S. Abdelkrim, Treatment characteristics of textile wastewater and removal of heavy metals using the electroflotation technique, Desalination, 228 (2008) 245-254.

[236] L. Ben Mansour, S. Chalbi, Removal of oil from oil/water emulsions using electroflotation process, Journal of Applied Electrochemistry, 36 (2006) 577-581.

[237] L. Ben Mansour, S. Chalbi, I. Kesentini, Experimental study of hydrodynamic and bubble size distributions in electroflotation process, Indian Journal of Chemical Technology, 14 (2007) 253-257.

[238] F.N. Crespilho, C.G. Santana, O.O. Rezende, Brazilian industrial coconut wastewater treatment by electroflotation, Quim. Nova, 27 (2004) 387-392.

[239] M. Kotti, N. Dammak, I. Ksentini, L. Ben Mansour, Effects of impurities on oxygen transfer rate in the electroflotation process, Indian Journal of Chemical Technology, 16 (2009) 513-518.

[240] S.E. Burns, S. Yiacoumi, C. Tsouris, Microbubble generation for environmental and industrial separations, Separation and Purification Technology, 11 (1997) 221-232.

[241] C. Jimenez, B. Talavera, C. Saez, P. Canizares, M.A. Rodrigo, Study of the production of hydrogen bubbles at low current densities for electroflotation processes, Journal of Chemical Technology and Biotechnology, 85 (2010) 1368-1373.

[242] Y. Fukui, S. Yuu, Removal of colloidal particles in electroflotation, Aiche Journal, 31 (1985) 201-208.

[243] X.M. Chen, G.H. Chen, P.L. Yue, Novel electrode system for electroflotation of wastewater, Environ. Sci. Technol., 36 (2002) 778-783.

[244] M. Boroski, A.C. Rodrigues, J.C. Garcia, L.C. Sampaio, J. Nozaki, N. Hioka, Combined electrocoagulation and TiO2 photoassisted treatment applied to wastewater effluents from pharmaceutical and cosmetic industries, Journal of Hazardous Materials, 162 (2009) 448-454.
[245] M. Boroski, A.C. Rodrigues, J.C. Garcia, A.P. Gerola, J. Nozaki, N. Hioka, The effect of operational parameters on electrocoagulation-flotation process followed by photocatalysis applied to the decontamination of water effluents from cellulose and paper factories, Journal of Hazardous Materials, 160 (2008) 135-141.
[246] S. Khoufi, F. Aloui, S. Sayadi, Treatment of olive oil mill wastewater by combined process electro-Fenton reaction and anaerobic digestion, Water Research, 40 (2006) 2007-2016.
[247] A.P. Buzzini, L.J. Patrizzi, A.J. Motheo, E.C. Pires, Preliminary evaluation of the electrochemical and chemical coagulation processes in the post-treatment of effluent from an upflow anaerobic sludge blanket (UASB) reactor, Journal of environmental management, 85 (2007) 847-857.
[248] X.H. Lei, T. Maekawa, Electrochemical treatment of anaerobic digestion effluent using a Ti/Pt-IrO2 electrode, Bioresource Technology, 98 (2007) 3521-3525.
[249] K. Yetilmezsoy, F. Ilhan, Z. Sapci-Zengin, S. Sakar, M.T. Gonullu, Decolorization and COD reduction of UASB pretreated poultry manure wastewater by electrocoagulation process: A post-treatment study, Journal of Hazardous Materials, 162 (2009) 120-132.
[250] A.M. Deshpande, S. Satyanarayan, S. Ramakant, Treatment of high-strength pharmaceutical wastewater by electrocoagulation combined with anaerobic process, in, IWA Publishing, 12 Caxton Street, London, SW1H 0QS, United Kingdom, 2010, pp. 463-472.
[251] J.A. Siles, M.A. Martin, A.F. Chica, A. Martin, Anaerobic co-digestion of glycerol and wastewater derived from biodiesel manufacturing, Bioresource Technology, 101 (2010) 6315-6321.
[252] G. Collins, S. McHugh, S. Connaughton, A.-M. Enright, A. Kearney, C. Scully, T. Mahony, P. Madden, V. O'Flaherty, New low-temperature applications of anaerobic wastewater treatment, Journal of Environmental Science and Health - Part A Toxic/Hazardous Substances and Environmental Engineering, 41 (2006) 881-895.
[253] S. Connaughton, G. Collins, V. O'Flaherty, Psychrophilic and mesophilic anaerobic digestion of brewery effluent: A comparative study, Water Research, 40 (2006) 2503-2510.
[254] S. Connaughton, G. Collins, V. O'Flaherty, Development of microbial community structure and actvity in a high-rate anaerobic bioreactor at 18C, Water Research, 40 (2006) 1009-1017.
[255] B.-Q. Liao, J. Kraemer, D. Bagley, Anaerobic Membrane Bioreactors: Applications and Research Directions, Critical Reviews in Environmental Science and Technology, 36 (2006) 489-530.
[256] M.F. Demirbas, M. Balat, Progress and recent trends in biogas processing, International Journal of Green Energy, 6 (2009) 117-142.
[257] H. Zhu, A. Stadnyk, M. Beland, P. Seto, Co-production of hydrogen and methane from potato waste using a two-stage anaerobic digestion process, Bioresource Technology, 99 (2008) 5078-5084.
[258] J.P. Steyer, O. Bernard, D.J. Batstone, I. Angelidaki, Lessons learnt from 15 years of ICA in anaerobic digesters, Water Science and Technology, 53 (2006) 25-33.
[259] M. Kanai, V. Ferre, S. Wakahara, T. Yamamoto, M. Moro, A novel combination of methane fermentation and MBR Kubota Submerged Anaerobic Membrane Bioreactor process, Desalination., 48 (2010) 964.
[260] S.H. Baek, K.R. Pagilla, Aerobic and anaerobic membrane bioreactors for municipal wastewater treatment, Water environment research : a research publication of the Water Environment Federation, 78 (2006) 133-140.
[261] A. Pierkiel, J. Lanting, Membrane-coupled anaerobic digestion of municipal sewage sludge, Water Science and Technology, 52 (2005) 253-258.
[262] S. Christian, S. Grant, P. McCarthy, D. Wilson, D. Mills, The first two years of full-scale anaerobic membrane bioreactor (AnMBR) operation treating high-strength industrial wastewater, Water Practice and Technology, 6 (2011).
[263] W.J. Gao, K.T. Leung, W.S. Qin, B.Q. Liao, Effects of temperature and temperature shock on the performance and microbial community structure of a submerged anaerobic membrane bioreactor, Bioresource Technology, 102 (2011) 8733-8740.

[264] M. Kanai, V. Ferre, S. Wakahara, T. Yamamoto, M. Moro, A novel combination of methane fermentation and MBR - Kubota Submerged Anaerobic Membrane Bioreactor process, Desalination, 250 (2010) 964-967.

[265] B.Q. Liao, K. Xie, H.J. Lin, D. Bertoldo, Treatment of kraft evaporator condensate using a thermophilic submerged anaerobic membrane bioreactor, Water Science and Technology, 61 (2010) 2177-2183.

[266] S.M. Lee, J.Y. Jung, Y.C. Chung, Novel method for enhancing permeate flux of submerged membrane system in two-phase anaerobic reactor, Water Research, 35 (2001) 471-477.

[267] G. Antonopoulou, K. Stamatelatou, N. Venetsaneas, M. Kornaros, G. Lyberatos, Biohydrogen and methane production from cheese whey in a two-stage anaerobic process, Industrial and Engineering Chemistry Research, 47 (2008) 5227-5233.

[268] B. Rincon, R. Borja, M.A. Martin, A. Martin, Kinetic study of the methanogenic step of a two-stage anaerobic digestion process treating olive mill solid residue, Chemical Engineering Journal, 160 (2010) 215-219.

[269] M.J. Park, J.H. Jo, D. Park, D.S. Lee, J.M. Park, Comprehensive study on a two-stage anaerobic digestion process for the sequential production of hydrogen and methane from cost-effective molasses, International Journal of Hydrogen Energy, 35 (2010) 6194-6202.

[270] S.G. Shin, G. Han, J. Lim, C. Lee, S. Hwang, A comprehensive microbial insight into two-stage anaerobic digestion of food waste-recycling wastewater, Water Research, 44 (2010) 4838-4849.

[271] A. American Public Health, A.D. Eaton, A. American Water Works, F. Water Environment, Standard methods for the examination of water and wastewater, APHA-AWWA-WEF, Washington, D.C., 2005.

[272] S. Ibeid, M. Elektorowicz, J.A. Oleszkiewicz, Electro-conditioning of activated sludge in a membrane electro-bioreactor for improved dewatering and reduced membrane fouling, Journal of Membrane Science, 494 (2015) 136-142.

[273] S.W. Hasan, M. Elektorowicz, J.A. Oleszkiewicz, Start-up period investigation of pilot-scale submerged membrane electro-bioreactor (SMEBR) treating raw municipal wastewater, Chemosphere, 97 (2014) 71-77.

[274] S. Ibeid, M. Elektorowicz, J.A. Oleszkiewicz, Novel electrokinetic approach reduces membrane fouling, Water Research, 47 (2013) 6358-6366.

[275] S. Philips, K. Rabaey, W. Verstraete, Impact of iron salts on activated sludge and interaction with nitrite or nitrate, Bioresource Technology, 88 (2003) 229-239.

[276] N. Parveen, S. Ahmad, G.G.H.A. Shadab, Iron induced genotoxicity: attenuation by vitamin C and its optimization, Interdisciplinary Toxicology, 7 (2014) 154-158.

[277] E. Farno, J.C. Baudez, R. Parthasarathy, N. Eshtiaghi, Impact of temperature and duration of thermal treatment on different concentrations of anaerobic digested sludge: Kinetic similarity of organic matter solubilisation and sludge rheology, Chemical Engineering Journal, 273 (2015) 534-542.

[278] J. Kozeny, Über kapillare leitung des wassers im boden, Akad. Wiss. Wien., 136 (1927) 271-306.

[279] P.A. Dias, T. Dunkel, D.A.S. Fajado, E. De León Gallegos, M. Denecke, P. Wiedemann, F.K. Schneider, H. Suhr, E.d.L. Gallegos, Image processing for identification and quantification of filamentous bacteria in in situ acquired images, BioMedical Engineering OnLine, 15 (2016) 1-19.

[280] A.S. Ziegler, S.J. McIlroy, P. Larsen, M. Albertsen, A.A. Hansen, N. Heinen, P.H. Nielsen, Dynamics of the Fouling Layer Microbial Community in a Membrane Bioreactor, PLoS ONE, 11 (2016) 1-14.

[281] K. Bani-Melhem, Z. Al-Qodah, M. Al-Shannag, A. Qasaimeh, M. Rasool Qtaishat, M. Alkasrawi, On the performance of real grey water treatment using a submerged membrane bioreactor system, Journal of Membrane Science, 476 (2015) 40-49.

[282] M. Lousada-Ferreira, J.B. van Lier, J.H.J.M. van der Graaf, Impact of suspended solids concentration on sludge filterability in full-scale membrane bioreactors, Journal of Membrane Science, 476 (2015) 68-75.

[283] A.S. Koparal, Y.S. Yildiz, B. Keskinler, N. Demircioglu, Effect of initial pH on the removal of humic substances from wastewater by electrocoagulation, Separation and Purification Technology, 59 (2008) 175-182.

[284] C.F. Baes, R.E. Mesmer, The hydrolysis of cations, Wiley, 1976.

[285] A.J. Meixner, Reaction of Aluminum with Water and Sodium Hydroxide, in, 2005.

[286] M. Citeau, J. Olivier, A. Mahmoud, J. Vaxelaire, O. Larue, E. Vorobiev, Pressurised electro-osmotic dewatering of activated and anaerobically digested sludges: Electrical variables analysis, Water Research, 46 (2012) 4405-4416.

[287] M. Citeau, O. Larue, E. Vorobiev, Influence of salt, pH and polyelectrolyte on the pressure electro-dewatering of sewage sludge, Water Research, 45 (2011) 2167-2180.

[288] Y.-l. Luo, Z.-h. Yang, Z.-y. Xu, L.-j. Zhou, G.-m. Zeng, J. Huang, Y. Xiao, L.-k. Wang, Effect of trace amounts of polyacrylamide (PAM) on long-term performance of activated sludge, Journal of Hazardous Materials, 189 (2011) 69-75.

[289] X. Yan, R. Gerards, L. Virens, I. Vankelecom, Hollow fiber membrane fouling and cleaning in a membrane bioreactor for molasses wastewater treatment, Desalin. Water Treat., 18 (2010) 192-197.

[290] E. Filloux, W. Gernjak, H. Gallard, J.P. Croue, Investigating the relative contribution of colloidal and soluble fractions of secondary effluent organic matter to the irreversible fouling of MF and UF hollow fibre membranes, Separation and Purification Technology, 170 (2016) 109-115.

[291] Y. Xiong, M. Harb, P.-Y. Hong, Characterization of biofoulants illustrates different membrane fouling mechanisms for aerobic and anaerobic membrane bioreactors, Separation and Purification Technology, 157 (2016) 192-202.

[292] J. Bartacek, J. Zabranska, P.N.L. Lens, Developments and constraints in fermentative hydrogen production, Biofuels, Bioproducts and Biorefining, 1 (2007) 201-214.

[293] J. Shayegan, F. Ghavipanjeh, P. Mirjafari, The effect of influent COD and upward flow velocity on the behaviour of sulphate-reducing bacteria, Process Biochemistry, 40 (2005) 2305-2310.

[294] D. Jeison, C.M. Plugge, A. Pereira, J.B.v. Lier, Effects of the acidogenic biomass on the performance of an anaerobic membrane bioreactor for wastewater treatment, Bioresource Technology, 100 (2009) 1951-1956.

[295] Y. Zhao, C. Feng, Q. Wang, Y. Yang, Z. Zhang, N. Sugiura, Nitrate removal from groundwater by cooperating heterotrophic with autotrophic denitrification in a biofilm–electrode reactor, Journal of Hazardous Materials, 192 (2011) 1033-1039.

Appendices

Appendices provide supplementary information to the main thesis. Appendix A provides information on analytical methods of analyses. Appendix B contains supplementary information generated during the SRM in Phase IV.

Appendix A: Analytical Methods

This appendix was prepared to provide a detailed description of the approach and calculations for each of the analytical assessments. The appendix was separated into sections, each pertaining specifically to physical-chemical and biological parameters. A general description of analytical methods is presented below.

Physical and Chemical Parameters

Methods for pH, Oxidation-Reduction Potential (ORP), and Temperature Analyses

The values pH, ORP and temperature were measured using a pH meter model 215 glass electrode (Denver Instrument, USA). Calibration of pH, and DO meters was conducted once a day before analyses at room temperature (20 ± 1 °C).

Total Suspended Solids and Volatile Suspended Solids

1.) Total Suspended Solids.

1.1. On a clean piece of paper filter pads were laid out for numbering.

1.2. A Sharpie permanent very fine point black marker was used to sequentially number each pad outside edge with a unique label.

1.3. After pads have been labeled, they were placed in prewashed with distilled water Pyrex dishes and dried overnight at 105° C in an oven for 30 min.

1.4. When ready to weigh, pads were removed from oven and placed into a desiccator to cool to room temperature.

1.5. Turn on analytical balance and checked calibration.

1.6. After pads cooled to room temperature, pads were weighted individually on a balance and data was entered into respective spread sheets and stored in labeled boxes for future use.

1.7. When ready to sample, numbered pad were placed onto filtering apparatus.

1.8. A known volume of sample was filtered through the filter pad.

1.9. Pads were washed well with deionized water to rinse down filter tower and remove any residues from the pads.

1.10. Pads were folded in half, sample side in and placed into a labeled foil pouch and then placed in in a freezer to be stored at -20° C. When ready to analyze, opened pouch were placed with sample in 105° C drying oven overnight.

1.11. Steps 1.4. – 1.7 were repeated for all samples.

1.12. TSS value was calculated according to Formula A.1:

$$TSS \left(\frac{mg}{L}\right) = \frac{(Wpost(g) - Wpre(g)) \times 1000}{Sample\ Volume\ (L)} \tag{A.1}$$

Volatile Suspended Solids.

2.1. Pads were placed straight from box into a crucible and were combusted at 550° C in a muffle furnace for 1.5 hours.

2.2. Pads were placed to an oven at 105° C for storage until ready to use.

2.3. Steps 1.4 – 1.7 were reproduced for all the samples.

2.4. After pads cooled to room temperature, pads were weighted individually on a balance and data was entered into respective spread sheets and stored in labeled Petri dishes for future use.
2.5. When ready to sample, numbered pad were placed onto filtering apparatus.

2.6. Once TSS values were determined pads were placed into numbered porcelain crucibles and.

2.7. Samples were combusted at 550° C in a muffle furnace for 1.5 hours.

2.8. Steps 1.4 – 1.7 were repeated for all samples.

2.9. Calculate VVS according to Formula A.2:

$$VSS \left(\frac{mg}{L}\right) = \frac{(Wpost(g) - Wcombust(g)) \times 1000}{Sample\ Volume\ (L)} \tag{A.2}$$

Procedure for Measuring Specific Resistance to Filtration

100 mL of sludge were withdrawn from the elector-bioreactor for the specific resistance to filtration tests. The SRF measurements were conducted every 10 days during the entire experiment according to a procedure described in Appendix A.

Figure A.1 depicts the Buchner funnel apparatus used for the determination of the SRF. Ashless filter papers (Cat. No. 1440-110, Fisher Scientific, Canada) were used to determine the SRF. 100 mL sample of the mixed liquor suspension was withdrawn for each SRF test. The method of analysis was conducted as follows:
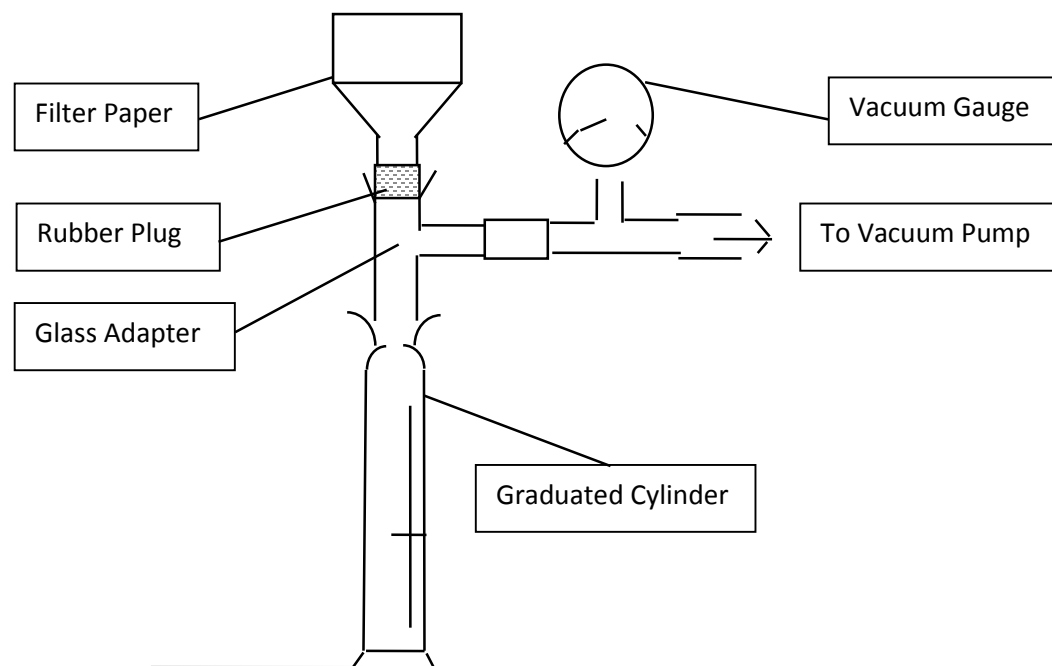
Figure A.1. Buchner funnel test apparatus used for the determination of the SRF

The pressure drop (ΔP) across the cake in the Buchner funnel can be calculated as:

$$\Delta P = (R_c + R_m)\mu v \qquad (A.3)$$

Where:

R_c is a resistance term for the cake

R_m is a resistance term for the filter

μ = viscosity of the filtrate

v = face velocity of filtrate

R_c is a function of the sludge physical properties and the cake thickness and hence R_c can be calculated as:

$R_c = \xi m_c$

where: ξ = specific cake resistance

   m_c = a measure of the thickness of the accumulated cake = $w_s V/A$

where: w_s = mass of solids per volume of sludge

   V = volume of filtrate produced at time "t"

   A = surface area of filter

In the Buchner funnel test the face velocity at time "t" is equal to:

$$v = \frac{dV}{dt} \times \frac{1}{A} \tag{A.4}$$

Substituting for v and R_c and re-arranging, we see that:

$$\frac{dt}{dV} = \left(\frac{\xi w_s V}{A} + R_m \right) \frac{\mu}{A \Delta P} \tag{A.5}$$

Integration between (0,0) and (t,V) gives:

$$\frac{t}{V} = \frac{\mu \xi w_s}{2 A^2 \Delta P} V + \frac{\mu R_m}{A \Delta P} \tag{A.6}$$

Therefore, the constant pressure filtration produces a linear plot of t/V vs V where the slope and intercept can be used to determine the specific cake resistance ξ and the resistance Rm of the filtering medium.

Procedure for Volume Measurement:

1. Samples of digested sludge were obtained from the reactor.

2. Concentration of total solids in the sludge was measure according to process described in the section MLSS/MLVSS measurement.

3. The Buchner funnel apparatus was arranged as shown in Figure A.1. The area of the funnel, the area of the filter paper and that of the woven wire drainage base was recorded.

4. For each sample the filter paper and crucible to be used in drying the cake sample were weighted.

5. The filter paper was sealed by moistening it before placing it in the funnel, then the vacuum was adjusted to 50 kPa.

6. 100 ml of sludge was to the Buchner funnel.

7. Vacuum was applied at zero time and the filtrate volume was recorded at preselected gradually increasing time intervals starting with fifteen seconds. The manometer readings were recorded every five minutes. Monitoring was continuing until the vacuum broke or until almost all filtrate was collected.

8. The filter cake and paper were carefully removed from the funnel, placed in the crucible and weighted. The crucible and its contents were placed in the oven to dry at 105°C. The dried samples will be weighed once dry and the results reported. This value was used to determine the mass of solids deposited on the filter (W).

Analysis

1. The following values were recorded:

P – the pressure drop across the filter

A – the area of the active filter paper

2. The weight of cake solids per unit volume of filtrate was calculated, $w = W/V$. This value was the grams of dry sludge solids per unit of filtrate in gm/cm^3.

3. The filtration data with the calculation of t/V for the recorded t and V was calculated. t/V measured in seconds/millilitre.

4. t/V versus V was plotted and determined the slope (b) of the straight line which was best approximated the graphical relation.

5. The average specific resistance for each sample was calculated according to the formula A5:

$$\xi = \frac{2bPA^2}{uw} \text{ in sec}^2/\text{gram} \tag{A.7}$$

Procedure for COD Analysis

To analysis COD samples, the following procedure was followed:

1 - All the samples were filtered using 0.45 pm filter paper.

2- COD heater block was preheated to 150° Celsius.

3- The cap from a COD twist-cap vial was removed.

4- A 2.5 mL sample was added carefully to COD vial such that it formed a layer on top of reagents.

5- The twist cap was replaced.

6- The contents of the sealed vial were mixed by shaking.

7- Standards and blanks were processed exactly as the samples.

8- The twist-cap vial was placed in a COD heater block for 2 hours.

9- After 2 hours, the vial was removed from the heater block and allowed for cooling.

10-The suspended precipitate was allowed to settle and the outside of the vial was clean before taking the measurements.

11-As described by the manufacture, Method A was used for standard Range reagent (20-900 mgL^{-1} COD) or method B was used for low Range gent (5-150 mgL^{-1} COD).

(a) The wavelength of the spectrophotometer was set to 600 nm and using a procedural blank, zero the absorbance reading.

(b) Use the highest standard (up to 150 mgL^{-1} COD) to set spectrophotometer to zero absorbance at 440 nm.

12- The absorbance of each standard and sample on the spectrophotometer was read.

13-A graphic calibration curve was prepared by plotting the absorbance of the standards versus their known concentration.

14-The sample absorbance was compared to the graphic calibration curve to determine COD concentrations.

Procedure for Ammonia- Nitrogen (NH₃-N) Analysis

A 0.1 mL of sample was added to one AmVer™ Diluent regent test N tube for high range ammonia nitrogen. This presented the prepared sample.

A 0.1 mL of ammonia-free water was added to one AmVer™ Diluent regent test N tube for high range ammonia nitrogen. This presented the blank sample.

The contents of one ammonia salicylate regent powder pillow was added to each sample in step 1 and 2.

The contents of one ammonia cyanurate regent powder pillow was added to each sample in step 1 and 2.

The vials were caped tightly and shacked thoroughly to dissolve the powder.

The contents in each vial in the step 5 were left for 20- minute reaction period.

The vial of the blank sample was placed into the cell holder, and the Zero bottom was touched. The display showed 0.00 mgL^{-1} NH₃-N.

The vial of the sample was placed into the cell holder, and the Read bottom was touched. The display showed the concentration of NH₃-N in mgL^{-1}.

Procedure for Nitrate- Nitrogen (NO₃-N) Analysis

1- A 25 mL graduated mixing cylinder was filled with 15 ml of the sample.

2- The contents of one NitraVer 6 Reagent powder were added to the cylinder.

3- The cylinder was shaken vigorously for three minutes.

4- The contents in the previous step were left for a 2- minute reaction period.

5- A 10 mL of the sample from step 4 was poured into a clean round sample cell.

6- The contents of one NitraVer3 Reagent powder were added to the sample in step

5. This presented the prepared sample.

7- The sample in step 6 was shaken gently for 30 seconds. A pink color was developed when the nitrate was presented.

8- The contents in the step 6 were left for 15- minute reaction period.

9- When the reaction period finished, a second 10 mL of the original sample is filled in another clean sample cell. This presented the blank sample.

10-The blank sample was placed into the cell holder, and the Zero bottom was touched. The display showed 0.00 mgL^{-1} NO$_3$-N.

11-The prepared sample was placed into the cell holder, and the Read bottom was touched. The display showed the concentration of NO$_3$-N in mgL^{-1}.

Procedure for TP Analysis

1- A 25 mL graduated mixing cylinder was filled with 25 mL of the sample.

2- A 1 mL of Molybdate reagent was added to the sample in step 1 using a 1 –mL calibrated dropper.

3- A 1 mL of Amino Acid reagent solution was added to the contents in step 2 using a 1 -mL calibrated dropper.

4- The contents in step 3 were mixed for several times. This presented the prepared sample. A blue color was developed when the phosphate was presented.

5- The contents in step 4 were left for 10- minute reaction period.

6- During the reaction period, a 25 mL graduated mixing cylinder was filled with another 25 mL of the sample. This presented the blank sample.

7- When the reaction period done, the blank sample was placed into the cell holder and the Zero bottom was touched. The display showed 0.00 mgL^{-1} PO$_4$$^{3-}$.

8- The prepared sample was placed into the cell holder and the Read bottom was touched. The display showed the PO4^{3-} concentration as in mgL^{-1}.

Appendix B: Statistical Analysis SRM

This appendix provides additional description of calculations for COD, phosphorus and nitrogen removal efficiency design by SRM using Minitab® 17.1.0 software. The appendix was separated into sections, each dedicated to specifically to particular pollutant of interest. An output of software is presented below.

Prediction for COD Removal

```
Regression Equation in Uncoded Units

% COD = -51.9 + 20.91 pH + 6.13 CD + 1.38 MLVSS - 1.678 pH*pH + 0.0183 CD*CD
        + 0.473 MLVSS*MLVSS - 0.166 pH*CD + 0.743 pH*MLVSS - 0.6380 CD*MLVSS


Variable  Setting
pH              7
CD             15
MLVSS           8


    Fit    SE Fit         95% CI               95% PI
97.2475  0.500154  (95.9618, 98.5332)  (95.2836, 99.2114)


Variable  Setting
pH              7
CD           17.5
MLVSS         6.5


    Fit    SE Fit         95% CI               95% PI
94.9733  0.333436  (94.1162, 95.8305)  (93.2591, 96.6876)


Variable  Setting
pH              6
CD           17.5
MLVSS           8


    Fit    SE Fit         95% CI               95% PI
96.2563  0.500154  (94.9706, 97.5419)  (94.2923, 98.2202)


Variable  Setting
pH              7
CD             15
MLVSS           5


  Fit    SE Fit         95% CI               95% PI
87.75  0.500154  (86.4643, 89.0357)  (85.7861, 89.7139)


Variable  Setting
pH              8
CD             15
MLVSS         6.5
```

```
    Fit    SE Fit         95% CI            95% PI
89.5163  0.500154  (88.2306, 90.8019)  (87.5523, 91.4802)


Variable  Setting
pH              7
CD             20
MLVSS           8


  Fit     SE Fit         95% CI            95% PI
99.77   0.500154  (98.4843, 101.056)  (97.8061, 101.734)


Variable  Setting
pH              6
CD             15
MLVSS         6.5


    Fit    SE Fit         95% CI            95% PI
89.9963  0.500154  (88.7106, 91.2819)  (88.0323, 91.9602)


Variable  Setting
pH              7
CD           17.5
MLVSS         6.5


    Fit    SE Fit         95% CI            95% PI
94.9733  0.333436  (94.1162, 95.8305)  (93.2591, 96.6876)


Variable  Setting
pH              8
CD             20
MLVSS         6.5


    Fit    SE Fit         95% CI            95% PI
95.9938  0.500154  (94.7081, 97.2794)  (94.0298, 97.9577)


Variable  Setting
pH              8
CD           17.5
MLVSS           8


    Fit    SE Fit         95% CI            95% PI
97.1762  0.500154  (95.8906, 98.4619)  (95.2123, 99.1402)


Variable  Setting
pH              6
CD             20
MLVSS         6.5


    Fit    SE Fit         95% CI            95% PI
98.1338  0.500154  (96.8481, 99.4194)  (96.1698, 100.098)


Variable  Setting
pH              7
```

```
CD            17.5
MLVSS          6.5


    Fit    SE Fit        95% CI              95% PI
94.9733  0.333436  (94.1162, 95.8305)  (93.2591, 96.6876)


Variable  Setting
pH              6
CD           17.5
MLVSS           5


    Fit    SE Fit        95% CI              95% PI
93.7737  0.500154  (92.4881, 95.0594)  (91.8098, 95.7377)


Variable  Setting
pH              8
CD           17.5
MLVSS           5


    Fit    SE Fit        95% CI              95% PI
90.2338  0.500154  (88.9481, 91.5194)  (88.2698, 92.1977)


Variable  Setting
pH              7
CD             20
MLVSS           5


    Fit    SE Fit        95% CI              95% PI
99.8425  0.500154  (98.5568, 101.128)  (97.8786, 101.806)
```

Response Optimization: COD Removal

```
Parameters

Response  Goal      Lower  Target  Upper  Weight  Importance
% COD     Maximum   87.85  99.99              1            1


Variable Ranges

Variable  Values
pH        (6, 8)
CD        (15, 20)
MLVSS     (5, 8)


Solution

                                   % COD     Composite
Solution  pH        CD  MLVSS       Fit   Desirability
1         6.34343   20  5       100.554              1


Multiple Response Prediction

Variable  Setting
pH        6.34343
```

```
CD        20
MLVSS      5


Response     Fit  SE Fit       95% CI              95% PI
% COD     100.554   0.566  (99.098, 102.010)  (98.474, 102.633)
```

Prediction for TN Removal

```
Regression Equation in Uncoded Units

% TN = -123.3 + 34.0 pH + 6.60 CD + 5.56 MLVSS - 3.114 pH*pH - 0.097 CD*CD
       + 0.441 MLVSS*MLVSS + 0.411 pH*CD + 0.253 pH*MLVSS - 0.633 CD*MLVSS


Variable  Setting
pH             7
CD            15
MLVSS          8


    Fit    SE Fit        95% CI              95% PI
93.5508  1.51797  (89.6487, 97.4529)  (87.5903, 99.5113)


Variable  Setting
pH             7
CD          17.5
MLVSS        6.5


    Fit    SE Fit        95% CI              95% PI
92.7158  1.01198  (90.1145, 95.3172)  (87.5131, 97.9186)


Variable  Setting
pH             6
CD          17.5
MLVSS          8


    Fit    SE Fit        95% CI              95% PI
93.8962  1.51797  (89.9941, 97.7982)  (87.9357, 99.8567)


Variable  Setting
pH             7
CD            15
MLVSS          5


    Fit    SE Fit        95% CI              95% PI
82.8556  1.51797  (78.9536, 86.7577)  (76.8951, 88.8161)


Variable  Setting
pH             8
CD            15
MLVSS        6.5


    Fit    SE Fit        95% CI              95% PI
82.3599  1.51797  (78.4578, 86.2620)  (76.3994, 88.3204)
```

265

```
Variable  Setting
pH             7
CD            20
MLVSS          8


    Fit   SE Fit        95% CI             95% PI
98.5944  1.51797  (94.6923, 102.496)  (92.6339, 104.555)


Variable  Setting
pH             6
CD            15
MLVSS        6.5


    Fit   SE Fit        95% CI             95% PI
85.8337  1.51797  (81.9316, 89.7357)  (79.8732, 91.7942)


Variable  Setting
pH             7
CD          17.5
MLVSS        6.5


    Fit   SE Fit        95% CI             95% PI
92.7158  1.01198  (90.1145, 95.3172)  (87.5131, 97.9186)


Variable  Setting
pH             8
CD            20
MLVSS        6.5


    Fit   SE Fit        95% CI             95% PI
94.2107  1.51797  (90.3086, 98.1128)  (88.2502, 100.171)


Variable  Setting
pH             8
CD          17.5
MLVSS          8


    Fit   SE Fit        95% CI             95% PI
93.2393  1.51797  (89.3372, 97.1414)  (87.2788, 99.1998)


Variable  Setting
pH             6
CD            20
MLVSS        6.5


    Fit   SE Fit        95% CI             95% PI
93.5701  1.51797  (89.6680, 97.4722)  (87.6096, 99.5306)


Variable  Setting
pH             7
CD          17.5
MLVSS        6.5
```

```
    Fit   SE Fit         95% CI              95% PI
92.7158  1.01198  (90.1145, 95.3172)  (87.5131, 97.9186)


Variable  Setting
pH              6
CD           17.5
MLVSS           5


    Fit   SE Fit         95% CI              95% PI
88.7107  1.51797  (84.8086, 92.6128)  (82.7502, 94.6712)


Variable  Setting
pH              8
CD           17.5
MLVSS           5


    Fit   SE Fit         95% CI              95% PI
86.5345  1.51797  (82.6324, 90.4365)  (80.5739, 92.4950)


Variable  Setting
pH              7
CD             20
MLVSS           5


    Fit   SE Fit         95% CI              95% PI
97.3992  1.51797  (93.4971, 101.301)  (91.4387, 103.360)
```

Response Optimization: TN Removal

```
Parameters

Response  Goal     Lower  Target  Upper  Weight  Importance
% TN      Maximum  82.6   99.99             1            1


Variable Ranges

Variable  Values
pH        (6, 8)
CD        (15, 20)
MLVSS     (5, 8)


Solution

                              % TN     Composite
Solution  pH       CD  MLVSS   Fit    Desirability
1         7.11111  20  8     98.6337    0.922009


Multiple Response Prediction

Variable  Setting
pH        7.11111
CD        20
MLVSS     8
```

```
Response    Fit  SE Fit      95% CI            95% PI
% TN       98.63   1.52  (94.72, 102.55)  (92.67, 104.60)
```

Prediction for TP Removal

```
Regression Equation in Uncoded Units

% TP = 171.4 + 7.24 pH - 11.80 CD - 0.91 MLVSS - 0.401 pH*pH + 0.3798 CD*CD
       + 0.086 MLVSS*MLVSS - 0.117 pH*CD + 0.208 pH*MLVSS - 0.074 CD*MLVSS


Variable  Setting
pH              7
CD             15
MLVSS           8


   Fit    SE Fit       95% CI            95% PI
99.535  0.687953  (97.7666, 101.303)  (96.8337, 102.236)


Variable  Setting
pH              7
CD           17.5
MLVSS         6.5


 Fit    SE Fit        95% CI             95% PI
96.6  0.458636  (95.4210, 97.7790)  (94.2421, 98.9579)


Variable  Setting
pH              6
CD           17.5
MLVSS           8


   Fit    SE Fit       95% CI            95% PI
95.715  0.687953  (93.9466, 97.4834)  (93.0137, 98.4163)


Variable  Setting
pH              7
CD             15
MLVSS           5


   Fit    SE Fit       95% CI            95% PI
97.855  0.687953  (96.0866, 99.6234)  (95.1537, 100.556)


Variable  Setting
pH              8
CD             15
MLVSS         6.5


 Fit    SE Fit       95% CI            95% PI
99.32  0.687953  (97.5516, 101.088)  (96.6187, 102.021)


Variable  Setting
pH              7
```

```
CD               20
MLVSS             8


    Fit    SE Fit          95% CI              95% PI
99.925  0.687953  (98.1566, 101.693)  (97.2237, 102.626)


Variable  Setting
pH               6
CD              15
MLVSS          6.5


   Fit    SE Fit          95% CI              95% PI
96.88  0.687953  (95.1116, 98.6484)  (94.1787, 99.5813)


Variable  Setting
pH               7
CD            17.5
MLVSS          6.5


 Fit    SE Fit          95% CI              95% PI
96.6  0.458636  (95.4210, 97.7790)  (94.2421, 98.9579)


Variable  Setting
pH               8
CD              20
MLVSS          6.5


   Fit    SE Fit          95% CI              95% PI
99.68  0.687953  (97.9116, 101.448)  (96.9787, 102.381)


Variable  Setting
pH               8
CD            17.5
MLVSS             8


    Fit    SE Fit          95% CI              95% PI
98.195  0.687953  (96.4266, 99.9634)  (95.4937, 100.896)


Variable  Setting
pH               6
CD              20
MLVSS          6.5


   Fit    SE Fit          95% CI              95% PI
98.41  0.687953  (96.6416, 100.178)  (95.7087, 101.111)


Variable  Setting
pH               7
CD            17.5
MLVSS          6.5


 Fit    SE Fit          95% CI              95% PI
96.6  0.458636  (95.4210, 97.7790)  (94.2421, 98.9579)
```

```
Variable    Setting
pH               6
CD            17.5
MLVSS            5


   Fit    SE Fit         95% CI              95% PI
95.215  0.687953  (93.4466, 96.9834)  (92.5137, 97.9163)


Variable    Setting
pH               8
CD            17.5
MLVSS            5


   Fit    SE Fit         95% CI              95% PI
96.445  0.687953  (94.6766, 98.2134)  (93.7437, 99.1463)


Variable    Setting
pH               7
CD              20
MLVSS            5


   Fit    SE Fit         95% CI              95% PI
99.355  0.687953  (97.5866, 101.123)  (96.6537, 102.056)
```

Response Optimization: TP Removal

```
Parameters

Response  Goal      Lower   Target  Upper  Weight  Importance
% TP      Maximum   94.54   99.99            1          1


Variable Ranges

Variable  Values
pH        (6, 8)
CD        (15, 20)
MLVSS     (5, 8)


Solution

                            % TP      Composite
Solution  pH  CD  MLVSS     Fit  Desirability
1         8   15  8      100.666            1


Multiple Response Prediction

Variable  Setting
pH        8
CD        15
MLVSS     8


Response      Fit  SE Fit         95% CI              95% PI
% TP      100.666   0.939  (98.254, 103.079)  (97.506, 103.827)
```

Prediction for Discoloration

Regression Equation in Uncoded Units

% Color = 93.27 + 1.020 pH - 0.297 CD + 1.367 MLVSS - 0.0604 pH*pH + 0.02113 CD*CD
          - 0.0002 MLVSS*MLVSS + 0.0020 pH*CD - 0.0250 pH*MLVSS - 0.0627 CD*MLVSS

```
Variable  Setting
pH             7
CD            15
MLVSS          8
```

```
    Fit     SE Fit         95% CI              95% PI
99.9562  0.0882681  (99.7293, 100.183)  (99.6097, 100.303)
```

```
Variable  Setting
pH             7
CD          17.5
MLVSS        6.5
```

```
    Fit     SE Fit         95% CI              95% PI
99.5733  0.0588454  (99.4221, 99.7246)  (99.2708, 99.8759)
```

```
Variable  Setting
pH             6
CD          17.5
MLVSS          8
```

```
    Fit     SE Fit         95% CI              95% PI
99.6425  0.0882681  (99.4156, 99.8694)  (99.2959, 99.9891)
```

```
Variable  Setting
pH             7
CD            15
MLVSS          5
```

```
    Fit     SE Fit         95% CI              95% PI
99.2087  0.0882681  (98.9818, 99.4357)  (98.8622, 99.5553)
```

```
Variable  Setting
pH             8
CD            15
MLVSS        6.5
```

```
    Fit     SE Fit         95% CI              95% PI
99.5637  0.0882681  (99.3368, 99.7907)  (99.2172, 99.9103)
```

```
Variable  Setting
pH             7
CD            20
MLVSS          8
```

```
    Fit     SE Fit         95% CI              95% PI
```

```
99.7313  0.0882681  (99.5043, 99.9582)  (99.3847, 100.078)


Variable  Setting
pH              6
CD             15
MLVSS         6.5


    Fit     SE Fit        95% CI              95% PI
99.4812  0.0882681  (99.2543, 99.7082)  (99.1347, 99.8278)


Variable  Setting
pH              7
CD           17.5
MLVSS         6.5


    Fit     SE Fit        95% CI              95% PI
99.5733  0.0588454  (99.4221, 99.7246)  (99.2708, 99.8759)


Variable  Setting
pH              8
CD             20
MLVSS         6.5


    Fit     SE Fit        95% CI              95% PI
99.8187  0.0882681  (99.5918, 100.046)  (99.4722, 100.165)


Variable  Setting
pH              8
CD           17.5
MLVSS           8


  Fit     SE Fit        95% CI              95% PI
99.66  0.0882681  (99.4331, 99.8869)  (99.3134, 100.007)


Variable  Setting
pH              6
CD             20
MLVSS         6.5


    Fit     SE Fit        95% CI              95% PI
99.7162  0.0882681  (99.4893, 99.9432)  (99.3697, 100.063)


Variable  Setting
pH              7
CD           17.5
MLVSS         6.5


    Fit     SE Fit        95% CI              95% PI
99.5733  0.0588454  (99.4221, 99.7246)  (99.2708, 99.8759)


Variable  Setting
pH              6
CD           17.5
```

```
MLVSS           5


  Fit    SE Fit        95% CI            95% PI
99.29  0.0882681  (99.0631, 99.5169)  (98.9434, 99.6366)


Variable  Setting
pH             8
CD          17.5
MLVSS          5


   Fit     SE Fit       95% CI            95% PI
99.4575  0.0882681  (99.2306, 99.6844)  (99.1109, 99.8041)


Variable  Setting
pH             7
CD            20
MLVSS          5


   Fit     SE Fit       95% CI            95% PI
99.9237  0.0882681  (99.6968, 100.151)  (99.5772, 100.270)
```

Response Optimization: Discoloration

```
Parameters

Response  Goal      Lower  Target  Upper  Weight  Importance
% Color   Maximum   99.2   99.96              1           1


Variable Ranges

Variable  Values
pH        (6, 8)
CD        (15, 20)
MLVSS     (5, 8)

Solution

                          % Color      Composite
Solution  pH      CD  MLVSS    Fit  Desirability
1         7.03030 15  8    99.9563      0.995142


Multiple Response Prediction

Variable  Setting
pH        7.03030
CD        15
MLVSS     8


Response      Fit  SE Fit        95% CI             95% PI
% Color   99.9563  0.0883  (99.7294, 100.1833)  (99.6097, 100.3029)
```